

Topology, interactions, and disorder in one-dimensional quantum systems

Phd thesis

by

Nikolaos Kainaris

05.10.2016

Instructor: Prof. Dr. Alexander D. Mirlin

Topologie, Wechselwirkung und Unordnung in eindimensionalen Quantensystemen

Zur Erlangung des akademischen Grades eines

DOKTORS DER NATURWISSENSCHAFTEN

von der Fakultät für Physik
des Karlsruher Instituts für Technologie

genehmigte

DISSERTATION

von

Dipl. Phys. Nikolaos Kainaris
aus Bruchsal

Tag der mündlichen Prüfung: 20.10.2016
Referent: Prof. Dr. Alexander D. Mirlin
Korreferent: Prof. Dr. Jörg Schmalian

To my mother

Introduction

A recurring theme in modern condensed matter physics is the discovery and classification of novel phases of matter. The first systematic approach to characterize different phases was developed by Landau [1], who proposed to classify different phases by the symmetries that are broken at the phase transition. Many systems can be successfully described by this theory: crystalline solids, magnets or superconductors all fall into this category. The pattern of symmetry breaking leads to a unique order parameter, which takes a nonzero value only in the ordered phase.

One of the first times Landau's theory was challenged occurred when Klitzing *et al.* experimentally discovered that when a two dimensional (2D) electron gas is subjected to a strong magnetic field, its longitudinal conductance vanishes, while its Hall conductance is quantized to values $\nu_{\mathbb{Z}}e^2/h$, where $\nu_{\mathbb{Z}}$ is an integer [2]. By varying the strength of the magnetic field, a transition between Hall phases, characterized by different integers $\nu_{\mathbb{Z}}$, takes place, without the breaking of any additional symmetry. This quantum Hall effect (QHE) was theoretically explained in a single-particle picture by the spectral flow of Landau levels [3] and it was realized that these systems host metallic edge states coexisting with the insulating bulk. Semiclassically, the effect can be explained by imagining that electrons perform cyclotron motion on equipotential lines of the disorder potential and are therefore localized in the bulk while the electrons at the boundary perform skipping orbits leading to the emergence of one dimensional (1D) conducting channels at the edge. Most importantly, the measured quantized conductance is insensitive to the presence of impurities. Thouless, Kohmoto, Nightingale, and den Nijs [4] were the first to realize that the distinction between different quantum Hall phases is not a matter of symmetry but of topology. A given quantum Hall phase is not characterized by an order parameter, but rather by the *topological invariant* $\nu_{\mathbb{Z}}$ which counts the number of conducting edge modes.

Soon after the discovery of the QHE, theorists wondered if the effect can also take place in the absence of a magnetic field i.e. in systems with time-reversal symmetry (TRS). Related to this question, Haldane [5] studied a model of spinless electrons on a honeycomb lattice penetrated by a staggered magnetic flux. He found, that, although the total magnetic flux through the system is zero, electrons still form conducting edge channels. This provided the important conceptual realization that the emergence of the edge states originates from the nature of the gapped band structure of electrons and does not require Landau levels in particular.

An important breakthrough was attained several years later by Kane and Mele [6, 7] who showed that a variation of the Haldane model can be realized in a graphene sheet with spin-orbit coupling (SOC). The SOC effectively generates opposite magnetic fields for spin-up and spin-down electrons while conserving TRS. Metallic modes, energetically located within the bulk gap, appear at the edge of the sheet exactly as in Haldane's proposal. However, since TRS is conserved, they appear as Kramers pairs of electrons with opposite spin, propagating in opposite directions. The edge states are called *helical*, because the electron spin is locked to the propagation direction in such a way that the helicity, the projection of the momentum onto the spin, is a well defined quantum number. Crucially, due to Kramers theorem, elastic scattering between the edge states is prohibited and hence the modes are protected against Anderson localization. Kane and Mele showed that contrary to the QHE this novel insulating state is characterized by a \mathbb{Z}_2 topological invariant $\nu_{\mathbb{Z}_2} = 0, 1$. If the number of Kramers

pairs at the edge is even, impurity scattering between different pairs can gap the excitations at the edge. In the presence of an odd number of Kramers doublets at the edge, on the other hand, a single metallic pair always remains gapless. Physically, the \mathbb{Z}_2 invariant hence counts the number of Kramers doublets at the edge modulo two. Application of a longitudinal charge current generates a transverse spin-polarized bias, resulting in a quantized spin Hall conductance $G_s = 2e^2\nu_{\mathbb{Z}_2}/h$. In analogy to the QHE this effect is hence referred to as quantum spin Hall (QSH) effect.

It was soon realized, however, that, due to the tiny bulk gap, the QSH insulator cannot be experimentally realized in graphene. This led researchers to search for other candidate materials, with strong intrinsic SOC, that might show the QSH effect. In regard to that search, Bernevig, Hughes and Zhang [8] predicted that CdTe/HgTe/CdTe quantum wells behave under certain conditions as a 2D QSH insulator, which was experimentally confirmed only one year later by the Molenkamp group [9].

Over the last several years it was realized that the QHE and the QSH effect are but two examples of a wider class of materials, called Topological insulators (TI). These phases of matter possess a gap in the bulk electron spectrum, but cannot be continuously deformed into the vacuum without closing the gap or breaking a given set of symmetries. The nontrivial bulk topology goes hand in hand with the emergence of metallic modes at the boundary of the system that are protected against Anderson localization [10].

This realization led to a significant increase of experimental and theoretical activity in the field. On the experimental side a plethora of two- and three-dimensional materials, that exhibit topological phases, were discovered [11–13]. On the theoretical side, meanwhile, a full symmetry classification (periodic table of TIs) of noninteracting topological insulators and superconductors was established based on the study of lattice Hamiltonians [14] and field theory of disordered systems [10]. Both approaches were shown to be equivalent [15].

While the classification and properties of noninteracting topological insulators are well understood, much less is known about TIs with interactions. Although arguments exist [16], that states in the periodic table of TIs should remain stable against weak interactions, an exact criterion for the interaction strength is not known. In fact, sufficiently strong interactions are expected to give rise to novel topological phases, that are not adiabatically connected to the noninteracting ones. A remarkable example of the importance of interactions is provided by quantum wires with superconducting correlations. The mean-field interaction inside the wire is responsible for superconductivity which introduces an integer number of Majorana 0D end states [17–20]. These Majorana fermions are a particular example of topological boundary states which exhibit many exotic properties, the most stunning being that they obey non-Abelian statistics. This property together with their topological protection can in principle be used to implement fault-tolerant quantum computation schemes [21, 22]. Evidences for Majorana zero modes have been reported in recent experiments in heterostructures of semiconducting quantum wires and superconductors [23–26]. Including interaction between quasiparticles crucially affects the classification, yielding eight distinct states [27–29].

Electron-electron interactions also play a pivotal role for the transport properties of the helical edge modes of the QSH insulator. Unlike in the QHE the right and left moving edge modes in this system are not spatially separated but coexist at the same edge. Hence, the quasiparticles can interact with each other which raises questions regarding the stability of the conductance quantization for strong interactions [30, 31]. Moreover, while it is true that the electrons that constitute the Kramers pairs cannot be localized by elastic scattering off disorder, the same cannot be excluded for inelastic scattering mechanisms containing both electron-electron interaction and disorder.

Crucially, the effect of interactions is especially pronounced in 1D systems compared to their higher dimensional counterparts. In two and three dimensions, the interacting many-electron gas is in many

cases well described by Landau’s Fermi liquid theory, which expresses the excitations of the system as weakly interacting quasiparticles with renormalized parameters. In one dimension, in contrast, this description generically breaks down. Interacting electrons in one dimension are instead described by the Tomonaga-Luttinger theory [32–35]. Indeed, since a 1D particle cannot move without perturbing all the other ones, the low-energy excitations turn out to be collective ones; the bosonic plasmon excitations of the electron gas. The Luttinger liquid (LL) phase exhibits many exotic properties unique to electron systems in one dimension, such as spin-charge separation [35–39] and charge fractionalization [40–43]. From a theoretical point of view, 1D models provide a particularly attractive framework to study the effect of strong correlations since many of them are either exactly solvable or can be analyzed using powerful mathematical tools specific to 1D settings [35, 44]. Hence, the study of 1D quantum systems in topological materials is a natural starting point to gain a deeper understanding of the interrelation of topology and strong correlations.

This thesis will be concerned with all three aspects of transport in 1D quantum systems – topology, interactions and disorder – as well as their mutual interplay. We will both study concrete physical systems of current interest as well as propose novel materials and experimental setups that can be used to analyze the interplay of topology, interactions, and disorder in 1D systems. For the most part we will be interested in the transport properties of the helical edge modes that emerge at the boundaries of 2D TIs with preserved TRS subject to both electron-electron interaction and disorder scattering.

Topological insulators realize a holographic principle: the boundary physics crucially depends on the topological characteristics of the bulk. Consequently, the strongly correlated quantum liquid that emerges at the edge due to electron-electron interactions is distinct from previously studied 1D quantum liquids. Owing to its helical nature the edge modes have been termed helical Luttinger liquid (HLL). Transport properties of the HLL at the boundary of HgTe/HgCdTe structures in the TI regime were experimentally studied in Refs. [9, 45, 46]. In this situation the observed value of the conductance was close to $2e^2/h$, as expected for the ballistic transport in the QSH edge state. However, a clear suppression of the conductance from this value was identified in systems whose size exceeded the electron-electron scattering mean free path. One of the main goals of this thesis will be to develop low-energy theory of the HLL in the presence of both interactions and disorder and to discuss possible scattering mechanisms that lead to this suppression. In doing so, it will turn out to be crucial to include disorder scattering since the state does allow for inelastic backscattering off impurities [47–50], as the time-reversal invariance only protects the two states moving in opposite directions of the same energy, which form a Kramers doublet. The study of the transport properties of the HLL is not only of interest for the analysis of current experiments but also is of fundamental physical relevance, as the HLL presents an example of a novel quantum liquid that only emerges at the edge of TIs. In this context two natural questions arise. First, *How does the nontrivial topological origin of the HLL affect its transport properties compared to conventional LLs?* Second, *can the edge modes be gapped out by sufficiently strong interactions between electrons?*

The fact that dissipation in HLLs microscopically only originates from inelastic scattering makes it desirable to study experimental setups that specifically probe the electron-electron interaction inside TI edges. A prime candidate for such an experiment is the measurement of Coulomb drag between helical liquids. In a Coulomb drag experiment, current is driven in an “active” conductor (active edge in our setup), inducing an electrical field or current in a “passive” conductor (passive edge), with the frictional force being due to electron-electron interactions, without transfer of electrons between the subsystems. As such, Coulomb drag is a sensitive probe of inelastic electron-electron scattering. We will show that, due to its topological origin, the Coulomb drag between helical liquids differs in an essential way from Coulomb drag between TLLs. In particular we will discuss how the mechanism of plasmon-mediated

drag arises in such systems and affects the transport properties.

The unique properties of the edge modes of TIs crucially depend on the nature of the bulk gap. The quantum-well heterostructures that host the HLL at their boundaries are band insulators and the transition to the TI regime is achieved by band inversion. Strong interactions in 1D conductors provide an alternative way to generate spectral gaps. Electron-electron correlations in 1D systems can lead to a strong-coupling regime where spectral gaps are generated dynamically without spontaneous breaking of any continuous symmetry. In these phases the charge sector remains critical (gapless), however the spin sector acquires a gap. This leads immediately to the question: *Can one obtain states akin to a topological insulator when the gap is not present in the band structure, but dynamically generated by interactions?* The distinguishing feature of the helical edge modes is their protection against Anderson localization for not too strong interactions between them. Consequently, we ask the question: *What happens with such a strongly correlated topological state in the presence of disorder?*

These issues will be discussed in the work at hand.

Specifically, the remainder of this thesis is organized as follows. In two introductory chapters (Ch. 1 and Ch. 2) we present a basic introduction into aspects of quantum physics in one-dimension and topological phases of matter. In particular in Ch. 2 we review key experiments on transport properties of the HLL. In Ch. 3 we will be concerned with the transport properties of a single helical edge mode at the boundary of a 2D QSH insulator. As outlined before, the impact of strong interactions for the stability of the topological phase as well as signatures of interaction and disorder in the transport properties of the HLL represent important issues of current research. Specifically, we derive semiclassical expressions for the conductivity of interacting helical fermions in the presence of disorder as a function of the temperature and the frequency of the driving field. Possible strong coupling phases are discussed in the framework of a weak-coupling RG analysis. Next, in Ch. 4 we will be concerned with the Coulomb drag between clean HLLs. We will obtain analytical expressions for the drag conductivity, the central observable determining drag between quantum liquids, in a wide parameter regime using a combination of perturbative methods, bosonization and renormalization group transformations. In particular we uncover the mechanism of plasmon-mediated drag unique to the HLL. Finally, we will discuss the stability of the coupled HLL system in the case of strong inter-edge interactions. Ch. 5 will be concerned with the study of 1D conductors with strong SOC. We will show that strong interactions can drive the system into a nontrivial topological phase, where the spin sector of the LL is gapped, while the charge sector remains massless. This fascinating new topological phase exhibits many properties akin to topological band insulators. In particular we will show that the phase is stable against Anderson localization for moderately strong interaction strength and that it hosts gapless edge excitations with fractional properties.

For the convenience of the reader a summary of the acronyms as well as a list of notation and conventions commonly used in this thesis is given on pages 127 and 129, respectively.

Acknowledgments

First, I want to express my sincere gratitude to Prof. Alexander Mirlin for giving me the opportunity to work in his research group and for supervising my doctorate. I am deeply thankful for his support, the many interesting scientific discussions and his useful advice on scientific matters and beyond. In addition I would like to thank Prof. Jörg Schmalian for agreeing to co-referee this thesis.

Special thanks goes to my collaborators Igor V. Gornyi, Sam T. Carr, Dmitry G. Polyakov, Alex Levchenko, Raul A. Santos and Dmitri B. Gutman. I enjoyed doing research together and learned very much from our discussions.

I am also indebted to the Carl-Zeiss Stiftung for financial support during the time of my Phd.

I want to thank all those who proof read my thesis: Julia Link, Tim Ludwig, Philip Wollfarth, Mareike Hoyer, Matthias Bard and Mathias Scheurer.

Furthermore, I want to thank my roommates during my time at TKM, Mathias Scheurer, Matthias Bard, Mareike Hoyer, Patrik Hlobil and Elio König, for the nice atmosphere in my office. I also want to thank Fabienne Flatter for her help during my time as the “coffee administrator”.

During my time at the TKM I had the opportunity to participate in several “book seminars” about different topics of physics. I want to thank in particular Mathias Scheurer, Elio König and Matthias Bard for their participation in those seminars and for our great many scientific discussions.

Outside physics, I want to thank my family for their love and support over the years.

Finally, a big “thank you” goes to all members of TKM for the wonderful atmosphere. I really enjoyed my time at the institute.

Contents

Introduction	vii
Acknowledgments	xi
1 Fundamentals: Quantum physics in one dimension	1
1.1 The renormalization group	1
1.2 Bosonization	3
1.2.1 The Gaussian model	4
1.2.2 The Dirac equation	5
1.2.3 Bosonization relations	6
1.3 Interacting electrons in 1D: The Luttinger liquid paradigm	7
1.3.1 Spin or charge gap and the sine-Gordon model	10
1.4 Disorder in Luttinger liquids	12
1.4.1 Model for one-dimensional disordered systems	13
1.4.2 Renormalization of a single impurity in a Luttinger liquid	14
1.4.3 Many impurities: disordered Luttinger liquid	15
2 Fundamentals: Topological insulators	19
2.1 Definition of a topological insulator	19
2.1.1 Symmetry classification of Hamiltonians	20
2.1.2 Example: Su-Schrieffer-Heger model	22
2.2 \mathbb{Z}_2 topological insulators and helical edge states	25
2.2.1 Topological protection of the helical edge states	28
2.2.2 Experimental evidence for helical edge states	29
3 Electron transport in a disordered helical Luttinger liquid	33
3.1 The helical Luttinger model with broken axial spin symmetry	34
3.2 Conductivity of helical fermions	38
3.2.1 Conductivity of helical fermions: kinetic equation	39
3.3 Bosonization: The disordered helical Luttinger liquid	46
3.3.1 High-frequency conductivity of the disordered helical Luttinger liquid	50
3.4 Discussion of the semiclassical conductivity	54
3.5 Renormalization group treatment of the disordered helical Luttinger liquid	57
3.6 Summary of chapter 3	60
4 Coulomb drag between helical liquids	63
4.1 The model	64
4.2 Coulomb drag between helical edges: Kinetic theory	66
4.2.1 Kinetic equation	66
4.2.2 High-frequency Coulomb drag: Scattering rate	67

4.2.3	Low-frequency Coulomb drag	70
4.3	Intraedge interaction: Bosonization framework	73
4.3.1	First-order backscattering	74
4.3.2	Higher-order backscattering	76
4.3.3	Luttinger-liquid renormalization of the drag resistivity	78
4.3.4	Coulomb drag in the strong-coupling limit	80
4.4	Discussion of the drag resistivity	81
4.5	Summary of chapter 4	83
5	Emergent topological properties in one-dimensional conductors with spin-orbit coupling	85
5.1	Model for interacting one-dimensional electrons in the presence of SOC	86
5.1.1	Diagonalization of the non-interacting Hamiltonian	87
5.2	Interaction effects	89
5.2.1	Bosonization	90
5.2.2	Renormalization-group analysis	92
5.3	Disorder	94
5.3.1	Single impurity	94
5.3.2	Boundary zero modes	103
5.3.3	Disorder	105
5.3.4	Experimental signatures	106
5.4	Summary of chapter 5	106
	Conclusion	107
	List of publications	111
	Bibliography	113
	Acronyms	127
	Notations and conventions	129
	A Bosonization dictionary	131
	B Electron transport in a helical Luttinger liquid	135
B.1	Expressions for the current and diamagnetic susceptibility	135
B.2	Calculation of the conductivity	137
	C Renormalization group analysis of the disordered HLL	141
	D Coulomb drag between helical Luttinger liquids	149
D.1	Polarization operator for edge states of quantum spin Hall insulators	149
D.2	RPA-screened interaction	151
D.3	Calculation of high-frequency drag rate	153
D.3.1	High-frequency Coulomb drag: Particle-hole contribution	153
D.3.2	High-frequency Coulomb drag: Plasmon contribution	155

D.4	Second-order backscattering	158
D.5	Renormalization of the drag resistivity	160

1

Chapter 1

Fundamentals: Quantum physics in one dimension

The common theme of this thesis is the interplay of interactions, disorder and topology in one dimensional electron systems. For now we will focus on the first two key words “interaction” and “disorder”, postponing a discussion of topological effects to the next chapter.

In particular we will be concerned with transport in a one-dimensional electron system, where both disorder and interactions modify the transport properties more strongly compared to higher dimensions. In the absence of disorder, electron-electron interactions drive the system into a non-Fermi liquid phase known as LL. The distinctive feature of this state of matter is that the elementary excitations have no relation to free electrons, but rather are described by collective plasmon modes. Additionally, these bosonic modes carry spin and charge independently, a phenomenon known as spin-charge separation. As a consequence of the collective nature of the elementary excitations, even weak interactions between the electrons have profound consequences for the quantum state of the system [35, 44]. If interactions become strong they can lead to a strong-coupling regime where spectral gaps are generated dynamically without spontaneous breaking of any continuous symmetry.

On the other hand, it is known [51], that in the absence of interactions, even arbitrarily weak disorder leads to the localization of all electronic states in the system. The *dc*-conductivity is then zero, $\sigma(T) = 0$, for all temperatures T , since the temperature only determines the distribution function over the localized states.

If both, interactions and disorder, are present, the transport is determined by their mutual renormalization, with a metal-insulator transition at sufficiently strong attractive interaction.

The purpose of this chapter is twofold. First, we review, mostly for notational purposes, the powerful techniques of the renormalization group (Sec. 1.1) and bosonization (Sec. 1.2) that are at our disposal to solve problems in one dimension. We then discuss the impact of interactions, see Sec. 1.3, and disorder, Sec. 1.4, on the transport properties and phase diagram of 1D electrons.

1.1 The renormalization group

Here we will present only a very basic introduction to the renormalization group and refer the reader to the literature [52–54] for more details.

In condensed matter physics the renormalization group (RG) is a general term for methods that allow systematic investigations of a system’s behavior under scale changes. In particular one is often

interested in obtaining an effective low-energy theory by integrating out high energy degrees of freedom. A field theory is by definition a physical model defined on the continuum instead of a lattice. However, quantum fluctuations being at work at all scales, the theory is prone to accumulate all sorts of ultraviolet (UV) or infrared (IR) divergences. Therefore, a purely continuous theory makes no sense and we have to introduce an energy cutoff Λ that marks the range of applicability of the model. In condensed matter such a *regularization* is very physical, since we often study the effective low-energy theory of some lattice model, where the bandwidth provides a natural cutoff for the theory.

This procedure invariably introduces an energy scale Λ , which is part of the theory as one of the parameters along with other coupling constants, masses, velocities and so on. One must keep in mind though that a change in the cutoff Λ (through tracing out the high energy degrees of freedom) is accompanied by a change of all other parameters. Thus a field theory is not characterized by a fixed set of coupling constants but by a renormalization group trajectory in parameter space, which traces the change of parameters as the cutoff is lowered.

Let us outline how a generic (momentum) RG step is done. The problem we face, is that the theory is in general unaware of any clear cut separation of “fast” and “slow”¹ degrees of freedom. To nonetheless implement our scheme of integrating out “fast” modes we have to artificially define an energy $\Lambda' = b^{-1}\Lambda$, where $b > 1$, that separates slow ($\omega < \Lambda/b$) and fast ($\Lambda/b < \omega < \Lambda$) variables. Now we integrate out the fast fields and arrive at an effective action for the slow fields. The result may be twofold, either the algebraic structure of the action is changed completely or we get a new action that is identical to previous one except for (i) new values of the coupling constants and (ii) a decreased energy cutoff $\Lambda \rightarrow \Lambda' = b^{-1}\Lambda$. In the latter case the theory is called *renormalizable*. To compare the set of coupling constants with the previous ones we have to rescale momenta and energies, such that they have the same cutoff as before $(k, \omega) \rightarrow (bk, b\omega)$ ². Now one can iterate the procedure until the natural cutoff of the theory is reached (e.g. if temperature is the highest energy scale of the problem, the cutoff will be T). However, the utility of the RG relies on the recursive reproduction of the model at each step: one step alone already encodes all information about the renormalization properties of the model. These properties are condensed in the *generalized β function* which describes the flow of the set of parameters λ under the change of the control parameter

$$\beta(\lambda) = \frac{d\lambda}{d \ln b}. \quad (1.1)$$

Of importance for our purposes is the notion of a *fixed point*, i.e. a point in parameter space λ^* that is unaffected by the renormalization step ($\beta(\lambda^*) = 0$). Exactly at a fixed point the system is scale invariant. However, every system has at least one intrinsic length scale, the correlation length ξ . Consequently, at a fixed point we must have either $\xi = 0$ or $\xi = \infty$. On the other hand, a diverging correlation length is the hallmark of a second order phase transition. Therefore, we can identify fixed points as critical points of the underlying physical model.

In the vicinity (in a perturbative sense) of a fixed point the terms in the action, characterized by their coupling constants, fall into three categories: relevant, irrelevant and marginal. Relevant parameters grow algebraically under renormalization, irrelevant parameters decrease algebraically and marginal parameters undergo logarithmic variations.

¹With $\hbar \equiv 1$ energy and frequency are measured in the same units. Thus “fast” is equivalent to high energies and “slow” to low energies.

²In a Lorentz invariant theory it makes sense to scale energy and momentum with the same factor.

Effect of perturbations: Consider the perturbed action of a one-dimensional system

$$S = S_0 + \lambda \int dx d\tau O(x, \tau) \quad (1.2)$$

where S_0 is the fixed-point action, λ is a dimensionless coupling constant and O is an operator of scaling dimension Δ . The scaling dimension defines the properties of the operator under dilation of the space-time scales, $O'(bx, b\tau) = b^{-\Delta}O(x, \tau)$. Let us now perform a single RG step, that is we change the real space cutoff Λ^{-1} to a higher value $b\Lambda^{-1}$, where $b > 1$. In order to compare the new action with the previous one, we have to rescale spacetime as $(x, \tau) = (b^{-1}x', b^{-1}\tau')$, where (x, τ) now have the same cutoff as before. Thus

$$S' = S_0 + \lambda \int dx' d\tau' O(x', \tau') = S_0 + \lambda b^{2-\Delta} \int dx d\tau O(x, \tau). \quad (1.3)$$

Therefore, we can read off the change of the coupling constant,

$$\lambda'(b) = \lambda b^{2-\Delta} = \lambda(0) e^{(2-\Delta)\ln(b)}. \quad (1.4)$$

Let us assume that $b = 1 + \ell$ ($\ell \ll 1$) is close to unity (which means we "shave off" an infinitesimal layer in momentum space in each RG step), i.e. $\ln(b) \approx \ell$. Then we can encapsulate the information from the RG step in the differential equation $\frac{\lambda' - \lambda}{\ell} \simeq \frac{d\lambda}{d\ell} = \lambda(2 - \Delta)$. In other words the β function is given by

$$\beta(\lambda) = \frac{d\lambda}{d\ell} = \lambda(2 - \Delta). \quad (1.5)$$

The sign of the beta function tells us if a coupling constant grows ($\beta > 0$) or decreases ($\beta < 0$) under the RG. Thus, the perturbation is relevant if $\Delta < 2$, irrelevant if $\Delta > 2$ and marginal if $\Delta = 2$. A relevant operator is typically the source of a gap in the low-energy spectrum while irrelevant operators only change the properties of the theory in a perturbative sense.

1.2 Bosonization

The conventional description of the low-energy properties of interacting electrons in dimensions $D > 1$ is based on the Fermi-liquid theory.

Free fermions obey Fermi-Dirac statistics and their ground state at zero temperature is the filled Fermi sea. Excitations with respect to this ground state are electrons defined by their momentum, spin and charge. Since they are eigenstates of the Hamiltonian they have infinite lifetime. Landau's hypothesis was, that if we adiabatically switch on interactions, the fundamental quantum numbers and the statistics of the particles are left unchanged. However, their dynamical properties such as mass, velocity etc. get renormalized by the effect of interactions. The excitations are thus not the fundamental electrons anymore but are called quasiparticles. Heuristically, these are electrons dressed by surrounding density fluctuations. The affinity of the quasiparticles to eigenstates of the many-body system is shown by the spectral function $A(k, \epsilon)$; the spectral weight is centered around the quasiparticle dispersion $\xi(k)$ with width $\delta\epsilon \ll \xi(k)$ and quasiparticle weight Z_k .

While this description works well in higher dimensions, it breaks down for the description of one dimensional electrons in the presence of even arbitrarily weak interactions. The correction to the quasiparticle weight in second (lowest non-vanishing) order scales as $\propto \ln(\Lambda/\epsilon)$, transferring spectral

weight away from the quasiparticle pole. Furthermore, the second order corrections to the single particle density of states $\nu(\epsilon)$ at $\epsilon = 0$ and to the momentum distribution function $n(k) \propto \int d\epsilon A(k, \epsilon)$ are divergent at the Fermi points $\pm k_F$.

These divergencies signal that electron-electron interactions drive the system into a non-Fermi liquid phase known as LL. While a description of the Luttinger liquid state is possible within a fermionic treatment, an alternative and very powerful approach is bosonization, in which the theory is formulated in terms of bosonic degrees of freedom. This description hinges on the fact that particle-hole pairs, in the linear spectrum approximation, have a well defined excitation energy. For free electrons an excitation with energy ϵ , consisting of an arbitrary number of particle hole-pairs with total momentum q , only depends on that total momentum, $\epsilon = v_F q$. This degeneracy allows one to describe the fermionic excitations in terms of free bosonic excitations - the quantized density waves (plasmons) of the electron gas.

A thorough discussion of the Luttinger liquid and the bosonization technique is beyond the scope of this thesis and we refer to the literature [35, 44, 54, 55]. In this section, we will merely show the fermion to boson equivalence on the level of correlation functions of the field theories of free bosons and free electrons in 1D.

1.2.1 The Gaussian model

The model describing free massless bosons in one dimension is called the Gaussian model and is defined by the action

$$S_0 = \frac{1}{2} \int dx d\tau \left[v^{-1} (\partial_\tau \varphi)^2 + v (\partial_x \varphi)^2 \right] \quad (1.6)$$

where $\varphi(x, \tau)$ is a real scalar field and v is the velocity. At $T = 0$ it is straightforward to show that the single particle Green's function on a disk of radius R and a short distance cutoff a is given by

$$G(z, \bar{z}) = \langle \varphi(z, \bar{z}) \varphi(0, 0) \rangle = \frac{1}{4\pi} \ln \left(\frac{R^2}{z\bar{z} + a^2} \right). \quad (1.7)$$

where we introduced the complex coordinates

$$z = v\tau - ix, \quad \bar{z} = v\tau + ix, \quad (1.8)$$

It is also useful to study the behavior of exponentials of bosonic fields, called vertex operators. To avoid divergencies in the theory these operators have to be normal ordered. Thus, vertex operators don't multiply like ordinary exponentials but according to

$$e^{i\alpha\phi(z)} e^{i\beta\phi(z')} = e^{i\alpha\phi(z) + i\beta\phi(z')} e^{-\alpha\beta\langle\phi(z)\phi(z')\rangle} \quad (1.9)$$

which can be shown using the Campbell-Baker-Hausdorff-Formula [54].

Next, defining the correlation function of bosonic exponents,

$$F(1, 2, \dots, N) \equiv \langle e^{i\beta_1\varphi(z_1, \bar{z}_1)} \dots e^{i\beta_N\varphi(z_N, \bar{z}_N)} \rangle \quad (1.10)$$

one finds that

$$F(1, 2, \dots, N) = \prod_{i>j} \left(\frac{z_{ij} \bar{z}_{ij}}{a^2} \right)^{\beta_i \beta_j} \left(\frac{R}{a} \right)^{-(\sum_i \beta_i)^2 / 4\pi} \quad (1.11)$$

For an infinite system, $R \rightarrow \infty$, this yields the “neutrality” condition that the correlation function is only nonzero if

$$\sum_i \beta_i = 0. \quad (1.12)$$

From the result (1.11) we see that the scaling dimension of a vertex operator is $\exp(i\beta\varphi) : \Delta = \beta^2/4\pi$. Note that, on the level of correlation functions, the boson field φ decomposes into a holomorphic and an antiholomorphic part, which are functions of only z or \bar{z} , respectively. Hence, we can define chiral components of the boson fields as

$$\varphi(z, \bar{z}) = \phi_+(z) + \phi_-(\bar{z}). \quad (1.13)$$

It is customary to further define the dual field

$$\theta(z, \bar{z}) = \phi_+(z) - \phi_-(\bar{z}), \quad (1.14)$$

which satisfies $\partial_z \theta = \partial_z \varphi$ and $\partial_{\bar{z}} \theta = -\partial_{\bar{z}} \varphi$, or in space time coordinates $i\partial_\tau \varphi = -\partial_x \theta$. Hence, the dual field is related to the conjugate momentum $\Pi = -\partial_x \theta$ which, in the Hamilton formalism, obeys the canonical equal time commutation relation $[\hat{\varphi}(x), \hat{\Pi}(x')] = i\delta(x - x')$. The relation between the dual field and the conjugate momentum implies the non-local commutation relation between the bosonic φ and θ operators:

$$[\hat{\varphi}(x), \hat{\theta}(x')] = -i\Theta(x - x'), \quad (1.15)$$

where Θ is the Heaviside step function.

1.2.2 The Dirac equation

Let us now discuss the model of free one dimensional fermions without spin, described by the action

$$S_0 = \int dx d\tau \left[\bar{\psi}(x, \tau) \left(\partial_\tau - \frac{\partial_x^2}{2m} \right) \psi(x, \tau) \right], \quad (1.16)$$

where $\bar{\psi}, \psi$ are Grassmann fields. We note, that in contrast to higher dimensions, the 1D Fermi surface consists of only two points. Usually, the bandwidth Λ or the Fermi energy E_F by far exceed the energy scales of interest such as the temperature or applied voltage. Our interest thus lies in a model that captures the relevant physics close to the Fermi points. There are two consequences of this. First, the only relevant Fourier components of external fields are those close to zero or $\pm 2k_F$.³ Second, we can linearize the spectrum close to the Fermi points and expand the electron fields in chiral fields ψ_η , that destroy electrons close to the right ($\eta = +$) or left ($\eta = -$) Fermi point. These excitations are usually referred to as right- and left-movers. Since the wave packet of an electron in the vicinity of the Fermi surface is peaked around momenta $\pm k_F$, this decomposition takes the form

$$\psi(x, \tau) = \psi_+(x, \tau)e^{ik_F x} + \psi_-(x, \tau)e^{-ik_F x}, \quad (1.17)$$

In the Hamiltonian formalism these chiral fermions correspond to operators with commutation rules

$$\{\hat{\psi}_\eta(x), \hat{\psi}_{\eta'}^\dagger(x')\} = \delta(x - x')\delta_{\eta, \eta'}. \quad (1.18)$$

³That means that electrons can only be scattered forward or backward; there are no angles to play with.

Using the expansion (1.17) in (1.16) and neglecting oscillatory terms and higher order gradients we arrive at

$$S_0 \simeq \sum_{\eta=\pm} \int dx d\tau \bar{\psi}_\eta (\partial_\tau - i\eta v \partial_x) \psi_\eta, \quad (1.19)$$

with the Fermi velocity v . If we can safely neglect curvature corrections (these would become important e.g. at the bottom of the band) the action in Eq. (1.19) is a universal model for the low-energy excitations of one-dimensional electrons. The free propagators of the fermionic model are readily calculated

$$\langle \psi_+(z) \bar{\psi}_+(0) \rangle = \frac{1}{2\pi a} \frac{1}{z} \quad \text{and} \quad \langle \psi_-(z) \bar{\psi}_-(0) \rangle = \frac{1}{2\pi a} \frac{1}{\bar{z}}. \quad (1.20)$$

We can also include an external electromagnetic field via the standard minimal substitution $\partial_\mu \rightarrow \partial_\mu - ieA_\mu$.⁴ This enables us to calculate the current density $j = j_1$ and charge density $\rho = ij_0$ by variation of the action,

$$j_\mu = \frac{\delta S[A]}{\delta A_\mu}, \quad (1.21)$$

which yields:

$$\rho = e(\rho_+ + \rho_-), \quad (1.22)$$

$$j = e(\rho_+ - \rho_-). \quad (1.23)$$

Here we defined the chiral densities $\rho_\eta = \bar{\psi}_\eta \psi_\eta$.

1.2.3 Bosonization relations

If we define the correspondence

$$\psi_+(z) = \frac{1}{\sqrt{2\pi a}} e^{-i\sqrt{4\pi}\phi_+(z)}, \quad \psi_-(\bar{z}) = \frac{1}{\sqrt{2\pi a}} e^{i\sqrt{4\pi}\phi_-(\bar{z})}, \quad (1.24)$$

the correlation functions of the fermionic model in Eq. (1.20) and those of the bosonic exponentials in Eq. (1.11) are identical. In fact it turns out that the entire spectrum of the two models is identical and Eq. (1.24) is an exact operator identity (if one includes Klein factors to be introduced below). We are not going to prove this equivalence here but refer to the literature given at the beginning of this chapter. A bosonization dictionary with useful relations can be found in App. A.

While the bosonization formulas (1.24) are the basis of fermion-to-boson translation, their naive implementation often leads to errors. Take for example the density of right movers $\rho_+(x) = \bar{\psi}_+(x)\psi_+(x)$. It is formally infinite because there is an infinite number of holes occupying the states below the Fermi surface at point x . To regularize such infinities we have to normal order the operator. Equivalently, we can implement the procedure of *point splitting* by defining

$$\rho_+(z) \equiv \lim_{\epsilon \rightarrow 0} \left[\bar{\psi}_+(z+\epsilon)\psi_+(z-\epsilon) - \langle \bar{\psi}_+(z+\epsilon)\psi_+(z-\epsilon) \rangle \right], \quad (1.25)$$

⁴Remember $c \equiv 1$ and e is the fundamental charge. Furthermore, in the imaginary time formalism $A_0 = i\phi$.

and similar for the left moving current. This yields the expressions

$$\rho_+(z) = \frac{i}{\sqrt{\pi}} \partial_z \phi_R, \quad \rho_-(\bar{z}) = -\frac{i}{\sqrt{\pi}} \partial_{\bar{z}} \phi_L. \quad (1.26)$$

The particle current and density take the form

$$\rho = \rho_+ + \rho_- = \frac{1}{\sqrt{\pi}} \partial_x \varphi, \quad (1.27)$$

$$j = \rho_+ - \rho_- = \frac{1}{\sqrt{\pi}} \partial_x \theta. \quad (1.28)$$

The field φ is sometimes called *displacement field* because it measures the local deviations from the average density, while the field θ is called *phase field* due to its relation to the current.

The relations 1.24 describe the bosonization relations for spinless electrons. For real electrons with spin $\sigma = \uparrow, \downarrow$ they have to be adjusted in two ways. First, to ensure the correct anticommutation relations between fermions of different spin species, one has to introduce Hermitian operators called Klein factors $\hat{\kappa}_{\eta, \sigma}$ into the bosonization relations. These connect different fermionic Hilbert spaces in the operator formalism and obey the Clifford algebra: $\{\hat{\kappa}_{\eta, \sigma}, \hat{\kappa}_{\eta', \sigma'}\} = \delta_{\eta, \eta'} \delta_{\sigma, \sigma'}$. For many purposes the Klein factors can be projected out [54, 55] and oftentimes we will neglect them in this thesis.

Second, we introduce the spinful chiral bosonic fields $\phi_{\eta, \uparrow}$ and $\phi_{\eta, \downarrow}$. The full bosonization relations for spinful fermions then read as

$$\psi_{+, \sigma}(x) = \frac{\kappa_{\sigma}}{\sqrt{2\pi a}} e^{i\sqrt{4\pi}\phi_{+, \sigma}(x)}, \quad \psi_{-, \sigma}(x) = \frac{\kappa_{\sigma}}{\sqrt{2\pi a}} e^{-i\sqrt{4\pi}\phi_{-, \sigma}(x)}. \quad (1.29)$$

The chiral fields define the displacement and phase field similar to the spinless case $\varphi_{\sigma} = \phi_{+, \sigma} + \phi_{-, \sigma}$ and $\theta_{\sigma} = \phi_{+, \sigma} - \phi_{-, \sigma}$. It is often useful to work not with the spin fields but with the spin and charge components:

$$\varphi_c = \frac{1}{\sqrt{2}}(\varphi_{\uparrow} + \varphi_{\downarrow}), \quad \varphi_s = \frac{1}{\sqrt{2}}(\varphi_{\uparrow} - \varphi_{\downarrow}). \quad (1.30)$$

and the same for $\theta_{c, s}$.

Admittedly, at the moment it is not clear why the bosonization transformation is useful. This only becomes apparent after we include interactions between electrons in the next section.

1.3 Interacting electrons in 1D: The Luttinger liquid paradigm

The general pairwise interaction between 1D electrons (of one band) is of the form

$$S_{\text{int}} = \frac{1}{2} \int dx_1 dx_2 \bar{\psi}_{\sigma}(x_1, \tau) \psi_{\sigma}(x_1, \tau) V(x_1 - x_2) \bar{\psi}_{\sigma'}(x_2, \tau) \psi_{\sigma'}(x_2, \tau) \quad (1.31)$$

Here, we assume that the pairwise interaction potential $V(x_1 - x_2)$ is short range (screened by external gates). We need only its Fourier components close to $q = 0$ (V_f) and $q = \pm 2k_F$ (V_b), which describe forward and backward scattering. Using the low-energy decomposition of the electron fields in (1.17), the interaction processes naturally fall into four categories labeled by dimensionful coupling constants g_i . This classification is usually termed *g-ology* for this reason and is defined by the coupling constants

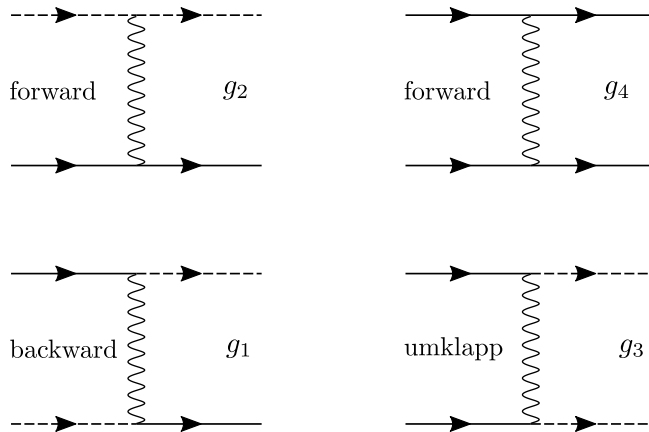


Figure 1.1: Interaction processes in a LL. Solid (dashed) lines denote right-moving (left-moving) electrons. The spin index has been suppressed.

g_4 (e-e forward scattering inside the same chiral branch), g_2 (e-e forward scattering between right- and left-movers), g_1 (e-e backscattering) and g_3 (e-e Umklapp scattering). Additionally we introduce subscripts which specify whether the spin of the two incoming electrons is parallel (\parallel) or antiparallel (\perp). The interaction part of the action then reads as $S_{\text{int}} = S_{\text{f}} + S_{\text{b}} + S_{\text{um}}$, with

$$S_{\text{f}} = \frac{1}{2} \sum_{\sigma, \sigma'} \sum_{\eta, \eta'} \int dx d\tau \left(g_{4\parallel} \delta_{\sigma, \sigma'} \delta_{\eta, \eta'} + g_{4\perp} \delta_{\sigma, \bar{\sigma}'} \delta_{\eta, \eta'} \right) \rho_{\eta, \sigma} \rho_{\eta', \sigma'} + \frac{1}{2} \sum_{\sigma, \sigma'} \sum_{\eta, \eta'} \int dx d\tau \left(g_{2\parallel} \delta_{\sigma, \sigma'} \delta_{\eta, \bar{\eta}'} + g_{2\perp} \delta_{\sigma, \bar{\sigma}'} \delta_{\eta, \bar{\eta}'} \right) \rho_{\eta, \sigma} \rho_{\eta', \sigma'} , \quad (1.32)$$

$$S_{\text{b}} = g_{1\perp} \sum_{\sigma} \int dx d\tau \bar{\psi}_{+, \sigma} \bar{\psi}_{-, \bar{\sigma}} \psi_{+, \bar{\sigma}} \psi_{-, \sigma} , \quad (1.33)$$

$$S_{\text{um}} = g_{3\perp} \sum_{\eta, \sigma} \int dx d\tau \bar{\psi}_{\eta, \sigma} \bar{\psi}_{\eta, \bar{\sigma}} \psi_{\bar{\eta}, \bar{\sigma}} \psi_{\bar{\eta}, \sigma} e^{-i4k_F x} . \quad (1.34)$$

The interaction processes are diagrammatically depicted in Fig. 1.1. The incoming spin in the backscattering term can be assumed to be antiparallel, since the case of parallel spins is included in the renormalization of the g_2 term via $g_{2\parallel} \rightarrow g_{2\parallel} - g_{1\parallel}$. In the Umklapp term the term with parallel spins vanishes due to the Pauli principle.

Two points are worth mentioning here. First, all coupling constants of the above action in general already contain renormalizations due to high-lying states and should be considered as effective coupling constants of the model. Second, we will neglect the Umklapp scattering in the remainder of this chapter, since it contains a highly oscillating exponential factor. It only has to be taken into account at commensurate filling, because of constraints set by crystal momentum conservation.⁵

To begin with, we neglect scattering across Fermi points (i.e. $g_{1\perp} = 0$). The model described by the action $S_{LL} = S_0 + S_{\text{f}}$ is then known as the *Tomonaga-Luttinger* model. The beauty of this model is that its bosonized form remains noninteracting (albeit with renormalized parameters). Applying the

⁵To see this consider the operator in momentum space e.g. $\bar{\psi}_{R, k} \bar{\psi}_{R, p} \psi_{L, k+q} \psi_{L, p-q}$ then we must have $k, p \simeq k_F$, $q \simeq -2k_F$. In order for all the operators to be near the Fermi points we must add a reciprocal lattice vector $Q = 2\pi/a_0$. In the case of half filling, $k_F = \pi/(2a_0)$, we have $Q = 4k_F$ and thus $p - q - Q$ is close to the left Fermi point as needed.

bosonization identities we find

$$S_{LL} = \sum_{\mu=c,s} \frac{1}{2v_\mu K_\mu} \int dx d\tau \left[v_\mu^2 (\partial_\tau \varphi_\mu)^2 + (\partial_x \varphi_\mu)^2 \right] \quad (1.35)$$

The model is determined by four parameters, the plasmon velocities v_μ and the Luttinger parameters K_μ , which are given by

$$K_\mu = \sqrt{\frac{1 - U_\mu}{1 + U_\mu}}, \quad (1.36)$$

$$v_\mu = u_\mu \sqrt{1 - U_\mu^2} \quad (1.37)$$

with

$$U_\mu = \frac{1}{2\pi u_\mu} (g_{2\parallel} \pm g_{2\perp}), \quad (1.38)$$

$$u_\mu = v_F + \frac{1}{2\pi} (g_{4\parallel} \pm g_{4\perp}), \quad (1.39)$$

where the upper sign corresponds to charge and the lower sign to spin. We see that the only role of g_4 forward scattering is to renormalize the Fermi velocity; it is therefore often neglected from the start. The result (1.35) shows the complete separation between spin and charge degrees of freedom - a phenomenon commonly referred to as spin charge separation.

We point out that it is not straightforward to derive the form of the coupling constants in (1.36) and (1.37) starting from the fermionic action in (1.31). By linearizing the spectrum around the Fermi surface and introducing left and right movers we effectively take a short cut to performing a rigorous RG treatment to derive the low-energy theory. The latter yields the flow to the LL fixed point but renormalizes the g-ology parameters. It is possible to fix the form of the coupling constants v_μ and K_μ by invoking the Pauli principle, Galilean invariance and spin SU(2) symmetry [56, 57]. The resulting expressions read as

$$\begin{aligned} v_\mu K_\mu &= 1, \\ K_c^{-1} &= \sqrt{1 + \frac{2V_f - V_b}{\pi v_F}}, \\ K_s^{-1} &= \sqrt{1 + \frac{V_b}{\pi v_F}}. \end{aligned} \quad (1.40)$$

Also the coupling constant of the Umklapp term is fixed to $g_{1\perp} = V_b$. It is important to keep in mind that if we want to model the low-energy theory of interacting electrons the coupling constants of the Luttinger model are not independent but obey the relations in (1.40).

Physically, the mapping of the interacting fermionic model to the free bosonic model in (1.35) means that the excitations of the Luttinger liquid are not single particle excitations, but bosonic density fields. The Luttinger liquid correlations manifest themselves for example in power law singularities of the single particle density of states at energy ϵ measured from the Fermi surface,

$$\nu(\epsilon)/\nu_0 \sim |\epsilon|^\alpha \quad (1.41)$$

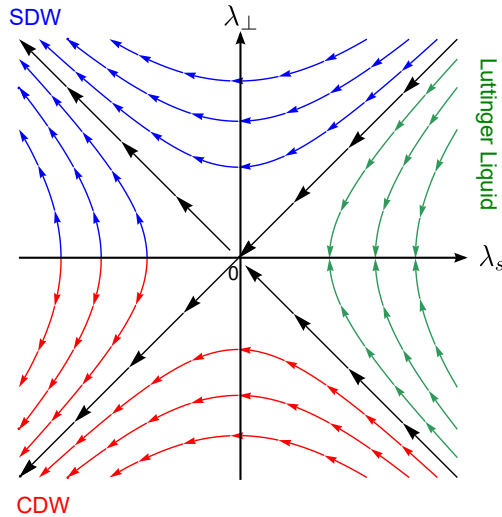


Figure 1.2: RG flow of the equations (1.43) for the dimensionless strength of backward (λ_{\perp}) and forward (λ_s) scattering electron-electron interaction potential of 1D fermions. If spin-rotational symmetry is not broken the bare parameters lie on the first bisecting (black) and the system flows towards the Luttinger liquid phase for repulsive interactions, $\lambda_{\perp} = \lambda_s > 0$ and to the charge-density wave (CDW) phase for attractive interactions, $\lambda_{\perp} = \lambda_s < 0$. In the latter case, the spin sector becomes gapped.

Here, ν_0 is the density of states in the absence of interactions and the exponent depends on the interaction strength. For tunneling into the bulk of a spin-rotational invariant electron liquid it is given by $\alpha = (K_c + 1/K_c - 4)/2$. The suppression of the density of states at zero energy signals, what we already mentioned at the beginning of this section: that no single particle states exist at the Fermi surface for electrons to tunnel into, they need a finite energy to convert into collective excitations before entering the bulk.

1.3.1 Spin or charge gap and the sine-Gordon model

If we take into account backscattering ($g_{1\perp}$), the field theory of interacting electrons can no longer be solved exactly by bosonization. Combined with the bosonized Luttinger model we get one of the most studied models in field theory, the sine-Gordon (SG) model $S = S_{LL} + S_{SG}$, with

$$S_{SG} = \frac{v_s g_{1\perp}}{2\pi^2 a^2} \int dx d\tau \cos\left(\sqrt{8\pi}\varphi_s\right) \quad (1.42)$$

This model is integrable and hence many exact properties are known about it. Most of the important properties can already be extracted from a perturbative RG treatment of the model. Note, that the scaling dimension of the cosine operator is $\Delta = 2K_s$. Naively we would expect that it is relevant for $K_s < 1$ and irrelevant for $K_s > 1$. However, K_s is subject to the RG flow itself and thus we have to study the coupled RG equations

$$\frac{d\lambda_s}{d\ell} = -\lambda_{\perp}^2, \quad \frac{d\lambda_{\perp}}{d\ell} = -\lambda_{\perp}\lambda_s. \quad (1.43)$$

where we expanded $K_s \simeq 1 + \lambda_s/2$ for weak interactions and defined the dimensionless coupling constant $\lambda_\perp = g_{1\perp}/\pi v_s$. The equations (1.43) were first obtained by Kosterlitz and Thouless [58] and are known as Berezinskii-Kosterlitz-Thouless (BKT) equations. The corresponding flow diagram is illustrated in Fig. 1.2. There are several important aspects to these equations. As we have already discussed, the bare coupling constants are fixed by spin SU(2) invariance to $\lambda_\perp^0 = \lambda_s^0 = V_b$. Hence the flow in Fig. 1.2 is constrained along the separatrix. If the electron-electron interaction is repulsive the system flows to a Luttinger liquid phase with renormalized Luttinger parameter and plasmon velocity. If, on the other hand, the interaction is attractive the flow is to a strong-coupling phase, the CDW phase, where interactions dynamically open a gap in the spin sector. There is also another strong-coupling fixed point, the spin-density wave (SDW) phase, that can only be realized, if spin-rotational invariance is broken, see the discussion in Ch. 5.

The nature of the strong-coupling fixed points can be studied by means of mean field theory. If the coupling constant of the cosine potential becomes strong, the field φ_s locks to one of the minima of the cosine potential $\sim g_{1\perp} \cos(\sqrt{8\pi}\varphi_s)$ to minimize the action. We can then define a local ‘‘order parameter’’ that characterizes the strong-coupling phase. As the charge mode, irrespective of the spin sector, always remains gapless, these local order parameters are never nonzero in the thermodynamic limit. Rather the phase of the system is identified with the order parameter with the slowest decaying correlations, see e.g. Ref [56, 59].

For definiteness we consider repulsive interactions in the charge sector, $K_c < 1$. In this case we have to study two possibilities for the order parameter. For $g_{1\perp} < 0$ the potential energy $\sim g_{1\perp} \cos(\sqrt{8\pi}\varphi_s)$ is minimized by $\varphi_s^{\text{CDW}} \equiv \sqrt{\pi/2} n$, where n is integer. For these mean-field configurations, $\langle \cos(\sqrt{2\pi}\varphi_s) \rangle \neq 0$ and the dominant correlations are described by the order parameter

$$\mathcal{O}_{\text{CDW}} = \frac{2}{\pi a} \sin(\sqrt{2\pi}\varphi_c) \cos(\sqrt{2\pi}\varphi_s) = \sum_{\sigma, \sigma'} \sum_{\eta, \eta' = \pm} \bar{\psi}_{\sigma, \eta} \sigma_{\sigma, \sigma'}^0 \tau_{\eta, \eta'}^x \psi_{\sigma', \eta'}. \quad (1.44)$$

In the second line we formulated the order parameter back in the basis of chiral fermions. The matrix σ^0 spin space signals the presence of spin singlets, while the matrix τ^x in chiral space signals that the charge degree of freedom fluctuates. This order parameter thus may be interpreted as a charge density wave phase.

On the other hand if $g_{1\perp} > 0$ the potential energy is minimized by $\varphi_s^{\text{SDW}} = \sqrt{\pi/2} (n + 1/2)$ and the order parameter

$$\mathcal{O}_{\text{SDW}} = \frac{2}{\pi a} \cos(\sqrt{2\pi}\varphi_c) \sin(\sqrt{2\pi}\varphi_s) = \sum_{\sigma, \sigma'} \sum_{\eta, \eta'} \bar{\psi}_{\sigma, \eta} \sigma_{\sigma, \sigma'}^z \tau_{\eta, \eta'}^x \psi_{\sigma', \eta'}, \quad (1.45)$$

becomes dominant since $\langle \sin(\sqrt{2\pi}\varphi_s) \rangle \neq 0$. The only difference between this order parameter and that in Eq. (1.44) is the presence of σ^z instead of σ^0 . This means, that one has an antiferromagnetic pattern of spins. We can thus interpret this phase as a spin density wave. A cartoon picture of the phases is depicted in Fig. 1.3.

Lastly, we discuss the nature of excitations in the massive phase, see Ref [44] and references therein. If the field φ_s is locked to one of the minima of the cosine potential, there is a spectral gap to excitations which are given by solitons in the field φ_s interpolating between adjacent minima. These solitons, also called *spinons*, are pictorially depicted in Fig. 1.3. There also exist antisolitons - mirror images of solitons. Additionally, there is a residual interaction between solitons, which is attractive for $K_s < 1/2$ and repulsive for $1/2 < K_s < 1$. In the attractive case, solitons and antisolitons can form bound states (*breathers*) with lower energy than the individual excitations. At exactly $K_s = 1/2$, the *Luther-Emery point*, the solitons are free and can be mapped to free massive fermions.

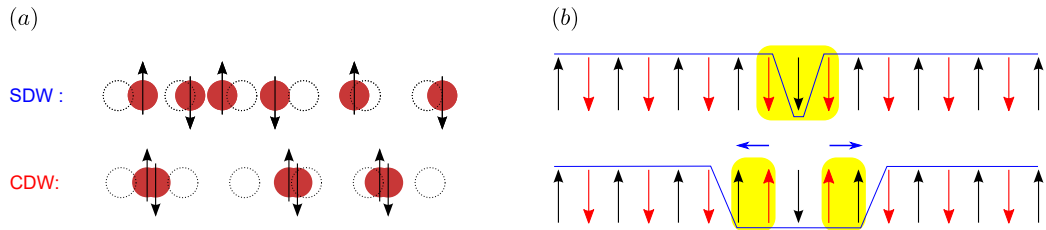


Figure 1.3: (a) Strong-coupling phases of the 1D electron gas with repulsive electron-electron interactions. Spin degrees of freedom order while charge degrees of freedom (red solid circles) fluctuate strongly around their average position (black open circles) (b) Excitations above the SDW ground state. The blue line denotes the local value of the spin displacement field φ_s . A flipped spin decomposes into a soliton and an antisoliton that each carry spin 1/2 and travel through the system as indicated by the blue arrows.

1.4 Disorder in Luttinger liquids

So far we discussed the physics of interacting one-dimensional electrons in the absence of disorder. Now let us discuss what happens if we introduce localized impurities into the system. This problem is of considerable practical relevance. Every physical realization of one-dimensional systems – semiconducting quantum wires, nanotubes, quantum Hall edges, etc. – generally contain imperfections such as dislocations, vacancies or charged impurities.

The goal of this section is to give a tailor-made introduction to the concepts required for the study of disordered one-dimensional systems and to review some key results known in the literature, see also [35, 60]. As mentioned, it is known [51] that arbitrarily weak disorder leads to the localization of all electronic states in the system, with the localization length ξ_{loc} given by the inverse scattering rate $v_F\tau$. The *dc*-conductivity then vanishes, $\sigma(T) = 0$, for any temperature T , since the temperature only determines the distribution over the localized states. The peculiarity of 1D electrons is, that the ballistic regime of free electrons crosses over directly to the localized regime in the presence of arbitrarily weak disorder, without any intermediate diffusive regime [60].

The transport properties of the localized system can be probed by the *ac*-response at an external frequency ω . In the limit of low frequencies $\omega\tau \ll 1$, the conductivity is given by the Berezinskii-Mott formula [61, 62]:

$$\text{Re } \sigma / \sigma_D = 4(\omega\tau)^2 \ln^2(\omega\tau), \quad (1.46)$$

where $\sigma_D = e^2\kappa v_F^2\tau$ and κ is the compressibility. In the opposite regime of high frequencies, $\omega\tau \gg 1$ the *ac*-conductivity follows the Drude law $\sigma(\omega) = \sigma_D / (1 - i\omega\tau)$.

The presence of electron-electron interaction changes this picture profoundly. In general interaction is responsible for two distinct main effects. First, it renormalizes the elastic scattering potential through the creation of particle-hole excitations (screening). In one dimension, this corresponds to the dressing of impurities by Friedel-oscillations, see the discussion in Sec. 1.4.2, which yields a temperature dependent scattering time $\tau(T)$ in the Drude formula.

The second effect of interactions is to break the phase-coherence of electrons. This introduces a new scale, the dephasing time τ_ϕ , into the problem - quasiclassically it corresponds to the time an electron can travel on average before it changes its phase through an inelastic scattering event.

Taking these effects into account, the conductivity of the interacting, disordered electron gas at sufficiently high temperatures is given by $\sigma(T) \simeq \sigma_D + \Delta\sigma_{wl}$ and is dominated by the temperature dependent Drude part. At lower temperatures, when $\sigma_D \sim \Delta\sigma_{wl}$, which is equivalent to $\tau(T) \sim \tau_\phi(T)$, the weak localization corrections become strong and trigger a metal-insulator transition towards a localized regime.

We will discuss the specific behavior in 1D system in more detail below. But first, we have to introduce a bit more formalism.

1.4.1 Model for one-dimensional disordered systems

We first discuss how to model random impurities in a field theoretical model. In the following we will only consider static impurities without intrinsic degrees of freedom, that could be excited in a scattering event. Hence, scattering off impurities is always elastic. In a specific system disorder is described by the continuous potential $U(x)$. However, the field $U(x)$ will differ from one system to another since the microscopic arrangement of impurities is always different. To obtain a description that only depends on a few characteristic parameters, we apply a statistical description where U is treated as random variable that is described by a probability distribution $\mathcal{P}[U]$, i.e. $\mathcal{P}[U_0]\mathcal{D}[U_0]$ is the probability that the specific potential U_0 is realized. This methodology is applicable if the system in question is “self-averaging”, which is expected to be the case when the phase coherence length is much smaller than the system size. The distribution is often chosen to be Gaussian, because due to the central limit theorem most distributions will become Gaussian if one considers a large ensemble of systems. The entire information about the distribution is contained in the moments

$$\langle U(x) \rangle_{\text{dis}} = 0, \quad (1.47)$$

$$\langle U(x)U(x') \rangle_{\text{dis}} = K(x - x'). \quad (1.48)$$

Here, the average is with respect to $\mathcal{P}[U]$,

$$\langle \dots \rangle_{\text{dis}} \equiv \int \mathcal{D}U \mathcal{P}[U] (\dots) \quad (1.49)$$

If the correlation length of disorder is much smaller than any other characteristic length scale of electrons, the disorder kernel can be chosen as a delta function, $K(x - x') = D\delta(x - x')$, where $D = n_{\text{imp}}U^2(q = 0)$, with the density of impurities n_{imp} , is a measure of the disorder strength.

When performing the disorder average one encounters the technical problem that the normalization of the path integral depends on the disorder configuration. One way to circumvent the problem is the replica trick which is based on the identity $\ln \mathcal{Z} = \lim_{N \rightarrow 0} (\mathcal{Z}^N - 1)/N$, where \mathcal{Z} denotes the partition function. Therefore, instead of studying one copy of the system with a random disorder potential it is more convenient to study N identical copies of the system with an effective disorder action. The fields in the replicated model then carry an additional replica index n and physical observables are obtained by taking the $N \rightarrow 0$ limit of correlation functions.

Let us now apply this formalism to obtain a model for one-dimensional disordered electrons. The disorder term in the action is simply

$$S_{\text{dis}} = \int dx d\tau U(x) \bar{\psi}_\sigma(x, \tau) \psi_\sigma(x, \tau). \quad (1.50)$$

If impurities are weak, $DE_F \ll 1$, disorder only produces effects close to the Fermi points. Consequently, impurities can only scatter forward ($q \sim 0$) with scattering amplitude \mathcal{U}_f or backward ($q \sim \pm 2k_F$) with

amplitude \mathcal{U}_b . It can be shown that \mathcal{U}_f is real, while \mathcal{U}_b is complex and that their correlation functions are given by

$$\langle \mathcal{U}_b(x)\mathcal{U}_b(x') \rangle = 0 \quad (1.51)$$

$$\langle \mathcal{U}_b(x)\mathcal{U}_b^*(x') \rangle = \langle \mathcal{U}_f(x)\mathcal{U}_f(x') \rangle = \langle U(x)U(x') \rangle \quad (1.52)$$

Furthermore, we can decompose the fermionic field ψ into right- and left-movers according to (1.17). The resulting low-energy disorder action is then $S_{\text{dis}} = S_{\text{dis,f}} + S_{\text{dis,b}}$, with

$$S_{\text{dis,f}} = \sum_{\sigma} \int dx d\tau \mathcal{U}_f(x) \left(\bar{\psi}_{+,\sigma} \psi_{+,\sigma} + \bar{\psi}_{-,\sigma} \psi_{-,\sigma} \right) \quad (1.53)$$

$$S_{\text{dis,b}} = \sum_{\sigma} \int dx d\tau \left[\mathcal{U}_b(x) \bar{\psi}_{+,\sigma} \psi_{-,\sigma} + \mathcal{U}_b^*(x) \bar{\psi}_{-,\sigma} \psi_{+,\sigma} \right].$$

In the bosonized form the disorder terms read as

$$S_{\text{dis,f}} = -\frac{2}{\sqrt{\pi}} \int dx d\tau \mathcal{U}_f(x) \partial_x \varphi_c \quad (1.54)$$

$$S_{\text{dis,b}} = -\frac{i}{4\pi a} \int dx d\tau \mathcal{U}_b(x) e^{-\sqrt{2\pi}\varphi_c} \cos(\sqrt{2\pi}\varphi_s) + \text{c.c.} \quad (1.55)$$

An important fact to notice is, that forward scattering can be completely removed⁶ by the transformation $\varphi_c \rightarrow \varphi_c + \int^x dy \mathcal{U}_f(y) K_c / (v_c \sqrt{\pi})$. As long as the observable one is interested in does not explicitly depend on the field φ_c , forward scattering can be neglected completely and we can set $\mathcal{U}_f = 0$ in the above expression. In particular this is the case for the current $j_c = -ie\sqrt{2/\pi}\partial_{\tau}\varphi_c$. It is then understood that the index “dis” always refers to backscattering processes.

1.4.2 Renormalization of a single impurity in a Luttinger liquid

As a first part of our analysis let us consider the effect of a single impurity, modelled by the potential $\mathcal{U}_b(x) = U(q = 2k_F)\delta(x)$. If we assume that the impurity potential is inversion symmetric, its Fourier components are real and the impurity is described by a single parameter. It was found in early works [63–66], that the density-density wave correlations of the LL yield a strong renormalization of the impurity potential. If the initial impurity potential is weak, the renormalized backscattering amplitude, seen by an electron with energy scale ϵ scales as

$$U(2k_F, \epsilon) \propto (\Lambda/|\epsilon|)^{\beta} \quad (1.56)$$

where the exponent β is determined by the interaction strength. For example, for the spinless electron gas, $\beta = 2 - 2K_c$. We see that, in this case, the potential grows if $K_c < 1$. An (infinitely) strong impurity potential perfectly reflects incoming electrons at any energy. Hence, as a result of this renormalization, an impurity in a system with sufficiently repulsive interaction can effectively decouple the wire into two independent parts, leading to a vanishing conductance at zero temperature.

Physically, this renormalization is due to the dressing of the impurity by Friedel oscillations: imagine a wavepacket of a right moving electron with characteristic momentum k_F colliding with an impurity at

⁶One may argue that this transformation also changes the backscattering part because $\mathcal{U}_b^* \rightarrow \mathcal{U}_b^* e^{2i \int^x dy \mathcal{U}_f(y) K_c / v_c}$. However, since \mathcal{U}_b was a random variable to begin with and its Gaussian statistics are not affected by the additional phase and the action is unchanged by this.

$x = 0$. The resulting wave amplitude to the left of the impurity $\Psi_+(x) \sim e^{ik_F x} + r e^{-ik_F x}$ will be a linear superposition of the incoming amplitude and the reflected amplitude, where r is the reflection coefficient. Therefore, the electronic density profile is given by $\rho(x) = |\Psi(x)|^2 \sim 1 + |r|^2 + 2 \operatorname{Re}(r e^{-2ik_F x})$. The oscillatory contribution is known as *Friedel oscillation*. In one dimension these decay rather slowly ($\sim 1/|x|$). The key point is, that electron waves approaching the impurity will not only notice the impurity potential but also the additional scattering potential off Friedel oscillations. Moreover the additional scattering potential creates secondary Friedel oscillations and so on. Therefore, even a weak impurity potential may be amplified by the effect of Friedel oscillations.

1.4.3 Many impurities: disordered Luttinger liquid

Let us now look at the case of many impurities. In order to perform the disorder average we introduce replicas φ_n . Using the Gaussian nature of the disorder distribution we can average over disorder configurations, $\langle \exp(-S_{\text{dis}}) \rangle_{\text{dis}} = \exp[-\frac{1}{2} \langle S_{\text{dis}}^2 \rangle_{\text{dis}}] \equiv \exp[-\frac{1}{2} S_D]$, to arrive at the disorder averaged action

$$\begin{aligned}
S &= \sum_n S_{\text{LL}}[\varphi_n] + \sum_n S_{\text{SG}}[\varphi_n] + \sum_{n,m} S_D[\varphi_n, \varphi_m], \\
S_{\text{LL}} &= \sum_{\mu=c,s} \frac{1}{2v_\mu K_\mu} \int dx d\tau \left[v_\mu^2 (\partial_\tau \varphi_{\mu n})^2 + (\partial_x \varphi_{\mu n})^2 \right], \\
S_{\text{SG}} &= \frac{v_s g_{1,\perp}}{2\pi^2 a^2} \int dx d\tau \cos(\sqrt{8\pi} \varphi_{sn}) \\
S_D &= \frac{D}{(\pi a)^2} \int dx d\tau_1 d\tau_2 \cos(\sqrt{2\pi}[\varphi_{cn}(1) - \varphi_{cm}(2)]) \cos(\sqrt{2\pi} \varphi_{sn}(1)) \cos(\sqrt{2\pi} \varphi_{sm}(2)).
\end{aligned} \tag{1.57}$$

The RG equations of the model for disordered Luttinger liquid in (1.57) has been derived by Giamarchi and Schulz [67]. The flow equations are given by

$$\begin{aligned}
\frac{dK_c}{d\ell} &= -\frac{1}{2} K_c^2 \frac{v_c}{v_s} \mathcal{D} \\
\frac{dK_s}{d\ell} &= -\frac{1}{2} [\mathcal{D} + \lambda_\perp^2] K_s^2 \\
\frac{dv_c}{d\ell} &= -\frac{v_c K_c}{2} \mathcal{D} \\
\frac{dv_s}{d\ell} &= -\frac{v_s K_s}{2} \mathcal{D} \\
\frac{d\lambda_\perp}{d\ell} &= (2 - 2K_s) \lambda_\perp - \mathcal{D} \\
\frac{d\mathcal{D}}{d\ell} &= (3 - K_c - K_s - \lambda_\perp) \mathcal{D}.
\end{aligned} \tag{1.58}$$

with the dimensionless quantities

$$\lambda_\perp = \frac{g_{1,\perp}}{\pi v_s}, \quad \mathcal{D} = \frac{2Da}{\pi v_s^2} \left(\frac{v_s}{v_c} \right)^{K_c}. \tag{1.59}$$

The equations describe not only the renormalization of interactions by disorder but also, vice versa, the renormalization of disorder by interactions. To understand the basic physical mechanisms behind

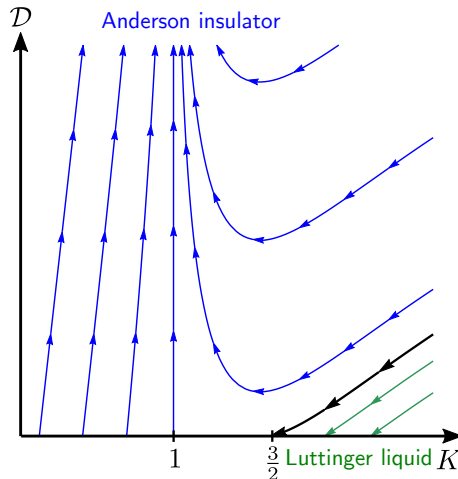


Figure 1.4: Flow diagram of the Giamarchi-Schulz RG 1.64. The parameter \mathcal{D} denotes the dimensionless disorder strength and K is the Luttinger parameter measuring the strength of electron-electron interactions. The black line, ending in the quantum critical point $K = 3/2$, separates the localized Anderson insulator phase from the delocalized Luttinger liquid phase.

this renormalization it is sufficient to study the limit of spinless fermions, formally $K_s = K_c = \tilde{K}$, $v_s = v_c = \tilde{v}$ and $\lambda_{\perp} = 0$. In this case the equations simplify to

$$d\tilde{K}/dl = -\tilde{K}^2\mathcal{D}/2, \quad (1.60)$$

$$d\tilde{v}/dl = -\tilde{v}\tilde{K}\mathcal{D}/2, \quad (1.61)$$

$$d\mathcal{D}/dl = (3 - 2\tilde{K})\mathcal{D}. \quad (1.62)$$

There is one subtlety to these equations. Naively one could think, that Eq. (1.60) gives the unphysical prediction, that interaction is generated by disorder if we start from the noninteracting fixed point $\tilde{K} = 1$. However, the parameters \tilde{K} and \tilde{v} , as a consequence of how the RG was derived, already contain admixtures of disorder and $\tilde{K} = 1$ is not the correct condition for the clean fixed point. In terms of the true Luttinger constant the equations read as [60]

$$\frac{dK}{dl} = -\frac{1}{2} \left[K^2 - \frac{(1 + K^2)(3 - 2K)}{2} \right] \mathcal{D}, \quad (1.63)$$

$$\frac{d\mathcal{D}}{dl} = (3 - 2K)\mathcal{D}, \quad (1.64)$$

Here, we dropped the equation for the velocity, since it does not couple to the other equations. Note, that now K does not flow if we start at the clean fixed point $K = 1$. The flow diagram is depicted in Fig. 1.4. There are two types of fixed points of the flow, a strong-coupling fixed point at $K = 1$, $\mathcal{D} \rightarrow \infty$ which can be identified as the Anderson localized phase and the line of Luttinger liquid fixed points with renormalized parameter $K = K^*$ and $\mathcal{D} \rightarrow 0$. At sufficiently strong attractive interaction and weak disorder strength, (1.64) predicts a metal insulator transition at zero temperature by lowering the parameter K below the critical value $3/2$. On the other hand, repulsive interactions are expected to enhance the disorder induced localization.

If the flow of disorder is to strong coupling, there exists a temperature where the disorder coupling constant becomes of order unity and the system enters a strong-coupling regime, where the Drude

approach breaks down. This temperature is determined by the condition $T\tau(T) \sim 1$. Physically, this is because the Friedel oscillations are cut at scales of the disorder induced mean free path. At higher temperatures, the equations describe the temperature dependence of an effective scattering time for scattering off impurities dressed by Friedel oscillations, thus yielding a temperature dependence of the Drude conductivity,

$$\sigma_D \propto (T/\Lambda)^{2\beta} \tag{1.65}$$

with the same β as in the single impurity case.

It is important to emphasize, that the RG approach only captures the renormalization of the Drude conductivity due to T-dependent screening, but does not accurately describe the weak localization corrections to the conductivity, which arise from coherent scattering on several impurities and therefore only appear in the RG equations in $\mathcal{O}(\mathcal{D}^3)$. The weak localization correction becomes strong at the temperature T_1 , when $|\Delta\sigma_{wl}(T_1)| \gtrsim \sigma_D(T_1)$, which in 1D is equivalent to the condition $\tau_\phi(T_1) \sim \tau_D(T_1)$. The onset of strong localization is determined by this condition which yields a higher threshold temperature than the temperature where the renormalized disorder strength becomes strong.

2

Chapter 2

Fundamentals: Topological insulators

In this chapter we give a short introduction into the concept of topology in condensed matter physics and introduce the notion of a TI. In particular we are interested in the transport properties of the gapless edge modes that emerge at the boundary of two-dimensional TIs. For a further study of the field we refer the reader to one of the many good reviews on the topic of topological in materials [13, 68–70].

We begin by defining the notion of a TI in Sec. 2.1. To this end we explain how insulating phases may be classified according to the presence or absence of certain antiunitary symmetries and how they can be characterized by a topological invariant in Sec. 2.1.1 and illustrate these concepts on the example of the Su-Schrieffer-Heeger model in Sec. 2.1.2. We then switch gears and focus on a specific class of TIs the \mathbb{Z}_2 quantum-spin Hall insulators in two-dimension in Sec. 2.2. We will discuss their theoretical description, with special emphasis on the transport properties of the helical edge states that emerge at their boundaries (Sec. 2.2.1) and their experimental signatures (Sec. 2.2.2).

2.1 Definition of a topological insulator

A topological state, within a given symmetry class, describes a gapped fermionic system that cannot be adiabatically deformed into the vacuum. By adiabaticity we mean in this context the following. Any gapped system can generically be described by a Hamiltonian. It turns out that the space of all Hamiltonians decomposes into several equivalence classes according to the absence or presence of certain antiunitary symmetries in the system. The notion of topology then originates from the fact that Hamiltonians of a given symmetry class cannot be continuously deformed into each other by changing the parameters of the model without closing the gap or breaking the symmetries of the corresponding symmetry class. By definition, a topologically trivial insulator is one that can be adiabatically deformed into the vacuum; all other insulating phases are called topologically non-trivial.

The gap can have several physical origins. It can arise in band insulators, i.e. the gap between occupied valence and unoccupied conduction bands, in superconductors due to a Cooper instability or it can arise dynamically, without breaking of any spontaneous symmetry, due to strong correlation in 1D materials (Ch.5). In any case the nontrivial topology of the bulk leads to the emergence of gapless edge modes at the boundary to a topologically trivial state. These gapless degrees of freedom are completely robust against disorder. That means we can add any random perturbation or potential of arbitrary strength to the Hamiltonian of the TI and the edge states will not develop a gap (as long as the perturbations preserve the antiunitary symmetries of the model and do not close the bulk gap).

Cartan label	Θ^2	Ξ^2	Π^2	d=1	d=2	d=3	d=4	d=5	d=6	d=7	d=8
A	0	0	0	0	\mathbb{Z}	0	\mathbb{Z}	0	\mathbb{Z}	0	\mathbb{Z}
AIII	0	0	1	\mathbb{Z}	0	\mathbb{Z}	0	\mathbb{Z}	0	\mathbb{Z}	0
AI	+1	0	0	0	0	0	\mathbb{Z}	0	\mathbb{Z}_2	\mathbb{Z}_2	\mathbb{Z}
BDI	+1	+1	1	\mathbb{Z}	0	0	0	\mathbb{Z}	0	\mathbb{Z}_2	\mathbb{Z}_2
D	0	+1	0	\mathbb{Z}_2	\mathbb{Z}	0	0	0	\mathbb{Z}	0	\mathbb{Z}_2
DIII	-1	+1	1	\mathbb{Z}_2	\mathbb{Z}_2	\mathbb{Z}	0	0	0	\mathbb{Z}	0
AII	-1	0	0	0	\mathbb{Z}_2	\mathbb{Z}_2	\mathbb{Z}	0	0	0	\mathbb{Z}
CII	-1	-1	1	\mathbb{Z}	0	\mathbb{Z}_2	\mathbb{Z}_2	\mathbb{Z}	0	0	0
C	0	-1	0	0	\mathbb{Z}	0	\mathbb{Z}_2	\mathbb{Z}_2	\mathbb{Z}	0	0
CI	+1	-1	1	0	0	\mathbb{Z}	0	\mathbb{Z}_2	\mathbb{Z}_2	\mathbb{Z}	0

Table 2.1: Periodic table of topological states of matter. The notation for the symmetries and topological invariants is explained in the main text. The whole table is periodic as a function of the dimension with periodicity 8 (“Bott periodicity”)

The addition of any perturbation only adiabatically maps Hamiltonians within one symmetry class onto each other which may change the exact form of the boundary modes but does not change their presence.

In the following we will elaborate on the classification of random Hamiltonians and give a minimal example of a TI to further explain these concepts.

2.1.1 Symmetry classification of Hamiltonians

As we already mentioned above, symmetries of the Hamiltonian play a key role in characterizing topological phases. As is well known [71] all symmetry operations are either described by unitary or antiunitary operators. It turns out that unitary symmetries are irrelevant for the topological classification, since they always allow for block diagonalization of the Hamiltonian. Consider for example spin rotation invariance around the z-direction for spin 1/2 particles. If S_z is conserved, the Hamiltonian can be brought into block diagonal form, where the blocks correspond to $S_z = \{\uparrow, \downarrow\}$ respectively. Therefore, one must study the symmetry properties of these blocks of irreducible Hamiltonians in terms of the most basic symmetries. These are TRS Θ and charge-conjugation or particle-hole symmetry (PHS) Ξ , which are represented by antiunitary operators when acting on the single particle Hilbert space. Every antiunitary operator can be expressed through the combination of a unitary matrix U and complex conjugation \mathcal{K} . Now consider the Hamiltonian of non-interacting fermions with translation invariance in second quantized language

$$\hat{H} = \sum_{\alpha, \beta} \int_{\mathbf{k}} \hat{\psi}_{\alpha}^{\dagger}(\mathbf{k}) \mathcal{H}_{\alpha, \beta}(\mathbf{k}) \hat{\psi}_{\beta}(\mathbf{k}), \quad (2.1)$$

where α, β are arbitrary quantum numbers and $\mathcal{H}_{\alpha, \beta}(\mathbf{k})$ is the first quantized Hamiltonian. The Hamiltonian is symmetric under TRS or PHS if it commutes with the respective antiunitary operator. In terms of the single-particle Hamiltonian this can be expressed as

$$\Theta \mathcal{H}(\mathbf{k}) \Theta^{-1} = + \mathcal{H}(-\mathbf{k}), \quad (2.2)$$

$$\Xi \mathcal{H}(\mathbf{k}) \Xi^{-1} = - \mathcal{H}(-\mathbf{k}). \quad (2.3)$$

It is easy to see that there are 10 distinct ways for a system to respond to the action of TRS and charge conjugation. Time reversal can either be absent ($\Theta = 0$) or present. If the system is time reversal invariant the antiunitary operator can square to either $+1$ or -1 which is usually denoted as $\Theta^2 = \pm 1$. The same applies for charge conjugation and therefore we are left with $3 \times 3 = 9$ possible classes. To completely specify the behavior under Θ and Ξ one also has to introduce the combined chiral symmetry, $\Pi = \Theta\Xi$, which is unitary and transforms the Hamiltonian as

$$\Pi \mathcal{H}(k) \Pi^{-1} = -\mathcal{H}(-k). \quad (2.4)$$

The behavior under Π is always uniquely fixed, except for the case $\Theta = \Xi = 0$. In this case, Π is either a symmetry of the Hamiltonian ($\Pi = 1$) or it is not ($\Pi = 0$).

Hence, there exist 10 classes of random Hamiltonians called Cartan-Altland-Zirnbauer symmetry classes [72, 73]. It was shown that the same classes can be used to classify topological states of matter in all dimensions. The full symmetry classification of noninteracting TIs and topological superconductors has been developed based on the analysis of lattice Hamiltonians [10] and of field theories of disordered systems [14]. Both approaches turn out to be equivalent [15, 69] and yield the table of TIs in different dimensions in Tab. 2.1. To illustrate how the table is constructed we discuss the specific example of class A TIs following the analysis of Ref. [74].

For simplicity let us consider a translationally invariant band insulator. Due to the translation invariance Bloch's theorem holds i.e. eigenstates of the Hamiltonian are characterized by the crystal momentum \mathbf{k} in the first Brillouin zone (1BZ) and the band index n :

$$\mathcal{H}(\mathbf{k}) |u_n(\mathbf{k})\rangle = \epsilon_n(\mathbf{k}) |u_n(\mathbf{k})\rangle. \quad (2.5)$$

We define the projector onto the filled Bloch states for any $\mathbf{k} \in 1\text{BZ}$ as

$$P(\mathbf{k}) = \sum_n^{\text{filled}} |u_n(\mathbf{k})\rangle \langle u_n(\mathbf{k})|. \quad (2.6)$$

It turns out to be more useful to work with the "simplified Hamiltonian" $Q(\mathbf{k})$ defined as

$$Q(\mathbf{k}) = 1 - 2P(\mathbf{k}), \quad (2.7)$$

which is obtained from H by assigning to the m filled states the eigenvalue (-1) and to the l empty states the eigenvalue $(+1)$, while leaving the eigenfunctions unchanged. If we are only interested in topological properties, we can always deform $H(\mathbf{k})$ by adding perturbations until it acquires the form of $Q(\mathbf{k})$. Let us see how we can use the matrix Q to identify topological materials by considering the simplest class, class A, where no symmetry conditions are imposed on the Hamiltonian. Then \mathcal{H} is an arbitrary Hermitian matrix and Q a unitary matrix $Q \in U(m+l)$. However, because relabelling filled and empty states amongst themselves leaves the physics unchanged, Q is actually a map from the 1BZ to the so called Grassmannian $U(m+l)/[U(m) \times U(l)]$:

$$\begin{aligned} Q : \quad 1\text{BZ} &\rightarrow U(m+l)/[U(m) \times U(l)], \\ \mathbf{k} &\rightarrow Q(\mathbf{k}). \end{aligned} \quad (2.8)$$

Let us summarize. As long as the bulk gap is not closed we can deform the Hamiltonian of the system by adding perturbations until it takes the form of Q . If we want to ask the question how many distinct gapped phases a system possesses this is equivalent to asking how many different maps $Q(\mathbf{k})$ there are

that can't be continuously deformed into each other. The answer to this question is given by homotopy theory.

Let us quickly review some mathematical basics. In quantum field theory we are mostly interested in mappings from compactified d-dimensional space time¹ into the target manifold M of fields ϕ of the theory, i.e.

$$\begin{aligned}\phi : S^d &\rightarrow M, \\ \mathbf{x} &\rightarrow \phi(\mathbf{x}).\end{aligned}\tag{2.9}$$

We will consider two fields to be equivalent, $\phi_1 \sim \phi_2$, if they can be continuously deformed into each other, i.e. if there exists a continuous mapping ("homotopy") Φ ,

$$\begin{aligned}\Phi : S^d \times [0, 1] &\rightarrow M, \\ (\mathbf{x}, a) &\rightarrow \Phi(\mathbf{x}, a),\end{aligned}\tag{2.10}$$

such that $\Phi(\mathbf{x}, 0) = \phi_1(\mathbf{x})$ and $\Phi(\mathbf{x}, 1) = \phi_2(\mathbf{x})$. The equivalence class containing all fields homotopic to ϕ is denoted by $[\phi]$. The set of all topological equivalence classes $\{[\phi]\}$ of mappings $\phi : S^d \rightarrow M$ is called the d-th homotopy group $\pi_d(M)$. The homotopy groups of the target manifold in the above case are well-known and in $d = 2, 3$ dimensions we have

$$\pi_2(U(m+l)/[U(m) \times U(l)]) = \mathbb{Z},\tag{2.11}$$

$$\pi_3(U(m+l)/[U(m) \times U(l)]) = \{1\}.\tag{2.12}$$

This suggests that for any integer $\nu_{\mathbb{Z}} \in \mathbb{Z}$ there exists a topologically distinct band insulator in $D = 2$ dimensions in symmetry class A. Hence, we see that similar to the concept of an order parameter that characterizes symmetry broken phases, TIs can be assigned a topological index that specifies their topological phase. TIs with different topological indices cannot be continuously deformed into one another without a topological quantum phase transition. In the particular example of class A, the topological state of matter is the quantum Hall effect and the topological invariant $\nu_{\mathbb{Z}}$ measures the number of chiral edge modes that emerge at its boundary. When this number changes we indeed have a quantum phase transition - the quantum Hall transition. The fact that the third homotopy group is trivial also tells us that there are no quantum Hall effects in three dimensions.

Besides \mathbb{Z} TIs there exist also $\mathbb{Z}_2 = \{0, 1\}$ TIs. In this case the insulator can only be trivial ($\nu_{\mathbb{Z}_2} = 0$) or topological $\nu_{\mathbb{Z}_2} = 1$.

To illustrate the concepts discussed in this section we will now analyze a specific model of a TI and explicitly calculate the topological invariant.

2.1.2 Example: Su-Schrieffer-Heger model

To present a simple model that exhibits a topologically nontrivial phase we study the Su-Schrieffer-Heeger (SSH) model, which was originally proposed in Ref. [75] for the description of polyacetylene chains, 1D chains ($[C_2H_2]_n$) of carbon atoms. In this system the Peierls instability leads to a distortion

¹The fields ϕ take values in spacetime \mathbb{R}^d . However, to keep the action finite we have to impose the condition $\phi(\mathbf{x}) \rightarrow \text{const.}$ for $|\mathbf{x}| \rightarrow \infty$. Thus the base manifold of the fields is actually isomorphic to the d-dimensional unit sphere $\mathbb{R}^d \cup \{\infty\} \simeq S^d$.

of the periodic 1D lattice and creates different hopping strengths between neighboring atoms. The Hamiltonian of the model is then given by

$$H = \sum_j \left[(t + \delta t) a_j^\dagger b_{j+1} + (t - \delta t) a_{j+1}^\dagger b_j + \text{H.c.} \right] \quad (2.13)$$

where t denotes the nearest neighbor hopping amplitude, δt is the hopping anisotropy and a_j or b_j destroys an electron at site j of sublattice A or B , respectively. We assume periodic boundary conditions and set the lattice spacing between atoms of the same sublattice species to unity, $a_0 = 1$. We perform a Fourier transform to momentum space, i.e. a mapping $j \rightarrow k \in [-\pi, \pi) \cong S_1$ and introduce the vector $\mathbf{c}_k = (a_k, b_k)^T$. Then the Hamiltonian takes the form

$$H = \sum_k \mathbf{c}_k^\dagger \mathcal{H}(k) \mathbf{c}_k, \quad (2.14)$$

with the single particle Hamiltonian $\mathcal{H}(k) = \mathbf{d}(k) \boldsymbol{\tau}$, where $\boldsymbol{\tau}$ denotes the vector of Pauli matrices in sublattice space. The components of the vector \mathbf{d} read as

$$d_1(k) = (t + \delta t) + (t - \delta t) \cos k, \quad d_2(k) = (t - \delta t) \sin k, \quad d_3(k) = 0. \quad (2.15)$$

By diagonalizing the single particle Hamiltonian we obtain the spectrum

$$E_{\pm}(k) = \pm |\mathbf{d}(k)| = 2 \sqrt{t^2 \cos^2(k/2) + \delta t^2 \sin^2(k/2)}. \quad (2.16)$$

In particular we note that the system is a band insulator at half filling $k_F = \pi$.

It is easy to check that the antiunitary symmetries of the system can be represented in sublattice space as $\Theta = \mathcal{K}$, $\Xi = \sigma_z \mathcal{K}$ and $\Pi = \sigma_z$, hence TRS and PHS obey $\Theta^2 = \Xi^2 = +1$ and $\Pi^2 = 1$, which places the Hamiltonian into the class BDI. According to Tab. 2.1 the class BDI supports a \mathbb{Z} TI in 1D. To analyze the topological properties of the Hamiltonian we define the simplified Hamiltonian $Q(k) = [d_1(k) + id_2(k)]/|\mathbf{d}(k)|$, which is a mapping from $S^1 \rightarrow S^1$ and can therefore be classified by an integer since $\pi_1(S^1) = \mathbb{Z}$. This *winding number* can be defined as

$$\nu_{\mathbb{Z}} = \frac{i}{2\pi} \int_{-\pi}^{\pi} dk Q^{-1} \partial_k Q. \quad (2.17)$$

It counts the number of times the vector \mathbf{d} winds around the origin as k transverses the 1BZ zone. In the SSH model the winding number is either 0 or 1 depending on whether $\delta t > 0$ or $\delta t < 0$. The topologically distinct configurations are depicted pictorially in Fig. 2.1. It is clear, that the winding numbers cannot be adiabatically transformed into each other by changing parameters of the Hamiltonian. Only, when $\delta t = 0$, in which case the band gap closes is the winding number not defined and may change between values. The winding number is therefore an example of an topological index.

Bulk boundary correspondence and edge states. We now show that a nontrivial bulk topology leads to the emergence of zero energy bound states at the boundary to a topologically trivial insulator. Consider therefore the boundary between two copies of the SSH chain with opposite sign of the parameter δt . It is convenient to study the low-energy theory of the SSH model. To this end we expand momenta around the Fermi momentum $k = \pi + q$ with $|q| \ll \pi$ and assume $\delta t \ll t$. The Hamiltonian $\mathcal{H}(q)$ then describes massive Dirac fermions with spectrum $E_{\pm}(q) \simeq \pm \sqrt{(vq)^2 + m^2}$, with mass $m = 2\delta t$ and velocity $v = ta_0$.

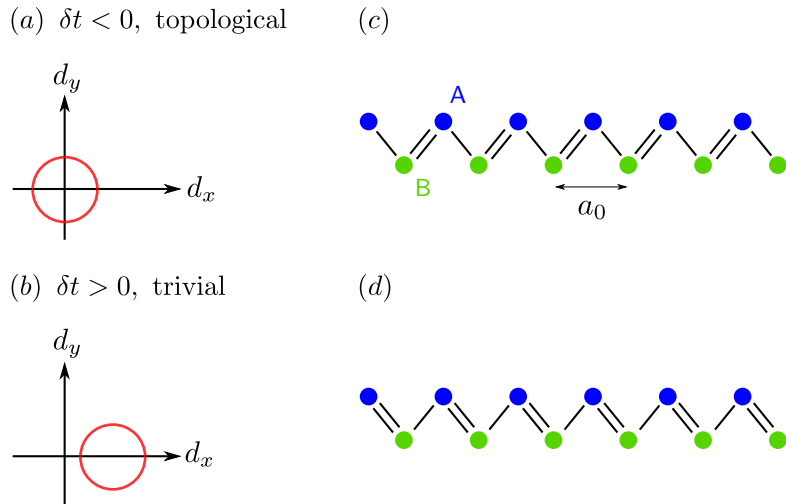


Figure 2.1: Two copies of the SSH chain with different bond configurations, corresponding to different signs of the parameter δt ; (c) corresponds to $\delta t < 0$ and (d) to $\delta t > 0$. The two configurations are characterized by a topological (a) or trivial (b) winding number.

Two coupled chains with opposite sign of the mass can be modelled by a continuous mass function $m(x)$ in the Hamiltonian. In real space the single particle Hamiltonian takes the form

$$\mathcal{H}(x) = -iv\partial_x\tau_y + m(x)\tau_x . \quad (2.18)$$

Due to the chiral symmetry of the model the Hamiltonian anticommutes with τ_z and therefore the eigenstates at energy E have the property $\tau_z|\psi_E\rangle = |\psi_{-E}\rangle$. Multiplying the Schrödinger equation for the zero mode $\mathcal{H}(x)\psi_0(x) = 0$ by $i\tau_x$ from the right and using the fact that the zero mode is an eigenstate of τ_z with eigenvalue 1, one arrives at the equation

$$v\partial_x\psi_0(x) = m(x)\psi_0(x) . \quad (2.19)$$

The wavefunction of the zero energy state then reads as

$$\psi_0(x) = \begin{pmatrix} 1 \\ 0 \end{pmatrix} e^{-\frac{1}{v}\int_{-\infty}^x dx' m(x')} . \quad (2.20)$$

The emergence of zero-energy modes at the interface between topologically distinct phases is not a special property of the SSH model but is a general phenomenon known as bulk-boundary correspondence. Whether the edge modes are real, so called Majorana fermions, or complex, i.e. Dirac fermions, depends on whether the system has a PHS. In the SSH model the edge states are real, but in the Bernevig-Hughes-Zhang (BHZ) model to be discussed below the edge states turn out to be Dirac fermions as the Hamiltonian belongs to class AII without PHS. The number of bound states is determined by the topological invariant to the right and left of the boundary, $|\nu_R - \nu_L| = \text{number of zero modes}$.

The bulk-boundary correspondence can be understood intuitively in the above example, when $m(x)$ is a smoothly varying function. Then the mass interpolates between positive and negative values and therefore must vanish at some point, independent of the exact form of the function $m(x)$.

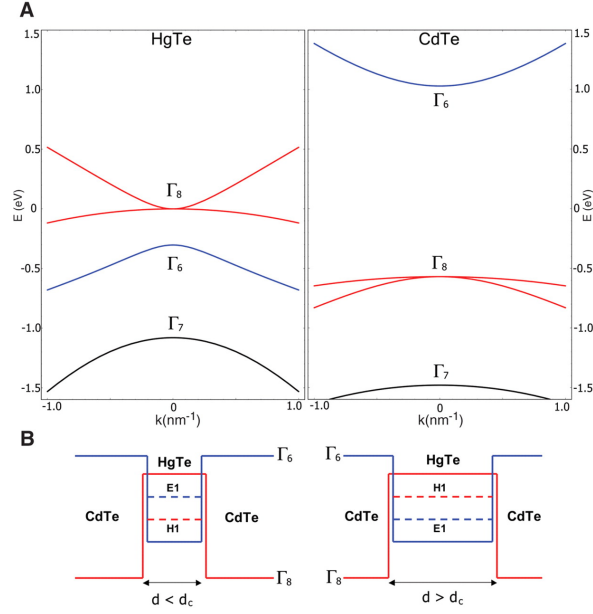


Figure 2.2: (A) Band structure of HgTe and CdTe near the Γ point. The band gap in the former is inverted, i.e. the Γ_8 band lies above the Γ_6 . (B) The bandstructure of thin quantum wells ($d < d_c$) resembles the CdTe bulk with band gap $M = (E_1 - H_1)/2 > 0$, while thick quantum wells ($d > d_c$) have an inverted band structure like CdTe with $M < 0$. From Ref. [13].

2.2 \mathbb{Z}_2 topological insulators and helical edge states

The properties discussed in the previous sections are general and hold for all topological materials. In the remainder of the chapter we will focus exclusively on TIs of the class AII in two dimensions with conserved TRS. The first experimentally observed TI in this class was discovered in HgTe/CdTe quantum wells [9]. Since a majority of this thesis will be devoted to the study of transport properties in the edge states of such 2D TIs we will discuss the host materials in some detail.

In this section we review the basic electronic structure of the semiconductors HgTe and CdTe and derive a simple model, following [8, 76], to describe the physics of the subbands of HgTe/CdTe quantum wells that are important for the topological nature of the material.

For both HgTe and CdTe the important bands near the Fermi level are close to the center of the Brillouin zone (Γ point). Quite generally one can picture the bands in solids as combinations of atomic orbitals of the constituent atoms. If two atoms are brought close together, the orbitals can overlap in two ways to form bonding or antibonding molecular orbitals. Normally, one concentrates on the antibonding s-type orbitals that make up the valence band and the bonding p-type orbitals that build the conduction band. Near the Γ point these are twice (s-type) or sixfold (p-type) degenerate due to the spin degree of freedom. If we take into account SOC, the bands become mixed and are characterized by their total angular momentum j i.e. we have quantum numbers (j, m_j, l, s) .

The important point is, that the band structure in HgTe is inverted because of the large SOC in heavy materials like Hg. That means that the Γ_8 band lies above the Γ_6 band in this material, see Fig. 2.2. For small quantum well thicknesses, we expect that the band structure of the quantum well behaves just as the one of CdTe with normal band ordering. However, as we increase the thickness above some critical

value d_c , the bandstructure will be determined by the properties of HgTe and become inverted (see Fig. 2.2). In the inverted regime the bands naturally have to cross at the boundaries which, according to the bulk-boundary correspondence, leads to the emergence of massless edge states. We therefore expect a topological quantum phase transition as a function of quantum well thickness in this material.

To derive an explicit model for this system, we consider the band structure of the quantum well. The conduction band consists of the doublet $|\Gamma_6, j = 1/2, m_j = \pm 1/2\rangle^2$ while the valence band is made of the quadruplet $|\Gamma_8, j = 3/2, m_j = \pm 1/2\rangle, |\Gamma_8, j = 3/2, m_j = \pm 3/2\rangle$ and the doublet $|\Gamma_7, j = 1/2, m_j = \pm 1/2\rangle$. The $j = 3/2$ bands are degenerate at the Γ point and have different curvatures (effective masses) away from it. Therefore, they are referred to as heavy and light hole bands. The Γ_7 band is split off by SOC and will be disregarded in the following.

In quantum wells grown in [001] direction the spherical symmetry is broken down to an axial rotation symmetry in the plane. The six bands therefore combine to form the spin up and down states of the quantum well subbands E1, H1 and L1. The L1 subband is separated from the other two and we will neglect it, leaving an effective four band model. At the Γ point with in-plane momentum $k_{\parallel} = 0$, m_j is still a good quantum number. The quantum well states $|E1, m_j = \pm 1/2\rangle$ are then linear combinations of states $|\Gamma_6, j = 1/2, m_j = \pm 1/2\rangle$ and $|\Gamma_8, j = 1/2, m_j = \pm 1/2\rangle$ while $|H1, m_j = \pm 3/2\rangle$ are made of $|\Gamma_8, j = 3/2, m_j = \pm 3/2\rangle$, respectively. Therefore, the quantum well states are given by the ordered basis $\{|E1, \uparrow\rangle, |H1, \uparrow\rangle, |E1, \downarrow\rangle, |H1, \downarrow\rangle\}$.³ The states $|E1, \sigma\rangle$ are Kramers partners, as well as $|H1, \sigma\rangle$ and therefore all matrix elements between them must vanish due to Kramers theorem. Furthermore, since $|E1, \sigma\rangle$ and $|H1, \sigma\rangle$ originate from s-like and p-like bands respectively, they have opposite parity. Hence, every mixed matrix element connecting them must be odd under parity, while matrix elements between the states must be even. These symmetry considerations lead to the effective BHZ Hamiltonian for momenta close to the Γ point:

$$H(k_x, k_y) = \begin{pmatrix} h(\mathbf{k}) & 0 \\ 0 & h^*(-\mathbf{k}) \end{pmatrix}, \quad (2.21)$$

with the 2×2 matrix

$$h(\mathbf{k}) = \epsilon(\mathbf{k})\mathbb{1}_2 + d_i(\mathbf{k})\sigma_i, \quad (2.22)$$

Here, $\epsilon(\mathbf{k}) = C - D(k_x^2 + k_y^2)$, $\mathbf{d}(\mathbf{k}) = [Ak_x, -Ak_y, M(\mathbf{k})]^T$, $M(\mathbf{k}) = M - B(k_x^2 + k_y^2)$ and A, B, C, D, M are material parameters that depend on the specific geometry of the setup. The two blocks of the Hamiltonian $h(\mathbf{k})$ and $h^*(-\mathbf{k})$ correspond to the Hamiltonians of anomalous quantum Hall insulators and are related by TRS. The model thus can be understood as two time reversed copies of the quantum Hall effect in opposite magnetic field. While each copy breaks TRS their combination is time-reversal symmetric.

Each block can be characterized by a topological invariant, the Chern number, ν_+ and ν_- respectively. The Chern numbers are given by $\nu_{\pm} = \pm[\text{sgn}(M) + \text{sgn}(B)]/2$ and therefore there exist two topologically distinct massive phases. The trivial phase in which the topological invariants vanish ($\text{sign}(MB) = -1$) and the topological regime with finite Chern number ($\text{sign}(MB) = +1$). The bulk is gapped in both cases with a band gap ~ 30 meV.

²The notation Γ_6, Γ_8 etc. originates from the group theoretical classification of irreducible representations of the crystal symmetries which determine the way wavefunctions transform at the Γ point.

³For Γ_6 states we have $l=0$ which implies that $m_j = \pm 1/2$ is the same as $s = \pm 1/2$. On the other hand, for Γ_8 $l=1$ and $m_j = \pm 3/2$ is also the same as $s = \pm 1/2$ therefore we introduced the notation $s = 1/2 = \uparrow$ and $s = -1/2 = \downarrow$.

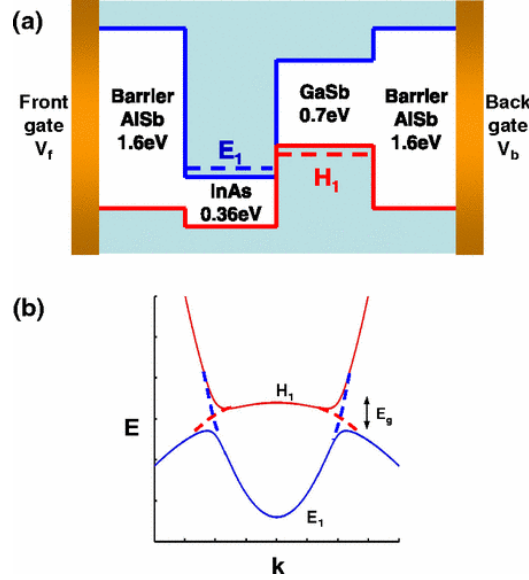


Figure 2.3: (a) *AlSb/InAs/GaSb/AlSb heterostructure: the electron valence subband E_1 is localized in the InAs layer, while the hole conduction subband is located in the GaSb layer.* (b) *When the hole band is tuned above the electron band, tunneling between the layers opens a hybridization gap. In this regime, gapless edge modes, energetically located within the band-gap, appear at the boundary of the quantum well. From Ref. [77].*

However, in the topological phase edge states emerge at the boundary of the sample, whose spectrum lies inside the bulk gap, see Fig 2.3. One finds, that the helical edge states are Dirac fermions with spectrum,

$$E_{\uparrow,\downarrow}(k_y) = \pm v_F k_y \quad (2.23)$$

where $v_F = A$ and for HgTe/CdTe quantum wells $A \simeq 5 \cdot 10^5 \text{m/s}$. Since the model describes two time reversed copies of the quantum Hall effect, two edge modes appear at the interface of the sample to the vacuum. They are Kramers partners of counterpropagating electrons with opposite spin. Due to the fixed relation between spin and momentum they have been termed helical edge states.

The number of counterpropagating edge modes is measured by the Chern numbers and determines the Hall conductance. While the total Chern number $\nu_c = \nu_+ + \nu_-$ vanishes, the spin Chern number, $\nu_s = \nu_+ - \nu_-$ is finite. By definition the charge and spin Hall conductance is $G_{xy}^{(c,s)} = \frac{e^2}{h} \nu_{c,s}$, and hence $G_c = 0$ while $G_s = 2e^2/h$ is quantized. The 2D TI is thus also referred to as QSH insulator.

An experimental difficulty that arises in the described setup is that the topological nature basically depends on the quantum well thickness and can not be changed in situ.

Another material that shows the QSH effect are AlSb/InAs/GaSb/AlSb heterostructures shown in Fig. 2.3. Because the valence band of GaSb is higher in energy than the conduction band of InAs, the conduction band and valence band of the quantum well are spatially separated. In the inverted regime $E_1 < H_1$ the bands cross at some finite wavevector, but due to tunneling between the electron and hole layers a hybridization gap $\sim 4 \text{meV}$ is opened, rendering the bulk insulating. Following the ideas developed in the previous discussion, the quantum well should be in the topological phase in the inverted regime and in the trivial phase in the normal regime. One major advantage of this experimental

setup is that the band alignment and the Fermi energy can be tuned by back and front gates, as shown in Fig. 2.3.

Let us make one more remark concerning the BHZ model (2.21). The model predicts the existence of helical edge states at the boundaries of 2D TIs. In the derivation of the model the bulk-inversion asymmetry (BIA) and structural-inversion asymmetry (SIA) of the quantum well have been neglected. This is not always justified [78, 79]. In InAs/GaSb heterostructures both BIA and SIA are always present and also in HgTe/CdTe the application of an electric field in the z -direction may break lead to SIA. Therefore, the general Hamiltonian should contain additional SOC terms that arise due to the broken inversion symmetry. Of course such inclusion does not change the topological phase of the system since the terms do not break TRS. However, in the presence of SOC the spin in z -direction is no longer conserved so that the edge states do not have a fixed spin polarisation anymore. At fixed energy the Kramers partners at momenta k and $-k$ still have opposite spin but the spin polarisation changes with momentum and there is a finite overlap between right and left moving states at momenta k and k' if $k \neq -k'$. This leads to new allowed scattering mechanisms, as discussed in Ch. 3.

2.2.1 Topological protection of the helical edge states

If the Fermi energy is tuned into the bulk gap of a trivial insulator electron transport is inhibited. On the other hand, if one tunes the Fermi energy inside the bulk gap of a TI charge transport is possible due to the presence of edge states. The transport properties of the edge states are particularly interesting because the helical modes are topologically protected, i.e. they cannot be localized by arbitrarily strong disorder as long as TRS is not broken. Here, we present an argument due to Kane and Mele [6] that helical electrons are robust against elastic scattering of impurities as long as TRS is preserved.

Consider an edge that is disordered in a finite region and clean outside that region. The conductance of the system can be found by solving the corresponding scattering problem. For a noninteracting system the eigenstates in the clean region at any given energy can be expanded in plane waves with the amplitudes ϕ_{in} of the incoming waves and the outgoing waves ϕ_{out} , where $\phi = (\phi_+, \phi_-)^T$ consists of the amplitudes of left and right moving edge states. Due to the spin-momentum locking right movers have spin-up and left movers have spin down. In particular the time-reversal operator can be represented in chiral space by the same form as for spin 1/2 fermions as $\Theta = i\sigma_y\mathcal{K}$. The scattering that occurs in the disordered region is characterized by the unitary 2×2 matrix S , which relates incoming and outgoing states $\phi_{\text{out}} = S\phi_{\text{in}}$. Time reversal symmetry switches the direction of propagation, which yields the relation between the amplitudes and the time reversed (TR) amplitudes $\phi_{\text{out}}^{\text{TR}} = i\sigma_y\phi_{\text{in}}$ and $\phi_{\text{in}}^{\text{TR}} = i\sigma_y\phi_{\text{out}}$. Since the TR amplitudes are again related by the S matrix, $\phi_{\text{out}}^{\text{new}} = S\phi_{\text{in}}^{\text{new}}$ we find the constraint

$$S = \sigma_y S^T \sigma_y. \quad (2.24)$$

It is straightforward to show that this implies that the S-matrix has to be diagonal, i.e. electrons in the disordered region are not backscattered. It follows that, unless TRS is broken, electrons are perfectly transmitted along the disordered region. Eigenstates at any energy inside the region are extended at $T = 0$ and the edge transport is ballistic with the quantized conductance $G = 2e^2/h$. This argument, however holds only for scattering between Kramers pairs. If there are two sets of Kramers pairs at the edge, elastic scattering between different pairs is allowed and localizes both pairs of edge modes. This shows that the QSH insulator is characterized by a \mathbb{Z}_2 invariant in the bulk [6], which corresponds to an even (topologically trivial) or odd (topologically nontrivial) number of Kramers pairs at the edge.

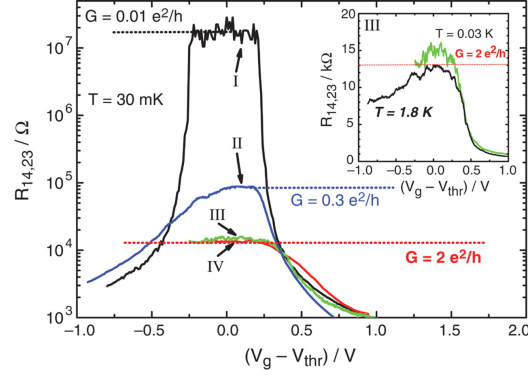


Figure 2.4: Four terminal resistance $R_{14,23}$ as a function of the gate voltage V_g that controls the chemical potential. The measurement is performed at temperature $T = 30$ mK and zero magnetic field. Different curves correspond to different samples: (I, black) device size $(20.0 \times 13.3) \mu\text{m}^2$ in the trivial regime; (II, blue) device size $(20.0 \times 13.3) \mu\text{m}^2$ in the topological regime; (III, green) device size $(1.0 \times 1.0) \mu\text{m}^2$ in the topological regime; (IV, red) device size $(1.0 \times 0.5) \mu\text{m}^2$ in the topological regime. The inset shows the temperature dependence of the resistance. The behavior of the curves is discussed in the main text. From Ref. [9].

2.2.2 Experimental evidence for helical edge states

A possible way to show the existence of edge states experimentally is through transport measurements at the sample edges. If the TI is in the topologically nontrivial regime and the Fermi energy is tuned inside the bulk gap the current is expected to be carried solely by the ballistic edge modes. The resistance in a multi-terminal setup then can be obtained by the Landauer-Büttiger formalism. The current flowing out of the i -th contact into the sample due to the applied voltages V_j at the contacts is given by

$$I_i = \frac{e^2}{h} \sum_j (T_{ji} V_i - T_{ij} V_j), \quad (2.25)$$

where T_{ij} is the transmission probability from the i -th to the j -th electrode. Due to TRS $T_{ij} = T_{ji}$ and since Kramers theorem prohibits backscattering between Kramers partners all entries except $T_{i,i+1} = T_{i+1,1} = 1$ vanish. The total current is conserved in the sense that $\sum_i I_i = 0$. Furthermore a voltage lead j is defined by the condition that it draws no net current, i.e. $I_j = 0$ and we have to identify the $i = N+1$ electrode with $i = 1$. The first experimental evidence of topologically protected edge transport was reported in [9], where the authors measured the four-terminal resistance $R_{14,23} = I_1 - I_4 / (V_2 - V_3)$. The results of the measurement are depicted in Fig. 2.4. For the setup considered in the experiment, Eq. (2.25) predicts $R_{14,23} = h/2e^2$, which is in good agreement with the experimentally measured curves for short samples (green and red) with device size $1 \times 1 \mu\text{m}^2$. For larger samples of size $20 \times 13.3 \mu\text{m}^2$ (blue curve) the conductance deviates significantly from the predicted value. In the latter case the system size is much larger than the mean free path of the system $\ell_{ee} \sim 1 \mu\text{m}$. This suggests that electron-electron scattering leads to nonuniversal corrections to the quantized conductance in these systems. Possible scattering mechanisms in helical edge modes will be discussed in detail in Ch. 3. The black curve is measured in the topologically trivial regime where no edge states are present and therefore shows much larger resistance than the other curves. Lastly, the inset shows that the conductance is

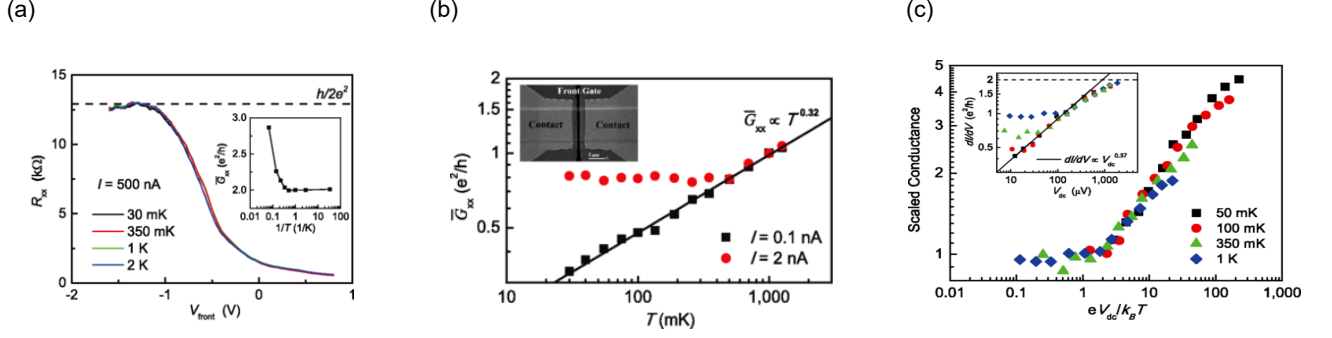


Figure 2.5: Measurement of the temperature (a) and (b) and voltage dependence (c) of the conductance of helical edge modes in InAs/GaSb quantum wells. Figures from [45].

only weakly temperature dependent, a point to which we will return shortly.

The quantization of conductance in the inverted regime and deviations from the perfect conductance for larger samples have also been observed in multiterminal measurements in InAs/GaSb quantum wells [12, 45, 80].

The transport measurements confirm the physical picture of topologically protected edge states, but do not shed light on the spin polarization. The fact that the edge states indeed are helical was confirmed in measurements on split-gated H-bar nanostructures, where QSH and spin Hall transport take place in the same device [81]. The spin Hall effect can be used as a spin current injector into the QSH region which allows for an electrical measurement of the spin polarization.

In addition the helical edge states of 2D TIs have been imaged explicitly in real space in Ref. [82, 83]. Here, the experimentalists used a scanning superconducting interference device (SQUID) to image the magnetic field produced by the current through a Hall bar and reconstructed the current density from the signal. The results confirm edge transport in the topological regime.

In Ch. 3 we will discuss in detail possible scattering mechanisms that may lead to conductance corrections beyond the ballistic regime. However, since elastic scattering is forbidden due to TRS at any energy scale, the mechanisms are necessarily inelastic and lead to power law corrections to the conductance $\delta G \sim \epsilon^\alpha$. Here, $\epsilon = \max(T, eV)$ and the exponent depends on the Luttinger parameter due to the one-dimensional nature of the edge states. It is important to emphasize, that the condition

$$k_B T \gg eV \quad (2.26)$$

corresponds to very small bias currents in experiment. In the ballistic regime, $G \sim 2e^2/h$, the voltage is proportional to the current $V \sim (h/2e^2) \cdot I$ and thus the condition (2.26) can be expressed as [70]

$$T [\text{mK}] \gg 150 \cdot I [\text{nA}]. \quad (2.27)$$

Since the experiments discussed above have been performed for bias currents of the order of 100 nA, the temperature dependence could only be observed for temperatures $T \gg 15\text{K}$ for which bulk effect become important and make it experimentally difficult to measure the edge current. This might explain the temperature independent nature of the conductance corrections in the above measurements.

Due to the experimentally difficult nature of the measurements, the first experimental observation of temperature dependence of the conductance was reported only recently in Ref. [46]. The results of the experiment, performed on systems with edge length $L \sim 1.2 \mu\text{m}$ are shown in Fig. 2.5. When the

chemical potential is tuned inside the bulk gap the longitudinal resistance shows a quantized plateau that persists for temperatures from 30 mK up to 2 K. The resistance is measured for a bias current of 500 nA, so that (2.27) is not fulfilled for any of the curves. Consequently, the plateau is temperature independent. For higher temperatures bulk states contribute to the transport leading to an increased conductance, as is shown in the inset. Fig. 2.5 (b) shows the conductance as a function of the temperature on a log-log plot for two different bias currents and in a temperature regime, where the conductance can safely be attributed to the edge modes. For temperatures, where (2.27) is fulfilled the curves collapse onto the line corresponding to the power law $G \propto T^{0.32}$. Finally, the experimentalists also studied the voltage dependence of the conductance for $I_{\text{bias}} = 0.1 \text{ nA}$ and temperatures $T \ll eV$. The result is depicted in Fig. 2.5 (c). The main plot illustrates that all measured curves collapse onto a single curve $G \propto V^{0.37}$ by scaling the measured dI/dV .

The non-integer power laws for the temperature and voltage dependence of the edge conductance suggest that the edge modes form a helical Luttinger liquid, where inelastic electron-electron interactions lead to corrections to the quantized conduction. The Luttinger constant in the material has been determined experimentally as $K \simeq 0.22$. For a discussion of the possible microscopic scattering mechanisms and a comparison to this experiment we refer to Ch. 3.

3

Chapter 3

Electron transport in a disordered helical Luttinger liquid

This chapter is devoted to the discussion of electron transport in a disordered HLL. As we have discussed in Sec. 2.2 the HLL is a novel type of 1D quantum liquid that emerges at the edge of a 2D QSH insulator [6, 13, 68, 76] and consists, in its most conventional form protected by time-reversal symmetry, of two counterpropagating Kramers conjugate modes. In an “ideal” helical edge, the electron spin is conserved for each of the chiral modes. Electron-electron backscattering between the modes, as well as backscattering by nonmagnetic inhomogeneities, is then prohibited by the combination of the spin-axial and time-reversal symmetries. As a consequence, charge transport through the ideal helical edge is characterized by a quantized conductance $G_0 = 2e^2/h$, at any temperature T , also in the presence of nonmagnetic disorder. This conductance quantization has been experimentally observed at the edges of short HgTe/CdTe [9, 84] and InAs/GaSb [12, 45, 80] quantum wells.

As we have seen in Sec. 2.2.2, transport measurements on larger samples, however, show clear deviations from the quantized conductance. The fact that these deviations appear only for scales larger than the mean free path due to electron-electron interaction $\ell_{ee} = v_F \tau_{ee}$ suggests that interactions between right- and left-movers at the edge are the source of dissipation. Since backscattering in an ideal helical liquid is inhibited by the spin-axial symmetry this in turn means that the S_z symmetry at the edge must be broken.

The goal of this chapter is twofold. First, we derive a model for the HLL with broken spin axial-symmetry by taking into account Rashba-type spin-orbit coupling, which is naturally induced by broken inversion symmetry about the plane of the semiconductor heterostructure. Second, we calculate the conductivity of this “generic” HLL in the presence of both electron-electron interaction and disorder, which allows us to make predictions about transport properties of large samples. While impurity scattering alone does not affect transport due to the topological protection of the edge states, we will show that the dressing of impurities by interaction generates effective scattering processes that govern transport at low temperatures.

The chapter is organized as follows. In Sec. 3.1 we introduce the model we are going to study, that describes interacting helical electrons in the presence of SOC and nonmagnetic disorder. We then go on to calculate the conductivity of an infinitely long edge channel for this model. First, we consider weak interactions and low frequencies of the applied electric field in the framework of a kinetic equation in Sec. 3.2. Subsequently, in Sec. 3.3 we complement these results by obtaining the conductivity for arbitrary strength of forward scattering interaction and high frequencies using bosonization and the

linear response formalism. The combination of both approaches enables us to make predictions for the temperature and frequency dependence of the conductivity in a wide parameter regime. The results of the perturbative approach are summarized and discussed in Sec. 3.4. Finally, we perform a weak coupling RG analysis of the disordered HLL in Sec. 3.5 in order to discuss the temperature behavior of the conductivity at lowest temperatures before summarizing in Sec. 3.6.

This chapter is based in part on Refs. [85, 86].

3.1 The helical Luttinger model with broken axial spin symmetry

Let us start by discussing the model we are going to study. The Hamiltonian of electrons at the edge of a two-dimensional QSH insulator consists of four parts $H = H_{\text{kin}} + H_{\text{SO}} + H_{\text{int}} + H_{\text{dis}}$. The kinetic part takes the form

$$H_{\text{kin}} = \int_k \psi_{\sigma}^{\dagger}(k) \epsilon_{\sigma}(k) \psi_{\sigma}(k). \quad (3.1)$$

Here, $\psi_{\sigma}(k)$ annihilates an electron with spin $\sigma = \uparrow, \downarrow$ in the z -direction (growth direction of the quantum well) and with momentum k parallel to the edge. The model of edge electrons we want to study should be invariant under time-reversal and therefore the Hamiltonian has to commute with the time reversal operator Θ . For spinful electrons Θ squares to $\Theta^2 = -1$ and can be parametrized as $\Theta = i\sigma_y \mathcal{K}$, where σ_i with $i = x, y, z$ denote the Pauli matrices in spin space and \mathcal{K} is complex conjugation. Time reversal symmetry then constrains the dispersion as $\epsilon_{\sigma}(k) = \epsilon_{\bar{\sigma}}(-k)$. We will assume that the spectrum is linear in the whole momentum range $k \in [-\Lambda/v_F, \Lambda/v_F]$, where Λ denotes the UV-cutoff of our theory (the bulk gap). The dispersion takes the form:

$$\epsilon_{\uparrow}(k) = v_F k, \quad \epsilon_{\downarrow}(k) = -v_F k \quad (3.2)$$

Here, v_F denotes the Fermi velocity and the momentum is measured from the crossing point of the spectrum which we will refer to as Dirac point. Note that right-moving modes correspond to spin up and left-moving modes to spin down - due to this special relation between the spin and the dispersion the excitations are dubbed helical electrons.

As we mentioned in the introduction to this chapter, spin orbit coupling arises naturally in semiconductor heterostructures, due to broken inversion symmetry. The strong SOC in these systems creates a band inversion in the topologically nontrivial regime and leads to the emergence of edge states in the first place. We will not derive the form of the SOC term at the edge from a microscopic theory here, but rather anticipate its form by symmetry arguments. The most generic SOC term we can write reads as

$$H_{\text{SO}} = \int_k \psi_{\sigma}^{\dagger}(k) \alpha_i(k) \sigma_{\sigma, \sigma'}^i \psi_{\sigma'}(k), \quad (3.3)$$

where TRS constrains the (real) expansion coefficients to be antisymmetric $\alpha_i(k) = -\alpha_i(-k)$. In the presence of this term the axial spin symmetry is broken and the quadratic part $H_0 = H_{\text{kin}} + H_{\text{SO}}$ of the Hamiltonian is no longer diagonal. We will return to this point shortly after introducing electron-electron interaction and disorder.

We assume that electrons interact via a short-range (screened by external gates) interaction potential $V(x - x')$. Additionally, we introduce weak ($D \ll \mu$) white-noise disorder, characterized by the

correlation function

$$\langle U(x)U(x') \rangle_{\text{dis}} = D \delta(x - x') \quad (3.4)$$

Here, $D = n_{\text{imp}}U^2(q=0)$, with the impurity concentration n_{imp} , is a measure for the disorder scattering strength. The interaction and disorder terms in the Hamiltonian take the form

$$H_{\text{int}} = \frac{1}{2} \int_{k,k',q} \sum_{\sigma\sigma'} \psi_{\sigma}^{\dagger}(k) \psi_{\sigma}(k-q) V(q) \psi_{\sigma'}^{\dagger}(k') \psi_{\sigma'}(k'+q), \quad (3.5)$$

$$H_{\text{dis}} = \int_{k,q} \sum_{\sigma} U(q) \psi_{\sigma}^{\dagger}(k) \psi_{\sigma}(k-q). \quad (3.6)$$

Let us now proceed to rediagonalize the quadratic part of the Hamiltonian in the presence of SOC. If we introduce the vector of fermionic fields,

$$\mathbf{\Psi}^{\dagger}(k) = (\psi_{\uparrow}^{\dagger}(k), \psi_{\downarrow}^{\dagger}(k)), \quad (3.7)$$

the noninteracting, clean Hamiltonian takes the form

$$H_0 = \int_k \mathbf{\Psi}^{\dagger}(k) \mathcal{H}(k) \mathbf{\Psi}(k), \quad (3.8)$$

with the hermitian matrix

$$\mathcal{H}(k) = \begin{pmatrix} v_F k + \alpha_3(k) & \alpha_{\parallel}(k) \\ \alpha_{\parallel}^*(k) & -v_F k - \alpha_3(k) \end{pmatrix}. \quad (3.9)$$

Here, we defined the function $\alpha_{\parallel}(k) = \alpha_1(k) - i\alpha_2(k)$. The subscript \parallel describes the fact that $\alpha_{\parallel}(k)$ is defined by the spin orbit components parallel to the 2D TI plane. The function $\alpha_{\parallel}(k)$ can always be chosen to be real by absorbing a momentum dependent phase into the definition of the fermionic fields.

Being bilinear in the spinor $\mathbf{\Psi}$, the Hamiltonian H_0 can be brought into diagonal form by the unitary transformation,

$$\begin{pmatrix} \psi_{+}(k) \\ \psi_{-}(k) \end{pmatrix} = B(k) \mathbf{\Psi}(k) = \begin{pmatrix} \cos \theta_k & -\sin \theta_k \\ \sin \theta_k & \cos \theta_k \end{pmatrix} \begin{pmatrix} \psi_{\uparrow}(k) \\ \psi_{\downarrow}(k) \end{pmatrix}. \quad (3.10)$$

Setting $2\theta_k = \arctan \alpha_{\parallel}(k)/[v_F k + \alpha_3(k)]$ the quadratic part takes the form

$$H_0 = \sum_{\eta} \int_k \psi_{\eta}^{\dagger}(k) \epsilon_{\eta}(k) \psi_{\eta}(k), \quad (3.11)$$

where the dispersion relation is given by $\epsilon_{\eta}(k) = [\alpha_{\parallel}^2(k) + (\alpha_3(k) + v_F k)^2]^{1/2}$. Performing the rotation (3.10) in Eqs. (3.5) and (3.6), we obtain the interaction and disorder Hamiltonians in the chiral basis as

$$H_{\text{int}} = \frac{1}{2} \int_{k,q,p} \sum_{\eta_1 \eta_2} \sum_{\eta_3 \eta_4} V(q) \left[B^{\dagger}(k) B(k-q) \right]_{\eta_1, \eta_2} \left[B^{\dagger}(p) B(p+q) \right]_{\eta_3, \eta_4} \times \psi_{\eta_1}^{\dagger}(k) \psi_{\eta_2}(k-q) \psi_{\eta_3}^{\dagger}(p) \psi_{\eta_4}(p+q), \quad (3.12)$$

$$H_{\text{dis}} = \int_{k,q} \sum_{\eta_1 \eta_2} U(q) \left[B^{\dagger}(k) B(k-q) \right]_{\eta_1, \eta_2} \psi_{\eta_1}^{\dagger}(k) \psi_{\eta_2}(k-q). \quad (3.13)$$

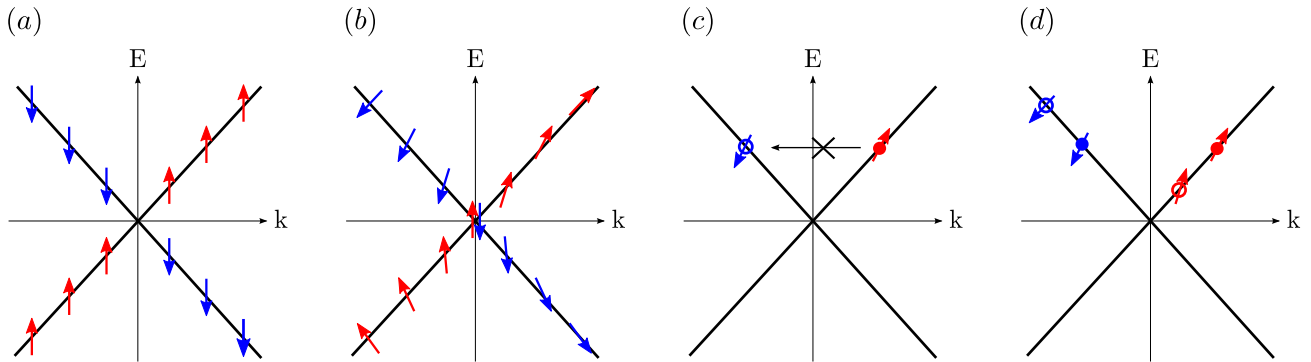


Figure 3.1: Illustration of the spin orientation and dispersion of (a) an ideal helical liquid with well defined spin-orientation and (b) a generic helical liquid. In an ideal HLL no scattering processes (elastic or inelastic) between quasiparticles of different chirality can take place because their states are orthogonal in spin space. (c) Elastic scattering in the generic HLL is forbidden due to Kramers theorem, that ensures that states at fixed energy have opposite spins. Filled (empty) circles denote occupied (unoccupied) states (d) Inelastic scattering in the generic HLL is allowed but is suppressed by the spin momentum locking - for weak spin-orbit coupling the spin-orientation changes only slowly as a function of the momentum, so that right- and left-moving particles have nearly opposite spin.

To simplify the expression we make two assumptions. First, for small momenta and isotropic spin orbit coupling we expand $\alpha_3(k) = \alpha_{\parallel}(k) \simeq \alpha k + \beta k^3$. Second, using realistic values for the parameters in HgTe/CdTe quantum wells [87] we estimate $v_F \simeq 5 \times 10^5$ m/s and $\alpha \simeq 1, 2 \times 10^4$ m/s. This means we can consider the SOC as a weak perturbation to the kinetic energy of the edge electrons and expand our results to leading order in $\alpha/v_F \ll 1$.

In the lowest order in this expansion the rotation angle θ_k takes the form $\theta_k \simeq \theta_0 + k^2/k_0^2$, with $\theta_0 \simeq \alpha/v_F$ and $k_0^2 = v_F/\beta$. The regime of “small” momenta is then defined by the condition $k \ll k_0$. The first order expansion of the angle θ_k corresponds to a constant rotation independent of the momentum, which we will neglect in the following.

Using the approximations outlined above, the unitary transformation between the chiral and spin basis in Eq. (3.10) takes the form

$$\begin{pmatrix} \psi_+(k) \\ \psi_-(k) \end{pmatrix} \simeq \begin{pmatrix} 1 & -k^2/k_0^2 \\ k^2/k_0^2 & 1 \end{pmatrix} \begin{pmatrix} \psi_{\uparrow}(k) \\ \psi_{\downarrow}(k) \end{pmatrix}. \quad (3.14)$$

This form of the rotation matrix has first been proposed in [48] based on symmetry arguments alone.

Note that the chiral operators ψ_{\pm} involve superpositions of \uparrow and \downarrow electrons, i.e. the quasiparticle states have no well defined spin in z-direction. In the limit of vanishing SOC ($k_0 \rightarrow \infty$) we recover the spin momentum locking, characteristic of the ideal helical liquid. For large but finite k_0 the spin orientation changes as a function of momentum, which is schematically depicted in Fig. 3.1.

Using the approximation in Eq. (3.14) the product appearing in Eqs. (3.12) and Eq. (3.13) can be written as

$$\left[B^{\dagger}(k)B(p) \right]_{\eta_1, \eta_2} \simeq b_{\eta_1, \eta_2}(k, p) \equiv \delta_{\eta_1, \eta_2} - \eta_1 \delta_{\eta_1, \bar{\eta}_2} \frac{k^2 - p^2}{k_0^2}. \quad (3.15)$$

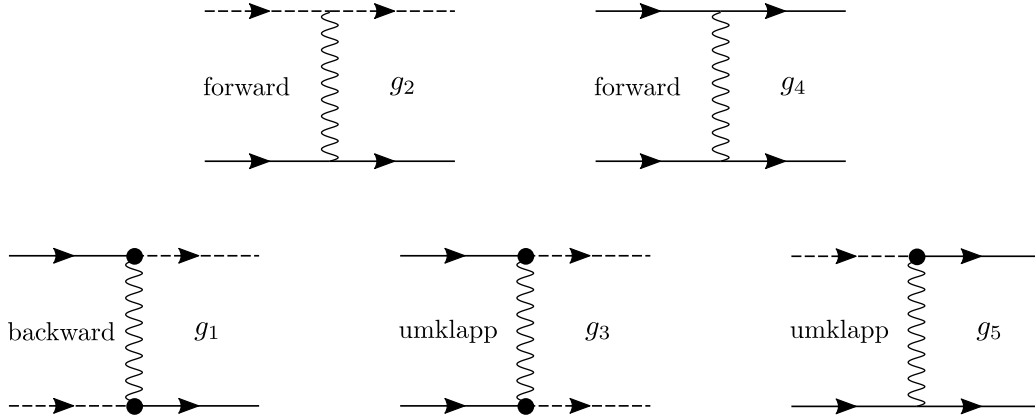


Figure 3.2: Two-particle electron-electron scattering processes in a helical Luttinger liquid. Full (dotted) lines denote right- (left-) moving quasiparticles, wiggly lines denote electron-electron interaction and a full circle denotes the vertex function $b_{\eta_{out}, \eta_{in}}(k_{out}, k_{in})$ introduced in the main text.

Substituting this into the interaction and disorder Hamiltonians in Eq. (3.12) and Eq. (3.13) and expanding the quadratic part to leading order in both α/v_F and k/k_0 , we arrive at the *helical Luttinger model*, $H = H_0 + \sum_{i=1}^5 H_i + H_f + H_b$. Thereby, the quadratic Hamiltonian reads as

$$H_0 = \sum_{\eta} \int_k \psi_{\eta}^{\dagger}(k) \epsilon_{\eta}(k) \psi_{\eta}(k), \quad (3.16a)$$

where the dispersion relation is given by $\epsilon_{\eta}(k) = v_F \eta k$. The interaction part can be organized in the spirit of the g-ology as

$$\begin{aligned} H_1 &= g_1 \int_{k,p,q} \sum_{\eta} \psi_{\eta}^{\dagger}(k) b_{\eta, \bar{\eta}}(k, k-q) \psi_{\bar{\eta}}(k-q) \psi_{\eta}^{\dagger}(p) b_{\bar{\eta}, \eta}(p, p-q) \psi_{\eta}(p+q), \\ H_2 &= g_2 \int_{k,p,q} \sum_{\eta} \psi_{\eta}^{\dagger}(k) \psi_{\eta}^{\dagger}(p) \psi_{\bar{\eta}}(p+q) \psi_{\eta}(k-q), \\ H_3 &= g_3 \int_{k,p,q} \sum_{\eta} \psi_{\eta}^{\dagger}(k) b_{\eta, \bar{\eta}}(k, k-q) \psi_{\bar{\eta}}(k-q) \psi_{\eta}^{\dagger}(p) b_{\eta, \bar{\eta}}(p, p+q) \psi_{\bar{\eta}}(p+q), \\ H_4 &= g_4 \int_{k,p,q} \sum_{\eta} \psi_{\eta}^{\dagger}(k) \psi_{\eta}^{\dagger}(p) \psi_{\eta}(p+q) \psi_{\eta}(k-q), \\ H_5 &= g_5 \int_{k,p,q} \sum_{\eta} \psi_{\eta}^{\dagger}(k) b_{\bar{\eta}, \eta}(k, k-q) \psi_{\eta}(k-q) \psi_{\eta}^{\dagger}(p) \psi_{\eta}(p+q) + \text{H.c.} . \end{aligned} \quad (3.16b)$$

Here, we assumed that the interaction potential is sufficiently short-ranged such that we can replace its Fourier transform by a constant, $V(q) = V_0 \in \mathbb{R}$. This yields the dimensionful g-ology constants $g_1 = g_2 = g_3 = g_4 = g_5 = V_0$. However, the parameters of the above Hamiltonian include in general renormalization due to high lying states and should in general be considered as independent, effective parameters of the theory, cf. the discussion in Sec. 1.3. A diagrammatic depiction of the scattering processes is shown in Fig. 3.2.

Finally, the disorder term takes the form $H_{\text{dis}} = H_f + H_b$, with

$$\begin{aligned}
H_f &= U_0 \int_{k,q} \sum_{\eta} \psi_{\eta}^{\dagger}(k) \psi_{\eta}(k-q) , \\
H_b &= U_0 \int_{k,q} \sum_{\eta} \psi_{\eta}^{\dagger}(k) b_{\eta,\bar{\eta}}(k, k-q) \psi_{\bar{\eta}}(k-q) .
\end{aligned}
\tag{3.16c}$$

Here, the first term describes forward scattering (scattering inside the same chiral branch) and the second term backscattering (scattering from one chiral branch to the other) off impurities. We assumed that impurity potential is short-range, which allows us to replace its Fouriertransform by a constant $U(q=0) \equiv U_0$. The Hamiltonian in Eqs. (3.16a), (3.16b) and (3.16c) defines the theory of helical fermions we wish to study in this chapter. Although the theory is in principle defined for all momentum scales $|k| < \Lambda/v_F$, scattering between electrons of different chirality, and conjoined Luttinger liquid renormalization only sets in on scales $|k| < k_0$, since the matrix elements of B connecting the spin and chiral basis are strongly oscillating for larger momenta.

The helical Luttinger model is very similar to the spinless Luttinger model introduced in Ch. 1.3, except for two important aspects.

The first and main difference is the presence of the factors $b_{\eta_1,\eta_2}(k,p)$ in the interaction and disorder part of the Hamiltonian. These factors appear when a particle changes its chirality in a scattering process and ensure that no elastic scattering between Kramers partners (for which $k = -p$) can take place, see Fig. 3.1 (c). Inelastic scattering between particles of opposite chirality, on the other hand, is allowed but suppressed by powers of k_0^{-2} . For weak spin-orbit coupling the chiral states in Eq. (3.14) only have a small admixture of states of the opposite spin direction, the overlap between states of different chirality is therefore small ($\propto k_0^{-2}$). This is schematically depicted in Fig. 3.1 (d).

The other difference is related to the population of eigenstates at thermal equilibrium. The conventional Luttinger model is obtained by linearizing the spectrum of fermions around the Fermi energy defining left and right movers with linear spectrum. The theory is then defined for temperatures $T \ll \mu$, where the linearization is valid. In the helical Luttinger model, we assume that T can be larger than the difference between μ and the Dirac point, so that real scattering events, that involve electron states around the Dirac point are not necessarily thermally suppressed. Therefore, Umklapp processes (g_3 and g_5), that usually would only appear in lattice theories at commensurate filling, appear in the Hamiltonian in Eq. (3.16b).

In particular in the g_5 process, energy and momentum conservation necessitate that one of the particles (incoming or outgoing) is exactly at the Dirac point, see Fig. 3.4. This scattering process is therefore unique to the helical Luttinger model and we will see that it drastically changes the transport properties of the HLL compared to the LL.

3.2 Conductivity of helical fermions

The goal of the remainder of this chapter is to study the transport properties of the helical Luttinger model defined in Eqs. (3.16a), (3.16b) and (3.16c). The key quantity characterizing transport in a system is the conductivity

$$\sigma(q, \omega) = j(q, \omega) / E(q, \omega) ,
\tag{3.17}$$

where $j(q, \omega)$ is the current density and $E(q, \omega)$ is an external electric field. In a macroscopic system, one takes the limit $q \rightarrow 0$ first, which corresponds to a uniform, but time dependend electric field. For lack

of better nomenclature we will refer to the quantity $\sigma(q=0, \omega)$ as the conductivity as well. In particular we are interested in the resistivity $\rho = [\text{Re}\sigma(0, 0)]^{-1} = E_0^2/(-\dot{Q})$, which measures the energy $(-\dot{Q})$ that is dissipated due to scattering in the edge if we apply a homogeneous *dc* field $E(q, \omega) = E_0\delta(q)\delta(\omega)$ to the system [57].

The opposite order of limits ($\omega \rightarrow 0$, q finite), corresponds to the situation when a static electric field is applied to part of the edge. The electric field can be nonuniform, but we will demand that the voltage $V = \int dx E(x)$ is finite. In this case it is often more convenient to introduce the conductance $G = I/V$.

Before we introduce the formalism to calculate the conductivity, let us first review the role of symmetries on the allowed microscopic scattering mechanisms in the system. Microscopically, the current operator of the relativistic low-energy theory of the helical electrons defined in Eq. (3.16a) is given by

$$J_0 = ev_F(N_+ - N_-), \quad (3.18)$$

where N_{\pm} denotes the total number of right- and left-movers, respectively. Electrical resistivity is created by perturbations that do not commute with the current operator. These perturbations correspond to scattering events that change the chirality of electrons.

As we have already discussed, elastic backscattering between Kramers partners remains exactly forbidden by TRS. As a result, the $T = 0$ conductance is given by the quantized value G_0 , independently of the strength of disorder (as long as the bulk remains insulating). However, at $T > 0$ inelastic backscattering processes are generically present in the model with broken spin-axial symmetry and will give rise to dissipation.

3.2.1 Conductivity of helical fermions: kinetic equation

Our starting point for the calculation of transport properties of helical fermions is the kinetic equation for pair collisions in a homogeneous edge of a topological insulator. It suffices to consider only pair collisions, since (single-particle) elastic scattering is strictly prohibited by Kramers theorem to any order.

The kinetic equation can be used to derive observables of physical interest such as the conductivity, on length scales much larger than the collision mean free path ℓ_{ee} ¹ yet smaller than macroscopic scales, such as the length over which the drop of an external voltage occurs. Furthermore, we have to assume that the system is subject to some external source of dephasing, such that the dephasing length ℓ_{ϕ} is much shorter than ℓ_{ee} . This assumption is important because the kinetic equation only describes collisions, where the electrons have no memory of previous scattering events, and is therefore not able to capture quantum interference corrections, such as weak localization.

Under these conditions the evolution of the distribution function² $f_{\eta}(k, t)$ of electrons of chirality η at momentum k and time t is governed by a kinetic equation. We consider the response of edge electrons with equilibrium temperature T and chemical potential μ to the application of a homogeneous electric field E . The corresponding kinetic equation reads as

$$\partial_t f_{\eta_1}(k_1, t) - eE\partial_k f_{\eta_1}(k_1, t) = \text{St}_{\eta_1}[f], \quad (3.19)$$

¹Since elastic scattering is forbidden by TRS at any energy scale, the mean free path is generated by inelastic scattering processes only. Therefore we associate $\ell = \ell_{ee}$.

²In general the distribution function depends on both the momentum k and the position x . It is then understood that one considers a wave packet with both k and x approximately defined, but always such that the uncertainty relation $\Delta x \Delta k \sim 1$ is fulfilled. In the case of a homogeneous edge studied here the spatial dependence is neglected.

where $\text{St}_\eta[f]$ denotes the collision integral for right- or left-movers, which contains all the information about scattering of electrons. It is given by

$$\begin{aligned} \text{St}_{\eta_1}[f] &= (2\pi)^2 \int_{k_2, k_1', k_2'} \sum_{\eta_2, \eta_1', \eta_2'} \mathcal{M}(1, 2, 1', 2') \delta(\epsilon_1 + \epsilon_2 - \epsilon_{1'} - \epsilon_{2'}) \delta(k_1 + k_2 - k_{1'} - k_{2'}) \\ &\times \{f(1')f(2')[1 - f(1)][1 - f(2)] - f(1)f(2)[1 - f(1')][1 - f(2')]\}, \end{aligned} \quad (3.20)$$

where we introduced the joint index $1 \equiv (k_1, \eta_1)$ and the single particle energies $\epsilon_i = v_F \eta_i k_i$. The function \mathcal{M} describes the probability for transitions between the eigenstates $|1, 2\rangle$ and $|1', 2'\rangle$ of the clean, noninteracting Hamiltonian. The probability in Fermi's golden rule approximation takes the form

$$\mathcal{M}(1, 2, 1', 2') = \left| \langle 1'2' | \mathcal{T} | 12 \rangle \right|^2, \quad (3.21)$$

with the T-matrix

$$\mathcal{T} \simeq (H_{\text{dis}} + H_{\text{int}}) + (H_{\text{dis}} + H_{\text{int}}) G_0 (H_{\text{dis}} + H_{\text{int}}) + \dots. \quad (3.22)$$

Here, the Green's function operator is defined as

$$G_0 = \frac{1}{\epsilon_i - H_0 + i\delta}, \quad \delta \rightarrow 0+. \quad (3.23)$$

where $\epsilon_i = \epsilon_1 + \epsilon_2$ denotes the energy of the initial state. If the external electric field is weak, the distribution function will not differ significantly from the thermal Fermi-Dirac distribution. It is then convenient to represent the solution of Eq. (3.19) in terms of the functions $g_\eta(k, \omega)$ as

$$f(1) = n_F(1) - g(1)n_F(1)(1 - n_F(1)) \quad (3.24)$$

where $n_F(1) = \{1 + e^{[\epsilon(1) - v_F k_F]/T}\}^{-1}$ is the thermal distribution function. Linearizing the kinetic equation in Eq. (3.19) in g we obtain (in the frequency representation)

$$-i\omega g(1) - \frac{eE v_F \eta_1}{T} = \text{st}_{\eta_1}[g] \quad (3.25)$$

with the linearized collision integral

$$\begin{aligned} \text{st}_{\eta_1}[g] &= 4 \times (2\pi)^2 \int_{k_2, k_1', k_2'} \sum_{\eta_2, \eta_1', \eta_2'} \mathcal{M}(1, 2, 1', 2') \delta(\epsilon_1 + \epsilon_2 - \epsilon_{1'} - \epsilon_{2'}) \delta(k_1 + k_2 - k_{1'} - k_{2'}) \\ &\times \zeta^{-2}(1) n_F(1) n_F(2) [1 - n_F(1')][1 - n_F(2')] \{g(1') + g(2') - g(1) - g(2)\} \end{aligned} \quad (3.26)$$

and

$$\zeta(1) = \cosh[(\epsilon_1 - \mu)/2T]. \quad (3.27)$$

By solving the kinetic equation in (3.25), we find the electronic distribution function g . This, in turn, allows us to obtain any physical observable of interest. In particular we will be interested in the conductivity which is obtained as

$$\sigma(\omega) = -\frac{e}{E} \int_k \sum_\eta v_\eta(k) f_\eta(k, \omega), \quad (3.28)$$

where $v_\eta(k) = v_F \eta$. Analytical results for the conductivity can be obtained in the high- ($\omega \tau_{\text{ee}} \gg 1$) and low-frequency ($\omega \tau_{\text{ee}} \ll 1$) limits, where τ_{ee} denotes the inelastic electron-electron scattering time.

High-frequency conductivity

In the high-frequency limit we obtain the conductivity by iterating the integral equation in Eq. (3.25) once. To zeroth order we neglect any electron-electron collisions, which yields the distribution function $g^{(0)}(1) = eEv_F\eta_1/(-i\omega + 0)T$. The next order is obtained by solving Eq. (3.25) with the collision integral $\text{st}_{\eta_1}[g^{(0)}]$. The resulting distribution function is then used to calculate the conductivity in Eq. (3.28) which takes the form

$$\text{Re } \sigma = \frac{e^2 v_F}{2\pi\omega^2} \frac{1}{\tau_{ee}^\infty} \quad (3.29)$$

for $\omega\tau_{ee}^\infty \gg 1$. The symbol ∞ is used to emphasize that the conductivity is calculated in the high-frequency regime. The high-frequency electron-electron scattering rate is given by

$$\begin{aligned} \frac{1}{\tau_{ee}^\infty} &= \frac{(2\pi)^3}{T} \int_{k_1, k_2, k_1', k_2'} \sum_{\eta_1, \eta_2, \eta_1', \eta_2'} \mathcal{M}(1, 2, 1', 2') \delta(\epsilon_1 + \epsilon_2 - \epsilon_{1'} - \epsilon_{2'}) \delta(k_1 + k_2 - k_{1'} - k_{2'}) \\ &\times n_F(1)n_F(2)[1 - n_F(1')][1 - n_F(2')] (\eta_1\eta_{1'} + \eta_1\eta_{2'} - 1 - \eta_2\eta_1) \end{aligned} \quad (3.30)$$

One result, we obtain immediately from this expression, is that scattering processes, that do not change the chirality of the particles, do not yield a finite scattering rate. For instance, for g_1 -type processes we have $\eta_1 = \eta_2' \neq \eta_{1'} = \eta_2$ and thus the sum of products of chiral factors in Eq. (3.30) vanishes.

For weak interactions, $g_i/v_F \ll 1$ and weak impurity scattering ($D \ll \mu$) we can calculate the rate perturbatively by expanding the T-matrix in Eq. (3.22) up to second order. Thereby, the impurity Hamiltonian is replaced by the Hamiltonian of a single impurity times the density of impurities n_{imp} (first Born-approximation).

Since elastic scattering is exactly prohibited to any order, the first order expansion is equivalent to the (inelastic) scattering rate of the clean system. In second order there appear corrections to the clean rate, but also rates due to combined processes involving both disorder and electron-electron scattering.

Inelastic scattering rate for the clean system: To first order in an expansion in the T-matrix the scattering probability is given by $\mathcal{M}(1, 2, 1', 2') = |\langle 1'2' | H_{\text{int}} | 12 \rangle|^2$, with the interaction Hamiltonian defined in Eq. (3.16b). Substituting this into the expression for the electron-electron scattering rate in Eq. (3.30), we obtain

$$\frac{1}{\tau_{ee, g_5}^\infty} = \left(\frac{g_5}{v_F}\right)^2 \left(\frac{T}{v_F k_0}\right)^4 f\left(\frac{\mu}{T}\right) T \quad (3.31)$$

with the dimensionless function

$$f(\tilde{\mu}) = \frac{1}{2\pi} \int dx dy \frac{(x^2 - y^2)^2}{\cosh(\frac{x-\tilde{\mu}}{2}) \cosh(\frac{y-\tilde{\mu}}{2}) \cosh(\frac{x+y-\tilde{\mu}}{2}) \cosh(\frac{\tilde{\mu}}{2})}. \quad (3.32)$$

Note, that the g_5 process is the only electron-electron scattering mechanism that generates a finite inelastic scattering rate – a point to which we will return shortly. Let us first discuss the behavior of the scattering rate as a function of temperature. For low temperatures $T \ll \mu$, we obtain the asymptotic behavior of the function f as $f(\tilde{\mu}) \simeq (44\pi/45)\tilde{\mu}^6 e^{-\tilde{\mu}}$ [86], which yields the rate

$$\frac{1}{\tau_{ee, g_5}^\infty} \simeq \frac{44}{45\pi} \left(\frac{g_5}{v_F}\right)^2 \left(\frac{k_F}{k_0}\right)^4 \left(\frac{\mu}{T}\right) \mu e^{-\frac{\mu}{T}}, \quad \text{for } \mu \gg T. \quad (3.33)$$

The inelastic scattering is thermally activated in this regime, since momentum and energy conservation restrict one of the incoming (outgoing) particles in g_5 scattering events to sit exactly at the Dirac point, see Fig. 3.4. For low temperatures the probability that this one state is empty (full) is exponentially small which triggers the exponential suppression of the scattering rate.

For higher temperatures, $T \gg \mu$, we expand $f(\tilde{\mu}) \simeq 306.02$, which yields the rate

$$\frac{1}{\tau_{\text{ee},g_5}^\infty} \simeq 306.02 \left(\frac{g_5}{v_F}\right)^2 \left(\frac{T}{v_F k_0}\right)^4 T, \quad \text{for } T \gg \mu. \quad (3.34)$$

The parametric dependence of the scattering rate is determined by the product of the available phase space $\sim T$ and the absolute square of the probability amplitude of the involved scattering process. In the g_5 scattering amplitude one of the incoming particles changes its chirality, which is suppressed by a small factor $(T/v_F k_0)^2$ due to the spin-momentum locking. The high power of the scattering rate in the temperature can therefore be attributed to the small matrix element for scattering between states of opposite chirality.

Let us at this point address two important conceptual points. First, how is it possible that interactions that conserve momentum, such as the g_5 term, lead to current relaxation? This is surprising since in conventional Fermi liquids translational invariance implies momentum conservation and entails the persistence of currents in the absence of momentum nonconserving interactions such as impurity scattering. However, in the present case we are dealing with an effective low-energy theory in which the current of the model (3.18) is determined by the number of left and right movers. In particular, momentum conservation does not imply current conservation. Current relaxation arises from the scattering of right to left movers or vice versa. While these scattering processes conserve quasimomentum in the effective low-energy theory, they are in fact Umklapp processes in a superordinate lattice model.

Second, why is the g_5 process the only g-ology scattering process that generates dissipation? As we have already discussed, only processes that change the chirality of electrons generate a finite resistivity. Consequently, forward scattering processes (g_2 and g_4) and the backscattering process (g_1) do not produce a finite transport scattering rate. The case of the g_3 Umklapp term, on the other hand, is more subtle. This scattering process obviously changes the chirality of the incoming electrons. The reason why it nonetheless does not lead to any dissipation is intimately linked to the conservation laws of the helical Luttinger model.

Consider the translation operator P_T and the particle current J_0 of the free Hamiltonian in Eq. (3.16a),

$$P_T = \sum_\eta \int_k \psi_\eta^\dagger(k) k \psi_\eta(k), \quad \text{and} \quad J_0 = \sum_\eta \int_k \psi_\eta^\dagger(k) \eta \psi_\eta(k). \quad (3.35)$$

Both commute with H_0 and therefore measure conserved quantities. For the case of a clean LL, it was first realized in Ref. [88] that there exists a hidden conserved quantity, the linear combination $P_0 = P_T + k_F J_0$, that can be identified as the total momentum of the Hamiltonian and is therefore conserved, but also commutes with a single Umklapp term. It is straightforward to show, using the expressions in Eq. (3.16b), that H_3 commutes with the total momentum while H_5 does not. Thus, although the g_3 term breaks the conservation of current, there is another conservation law that is preserved by this particular Umklapp term. If this conservation law is obeyed it is impossible to relax a finite current, and therefore the conductivity remains infinite even at finite temperature. Since the conservation of the total momentum is only broken due to g_5 Umklapp terms, we expect that g_5 processes generate a finite conductivity, while g_3 processes do not, which is consistent with the calculation above.

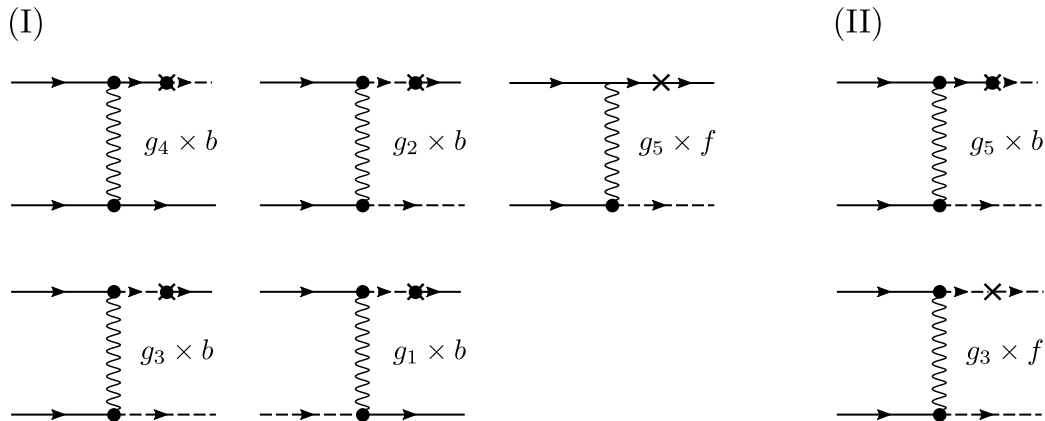


Figure 3.3: Diagrammatic representation of the scattering amplitude of the scattering processes that appear in the second order expansion of the T -matrix and are relevant for the calculation of the conductivity. Here, full (dotted) lines denote right- (left-) moving quasiparticles, wiggly lines denote electron-electron interaction, crosses represent scattering off an impurity and full circles denote the spin-momentum locking vertex factors $b_{k_{in}, k_{out}}$. The diagrams are grouped into two classes (I) and (II) according to the number of incoming electrons that change their chirality during the scattering process.

Higher order scattering processes: To the second order of the weak coupling expansion of the T -matrix the transport scattering rate is given by Eq. (3.30) with the transition probability $\mathcal{M}(1, 2, 1', 2') = |\langle 1'2' | (H_{\text{dis}} + H_{\text{int}}) G_0 (H_{\text{dis}} + H_{\text{int}}) | 12 \rangle|^2$. The matrix element contains three distinct types of scattering mechanisms. First, there are processes where both particles are (independently) scattered by an impurity and then propagate freely before scattering off another impurity. As we have already discussed such elastic scattering events do not yield a finite scattering rate and will therefore not be considered. Similarly, there exist processes that include two electron-electron interactions. Diagrammatically, these correspond to calculating the two particle scattering amplitude with full Greens functions, where the infinitesimal lifetime is replaced by the electronic self energy. Being quartic in the interaction strength such processes represent corrections to the rate derived in Eq. (3.31) and will not be considered here. This leaves us with the third type of processes: scattering event where one incoming (outgoing) particle scatters off an impurity undergoes a free propagation and then interacts with the other incoming particle via the electron-electron interaction. Thereby, the impurity scattering can be either of the forward or backward type and the interaction line can be any of the 5 g-ology processes, which leaves us with 10 types of combined scattering processes. Using the intuition obtained from the first order of perturbation theory we expect that only processes that change the total number of right or left movers can affect current. This is confirmed in the explicit calculation. The remaining processes, that are relevant for the transport scattering rate are diagrammatically depicted in Fig. 3.3.

We note that we can classify the different processes by how many of the incoming electrons change their chirality during the scattering process. First, there are processes that change the chirality of a single incoming particle which we will refer to as “1P processes”. Second, we have scattering processes that change the chirality of both incoming particles which we will dub “2P processes”. We stress that these processes are inelastic, due to the electron-electron scattering, but do not conserve momentum, since they also contain scattering off one impurity. The composite processes are depicted in Fig. 3.4.

Calculating the transport scattering rate for these processes explicitly we obtain

$$\begin{aligned} \frac{1}{\tau_{ee,1P}^\infty} &\simeq c_1 \left[g_5^2 D_f + 2^9 g_3^2 D_b \left(\frac{k_F}{k_0} \right)^8 \right] \left(\frac{T}{v_F k_0} \right)^4 \\ \frac{1}{\tau_{ee,2P}^\infty} &\simeq c_2 \left[g_3^2 D_f + 2g_1^2 D_b \left(\frac{k_F}{k_0} \right)^4 \right] \left(\frac{k_F}{k_0} \right)^2 \left(\frac{T}{v_F k_0} \right)^6, \end{aligned} \quad (3.36)$$

with the numerical constants

$$c_1 = \frac{4}{\pi^2} \int dx_1 dx_2 dx_3 \frac{(x_1 - x_2)^2}{\cosh(x_1) \cosh(x_2) \cosh(x_3) \cosh(x_1 + x_2 + x_3)} \simeq 21.06, \quad (3.37)$$

$$c_2 = \frac{2^9}{\pi^2} \int dx_1 dx_2 dx_3 \frac{(x_1 - x_2)^2 (x_1 + x_2 + 2x_3)^2}{\cosh(x_1) \cosh(x_2) \cosh(x_3) \cosh(x_1 + x_2 + x_3)} \simeq 1.14 \times 10^4 \quad (3.38)$$

In (3.36), the first line describes the scattering rate due to “1P” type processes, while the second line corresponds to “2P” type processes and we introduced the strength of impurity forward ($D_f \equiv D$) and backward ($D_b \equiv D$) scattering to highlight the type of impurity scattering that participates in a given scattering process. Note that composite scattering events that contain forward scattering off disorder are always parametrically larger by factors of $(k_0/k_F)^2$ than the ones containing backscattering off disorder, since they contain less backscattering vertices; see also Fig. 3.3.

The composite scattering processes, together with the g_5 Umklapp term determine the behavior of the high-frequency conductivity. To leading order in the dimensionless strength of electron-electron interaction and disorder scattering it is given by (3.29) with the scattering rate,

$$\frac{1}{\tau_{ee}^\infty} = \frac{1}{\tau_{ee,g_5}^\infty} + \frac{1}{\tau_{ee,1P}^\infty} + \frac{1}{\tau_{ee,2P}^\infty}, \quad (3.39)$$

where the rates are defined in Eqs. (3.31) and (3.36). In the case of weak interactions studied in this section, the 1P scattering rate is parametrically larger than the 2P scattering rate by a factor of $(k_0/k_F)^2 (v_F k_0/T)^2$ and we can neglect the latter. However, it turns out that 2P processes are the dominant scattering mechanism at low temperatures for $K < 2/3$ when we include Luttinger liquid effects in Sec. 3.3.

It is instructive to study the behavior of the transport scattering rate in the regimes of high and low temperatures, compared to μ , separately. For low temperatures, the rate due to g_5 processes is exponentially small, see Eq. (3.33). We remind the reader that the exponential suppression originates from the fact that momentum and energy conservation force one of the particles to be at the Dirac point deep within the filled Fermi sea. The 1P process is very similar to the g_5 process, but contains scattering off impurities. If we include disorder, momentum conservation is broken and the phase space requirements for the process are relaxed, which removes the exponential suppression. Thus at low temperatures, the scattering rate is dominated by the contribution due 1P processes and hence $\text{Re } \sigma \sim 1/\tau_{ee,1P}^\infty$. At high temperatures, on the other hand, the rate due to g_5 Umklapp processes is parametrically larger than the 1P rate by a factor T/D_f . The parameter originates from the comparison of the available phase space and the transition matrix elements of both processes. The 1P process contains one impurity scattering event and is therefore of higher order in the impurity strength D_f . On the other hand the available phase space for this process is higher, since it is not constricted by

momentum conservation. The difference in phase space yields the factor T^{-1} , relative to the Umklapp process. At high temperatures $T \gg \mu \gg D_f$, the higher phase space is more important and the conductivity behaves as $\text{Re}\sigma \sim 1/\tau_{\text{ee},g_5}^\infty$. The same reasoning qualitatively still applies once we take Luttinger liquid renormalization into account in Sec. 3.3.

Naively, one might think that, in the spirit of the Drude theory, or the memory function formalism, with the memory function expanded to lowest order in disorder and interaction, the high-frequency scattering time τ_{ee}^∞ also defines the transport properties in the dc limit ($\omega \rightarrow 0$) with the conductivity given as $\sigma \sim \tau_{\text{ee}}^\infty$. As we will see in the next section, this assumption turns out to be true for the composite 1P and 2P processes; however, it fails for the g_5 Umklapp processes.

Low-frequency conductivity

Let us now discuss the behavior of the conductivity in the *dc* limit, $\omega \rightarrow 0$. As we have seen in the previous section, the conductivity is determined by g_5 type Umklapp processes and composite processes containing both disorder and interaction. We classified these processes according to the number of incoming electrons that change their chirality during the scattering event as 1P and 2P processes. In order to simplify the subsequent calculations we introduce effective Hamiltonians for these composite processes:

$$H_{1\text{P}} = g_{1\text{P},1} U_0 \int_{k,p,q,q'} \sum_{\eta} q \psi_{\eta}^{\dagger}(k) \psi_{\bar{\eta}}^{\dagger}(p) \psi_{\eta}(q) \psi_{\eta}(q') + \text{H.c.}, \quad (3.40)$$

$$H_{2\text{P}} = g_{2\text{P}} U_0 \int_{k,p,q,q'} \sum_{\eta} k q \psi_{\eta}^{\dagger}(k) \psi_{\eta}^{\dagger}(p) \psi_{\bar{\eta}}(q) \psi_{\bar{\eta}}(q'), \quad (3.41)$$

with the coupling constants

$$g_{1\text{P},1} = \sqrt{2} \frac{g_5}{k_0^2} \quad \text{and} \quad g_{2\text{P}} = 8 \frac{g_3 k_F}{k_0^4}. \quad (3.42)$$

These operators appear in the second order of the perturbative RG procedure performed in App. C. The RG is most conveniently performed in the bosonized language and we obtain the operators in Eqs. (3.40) and (3.41) by refermionization. Their coupling constants are fixed by demanding that the high-frequency scattering rate calculated with the composite operators reproduces the results obtained by the perturbative expansion of the T-matrix in (3.36). In the values of the coupling constants we neglected terms $\propto D_b$ since they are accompanied by powers of k_F/k_0 making them subleading.

To study transport behavior in the *dc* limit we explicitly solve the kinetic equation (3.25) for the distribution function $g_{\eta_1}(k_1, \omega)$ in the limit $\omega \rightarrow 0$ for each of the composite scattering processes in Eqs. (3.40) and (3.41) and the g_5 Umklapp process in Eq. (3.16b), separately. Once the distribution functions are known, we obtain the contribution of each process to the conductivity through Eq. (3.28). To lowest order in the coupling constants, the conductivity is then just the sum of all individual contributions. Some details of this calculation are outlined in App. B of Ref. [85]. As a result we obtain the conductivity for $\omega \rightarrow 0$ in the form

$$\sigma(\omega = 0) = \frac{2e^2 v_F}{h} \left(\tau_{\text{ee},g_5}^{-1} + \tau_{\text{ee},1\text{P}}^{-1} + \tau_{\text{ee},2\text{P}}^{-1} \right)^{-1} \quad (3.43)$$

Here, the dc transport scattering rate of the clean system reads as

$$\tau_{\text{ee},g_5}^{-1} \simeq g_5^2 \left(\frac{T}{v_F k_0} \right)^4 T f_{\text{dc}} \left(\frac{\mu}{T} \right) \quad (3.44)$$

The function $f_{dc}(\tilde{\mu})$ behaves as $f_{dc}(\tilde{\mu}) \simeq 71.4$ for $\tilde{\mu} \ll 1$ and $f_{dc}(\tilde{\mu}) \simeq 1.2 \tilde{\mu}^5 \exp(-\tilde{\mu})$ in the limit $\tilde{\mu} \gg 1$.

The rates due to composite processes take the form

$$\begin{aligned} \tau_{ee,1P}^{-1} &\simeq 4.3 g_5^2 D_f \left(\frac{T}{v_F k_0} \right)^4, \\ \tau_{ee,2P}^{-1} &\simeq 1.5 \times 10^3 g_3^2 D_f \left(\frac{k_F}{k_0} \right)^2 \left(\frac{T}{v_F k_0} \right)^4. \end{aligned} \quad (3.45)$$

It is instructive to compare these rates with the ones obtained in the high-frequency limit. Let us first consider the clean system at high temperatures, $T \gg \mu$. In this regime the high-frequency rate in Eq. (3.31) and the dc rate in Eq. (3.44) are parametrically identical - they differ only by a factor of order unity. On the other hand, in the low temperature regime, $T \ll \mu$, the rates in Eqs. (3.33) and (3.44) differ by a parametrically large factor $\tau_{ee,g5}/\tau_{ee,g5}^\infty \sim \mu/T \gg 1$. This discrepancy can be attributed to the Pauli blocking of the state at the Dirac point. As we have discussed, each g_5 process involves one incoming or outgoing particle that occupies the state at exactly zero momentum. At high frequencies the state is frequently emptied due to the applied field. In the dc limit this can only happen due to thermal fluctuations that are suppressed as T/μ at low temperatures.

Finally, by comparing the scattering rates of composite events in the high-frequency regime (3.45) and the low-frequency regime (3.36), we see that they are identical up to a numerical prefactor.

We summarize, that the only parametric discrepancy between high and low-frequency transport scattering rates occurs in the clean rate for temperatures $T \ll \mu$, where the g_5 term is exponentially suppressed anyway. Hence, we conclude that the conductivity behaves Drude-like with the effective scattering rate $\tau_{ee}^{-1}(T) \simeq \tau_{ee,g5}^{-1}(T) + \tau_{ee,1P}^{-1}(T) + \tau_{ee,2P}^{-1}(T)$. That means the conductivity has the form

$$\sigma(\omega, T) = \frac{2e^2}{h} \frac{\tau_{ee}(T)}{1 - i\omega\tau_{ee}(T)}. \quad (3.46)$$

At the moment, we will postpone a discussion of the behavior of the conductivity to Sec. 3.4 after we have included the effect of Luttinger liquid renormalizations.

3.3 Bosonization: The disordered helical Luttinger liquid

In this section, we bosonize the helical Luttinger model which allows us to take forward scattering interactions, g_2 and g_4 , into account exactly.

To this end we first perform a Fourier transform of the model in Eqs. (3.16a)-(3.16c) to real space. The quadratic part of the Hamiltonian and the electron-electron forward scattering can be written similar to a conventional spinless Luttinger model as

$$H_0 = -iv_F \sum_{\eta} \int dx \psi_{\eta}^{\dagger} \partial_x \psi_{\eta} \quad (3.47)$$

and the Hamiltonian of electron-electron forward scattering reads as

$$H_4 + H_2 = \sum_{\eta, \eta'} \int dx (g_4 \delta_{\eta, \eta'} + g_2 \delta_{\bar{\eta}, \eta'}) \rho_{\eta} \rho_{\eta'}, \quad (3.48)$$

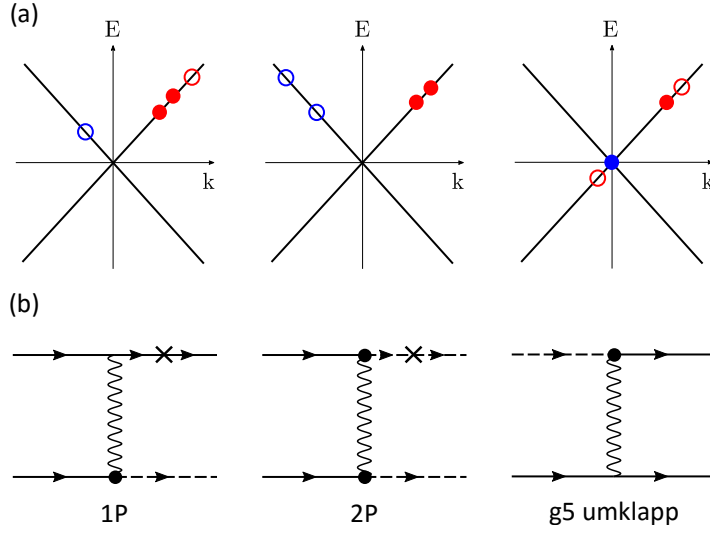


Figure 3.4: (a) Momentum configurations for two particle scattering in a HLL in the most important scattering channels. Full (empty) circles denote thermally occupied (empty) states. (b) Diagrammatic representation of the scattering amplitude of the scattering processes. Here, full (dotted) lines denote right- (left-) moving quasiparticles, wiggly lines denote electron-electron interaction, crosses represent scattering off an impurity and full circles denote the spin-momentum locking vertex factors $b_{\eta_{out}, \eta_{in}}(k_{out}, k_{in})$. “1P” and “2P” scattering processes denote effective inelastic scattering processes, that contain both electron-electron interaction and scattering off impurities, in which one and both of the incoming particles, respectively, change their chirality. Due to the presence of disorder, the total momentum is not conserved during the scattering. In the g_5 Umklapp term the incoming particle has to sit directly at the Dirac point, due to kinematic restraints set by momentum and energy conservation.

with the chiral densities $\rho_\eta = \psi_\eta^\dagger \psi_\eta$. Note, that we dropped the g_1 term in the expression above. For spinless electrons, this term is similar to the g_2 term, but contains more spatial gradients making it less relevant in the RG sense.

Next, the Umklapp part takes the form

$$H_3 = g_3 k_0^{-4} \sum_\eta \int dx (\partial_x^2 \psi_\eta^\dagger) \psi_\eta^\dagger \psi_\eta (\partial_x^2 \psi_\eta) \quad (3.49)$$

$$H_5 = g_5 k_0^{-2} \sum_\eta \int dx (\partial_x \rho) \left[(\partial_x \psi_\eta^\dagger) \psi_\eta + \text{H.c.} \right] \quad (3.50)$$

where $\rho = \rho_+ + \rho_-$ denotes the total fermionic density.

Finally, the disorder Hamiltonians read as

$$H_f = \sum_\eta \int dx U(x) \psi_\eta^\dagger(x) \psi_\eta(x) \quad (3.51)$$

$$H_b = k_0^{-2} \sum_\eta \int dx U(x) \left[\psi_\eta^\dagger \partial_x^2 \psi_\eta - (\partial_x^2 \psi_\eta^\dagger) \psi_\eta \right] \quad (3.52)$$

For weak interaction and disorder potentials, all relevant scattering processes take place close to the Fermi points. It is then convenient to introduce new fermionic fields R and L , for left- and right moving electrons, whose momenta are measured from the Fermi points. In real space this corresponds to the transformation

$$\psi_+(x) = R(x) e^{ik_F x}, \quad \psi_-(x) = L(x) e^{-ik_F x}. \quad (3.53)$$

As we have mentioned, the forward scattering term can be treated exactly using bosonization, with the fermionic fields represented in terms of the bosonic field $\varphi(x)$ and its dual field $\theta(x)$ as

$$R(x) = \frac{1}{\sqrt{2\pi a}} e^{i\sqrt{\pi}[\varphi(x) - \theta(x)]}, \quad (3.54)$$

$$L(x) = \frac{1}{\sqrt{2\pi a}} e^{-i\sqrt{\pi}[\varphi(x) + \theta(x)]}. \quad (3.55)$$

Here, $a \sim k_0^{-1}$ is the short-distance cutoff of the theory.

Since the subsequent calculations are most conveniently performed in the framework of a field theoretical description we also switch to the action $S = \int dx d\tau \{i\Pi \partial_\tau \varphi + H[\varphi, \Pi]\}$, where the canonical momentum is given by $\Pi = -\partial_x \theta$. The quadratic part of the helical Luttinger model including electron-electron forward scattering then takes the form

$$S_{LL} = \int dx d\tau \left\{ -i\partial_x \theta \partial_\tau \varphi + \frac{v}{2} [K(\partial_x \theta)^2 + K^{-1}(\partial_x \varphi)^2] \right\}. \quad (3.56a)$$

Here, K denotes the Luttinger parameter and v the plasmon velocity. In terms of the interaction parameters g_2 and g_4 they are given by

$$K = \sqrt{\frac{1 + \frac{g_4}{2\pi v_F} - \frac{g_2}{2\pi v_F}}{1 + \frac{g_4}{2\pi v_F} + \frac{g_2}{2\pi v_F}}} \quad \text{and} \quad v = v_F \sqrt{\left(1 + \frac{g_4}{2\pi v_F}\right)^2 - \left(\frac{g_2}{2\pi v_F}\right)^2}. \quad (3.56b)$$

Performing the bosonization procedure for the Umklapp part yields

$$S_3 = g_3 \frac{2}{\pi k_0^4 a^4} \int dx d\tau [(\partial_x \tilde{\varphi})^2 - (\partial_x \theta)^2] \cos(4\sqrt{\pi} \tilde{\varphi}), \quad (3.56c)$$

$$S_5 = g_5 \frac{2}{\pi k_0^2 a} \int dx d\tau (\partial_x^2 \tilde{\varphi})(\partial_x \theta) \sin(2\sqrt{\pi} \tilde{\varphi}), \quad (3.56d)$$

where we defined $\tilde{\varphi} \equiv \varphi - k_F x / \sqrt{\pi}$. Similarly, the disorder terms take the form

$$S_f = \frac{1}{\sqrt{\pi}} \int dx d\tau \mathcal{U}_f(x) \partial_x \varphi, \quad (3.56e)$$

$$S_b = -\frac{1}{2\pi k_0^2 a} \int dx d\tau \mathcal{U}_b(x) [\pi \partial_x \theta \partial_x \tilde{\varphi} + i\sqrt{4\pi} \partial_x^2 \theta] e^{-i\sqrt{4\pi} \tilde{\varphi}} + \text{H.c.} \quad (3.56f)$$

The forward and backward scattering impurity potentials are defined by the correlation functions

$$\langle \mathcal{U}_f(x) \mathcal{U}_f(x') \rangle_{\text{dis}} = D_f \delta(x - x'), \quad \langle \mathcal{U}_b(x) \mathcal{U}_b^*(x') \rangle_{\text{dis}} = D_b \delta(x - x') \quad (3.56g)$$

and zero for all other correlators.

Unlike in the Luttinger liquid model, the forward scattering term can not be removed by a gauge transformation of the field φ as we outlined in Sec. 1.4.1. The conventional shift $\varphi \rightarrow \varphi + \int^x dy \mathcal{U}_f(y) K / (v\sqrt{\pi})$ removes the term S_f from the action but reintroduces the disorder fields \mathcal{U}_f in the argument of the cosine of the Umklapp terms. As we have seen in the perturbative calculation of the conductivity for weak interaction strength, disorder forward scattering plays an important role for the transport properties of the disordered HLL by generating composite scattering processes when combined with Umklapp scattering.

The composite 1P and 2P processes appear in the second order of the perturbative RG procedure performed in App. C and have to be included into the action. They read as

$$\begin{aligned} S_{1P} &= g_{1P,1} (va)^{-1} \int dx d\tau \mathcal{U}_f(x) \partial_x^2 \theta \sin(\sqrt{4\pi} \varphi - 2k_F x) \\ &\quad + g_{1P,2} (va^2)^{-1} \int dx d\tau \mathcal{U}_f(x) \partial_x \theta \cos(\sqrt{4\pi} \varphi - 2k_F x), \\ S_{2P} &= g_{2P} (va^4)^{-1} \int dx d\tau \mathcal{U}_f(x) \sin(\sqrt{16\pi} \varphi - 4k_F x). \end{aligned} \quad (3.56h)$$

The values of the coupling constants at the UV scale are given in Eq. (3.42). They are fixed by the condition that the operators reproduce the results of the fermionic perturbation theory.³

We now perform the disorder average using the replica trick, as discussed in the Sec. 1.4. If we are interested in the behavior of the system at energy scales $\epsilon = \max(T, \omega) \ll \mu$, we can neglect terms in the action that are higher order in spatial derivatives, since they are less relevant in the RG sense.

³Note that the term with coupling constant $g_{1P,2}$ does not contribute to the conductivity in the lowest order of perturbation theory. Its value would have to be fixed by the perturbative calculation of other observables.

This yields the action of the *disordered helical Luttinger liquid*

$$\begin{aligned}
S_{\text{LL}} &= \sum_n \int dx d\tau \left\{ -i\partial_x \theta_n \partial_\tau \varphi_n + \frac{v}{2} [K(\partial_x \theta_n)^2 + K^{-1}(\partial_x \varphi_n)^2] \right\}, \\
S_3 &= \lambda_3 \frac{v}{a^2} \sum_n \int dx d\tau \cos(4\sqrt{\pi} \varphi_n - 4k_F x), \\
S_5 &= \lambda_{5,1} v \sum_n \int dx d\tau \partial_x^2 \theta_n \cos(2\sqrt{\pi} \varphi_n - 2k_F x) \\
&\quad - \lambda_{5,2} \frac{v}{a} \sum_n \int dx d\tau \partial_x \theta_n \sin(2\sqrt{\pi} \varphi_n - 2k_F x), \\
S_{2\text{P}} &= -\lambda_{2\text{P}} \frac{v^2}{a^3} \sum_{n,m} \int dx d\tau d\tau' \cos(2\sqrt{4\pi} [\varphi_n(x, \tau) - \varphi_m(x, \tau')]), \\
S_{1\text{P}} &= -\lambda_{1\text{P},1} v^2 a \sum_{n,m} \int dx d\tau d\tau' \partial_x^2 \theta_a(x, \tau) \partial_x^2 \theta_b(x, \tau') \cos(\sqrt{4\pi} [\varphi_n(x, \tau) - \varphi_m(x, \tau')]) \\
&\quad + \lambda_{1\text{P},2} v^2 \sum_{n,m} \int dx d\tau d\tau' \partial_x^2 \theta_a(x, \tau) \partial_x \theta_b(x, \tau') \sin(\sqrt{4\pi} [\varphi_n(x, \tau) - \varphi_m(x, \tau')]), \\
S_f &= -\mathcal{D}_f \sum_{n,m} \frac{v^2}{a} \int dx d\tau d\tau' \partial_x \varphi_n(x, \tau) \partial_x \varphi_m(x, \tau'), \\
S_b &= -\mathcal{D}_b \frac{v^2}{a} \sum_{n,m} \int dx d\tau d\tau' \partial_x \theta_n(x, \tau) \partial_x \theta_m(x, \tau') \cos(\sqrt{4\pi} [\varphi_n(x, \tau) - \varphi_m(x, \tau')]).
\end{aligned} \tag{3.57}$$

Here, $n, m = 1, \dots, N$ denote replica indices, where N is the number of replicas, and we defined the dimensionless coupling constants of the Umklapp terms $\lambda_3 = g_3 2k_F^2 / \pi^2 v k_0^4 a^2$, $\lambda_{5,1} = g_5 2k_F / \sqrt{\pi^3} v k_0^2 a$ and $\lambda_{5,2} = g_5 8k_F^2 / \sqrt{\pi^3} v k_0^2$, the dimensionless coupling constants of the composite terms $\lambda_{1\text{P},1} = g_{1\text{P}}^2 D_f / 4a^3 v^4$, $\lambda_{1\text{P},2} = g_{1\text{P},2}^2 g_{1\text{P},1}^2 D_f / 2a^3 v^4$ and $\lambda_{2\text{P}} = g_{2\text{P}}^2 D_f / 4(av)^4$ and the dimensionless coupling constants of the disorder terms $\mathcal{D}_f = D_f a / 2\pi v^2$ and $\mathcal{D}_b = D_b k_F^2 / 2\pi v^2 a k_0^4 + D_f g_{1\text{P},2}^2 / 4a^3 v^4$.

We point out, that if the chemical potential is tuned to the Dirac point ($k_F = 0$), we have to consider the original action in Eq. (3.56a)-(3.56h) instead of the action in (3.57).

3.3.1 High-frequency conductivity of the disordered helical Luttinger liquid

We now calculate the conductivity of the helical Luttinger liquid model (3.57) in linear response. The conductivity is obtained as [52]

$$\sigma(\omega, T) = -\frac{i}{\omega} \chi(k \rightarrow 0, i k_n \rightarrow \omega + i\delta), \quad \delta = 0 +. \tag{3.58}$$

where the susceptibility contains the current-current correlation function and the so-called diamagnetic term and reads as

$$\chi(x, \tau) = \chi^{\text{dia}}(x, \tau) + \langle j(x, \tau) j(0, 0) \rangle. \tag{3.59}$$

Here, the brackets include both the average over disorder and the average over quantum fluctuations described by the action in Eq. (3.57). In the presence of an electromagnetic field we couple the vector

potential to the canonical momentum via the minimal substitution $\partial_x \theta \rightarrow \partial_x \theta + \frac{e}{\sqrt{\pi}} A$ [44]. The current is then obtained by varying the action with respect to the vector potential

$$j = \delta S / \delta A|_{A=0} \quad (3.60)$$

and the diamagnetic susceptibility is obtained as

$$\chi^{\text{dia}}(x - x', \tau - \tau') = - \left\langle \frac{\delta S}{\delta A(x, \tau) \delta A(x', \tau')} \right\rangle \Big|_{A=0}. \quad (3.61)$$

Note that the vector potential does not only couple to the free action but also to the perturbations in Eq. (3.57). Therefore, we get additional contributions to the current and the diamagnetic susceptibility proportional to the coupling constants of the perturbations. These have to be taken into account in the perturbative calculation of the conductivity as well.

In the absence of any perturbations, the current is given by

$$j_0(x, \tau) = \frac{eKv}{\sqrt{\pi}} \partial_x \theta(x, \tau) \quad (3.62)$$

and the diamagnetic susceptibility is

$$\chi_0^{\text{dia}}(x - x', \tau - \tau') = \frac{e^2 v K}{\pi} \delta(x - x') \delta(\tau - \tau'). \quad (3.63)$$

From this we obtain the conductivity of a free HLL in linear response according to Eqs. (3.58) and (3.59):

$$\sigma_0(\omega) = \frac{2e^2}{h} \frac{ivK}{\omega + i\delta}. \quad (3.64)$$

The real part of the conductivity is therefore a simple delta peak, with *Drude weight* ivK . The system is a perfect conductor with infinite static conductivity [35]. To obtain a finite real part of the conductivity, which leads to dissipation in the system, we perform a perturbative expansion of the susceptibility to lowest nontrivial order in the considered scattering mechanism. In order to treat the effect of scattering processes perturbatively the corresponding scattering rate has to be the lowest energy scale in the problem. In particular we have to require $\omega \gg \tau_{ee}^{-1}$ which means the perturbative treatment only allows us to calculate the *ac* conductivity.

In the following, we will first discuss the conductivity in the clean case and then in the presence of disorder. Some details of the calculation are summarized in the Appendix B.2.

Clean case

In the weakly interacting case, we have identified the g_5 Umklapp interaction as the main source of resistivity in a clean system. Let us now study the conductivity induced by this process in the bosonic language. To lowest order in the coupling g_5 and in the regime $\omega, T \ll \mu$ we obtain the conductivity $\sigma = \sigma_0 + \sigma_{g_5}$, with

$$\sigma_{g_5}(\omega, T) = \left(\frac{g_5}{v} \right)^2 \frac{i}{\omega^3} \frac{e^2 v}{\pi} \left(\frac{k_F}{k_0} \right)^2 \mathcal{I}_K(\omega, T) \quad (3.65)$$

where the function $\mathcal{I}_K(\omega, T)$ is defined in Eq. (B.26) in the Appendix. The imaginary part of the conductivity (3.65) renormalizes the zeroth order result (3.64), which amounts to replacing the Luttinger parameter and plasmon velocity by their renormalized values at given energy scale $\epsilon = \max(T, \omega)$. Here, we are interested solely in the real part of the conductivity. It is useful to express the conductivity through the high-frequency scattering rate as $\text{Re } \sigma = \frac{e^2 v_F}{\pi \omega^2} (\tau_{ee}^\infty)^{-1}$ and to discuss the effective rate in the limit of low $T \ll \omega$ and high $T \gg \omega$ temperatures.

In the regime $\mu \gg \omega \gg T$ we obtain

$$\frac{1}{\tau_{g_5}^\infty(\omega)} \simeq f_1(K) \left(\frac{g_5}{v} \right)^2 \frac{v^2 k_F^2}{\omega} (k_F a)^{2K+2} e^{-\frac{\mu}{T}} e^{\frac{\omega}{2T}}. \quad (3.66)$$

where we defined the positive, dimensionless function

$$f_1(K) = -\frac{16}{\pi^3} \frac{1}{(k_0 a)^4} \sin(\pi K)^2 K^2 \left[(6+K)\Gamma(-K)\Gamma(-K-3) + \Gamma(-1-K)^2 \right]. \quad (3.67)$$

Note, that we did not discuss the regime $\omega \gg T$ beforehand, because it lies outside the region of applicability of the kinetic equation. We will return to this point at the end of this section

For high temperatures $\omega \ll T$, on the other hand, we obtain the transport rate

$$\frac{1}{\tau_{g_5}^\infty(\omega)} \simeq \frac{f_1(K)}{2} \left(\frac{g_5}{v} \right)^2 \frac{v^2 k_F^2}{T} (k_F a)^{2K+2} e^{-\frac{\mu}{T}}. \quad (3.68)$$

For weakly interacting electrons, $K \rightarrow 1$, $v \rightarrow v_F$, this agrees with the result obtained in the kinetic equation approach in Eq. (3.33). For a qualitative discussion of the behavior of the conductivity we refer to Sec. 3.4.

Note, that we could also have obtained the parametric dependence of (3.68) by scaling arguments. The full conductivity, apart from an unimportant numerical prefactor, can be obtained by substituting the renormalized coupling constant $g_5(\epsilon)$ into the equation for the scattering rate in Eq. (3.33). If one neglects the scaling of K , which only starts at order g_5^2 , the renormalized coupling can be obtained by power counting. The scaling dimension of the action in Eq. (3.56d) is $\Delta_{g_5} = K + 3$. It is important to realize that this scaling includes both the gradient terms, which are already included in the weak coupling result and the scaling of the cosine-operator which includes information about the Luttinger liquid renormalization. On this basis, the renormalized coupling constant reads as

$$g_5(\epsilon) = g_5 \left(\frac{\epsilon}{v k_0} \right)^{K+1}, \quad (3.69)$$

where we used that the renormalization only sets in on scales $v k_0 \ll \Lambda$. Above this scale all interactions that mix left- and right movers contain strongly oscillating terms and can be neglected. For a finite interaction radius, $d_0 \ll 1/k_0$, on the other hand, the UV cutoff would be of the order of v/d_0 (compare the discussion in Ch. 4.3).

Finally, we can make predictions about the regime of $\omega, T \gg \mu$. In this limit the system effectively behaves as if the chemical potential were at the Dirac point. To zeroth order we thus have to calculate the conductivity in the presence of the original g_5 term in Eq. (3.56d) at $k_F = 0$. Instead of performing the calculation explicitly, we will use the scaling arguments we just discussed to obtain the behavior of the conductivity. Substituting the renormalized coupling constant in Eq. (3.69) into the high-frequency

rate in Eq. (3.34) we obtain the renormalized rate

$$\frac{1}{\tau_{g_5^\infty}(\epsilon)} \sim \left(\frac{g_5(\epsilon)}{v} \right)^2 \epsilon = \left(\frac{g_5}{v} \right)^2 \left(\frac{\epsilon}{vk_0} \right)^{2K+2} \epsilon. \quad (3.70)$$

The parametric dependence of the clean conductivity as a function of the frequency or the temperature will be discussed in Sec. 3.4.

To summarize, we find, that for strong interactions, the power law exponents in the scattering rate are functions of the Luttinger parameter. Thereby, the correct parametric dependence of the scattering rate can be obtained by substituting the renormalized coupling constants at energy scale ϵ into the weak coupling kinetic equation results. Additionally, the combination of bosonization and the linear response calculation allows us to make predictions for the frequency range $\omega \gg T$, beyond the applicability of the kinetic equation formalism. In the kinetic equation the external field is treated classically, so it cannot be applied if the frequency becomes larger than the temperature. In this case one has to quantize the electric field and treat the interaction of photons with the electrons quantum mechanically. This regime becomes accessible in the present formalism.

Disordered case

In the presence of disorder the conductivity has additional contributions due to the composite 1P and 2P processes. One could naively expect that also the term S_b , that describes backscattering off disorder dressed by electron-electron forward scattering yields a finite contribution to the conductivity. However, we find that this contribution vanishes exactly, independently of the value of K .

If we calculate the conductivity in linear response to leading order in the coupling constants λ_{1P} , λ_{2P} and \mathcal{D}_b , we obtain

$$\sigma_{1P}(\omega, T) = \lambda_{1P,1} \frac{i}{\omega^3} \frac{e^2 v}{\pi} \frac{8v^3 K}{a^3} \left(\frac{\pi a T}{v} \right)^{2K+4} (3\mathcal{J}_{2K+4}(\omega, T) - 2\mathcal{J}_{2K+2}(\omega, T)), \quad (3.71)$$

$$\sigma_{2P}(\omega, T) = \frac{i}{\omega^3} \frac{e^2 v}{\pi} \frac{32\pi v^3 K^2}{a^3} \lambda_{2P} \left(\frac{\pi a T}{v} \right)^{8K} \mathcal{J}_{8K}(\omega, T), \quad (3.72)$$

$$\sigma_b = 0, \quad (3.73)$$

where $\mathcal{J}_{2K}(\omega, T)$ is defined in Eq. (B.20).

First, let us discuss the conductivity due to the composite operators in the limit of low and high temperature. To this end we again express the conductivity through the high-frequency scattering rate as $\text{Re } \sigma = \frac{e^2 v_F}{2\pi\omega^2} (\tau_{ee}^\infty)^{-1}$ and substitute the value of the coupling constants λ_{2P} and $\lambda_{1P,1}$ by their definition below (3.57).

In the limit $T \gg \omega$ this yields

$$\begin{aligned} \frac{1}{\tau_{ee,1P}^\infty} + \frac{1}{\tau_{ee,2P}^\infty} &= \frac{D_f}{v} \frac{1}{(ak_0)^4} \frac{2^6 K^4}{\pi^4} \left[4 \left(\frac{g_3}{v} \right)^2 \frac{\Gamma^2(4K)}{\Gamma(8K)\pi^4} \left(\frac{k_F}{k_0} \right)^2 \frac{1}{(ak_0)^2} \left(\frac{2\pi a T}{v} \right)^{8K-2} \right. \\ &\quad \left. + \left(\frac{g_5}{v} \right)^2 \frac{(K+1)}{\Gamma(2K+4)} \Gamma^2(K+1) \left(\frac{2\pi a T}{v} \right)^{2K+2} \right] \end{aligned} \quad (3.74)$$

and for $T \ll \omega$

$$\frac{1}{\tau_{ee,1P}^\infty} + \frac{1}{\tau_{ee,2P}^\infty} = \frac{D_f}{v} \left(\frac{v_F}{v}\right)^2 \frac{1}{(ak_0)^4} \frac{2^6 K^4}{\pi^4} \left[4 \left(\frac{g_3}{v}\right)^2 \frac{1}{\Gamma(8K)\pi^4} \left(\frac{k_F}{k_0}\right)^2 \frac{1}{(ak_0)^2} \left(\frac{a\omega}{v}\right)^{8K-2} + \left(\frac{g_5}{v}\right)^2 \frac{3}{K\Gamma(2K+4)} \left(\frac{\omega a}{v}\right)^{2K+2} \right] \quad (3.75)$$

In both limits the transport scattering rate behaves as a power law of temperature and frequency, where the exponent is a function of the Luttinger parameter. As in the clean case we could have derived the parametrical form of these rates by substituting the renormalized coupling constants

$$g_3(\epsilon) = g_3 \left(\frac{\epsilon a}{v}\right)^{4K-2}, \quad g_5(\epsilon) = g_5 \left(\frac{\epsilon a}{v}\right)^{K+1}, \quad (3.76)$$

at the scale $\epsilon = \max(T, \omega)$ into the results for $K = 1$ in Eq. (3.36). For a discussion of the conductivity of the disordered HLL we refer to Sec. 3.4

Now, let us discuss the result that the disorder backscattering term in Eq. (3.57) yields no finite conductivity even when dressed with arbitrarily strong forward scattering electron-electron interaction. In Appendix B.2 we show that, to the leading order in disorder strength D_b , the backscattering term does not lead to a finite scattering time for any value of K . Recall that the term $S_{\text{imp},b}$ originates from backscattering off impurities and should therefore have no impact on transport on its own in the absence of g_2 interaction at $K = 1$. However, we find that the conductivity does not only vanish for $K = 1$ but for arbitrary K meaning that even the combination of g_2 interaction and backscattering off impurities does not change the conductivity. This is also consistent with our fermionic analysis in Eq. (3.36), where no terms proportional to $D_b g_2^2$ appear. It was recently shown [89] that this statement is true to any order in the perturbation series. However, at the moment of writing, the origin of this conservation law remains an open question.

3.4 Discussion of the semiclassical conductivity

Let us now combine the results obtained so far. In particular we will be interested in the temperature dependence of the semiclassical dc resistivity $\rho = \sigma^{-1}(\omega = 0)$ of the disordered HLL and in the frequency dependence of the conductivity at fixed temperature.

First, we have checked by explicit calculation of the conductivity of weakly interacting electrons in the ac limit in Sec. 3.2.1 and in the dc limit in Sec. 3.2.1, that the conductivity behaves Drude like as

$$\sigma(\omega, T) = \frac{2e^2}{h} \frac{\tau_{ee}(\epsilon)}{1 - i\omega\tau_{ee}(\epsilon)}. \quad (3.77)$$

where $\tau_{ee}^{-1} = \tau_{ee,g_5}^{-1} + \tau_{ee,1P}^{-1} + \tau_{ee,2P}^{-1}$ is the renormalized scattering rate at energy scale ϵ . The effect of Luttinger liquid renormalizations on the rate can thereby be incorporated by substituting the renormalized interaction constants (3.76) into the kinetic equation results.

Combining the results of our different approaches, we obtain the dc resistivity $\rho = h/2e^2\tau_{ee}^{-1}$, with

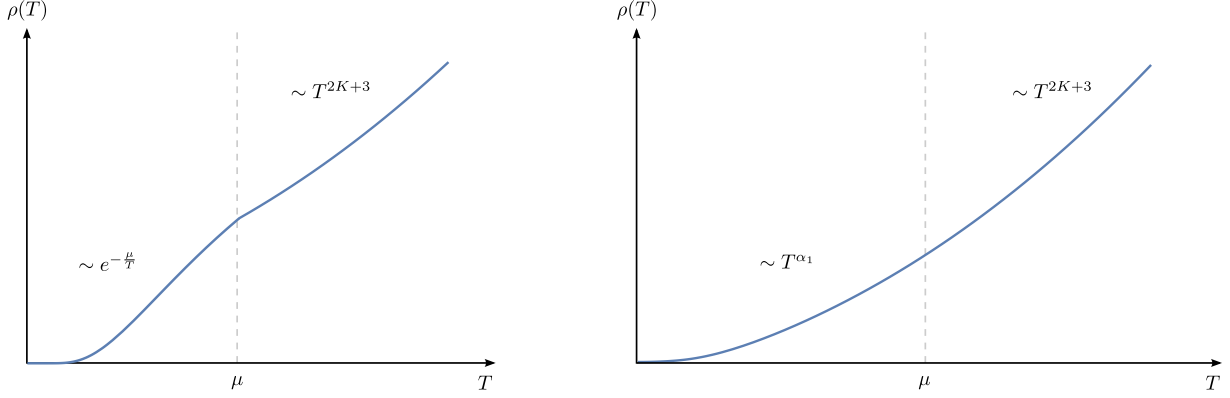


Figure 3.5: Behavior of the dc resistivity of the clean (left) and disordered (right) HLL as a function of temperature. At high temperatures the main source of resistivity is provided by g_5 Umklapp processes which yields $\rho \propto T^{2K+3}$. These scattering processes become thermally activated at temperatures $T < \mu$ and thus the behavior of the resistivity of the disordered HLL is dominated by the composite 1P and 2P processes instead. These scattering processes yield a behavior $\rho \propto T^{\alpha_1}$, with the exponent $\alpha_1 = 2K + 2$, for $K > 2/3$ and $\alpha_1 = 8K - 2$, for $K < 2/3$. At zero temperature the resistivity goes to zero, as long as $K > 1/2$.

the scattering rates

$$\begin{aligned}
 \tau_{ee,g5}^{-1} &\propto g_5^2 f_{dc} \left(\frac{\mu}{T} \right) \left(\frac{\epsilon}{vk_0} \right)^{2K+2} \epsilon, \\
 \tau_{ee,1P}^{-1} &\propto g_5^2 \left(\frac{\epsilon}{vk_0} \right)^{2K+2} D_f, \\
 \tau_{ee,2P}^{-1} &\propto g_3^2 \left(\frac{k_F}{k_0} \right)^2 \left(\frac{\epsilon}{vk_0} \right)^{8K-2} D_f,
 \end{aligned} \tag{3.78}$$

where $\epsilon = \max(\mu, T)$ and $f_{dc}(\tilde{\mu})$ behaves as $f_{dc}(\tilde{\mu}) = \text{const.}$ for $\tilde{\mu} \ll 1$ and $f_{dc}(\tilde{\mu}) \sim \tilde{\mu}^5 \exp(-\tilde{\mu})$ in the limit $\tilde{\mu} \gg 1$. The exact prefactors of the rates are in general functions of the Luttinger parameter and the dimensionless ratio ω/T and are difficult to obtain in general. Here, we will only discuss the parametric dependence of the total rate, which in turn determines the behavior of the resistivity.

The resistivity as a function of temperature is plotted schematically in Fig. 3.5 for both the clean (left) and disordered (right) HLL. In both cases the resistivity mirrors the behavior of the renormalized scattering rate τ_{ee}^{-1} and we can discuss them on equal footing. At high temperatures, the transport rate is dominated by the contribution of g_5 Umklapp terms and hence the resistivity decreases as temperature is decreased as $\rho \sim T^{2K+3}$. For temperatures $T \ll \mu$, the Umklapp term becomes thermally activated due to Pauli blocking of states close to the Dirac point. Hence, in the clean HLL the resistivity decreases exponentially as temperature is lowered reaching zero at $T = 0$. In the disordered case, on the other hand, the resistivity at low temperatures is determined by either 1P or 2P processes and decreases as a power law $\rho \sim T^{\alpha_1}$. The exponent is $\alpha_1 = 2K + 2$ for $K > 2/3$ and $\alpha_1 = 8K - 2$ for $1/2 < K < 2/3$. In any case the resistivity vanishes at zero temperature, due to the absence of phase space for inelastic scattering events. For even stronger interaction $K < 1/2$, electron-electron interactions become relevant

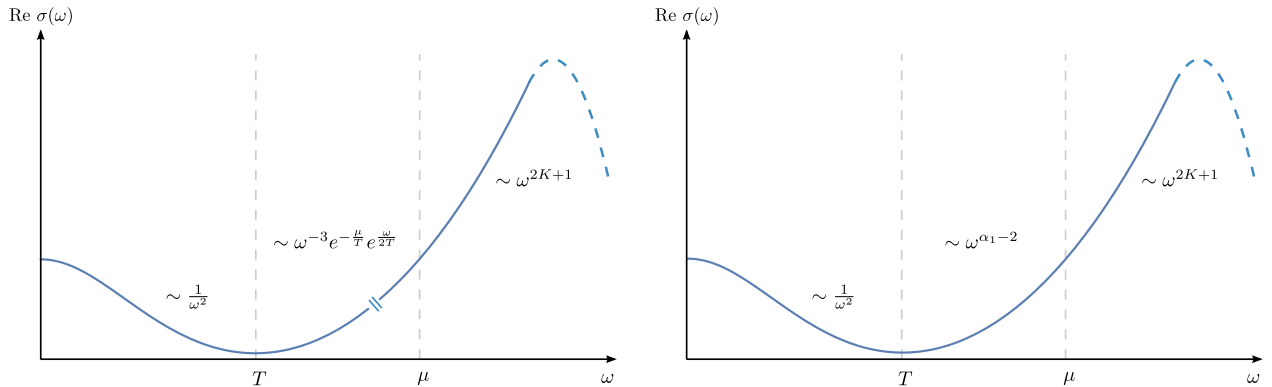


Figure 3.6: The real part of the conductivity of the clean (left) and disordered (right) HLL as a function of frequency. The behavior of the curves is discussed in the main text.

in the RG sense and a perturbative treatment is no longer viable. We discuss the behavior in this regime in the next section.

We have also studied the frequency dependence of the real part of the conductivity, which is plotted for the exemplary case $T < \mu$ in Fig. 3.6 for both the clean (left) and disordered (right) HLL. Let us first discuss the clean case. At high frequencies the conductivity is proportional to the renormalized scattering rate $\text{Re } \sigma \sim 1/\omega^2 \tau_{ee}(\omega)$, which yields a power law behavior $\text{Re } \sigma \sim \omega^{2K+1}$. At frequencies below the chemical potential the Umklapp process becomes thermally activated due to the Pauli blocking of the state at the Dirac point. The conductivity thus decreases as $\sim \omega^3 \exp(-\mu + 2\omega/2T)$ down to exponentially small values at frequencies of the order of the temperature. At even lower frequencies, the conductivity behaves Drude like with the renormalized scattering rate $\tau_{ee}(T)$, this means it begins to grow again as $\sim \omega^{-2}$ as frequency is lowered reaching a finite dc value at zero frequency. The dotted line at highest frequencies indicates that the conductivity has to decrease at frequencies above the UV scale of our theory $\sim vk_0$, lest the theory becomes unstable – remember that the real part of the conductivity at frequency ω is proportional to the average dissipated energy in the system in response to a ac field with frequency ω .

Now, let us turn to the discussion of the conductivity of the disordered HLL. Similarly, to the discussion above the conductivity behaves as a power law of frequency, where the power is determined by the dominant scattering mechanism. For frequencies $\omega \gg \mu$, the g_5 Umklapp process yields $\text{Re } \sigma \sim \omega^{2K+1}$. At lower frequencies the transport scattering rate is dominated by the composite 1P or 2P processes and we find $\text{Re } \sigma \sim \omega^{\alpha_1-2}$, with $\alpha_1 = 2K + 2$, for $K > 2/3$ and $\alpha_1 = 8K - 2$, for $K < 2/3$. At even lower frequencies, $\omega < T$, the renormalization of the scattering rate is cut at scales of the order of the temperature and the conductivity behaves as $\text{Re } \sigma \sim 1/\omega^2 \tau_{ee}(T)$, before transitioning into the dc regime where $\text{Re } \sigma \sim \tau_{ee}(T)(1 - \omega^2 \tau_{ee}^2(T))$.

Corrections to the quantized conductance of short edges. The electron-electron transport rate can also be used to make predictions about other physical quantities relevant for transport. In particular the dc conductance of a short edge with length $L \ll \ell_{ee}$ can be obtained as [57]

$$G \simeq \frac{2e^2}{h} \left(1 - \frac{L}{\ell_{ee}(T)} \right), \quad (3.79)$$

where $\ell_{ee}(T) = v_F \tau_{ee}^\infty(T)$. Roughly speaking, the frequency defines a characteristic length scale $L_\omega =$

v_F/ω and thus an infinite system at finite frequency is expected to behave similarly to a finite system at zero frequency. Technically, we can perform the substitution $(-i\omega + 0 \rightarrow 1/L)$ in the result for the ac conductivity and obtain the conductance as $G = \sigma/L$. The behavior of the conductance as a function of temperature is thus as follows. At zero temperature, $\ell_{ee}^\infty(T) \rightarrow \infty$ and charge transport through the helical edge is characterized by a quantized conductance $G_0 = 2e^2/h$, also in the presence of nonmagnetic disorder. At higher temperatures, on the other hand, forward scattering off impurities dressed by electron-electron interaction yields a finite scattering rate and hence a correction to the quantized conductance $\delta G = G_0 - G$, with $\delta G \sim T^{\alpha_1}$, for temperatures $T \ll \mu$. At higher temperatures g_5 Umklapp processes provide the fastest scattering mechanism and yield $\delta G \sim T^{2K+3}$. This agrees with the analysis of previous works [48, 49, 90].

Comparison with experimental data. As discussed in Ch. 2.2.2, the temperature dependence of the conductance of the HLL has been measured in InAs/GaSb heterostructures in [46]. The authors estimate a Luttinger constant $K = 0.22$ in the material and obtain a temperature scaling of the conductance $G \sim T^{0.32}$. At higher temperatures or voltages the conductance saturates to the quantized value $G_0 = 2e^2/h$. The nonuniversal power law is a clear indication of Luttinger liquid physics in QSH edges. Our theory predicts a power law correction $\delta G \sim T^{8K-2}$ which would agree with the measured exponent for $K = 0.29$. However, since the correction grows and hence the conductance decreases with increasing the energy scale, the saturation cannot be explained by the model we considered.

The observed behavior of the conductivity was attributed to the scattering of quasiparticles off a Kondo impurity [47]. At high temperatures, Kondo and two-particle scattering yield logarithmic corrections to the quantized conductance, leading to the saturation at the quantized value at highest energy scales. At low temperatures and for $K < 1/4$, on the other hand, the Kondo impurity becomes screened and transport proceeds by weak tunneling through the impurity potential. In this limit the conductance is predicted to behave as $\delta G \sim T^{\frac{1}{2K}-2}$. The experimentally observed value of the power law exponent is obtained from this formula if $K = 0.21$, which fits well with the experimentally measured value.

In summary, the experiment shows clear signs of Luttinger behavior in helical edge modes, but further measurements on a variety of samples are needed to pinpoint the exact microscopic scattering mechanisms behind the temperature dependence of the conductance.

3.5 Renormalization group treatment of the disordered helical Luttinger liquid

The results of the previous sections are valid if a perturbative expansion in powers of the coupling constants is possible. However, the coupling constants of the model are subject to renormalization upon lowering the temperature. There may thus exist a critical temperature below which the system undergoes a phase transition and the perturbative description breaks down. One way to handle this problem is to study how the coupling constants change under a rescaling of the short distance cutoff $a \rightarrow a' = ab$, with $b > 1$. For an infinitesimal RG step $b = 1 + \ell$, where $\ell = \ln(a'/a)$ we can derive the perturbative renormalization group equations that determine the flow of the coupling constants. A complete derivation of these equations can be found in App. C. The set of equations for $k_F a \ll 1$ is

given by

$$\begin{aligned}
\frac{dK}{d\ell} &= -\mathcal{D}_b K(1-K)(1-2K) - \lambda_3^2 K^2 + K^2(8K-2)\lambda_{2P}, \\
\frac{dv}{d\ell} &= -\mathcal{D}_b v(1-K)(1-2K) + K(8K-2)\lambda_{2P}v, \\
\frac{d\lambda_3}{d\ell} &= (2-4K)\lambda_3 - \mathcal{D}_f \lambda_3 K^2 + 2\mathcal{D}_b \lambda_3(1-K)(1-2K), \\
\frac{d\lambda_{2P}}{d\ell} &= (3-8K)\lambda_{2P}, \\
\frac{d\mathcal{D}_f}{d\ell} &= \mathcal{D}_f, \\
\frac{d\mathcal{D}_b}{d\ell} &= (1-2K)\mathcal{D}_b.
\end{aligned} \tag{3.80}$$

The equations are perturbative in the couplings $\mathcal{D}_f, \mathcal{D}_b, \lambda_{2P}$ and λ_3 but exact in K and v . We have dropped both λ_5 and λ_{1P} terms because they are irrelevant.

There are several important aspects to these equations. First, note that the equation for the velocity decouples from the others and can thus be dropped. Second, the flow of \mathcal{D}_f decouples from the other equations in the absence of the Umklapp term $\lambda_3 \rightarrow 0$. This is a good check for the validity of the equations, since it is well known that the disorder forward scattering term can be removed by a unitary transformation of the Hamiltonian in the absence of Umklapp terms [44]. The forward scattering itself always grows under renormalization. This does not indicate any instability of the system but just mirrors the fact, that the dimensionless coupling constant $\mathcal{D}_f = D_f a / 2\pi v^2$ grows, because the short distance cutoff a grows under renormalization. In other words there is no renormalization of the dimensionful coupling constant D_f . Nonetheless, there exists a scale $\ell^* \sim -\ln(\mathcal{D}_f)$, where $\mathcal{D}_f(\ell^*)$ becomes of order unity, at which we have to cut the renormalization of λ_3 due to forward scattering off disorder. Third, the flow equation for K in general contains the dimensionless functions $c_{1,2}$ defined in Eq. (C.34) in the Appendix. The exact form of these functions is not important and does depend on the cutoff procedure. What matters is that they are essentially one as long as $k_F a \ll 1$, which is the case discussed here, and vanish for $k_F a \gg 1$. The renormalization of the Luttinger parameter coming from the Umklapp term is thus suppressed on length scales x such that $k_F x$ is of order unity. This is physically plausible since the typical length scales of an electron in thermal equilibrium are of the order of the thermal length $x \sim v_F / T$, which leads to a strongly oscillating behavior of the cosine $\cos(4\sqrt{\pi}\varphi_\alpha - 4k_F x)$ at low temperatures $\mu/T \gg 1$. In this case we can effectively neglect the cosine term. At high temperatures, on the other hand, $k_F x \simeq 0$ and we can essentially neglect the $k_F x$ term in the argument of the cosine.

After having discussed some technical points, let us now discuss the consequences of the flow on the phase diagram of the disordered HLL. The set of equations (3.80) has a line of weak coupling Luttinger liquid fixed points at $\lambda_3 = \mathcal{D}_b = \lambda_{2P} = 0$ and a set of strong-coupling fixed points at $\lambda_3 \rightarrow \infty, \mathcal{D}_b \rightarrow \infty$ and $\lambda_3 \rightarrow -\infty, \mathcal{D}_b \rightarrow -\infty$ and $|\lambda_{2P}| \rightarrow \infty, \lambda_3 = \mathcal{D}_b = 0$. At this order in the RG the coupling λ_{2P} and the couplings λ_3 and \mathcal{D}_b do not influence each other. At higher order, on the other hand, the interplay between the couplings might change the nature of the fixed points.

Note that the flow of K is determined by a competition of the disorder and Umklapp terms. If the initial value is in the range $1/2 < K_0 < 1$, the disorder term and the 2P term increase K while the Umklapp term decreases K . If we assume, that the bare values of interaction and disorder strengths are of the same order, the renormalization due to Umklapp scattering can be neglected since it only

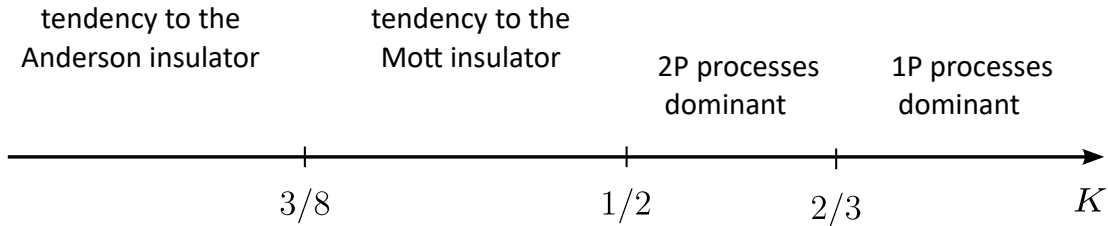


Figure 3.7: *Illustration of possible strong-coupling phases of the disordered HLL. For weak interactions $K > 1/2$ the edge is in the HLL phase. Transport at lowest temperatures is dominated by composite 1P processes for $K > 2/3$ and composite 2P processes for $K < 2/3$. For more repulsive interaction the weak coupling RG predicts multiple strong coupling phases. At $K < 1/2$ both disorder backscattering and Umklapp scattering become relevant and lead to a tendency towards a (disordered) Mott insulating phase. At $K < 3/8$ the 2P term becomes relevant, which leads to a tendency towards the Anderson insulating phase.*

appears in second order. In this case the disorder term wins and drives the system to more attractive interactions. This has important consequences for the behavior of the other coupling constants. Note that both the Umklapp term and the disorder backscattering term become relevant for $K < 1/2$ simultaneously. However, if the flow of K is to larger values, which is the case if we start with initial values above $K = 1/2$, this threshold value is never reached. Therefore, for temperatures $T \ll \mu$ or sufficiently weak interactions $K > 1/2$ our perturbative results for the conductivity in the previous section are perfectly valid. This constitutes the main result of our RG analysis.

Discussion of the strong-coupling phases. For strong repulsive interaction the weak coupling RG predicts various strong-coupling regimes. While the RG does not allow us to identify the nature of the strong-coupling phases, we can speculate on the behavior of the HLL by employing mappings to the spinless LL, whose strong-coupling fixed points are known. A plot of the values of K where, based on this mapping, different strong-coupling phases might emerge is presented in Fig. 3.7.

For $K < 1/2$ both the g_3 Umklapp term and the disorder backscattering term become relevant simultaneously and may drive the system into a strong-coupling phase. At the moment of writing this thesis, the nature of this strong-coupling fixed point is unknown. For the clean HLL with $\mathcal{D}_b = \lambda_{2P} = 0$ the theory can be mapped to the spinless Luttinger liquid at half filling with $K_{LL} = K_{HLL}/2$, which suggests that the strong-coupling fixed point corresponds to the Mott insulating phase. In this phase the field φ is pinned to one of the minima of the cosine. At zero temperature, the Umklapp term thus spontaneously breaks TRS and opens a gap in the electronic spectrum. At finite temperature, the TRS is restored by solitons that connect neighboring minima. The exponentially small density of thermally excited solitons triggers an exponentially large resistivity $\rho \sim e^{\Delta/T}$, with the excitation gap of the form $\Delta \sim vk_0(8K\lambda_{um})^{\frac{1}{2-4K}}$ [35]. In analogy to this phase we will refer to (the yet unknown) phase that emerges when both disorder and Umklapp terms become relevant as the (disordered) Mott phase.

Although, the Umklapp and disorder terms become relevant already at $K = 1/2$ neither of them leads to dissipation in our weak coupling analysis. The most important scattering mechanism at low temperatures and strong repulsive interactions is the composite 2P scattering. The corresponding term in the action becomes relevant at $K = 3/8$. It was pointed out in [87] that the model with the action $S = S_{LL} + S_{2P}$ can be mapped to the Giamarchi-Schulz model of the disordered spinless Luttinger

liquid with Luttinger parameter $K_{\text{LL}} = K_{\text{HLL}}/4$. As discussed in Sec. 1.4.3 this model exhibits a metal insulator transition with a quantum critical point at $K_{\text{LL}} = 3/2$, which corresponds to $K_{\text{HLL}} = 3/8$ in the model for the HLL. This mapping therefore suggests that the fixed point corresponds to the Anderson localized phase.

Another possible scenario is, that the topological properties of the HLL prevents the opening of a gap at the edge altogether. We speculate, that on the formal level of the effective edge theory, this “topological protection” might be related to the difference between the normal LL and HLL: The latter contains additional terms in the action namely $S_{1\text{P}}$ and S_5 . While in the weak coupling regime these are highly irrelevant, when the Umklapp, disorder and 2P terms enter the strong-coupling limit, they might become relevant again, destroying the quasi-long range order. The interplay between the different terms in higher order of the perturbative beta functions might additionally change the conclusions drawn above.

A somewhat similar situation was encountered in Ref. [15] devoted to 2D surface states of 3D topological insulators. There, the perturbative (weak-coupling) RG suggested localization due to Altshuler-Aronov-type corrections, but the topological protection remained and resulted in emergence of the critical state in the strong-coupling regime.

3.6 Summary of chapter 3

In this chapter we have discussed the transport properties of the disordered HLL that emerges at the boundaries of 2D TIs. We have demonstrated that these transport properties differ significantly from those of conventional LLs, due to the topological protection against elastic scattering and the presence of g_5 Umklapp processes, that can be thought of as unique to the HLL, since their kinetics necessarily require the presence of a Dirac point in the spectrum. In particular these Umklapp processes yield a *dc* conductivity at any temperature $T > 0$.

We have employed two complementing approaches to obtain the conductivity in a wide range of parameters. One is the kinetic equation approach (3.2.1) for weakly interacting helical fermions, that allowed us to obtain the semiclassical conductivity in the regime $\omega \ll T$. The other approach is bosonization combined with the linear response formalism which enables us to take into account Luttinger liquid effects and to describe frequencies $\omega \gg T$.

By combining both approaches we have demonstrated, that while the disordered HLL is topologically protected against elastic scattering, yielding a vanishing resistivity at $T = 0$, inelastic scattering generates a finite resistivity at $T > 0$, even in the absence of nonmagnetic impurities. For finite systems this converts into temperature dependent corrections to the quantized conductance.

Our main result concerns the behavior of the *dc* resistivity of the disordered HLL depicted in Fig. 3.5 as well as the frequency dependence of the conductivity in Fig. 3.6 and the corresponding transport scattering rates in Eq. (3.78). We find that the parametric dependence of the conductivity of a disordered HLL as a function of frequency is described by Drude’s law with the renormalized transport scattering rate $\tau_{\text{ee}}(\epsilon)$ where $\epsilon = \max(T, \omega)$. At energy scales above the chemical potential, the rate is determined by g_5 Umklapp processes. At lower energy scales, however, we find that the transport scattering rate is dominated by composite processes containing both electron-electron interaction and impurity scattering. Physically, these processes correspond to forward scattering off impurities dressed by interaction. Thereby, it is of conceptual importance that forward scattering off disorder, in contrast to disorder induced backscattering, plays the primary role in these combined effects.

Going beyond the semiclassical regime, we make predictions about possible strong-coupling regimes

using a perturbative RG analysis in Sec. 3.5. A detailed analysis of the strong-coupling phases in helical edge states remains a prospect for future work.

4 Chapter 4

Coulomb drag between helical liquids

In Ch. 3 we have studied the transport properties of helical edge states with broken spin-rotational invariance that emerge at the edges of 2D QSH insulators. One of our main findings was that dissipation in the edge states is generated solely by inelastic scattering, which microscopically originates from either electron-electron scattering or from scattering off impurities dressed by interaction. In light of the importance of electron-electron interaction for the transport properties it is desirable to study experimental setups that only probe the electron-electron interaction in helical edges disconnected from disorder scattering.

In this chapter, we therefore investigate the Coulomb drag between parallel clean edges of two identical QSH insulators, brought in proximity to each other, in the case of broken spin-rotational invariance. We assume that each of the edges hosts a single set of Kramers partners with a linear dispersion relation. In a Coulomb drag measurement, current is driven in an “active” conductor (active edge in our setup), inducing an electrical field or current in a “passive” conductor (passive edge), with the frictional force being due to electron-electron interactions, without transfer of electrons between the subsystems. As such, Coulomb drag is a sensitive probe of inelastic electron-electron scattering. For helical edges, Coulomb drag is particularly worthy of study because, as already mentioned above, inelastic electron-electron scattering is the only source of dissipation inside a single edge. A typical drag setup is depicted in Fig. 4.1. The key quantity characterizing friction is the drag resistivity,

$$\rho_D = -E_2/j_1 , \quad (4.1)$$

where j_1 is the current density driven in the active conductor and E_2 is the electric field applied to the passive conductor to compensate for the friction force and maintain zero current therein. In conventional one-dimensional systems (single-channel quantum wires), Coulomb drag has been intensively studied both theoretically [91–105] and experimentally [106–112]. In general, Coulomb drag in one dimension, independently of the particular form of the electron dispersion relation, can only occur in the presence of scattering that changes the chirality of electrons [104]. Therefore, there is no Coulomb drag between clean ideal HLLs, in which scattering between left- and right movers is strictly prohibited. Conversely, Coulomb drag between HLLs is only possible if there is a perturbation that breaks spin-rotational invariance of the edge modes.

One possibility to break the axial spin symmetry and lift the restriction on backscattering interactions between two HLLs is to apply an external magnetic (Zeeman) field [113]. However, the magnetic field also breaks TRS and generically gaps the edge modes.

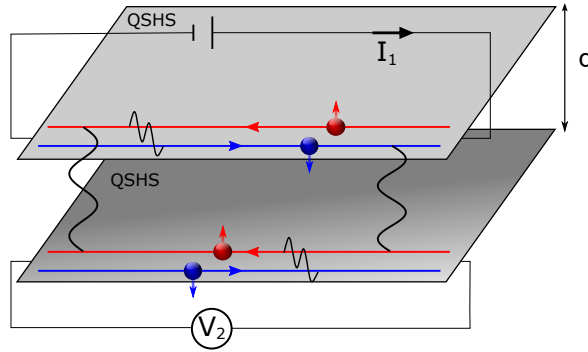


Figure 4.1: Schematics of a Coulomb drag measurement between helical edges of two QSH systems, brought into proximity of one another with distance d . Current I_1 is driven across the active edge and, through electron-electron interactions, voltage V_2 is induced in the passive edge.

Another possibility to destroy the spin-rotational invariance originates from spin-orbit coupling in the bulk of the QSH insulator. This is the model that we study in this chapter, within the framework introduced in Ch. 3 for a single helical edge. In this context it is important that, in contrast to the magnetic field-induced drag [113], TRS is preserved in this model, so that the topological nature of the edge states as Kramers partners remains intact. We will show that therefore the Coulomb drag between HLLs differs in an essential way both from Coulomb drag induced by the Zeeman field and from Coulomb drag between LLs.

The chapter is organized as follows. In Sec. 4.1, we formulate the model of two capacitively coupled helical edges with broken spin-rotational symmetry. The Coulomb drag between identical helical edges, first neglecting Luttinger liquid renormalizations, is calculated in Sec. 4.2 in the framework of a kinetic equation. The renormalization of the drag resistivity is included in Sec. 4.3, where we bosonize the theory and calculate the drag resistivity in linear response. To determine the behavior of the drag at lowest temperatures the perturbative calculation is supplemented by an RG calculation. The strong-coupling regime is discussed in Sec. 4.3.4. Section 4.5 concludes with a summary. Some of the technical details can be found in App. D.

This chapter is based in part on Ref. [114].

4.1 The model

We start by formulating our model for two helical liquids with broken spin-rotational invariance coupled by a screened Coulomb interaction (we neglect the tunneling between the edges). In substance, we employ the model proposed—for a single helical edge—introduced in Ch. 3 and extend it to the case of two edges. We consider two identical QSH systems, each with one Kramers pair at the edge, as shown in Fig. 4.1. Throughout the paper we assume that both edges are characterized by the same temperature T and chemical potential μ . The transverse size of the edge channels is assumed to be much smaller than the interedge distance d . We focus on Coulomb drag between infinitely long edges, i.e., the wavevector of the external perturbation in the response functions is sent to zero before taking the dc limit: this is the order of limits that defines the dc resistivity in general, and the dc-drag resistivity ρ_D in particular.

The kinetic part H_0 of the Hamiltonian is given by

$$H_0 = \sum_{\sigma\eta} \int_k (\eta v_F k - \mu) \psi_{k\sigma\eta}^\dagger \psi_{k\sigma\eta} , \quad (4.2)$$

where $\psi_{k\sigma\eta}$ is the electron operator at the momentum k in edge $\sigma = 1, 2$ with the chirality $\eta = \pm$, and v_F is the Fermi velocity (assumed to be the same for the two edges). The sum over k for each of the chiralities runs from $-\infty$ to ∞ (the bandwidth of 1D edge states is assumed to be larger than all other energy scales), with the chiral spectral branches crossing at $k = 0$ (“Dirac point”). In the ideal helical edge, the spin-locking axis is independent of k , so that the electron state $\tilde{\psi}_{k\sigma s}$ with a given spin projection $s = \uparrow, \downarrow$ coincides with $\psi_{k\sigma\eta}$.

As already discussed, we specialize to the model in which the spin-rotational invariance of the helical edges is broken by Rashba-type spin-orbit coupling in the bulk (for more detail, see Sec. 3.1). In the absence of spin-axial symmetry, $\tilde{\psi}_{k\sigma s}$ is generically a mixture of the chiral states $\psi_{k\sigma\eta}$ with both chiralities η . By TRS, the unitary transformation between the two basis sets (“spin” vs “chiral”) in the vicinity of the Dirac point has a universal form, as far as the dependence on k is concerned, to order $\mathcal{O}(k^2)$. Specifically [48],

$$\begin{aligned} \tilde{\psi}_{k\sigma\uparrow} &\simeq \psi_{k\sigma+} - \frac{k^2}{k_0^2} \psi_{k\sigma-} , \\ \tilde{\psi}_{k\sigma\downarrow} &\simeq \psi_{k\sigma-} + \frac{k^2}{k_0^2} \psi_{k\sigma+} , \end{aligned} \quad (4.3)$$

where k_0 is a model-dependent momentum scale which characterizes the strength of spin-orbit coupling (taken to be identical in the two edges). We assume that the spin-orbit interaction is a weak symmetry-breaking perturbation with $v_F k_0 \gg \max\{\mu, T\}$, so that the quadratic-in- k expansion (4.3) is sufficient for our purposes.

The density-density interaction term in the Hamiltonian is then written in the chiral basis, rotated with respect to the spin basis according to Eq. (4.3), as

$$H_{\text{int}} = \frac{1}{2} \sum_{\sigma, \sigma'} \sum_{\eta_1 \eta_2 \eta_3 \eta_4} \int_{kk'q} b_{\eta_1 \eta_4}(k+q, k) b_{\eta_2 \eta_3}(k'-q, k') V_{\sigma\sigma'}(q) \psi_{k+q, \eta_1 \sigma}^\dagger \psi_{k'-q, \eta_2 \sigma'}^\dagger \psi_{k' \eta_3 \sigma'} \psi_{k \eta_4 \sigma} , \quad (4.4)$$

where $V_{\sigma\sigma'}(q)$ is the Fourier component of the interaction potential inside ($\sigma = \sigma'$ equal to 1 or 2) and between ($\sigma \neq \sigma'$) the edges and

$$b_{\eta_1 \eta_2}(k_1, k_2) = \delta_{\eta_1 \eta_2} - \eta_1 \delta_{\eta_1, -\eta_2} \frac{k_1^2 - k_2^2}{k_0^2} . \quad (4.5)$$

We assume that the interactions in the double-edge system are screened by a nearby metallic gate. Note that—irrespective of the relation between the distance to the gate and the distance between the wires d —the interwire potential $V_{12}(q)$ starts to decay exponentially with increasing $|q|$ at $|q| \sim 1/d$ (see, e.g., Appendix A of Ref. [104]). For simplicity, we take $V_{11}(q) = V_{22}(q)$ to be given by a constant $V_{0\parallel}$ and $V_{12}(q)$ by a simple exponential $V_{0\perp} e^{-|q|d}$.

The presence of the factors (4.5) in the interacting part of the Hamiltonian for the helical liquid constitutes the key difference between the helical and conventional Luttinger models. Another difference to notice is related to the population of the eigenstates at thermal equilibrium. The conventional

Luttinger model is formulated for $T \ll \mu$, where the chemical potential μ is counted from the energy at which the chiral spectral branches meet [either at the bottom of the electron spectrum, linearized in the vicinity of the Fermi energy, or at the crossing point of two chiral branches with a linear dispersion relation, similar to Eq. (4.2)]. In the helical Luttinger model, we assume that T can be larger than the energy difference between μ and the Dirac point, so that the real scattering processes that involve the electron states at and around the Dirac point are not necessarily thermally suppressed.

4.2 Coulomb drag between helical edges: Kinetic theory

In this section, we consider Coulomb drag between helical edges within the model that neglects the LL renormalization of parameters due to the intraedge interactions. This model is justified for sufficiently high temperatures (the precise condition will be given below) and can be viewed as a direct counterpart of the approach employed in Ch. 3 for a single edge. Treating the interwire electron-electron interaction perturbatively, we solve the kinetic equation for two coupled helical edges and obtain the drag resistivity in the high-frequency (*ac*) and low-frequency (*dc*) regimes. These regimes are distinguished by the relation between the frequency of the driving field and the relevant inelastic relaxation rate. The discussion of the LL effects is postponed until Sec. 4.3 below, where we will complement the fermionic approach by the analysis of the bosonized theory including the LL effects.

4.2.1 Kinetic equation

Our starting point for the calculation of the drag resistivity is the kinetic equation for the pair collisions in a system of two spatially homogeneous edges:

$$\partial_t f_\sigma(1) - eE_\sigma \partial_{k_1} f_\sigma(1) = \text{St}_\sigma[f]. \quad (4.6)$$

Here, we have introduced the joint index $i \equiv (k_i, \eta_i)$ for the electron momentum and chirality, E_σ is the electric field, and f_σ is the electronic distribution function in edge σ . We first discard the intraedge interactions and will discuss their role in Sec. 4.2.3 below. The collision integral $\text{St}_\sigma[f]$ for $\sigma = 1$ is then given (to the lowest order in the interedge interaction) by

$$\begin{aligned} \text{St}_1[f] = & (2\pi)^2 \int_{k_{1'}, k_{2'}, k_2} \sum_{\eta_{1'}, \eta_{2'}, \eta_2} \left| V_{12}(k_{1'} - k_1, \epsilon_{1'} - \epsilon_1) \right|^2 \left| B_{\eta_{1'}, \eta_1}(k_{1'}, k_1) \right|^2 \left| B_{\eta_{2'}, \eta_2}(k_{2'}, k_2) \right|^2 \\ & \times \delta(k_1 + k_2 - k_{1'} - k_{2'}) \delta(\epsilon_1 + \epsilon_2 - \epsilon_{1'} - \epsilon_{2'}) \\ & \times \left\{ f_1(1') f_2(2') [1 - f_1(1)] [1 - f_2(2)] - f_1(1) f_2(2) [1 - f_1(1')] [1 - f_2(2')] \right\} \end{aligned} \quad (4.7)$$

with the single particle energies $\epsilon_i = v_F \eta_i k_i$. The collision integral for electrons in edge 2 is obtained by interchanging edge indices ($1 \leftrightarrow 2$). The dynamically Random phase approximation (RPA)-screened interaction $V_{12}(q, \Omega)$ is specified by Eq. (D.27) in App. D. It will turn out that we cannot neglect screening to lowest order in the interaction strength in the current problem since it introduces a novel plasmon scattering channel for the drag, as we will discuss later.

It is convenient to represent the distribution function in terms of the functions $g_\sigma(1)$ as

$$f_\sigma(1) = n_F(1) - g_\sigma(1) n_F(1) [1 - n_F(1)], \quad (4.8)$$

where $n_F(1) = [1 + \exp(\epsilon_1 - \mu)/T]^{-1}$ is the thermal distribution function. Linearizing Eq. (4.6) in g_σ we obtain (in the ω representation)

$$-i\omega g_\sigma(1) - \frac{v_F e E_\sigma \eta_1}{T} = \zeta^{-2}(1) \text{st}_\sigma[g], \quad (4.9)$$

where we defined the function

$$\zeta(1) = \frac{1}{\cosh[(\epsilon_1 - \mu)/2T]} \quad (4.10)$$

and the collision integral

$$\begin{aligned} \text{st}_1[g] &= 4 \times (2\pi)^2 \int_{k_2, k_{1'}, k_{2'}} \sum_{\eta_2, \eta_{1'}, \eta_{2'}} \left| V_{12}(k_{1'} - k_1, \epsilon_{1'} - \epsilon_1) \right|^2 \left| B_{\eta_{2'}, \eta_2}(k_{2'}, k_2) \right|^2 \left| B_{\eta_{1'}, \eta_1}(k_{1'}, k_1) \right|^2 \\ &\times \delta(\epsilon_1 + \epsilon_2 - \epsilon_{1'} - \epsilon_{2'}) \delta(k_1 + k_2 - k_{1'} - k_{2'}) n_F(1) n_F(2) [1 - n_F(1')] [1 - n_F(2')] \\ &\times \left\{ g_1(1') + g_2(2') - g_1(1) - g_2(2) \right\}. \end{aligned} \quad (4.11)$$

By solving the kinetic equation, we find the distribution function f_σ or, equivalently, g_σ , which allows us, in turn, to calculate the electric current in edge σ :

$$j_\sigma = \frac{ev_F}{4} \sum_{\eta_1} \int_{k_1} \eta_1 \zeta^2(1) g_\sigma(1). \quad (4.12)$$

The object of main interest in this section is the drag conductivity, defined as $\sigma_{12} = j_1/E_2$ under the condition that $E_1 = 0$.

4.2.2 High-frequency Coulomb drag: Scattering rate

In the high-frequency limit, the kinetic equation (4.9) can be solved iteratively. In the zeroth approximation one neglects collisions between particles altogether, which yields the distribution function

$$g_\sigma^{(0)}(k, \eta) = \frac{1}{-i\omega + 0} \eta \frac{v_F e E_\sigma}{T}. \quad (4.13)$$

Substituting this into the collision integral on the right hand side of Eq. (4.9), we obtain an equation for the next order approximation $g_\sigma^{(1)}$ which is then used in Eq. (4.12). The drag conductivity obtained in this approximation can be expressed as

$$\text{Re } \sigma_{12} = -\frac{e^2 v_F}{\pi \omega^2 \tau_D^\infty}, \quad \omega \tau_D^\infty \gg 1. \quad (4.14)$$

The symbol ∞ here is used to emphasize that the drag rate is calculated in the high-frequency regime. Since $g_\sigma^{(0)}$ is independent of k , the contribution of $\eta_{2'} = \eta_2$ to the collision integral for the particles in the active edge vanishes, thus requiring the backscattering of at least one particle involved in the collision process. The high-frequency drag rate defined by Eq. (4.14) then takes the form

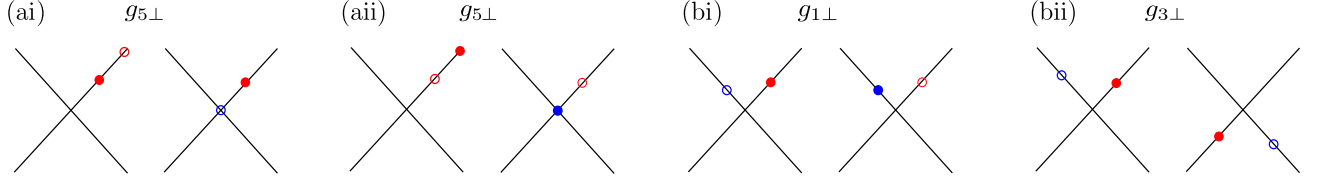


Figure 4.2: Momentum configurations for the interedge two-particle scattering in channels (a) and (b) as defined in Eq. (4.16) and the corresponding g-ology classification. The initial and final states in edge 1 and 2 are depicted as filled and empty circles, respectively. Blue circles denote left movers and red circles right movers. For $g_{5\perp}$ processes (channel a), the left mover is at zero energy while the right movers are close to the Fermi surface, due to constraints imposed by energy-momentum conservation. As explained in the text, the scattering rates for processes (ai) and (aii) cancel each other. The drag scattering rate is determined by $g_{1\perp}$ and $g_{3\perp}$ processes.

$$\begin{aligned} \frac{1}{\tau_D^\infty} = & -\frac{(2\pi)^3}{T} \int_{k_1, k_2, k_1', k_2'} \sum_{\eta_1, \eta_2, \eta_1'} \eta_1 \eta_2 \left| V_{12}(k_1' - k_1, \epsilon_1' - \epsilon_1) \right|^2 \left| B_{-\eta_2, \eta_2}(k_2', k_2) \right|^2 \\ & \times \left| B_{\eta_1', \eta_1}(k_1', k_1) \right|^2 \delta(\eta_1 k_1 + \eta_2 [k_2 + k_2'] - \eta_1' k_1') \delta(k_1 + k_2 - k_1' - k_2') \\ & \times n_F(1) n_F(2) [1 - n_F(1')] [1 - n_F(k_2', -\eta_2)]. \end{aligned} \quad (4.15)$$

The rate is a sum of 4 scattering channels:

$$\begin{aligned} \text{(ai)} \quad \eta_1 = \eta_1' \quad \text{and} \quad \eta_2 = \eta_1 & & \text{(bi)} \quad \eta_1 = -\eta_1' \quad \text{and} \quad \eta_2 = -\eta_1 \\ \text{(aii)} \quad \eta_1 = \eta_1' \quad \text{and} \quad \eta_2 = -\eta_1 & & \text{(bii)} \quad \eta_1 = -\eta_1' \quad \text{and} \quad \eta_2 = \eta_1 \end{aligned} \quad (4.16)$$

The different scattering channels are depicted in Fig. 4.2 together with their g-ology classification.

We first consider the scattering rates for processes (a) which correspond to g_5 processes in the g-ology classification. Denoting $k_1' - k_1 = q$ we find

$$\frac{1}{\tau_D^\infty, \text{(ai)}} = -\frac{\pi}{T} \int_{k_1, q} \sum_{\eta_1} \left| V_{12}(q, v_F q) \right|^2 \left(\frac{q}{k_0} \right)^4 n_F(1) n_F(q, \eta_1) [1 - n_F(q + k_1, \eta_1)] [1 - n_F(0, -\eta_1)] \quad (4.17)$$

$$\begin{aligned} \frac{1}{\tau_D^\infty, \text{(aii)}} &= \frac{\pi}{T} \int_{k_1, k_1'} \sum_{\eta_1} \left| V_{12}(q, v_F q) \right|^2 \left(\frac{q}{k_0} \right)^4 n_F(1) n_F(0, -\eta_1) [1 - n_F(q + k_1, \eta_1)] [1 - n_F(-q, \eta_1)] \\ &= \frac{\pi}{T} \int_{k_1, q} \sum_{\eta_1} \left| V_{12}(q, v_F q) \right|^2 \left(\frac{q}{k_0} \right)^4 n_F(1) n_F(q, \eta_1) [1 - n_F(q + k_1, \eta_1)] [1 - n_F(0, -\eta_1)]. \end{aligned} \quad (4.18)$$

In the last line here, we have first shifted momenta $q \rightarrow -q$ and $k_1 \rightarrow k_1 + q$ and then used the identity

$$n_F(1) n_F(2) [1 - n_F(1')] [1 - n_F(2')] = n_F(1') n_F(2') [1 - n_F(1)] [1 - n_F(2)]$$

which holds if $\epsilon_1 + \epsilon_2 = \epsilon_{1'} + \epsilon_{2'}$.

We thus notice that the scattering rates of the two g_5 processes cancel out. The corresponding scattering processes for $\eta_1 = +$ are schematically depicted in Fig. 4.2. The cancellation occurs because the processes (ai) and (aii) have the same thermal occupation factors but the change of velocity is reversed: in channel (ai) a right mover in edge 2 scatters to a left mover while in channel (aii) the process is reversed. Both processes thus give the contributions to the current in edge 2 of the same magnitude but with opposite signs, which leads to the cancellation observed above.

The high-frequency drag scattering rate is thus determined by the remaining sum of $g_{1\perp}$ backscattering (bi) and $g_{3\perp}$ Umklapp processes (bii):

$$\begin{aligned} \frac{1}{\tau_D^\infty} = & \frac{8\pi}{T k_0^8} \int_{q,Q} \frac{Q^4 q^4 |V_{12}(q, 2v_F Q)|^2}{\cosh\left(\frac{v_F q}{2T} + \frac{\mu}{T}\right) + \cosh\frac{v_F Q}{T}} \\ & \times \left[\frac{1}{\cosh\left(\frac{v_F q}{2T} + \frac{\mu}{T}\right) + \cosh\frac{v_F Q}{T}} - \frac{1}{\cosh\left(\frac{v_F q}{2T} - \frac{\mu}{T}\right) + \cosh\frac{v_F Q}{T}} \right]. \end{aligned} \quad (4.19)$$

Here, $q = k_1 - k_{1'}$ denotes the momentum transfer and $Q = (k_1 + k_{1'})/2$ the total momentum of the incoming (k_1) and outgoing ($k_{1'}$) particle in edge 1. Due to constraints set by the energy-momentum conservation in the collision kernel, the transferred frequency in the RPA interaction is set to $\epsilon_1 - \epsilon_{1'} = 2v_F Q$.

We point out that the rate vanishes if the chemical potential is tuned to the Dirac point, $\mu = 0$, because the system exhibits perfect particle-hole symmetry at this point. Technically, the vanishing occurs because the second term in brackets in Eq. (4.19), which is due to $g_{3\perp}$ Umklapp scattering, cancels the contribution of the first term that stems from $g_{1\perp}$ backscattering.

Before proceeding with the calculation of the drag rate, we elaborate on the importance of the RPA-screened interaction potential $V_{12}(q, 2v_F Q)$ which appears in the integrand in Eq. (4.19). The form of the interaction potential is derived in Appendix D.2 and reads as

$$V_{12}(q, \Omega) = \frac{V_0 e^{-|q|d} \left[(v_F q)^2 - \Omega^2 \right]^2}{\left[(\Omega + i\Gamma_+)^2 - \Omega_+^2 \right] \left[(\Omega + i\Gamma_-)^2 - \Omega_-^2 \right]}. \quad (4.20)$$

The potential has poles at the energies of the plasmon excitations,

$$\Omega_\pm = v_\pm(q) |q|, \quad (4.21)$$

where the plasmon velocities are given by

$$v_\pm(q) = \sqrt{1 + \alpha_\pm(q)} v_F. \quad (4.22)$$

or equivalently by Eq. (4.54) below obtained using bosonization. Here, the difference ($-$) and sum ($+$) of dimensionless intra- and interedge interaction constants are defined as

$$\alpha_\pm(q) = \alpha \left(1 \pm e^{-|q|d} \right) \quad (4.23)$$

and $\alpha = V_{0\parallel}/\pi v_F$ is the dimensionless interaction strength. Here and below, we make the assumption that $V_{0\parallel} = V_{0\perp} = V_0$, which simplifies the calculation but does not change the qualitative outcome of the results. In the presence of scattering that changes the chirality of electrons, the plasmon excitations acquire a finite decay rate Γ_{\pm} . To the lowest order in the dimensionless interaction, we find

$$\Gamma_{\pm}(q) = \alpha_{\pm}^2(q) \frac{v_F q}{8} \left(\frac{q}{k_0}\right)^4 \sinh \frac{v_F q}{2T} \times \left[\frac{1}{\cosh(\frac{v_F q}{2T} + \frac{\mu}{T}) + \cosh \frac{v_F q}{2T}} + \frac{1}{\cosh(\frac{v_F q}{2T} - \frac{\mu}{T}) + \cosh \frac{v_F q}{2T}} \right]. \quad (4.24)$$

The damping of plasmons becomes strong at the characteristic energy scale

$$T_{p0} = \frac{v_F}{d} \ln \frac{(k_0 d)^4}{\alpha} \quad (4.25)$$

as is discussed in App. D.3.2.

The appearance of plasmon poles in the screened backscattering interaction is a unique feature of the HLL and does not occur in the conventional LL. In the diagrammatic RPA expansion shown in Fig. D.1, the coupling to the chiral polarization bubbles that correspond to the plasmons of the system is always mediated by g_5 interaction lines. As we already mentioned, these interaction processes can only take place in the presence of a Dirac point in the spectrum. Therefore, while the drag rate due to $g_{5\perp}$ processes cancels exactly, these processes nonetheless influence the drag indirectly—by facilitating the coupling to plasmons in the RPA summation.

Returning to the explicit expression for the drag rate in Eq. (4.19), we point out that the contribution of the plasmon poles in the screened interaction and that of particle-hole excitations decouple and can be treated separately. Indeed, the integral over Q can be performed by contour integration in the complex plane. The drag rate is then given by the sum of the contribution of the plasmon poles (4.21) and the contribution of the thermal poles at

$$Q_n = \pm \frac{q}{2} + \frac{\mu}{v_F} + i\pi(2n-1) \frac{T}{v_F}$$

with $n \in \mathbb{Z}$. We therefore use the following approximate scheme to calculate the drag rate. We note that in the vicinity of the thermal poles we can approximate the RPA-screened interaction in Eq. (4.20) by the statically screened interaction $V(q, Q_n) \simeq V_0 e^{-|q|d}$. Here, we first neglected the plasmon rates $\Gamma_{\pm} \ll T$ and then performed an expansion to leading order in the dimensionless interaction strength α . The drag rate can thus be expressed as the sum of a particle-hole contribution, obtained by setting $V_{12}(q, Q) = V_0 \exp(-|q|d)$ in Eq. (4.19), and a plasmon contribution obtained by performing the integral in Eq. (4.19) using only the plasmon poles. This program is performed in Appendix D.3. The high-frequency drag rate is given by the sum of the particle-hole drag rate, derived in Appendix D.3.1, and the plasmon drag rate obtained in Appendix D.3.2. The behavior of the high-frequency rate is depicted in Fig. 4.4. For now we postpone a discussion of this behavior until we have included the effect of LL renormalization in Sec. 4.4 below.

4.2.3 Low-frequency Coulomb drag

In the low-frequency regime, one can no longer use the iterative solution employed in Sec. 4.2.2. In the spirit of the Drude theory, the rate $1/\tau_D^{\infty}$ can be expected to determine the drag also in the limit

$\omega \rightarrow 0$, with the dc-drag resistivity $\rho_D \sim 1/\tau_D^\infty$. This holds, in fact, as long as the intraedge relaxation rate $1/\tau_{ee}$ is much larger than the drag rate [104, 115–117]. The intraedge electron-electron scattering rate is determined by $g_{5\parallel}$ processes and reads as [85]

$$\frac{1}{\tau_{ee}} \propto \alpha^2 \left(\frac{T}{v_F k_0} \right)^4 T, \quad \text{for } T \gg \mu. \quad (4.26)$$

For temperatures $T \gg \mu$ the drag rate is determined by plasmons and smaller than the intraedge electron-electron scattering rate by a parametric factor $(\mu/T)^2$ for $T \ll T_{p0}$ [cf. Eq. (D.44)] and by a parametric factor of $(\mu/T)^2 (T_p/T)^7$ for $T \gg T_{p0}$ [cf. Eq. (D.47)]. We thus conclude that the dc-drag rate is determined by the same scattering time τ_D^∞ as the ac-drag for $T \gg \mu$.

For lower temperatures $T \ll \mu$ the dc electron-electron scattering rate is exponentially small, due to the kinematic phase space constraints and reads as [85]

$$\frac{1}{\tau_{ee}} \sim \alpha^2 \left(\frac{\mu}{v_F k_0} \right)^4 \frac{\mu}{T} e^{-\mu/T}, \quad \text{for } T \ll \mu. \quad (4.27)$$

For $T_1 \ll T \ll \mu$, the drag rate is again parametrically smaller than the relaxation rate, by a factor T/μ . By comparing the rate (4.27) with the high-frequency drag rate in Eq. (D.30), on the other hand, we find that $\tau_D^\infty/\tau_{ee} \sim \exp(-\mu/T + 4k_F d)$. Thus the dc-drag is determined by the same scattering rate as the ac one in the regime $T \gg v_F/d$ while we can make no a priori statement in the regime $\mu \gg v_F/d \gg T$.

Therefore, we will now solve the kinetic equation in the regime $\mu \gg v_F/d \gg T$ and determine the dc-drag rate using the explicit form of the distribution function. It will turn out that, although the high-frequency approximation is no longer justified in this regime, it nonetheless yields a parametrically correct drag resistivity.

We begin by considering the terms in the chirality summation in the collision integral in Eq. (4.11), which correspond to a different microscopic scattering mechanisms, one by one. First we notice, that the collision integral vanishes exactly for forward scattering processes ($g_{2\perp}$ and $g_{4\perp}$ in the g-ology notation) and therefore these processes do not contribute to the drag. In the case of $g_{2,\perp}$ processes, with $\eta_2 = \eta_{2'} = -\eta_{1'} = -\eta_1$ in Eq. (4.11), the vanishing of the collision integral has a straightforward interpretation. For a linear electron spectrum, these processes only exchange the energy and momentum of the incoming particles and therefore do not change the distribution function. The contribution due to $g_{4,\perp}$ processes, with $\eta_2 = \eta_{2'} = \eta_{1'} = \eta_1$ in Eq. (4.11), is more subtle. For this scattering process the delta functions ensuring momentum and energy conservation are identical and lead to a diverging contribution in the collision integral, which would be regularized by a finite system length: $\delta(k=0) \sim L$. If we take into account screening, the interaction will be given by Eq. (D.18). In the collision integral the interaction has to be evaluated at the frequency $\Omega = \pm v_F q$ where the imaginary part in Eq. (D.12) diverges and thus $|U(q, v_F q)|^2 \sim 1/[\delta(0)]^4$. We therefore conclude that, although the energy-momentum conserving delta functions diverge, the product of RPA-screened interaction and diverging delta function goes to zero in the limit of infinite system size, such that the collision integral due to forward scattering vanishes. For an analogous discussion of this cancellation in the context of spinful disordered LLs we refer to Ref. [118]. We also point out the similarity to graphene, where unscreened forward scattering also yields a divergent contribution to the collision integral. RPA regularizes this divergence for scattering angles smaller than α_g , the dimensionless strength of interaction in graphene, but nonetheless scattering with small scattering angles is still parametrically enhanced. In particular

one finds that the energy relaxation rate, which is dominated by the contribution of small scattering angles is much larger than the transport scattering rate, which is dominated by scattering processes with large scattering angles [116]. Finally, we will restrict the analysis to the regime $\mu \gg T$, where we can neglect all contributions from Umklapp terms to the collision integral.

The only source of dc drag is then $g_{1\perp}$ backscattering which corresponds to the term with $\eta_1 = -\eta_2 = \eta_{2'} = -\eta_{1'}$ in the sum over chiralities in Eq. (4.11). The set of kinetic equation in Eq. (4.9) then takes the form

$$\begin{aligned} -i\omega g_1(1) - \frac{v_F e E_1 \eta_1}{T} &= \text{st}_1[g], \\ -i\omega g_2(1) - \frac{v_F e E_2 \eta_1}{T} &= -\text{st}_1[g]. \end{aligned} \quad (4.28)$$

with the collision integral

$$\begin{aligned} \text{st}_1 &= \frac{1}{8v_F} \int_{k_{1'}} |V_{12}(k_1 - k_{1'})|^2 \frac{(k_1^2 - k_{1'}^2)^4}{k_0^8} \zeta^2(-\eta_1, k_{1'}) \\ &\times \{g_1(-\eta_1, k_{1'}) + g_2(\eta_1, k_1) - g_1(\eta_1, k_1) - g_2(-\eta_1, k_{1'})\}. \end{aligned} \quad (4.29)$$

The kinetic equations in (4.28) can be decoupled by defining the relative and absolute components

$$g_{\pm}(\eta, k) = (g_1(\eta, k) \pm g_2(\eta, k)) / 2, \quad (4.30)$$

and the (pseudo-) spin [sign + in Eq. (4.31)] and charge [sign - in Eq. (4.31)] components

$$g_{\pm}^{c,s}(k) = (g_{\pm}(R, k) \mp g_{\pm}(L, -k)) / 2. \quad (4.31)$$

The drag resistivity is obtained as [104]

$$\rho_D = \frac{E_1 - E_2}{j_-}, \quad (4.32)$$

where the relative current is given by

$$j_- = \frac{j_1 - j_2}{2} = \frac{ev_F}{2} \int_k \frac{g_-^c(k + k_F)}{\cosh^2\left(\frac{v_F k}{2T}\right)}. \quad (4.33)$$

We only consider the kinetic equations for the g_-^c functions, since these determine the transport properties of the system. We find

$$-i\omega g_-^c(k_1 + k_F) - \frac{v_F e (E_1 - E_2)}{2T} = \text{st}_c[g_-^c], \quad (4.34)$$

$$-i\omega g_+^c(k_1 + k_F) - \frac{v_F e (E_1 + E_2)}{2T} = 0, \quad (4.35)$$

where

$$\text{st}_c[g_-^c] \simeq -\frac{(2k_F^4)}{k_0^8} \int_{k_{1'}} |V_{12}(k_{1'} - k_1 - 2k_F)|^2 \frac{(k_{1'} - k_1 - 2k_F)^4}{\cosh^2\left(\frac{v_F k_{1'}}{2T}\right)} [g_-^c(k_{1'}) + g_-^c(k_1)]. \quad (4.36)$$

We now take the limit $\omega \rightarrow 0$ and assume $\omega g_-^c(\omega) \rightarrow 0$ for $\omega \rightarrow 0$ (which has to be confirmed selfconsistently). Eq. (4.34) then takes the form of an integral equation for the function g_-^c :

$$\frac{2v_F^2 e(E_1 - E_2)}{T} = \int \frac{dk_{1'}}{2\pi} \frac{(k_1 - k_{1'} - 2k_F)^4 (k_1 + k_{1'})^4 |V_{12}(k_1 - k_{1'} - 2k_F)|^2}{k_0^8 \cosh^2\left(\frac{v_F k_{1'}}{2T}\right)} \times [g_-^c(-k_{1'} + k_F) + g_-^c(k_1 + k_F)]. \quad (4.37)$$

In the regime $T \ll v_F/d \ll \mu$ we can replace the expression $k_{1'} - k_1 - 2k_F$ in the integrand by $2k_F$. If we introduce the dimensionless variables $x = v_F k_1/2T$ and $y = v_F k_{1'}/2T$ and the dimensionless function

$$G(x) = \frac{2^7}{\pi} \left(\frac{k_F}{k_0}\right)^4 \frac{|V_{12}(2k_F)|^2}{v_F^2} \frac{T k_0}{e(E_1 - E_2)} \left(\frac{T}{v_F k_0}\right)^5 g_-^c\left(\frac{2T}{v_F} x + k_F\right), \quad (4.38)$$

Eq. (4.37) takes the form

$$G(x) = \frac{1}{A(x)} \left(1 - \int dy \frac{(x-y)^4}{\cosh^2(y)} G(y)\right), \quad (4.39)$$

$$A(x) = \int dy \frac{(x-y)^4}{\cosh^2(y)} = \frac{7\pi^4}{120} + \pi^2 x^2 + 2x^4. \quad (4.40)$$

We solve the integral equation for $G(x)$ numerically and use Eqs. (4.32), (4.33) and (4.38) to express the drag conductivity as

$$\rho_D = \frac{2^9}{\lambda} \frac{1}{e^2} \left(\frac{k_F}{k_0}\right)^4 \frac{|V_{12}(2k_F)|^2}{v_F^2} \left(\frac{T}{v_F k_0}\right)^5 k_0, \quad (4.41)$$

with the constant

$$\lambda = \int dx \frac{G(x)}{\cosh^2(x)} \simeq 0.242. \quad (4.42)$$

We conclude, that the drag rate that determines the ac drag and the rate that determines the dc drag are parametrically equivalent in the regime $T \ll v_F/d \ll \mu$ as can be seen by comparing the results in Eqs. (D.30) and (4.41). At higher temperatures, the ac and dc-drag rates are exactly equivalent, since the intraedge electron relaxation rate is parametrically larger than the ac-drag rate, which legitimates the high-frequency expansion. This curious behavior is due to the fact that the g_5 scattering mechanism that sets the scale for relaxation, does not contribute directly to the drag which is determined by RPA renormalized g_1 and g_3 processes with higher scattering rates.

4.3 Intraedge interaction: Bosonization framework

Above, we have addressed the drag between helical edges within the framework of kinetic equation, neglecting Luttinger-liquid renormalization effects. In this section, we employ the bosonization approach to extend the above analysis to the lower temperatures, where the renormalization of the 1D theory leads, as usual, to the anomalous power-law temperature dependence of observables.

Since the renormalization effects in Luttinger liquids necessarily involve backscattering processes, the characteristic temperature scale at which the renormalization starts cannot exceed $T_d = v_F/d$. Indeed, the distance d between the edges determines the characteristic radius of the interedge interaction potential V_{12} , so that on smaller spatial scales one cannot treat this interaction as local. In fact, in addition to the scale d , the screening by external gates introduces another scale d_0 for the intraedge interaction, so that the renormalization becomes effective at $T < v_F/\max\{d, d_0\}$. For definiteness, we assume that $d \gtrsim d_0$ and hence treat the intraedge interactions V_{11}, V_{22} as local on the scale of d .

In what follows, we first bosonize the model and analyze the resulting phase diagram for two coupled helical edges. Next, we discuss the implications of the Luttinger renormalization effects for the drag resistivity.

4.3.1 First-order backscattering

For simplicity, we will concentrate on the case of sufficiently high densities, such that $k_F d \gg 1$ (or, equivalently, $\mu \gg T_d$). For relevant temperatures $T < T_d$, we then have $\mu \gg T$, so that transitions resulting from Umklapp interactions of two particles in the vicinity of the Dirac point are thermally suppressed. Neglecting them, the part of Eq. (4.4) that describes chirality-changing interactions reduces to backscattering in the vicinity of the Fermi surface. The Hamiltonian density simplifies, then, to $\mathcal{H} = \mathcal{H}_0 + \mathcal{H}_f + \mathcal{H}_b$, where \mathcal{H}_0 corresponds to the free Hamiltonian in Eq. (4.2) and $\mathcal{H}_{f,b}$ describes forward (f) and backward (b) scattering.

To write \mathcal{H} , it is convenient to introduce the electron operators at a given point in real space, for the right- and left-moving electrons, in the form

$$\psi_{\sigma+}(x) = R_\sigma(x)e^{ik_F x}, \quad \psi_{\sigma-}(x) = L_\sigma(x)e^{-ik_F x}, \quad (4.43)$$

where $R_\sigma(x)$ and $L_\sigma(x)$ vary slowly on the scale of k_F^{-1} . Specifically, \mathcal{H}_0 and \mathcal{H}_f are written similar to the conventional Luttinger model as

$$\mathcal{H}_0 = -iv_F \left(R_\sigma^\dagger \partial_x R_\sigma - L_\sigma^\dagger \partial_x L_\sigma \right) \quad (4.44)$$

and

$$\mathcal{H}_f = \sum_{\sigma\sigma'} \left(g_{2\parallel} \delta_{\sigma\sigma'} + g_{2\perp} \delta_{\sigma,-\sigma'} \right) \rho_{R\sigma} \rho_{L\sigma'} + \frac{1}{2} \sum_{\sigma\sigma'\eta} \left(g_{4\parallel} \delta_{\sigma\sigma'} + g_{4\perp} \delta_{\sigma,-\sigma'} \right) \rho_{\eta\sigma} \rho_{\eta\sigma'}, \quad (4.45)$$

where the chiral densities in \mathcal{H}_f are given by $\rho_{R\sigma} = R_\sigma^\dagger R_\sigma$ and $\rho_{L\sigma} = L_\sigma^\dagger L_\sigma$, and the coupling constants read $g_{4\parallel} = g_{2\parallel} = V_{11}(0)$ and $g_{4\perp} = g_{2\perp} = V_{12}(0)$. The backscattering part

$$\mathcal{H}_b = \sum_{\sigma\sigma'} \left(g_{1\parallel} \delta_{\sigma\sigma'} + g_{1\perp} \delta_{\sigma,-\sigma'} \right) h_\sigma^\dagger h_{\sigma'} \quad (4.46)$$

is represented in terms of R_σ and L_σ differently, compared to the conventional Luttinger model, with h_σ coming from the spatial gradient expansion:

$$h_\sigma = \left[(\partial_x R_\sigma^\dagger) L_\sigma - R_\sigma^\dagger (\partial_x L_\sigma) \right] a, \quad (4.47)$$

where a is the ultraviolet cutoff in real space. As discussed above, the local representation of the backscattering term is valid on spatial scales larger than d , hence $a \sim d$. The coupling constants for backscattering are given by

$$g_{1\parallel} = \frac{4k_F^2}{k_0^4 a^2} V_{11}(2k_F), \quad g_{1\perp} = \frac{4k_F^2}{k_0^4 a^2} V_{12}(2k_F). \quad (4.48)$$

Note that the ultraviolet scale a cancels out in Eq. (4.46).

The forward scattering term \mathcal{H}_f can be treated exactly by bosonization, with the fermionic fields represented in terms of the bosonic field $\varphi_\sigma(x)$ and its canonical conjugate $\theta_\sigma(x)$ as

$$R_\sigma(x) = \frac{1}{\sqrt{2\pi a}} e^{i\sqrt{\pi}[\varphi_\sigma(x) - \theta_\sigma(x)]}, \quad (4.49)$$

$$L_\sigma(x) = \frac{1}{\sqrt{2\pi a}} e^{-i\sqrt{\pi}[\varphi_\sigma(x) + \theta_\sigma(x)]}. \quad (4.50)$$

Changing from the ‘‘wire basis’’ ($\sigma = 1, 2$) to the basis of symmetric (+) and antisymmetric (−) fields

$$\varphi_\pm = (\varphi_1 \pm \varphi_2)/\sqrt{2}, \quad \theta_\pm = (\theta_1 \pm \theta_2)/\sqrt{2}, \quad (4.51)$$

the bosonized Hamiltonian density reads

$$\mathcal{H} = \sum_{\lambda=\pm} \frac{v_\lambda}{2} \left[K_\lambda (\partial_x \theta_\lambda)^2 + K_\lambda^{-1} (\partial_x \varphi_\lambda)^2 \right] + \frac{g_{1\perp}}{\pi} \left[(\partial_x \theta_+)^2 - (\partial_x \theta_-)^2 \right] \cos \left(2\sqrt{2\pi} \varphi_- \right), \quad (4.52)$$

where

$$K_\pm = \sqrt{\frac{1 - U_\pm}{1 + U_\pm}}, \quad (4.53)$$

$$v_\pm = u_\pm \sqrt{1 - U_\pm^2} \quad (4.54)$$

with

$$U_\pm = \frac{1}{2\pi u_\pm} \left(g_{2\parallel} \pm g_{2\perp} \right), \quad (4.55)$$

$$u_\pm = v_F + \frac{1}{2\pi} \left(g_{4\parallel} \pm g_{4\perp} \right). \quad (4.56)$$

Note, that the parameters do not contain $g_{1\parallel}$ interaction, unlike in the model of coupled LLs. In the present theory the $g_{1\parallel}$ term contains additional gradients and can thus be neglected with respect to the $g_{2\parallel}$ term.

Because of the $g_{1\perp}$ scattering processes, the coupling constants for the double-edge system described by the Hamiltonian (4.52) are subject to renormalization. Under a renormalization-group (RG) transformation that keeps the quadratic term in Eq. (4.52) invariant, the scaling dimension for the backscattering operator is obtained as $2K_- + 2$, with 2 coming from the spatial gradients. That is, backscattering is irrelevant in the RG sense, with the coupling constant

$$\alpha_b = \frac{g_{1\perp}}{2\pi v_-} \quad (4.57)$$

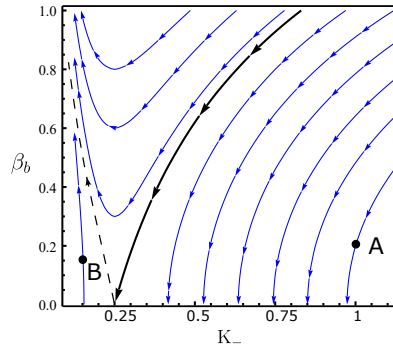


Figure 4.3: Renormalization-group flow of the coupling constant for interwire second-order backscattering β_b vs the Luttinger constant for the relative charge mode K_- . The separatrix between the strong- and weak-coupling phases (thick black line) terminates at a strongly-interacting point with $K_- = 1/4$.

scaling with T as

$$\alpha_b(T) = \alpha_{b0} \left(\frac{T}{T_d} \right)^{2K_-}, \quad (4.58)$$

where α_{b0} is the bare coupling.

We will return to the scaling behavior of “first-order backscattering” in Sec. 4.3.3, when calculating ρ_D . For now, we proceed with the RG treatment of Eq. (4.52). The discussion above brought up an important point that the theory with \mathcal{H} from Eq. (4.52) is weakly coupled, provided no additional couplings that become relevant are generated by the RG transformation. In fact, as we discuss in Sec. 4.3.2, second-order backscattering processes do become relevant for sufficiently strong forward-scattering interactions.

4.3.2 Higher-order backscattering

As already mentioned in Sec. 4.3.1, the backscattering operator in Eq. (4.52), which is itself irrelevant, can generate relevant operators under the RG transformation. These describe higher-order backscattering processes. Among the additional backscattering terms in the rescaled Hamiltonian, the relevancy is the highest for the term proportional to the next-order harmonic of the field φ_- , i.e., to $\cos(4\sqrt{2\pi}\varphi_-)$. Importantly, the emergent additional backscattering interaction is not suppressed by spatial gradient terms in the prefactor of the cosine, in contrast to Eq. (4.52). Specifically, as shown in Appendix D.4, the perturbative (in $\alpha_b \ll 1$) RG yields the $\cos(4\sqrt{2\pi}\varphi_-)$ term at two-loop order. The resulting effective action reads $S = S_0 + S_1 + S_2$, where

$$\begin{aligned} S_0 &= \frac{v_-}{2K_-} \int dx d\tau \left[\frac{1}{v_-^2} (\partial_\tau \varphi_-)^2 + (\partial_x \varphi_-)^2 \right], \\ S_1 &= 2v_- \alpha_b \int dx d\tau \left[(\partial_x \theta_+)^2 - (\partial_x \theta_-)^2 \right] \cos \left(2\sqrt{2\pi} \varphi_- \right), \\ S_2 &= \frac{v_- \beta_b}{\pi a^2} \int dx d\tau \cos \left(4\sqrt{2\pi} \varphi_- \right). \end{aligned} \quad (4.59)$$

The structure of the term S_2 suggests its interpretation as describing the processes of correlated four-fermion backscattering. A similar term with doubled harmonics is generated under the RG in disordered helical edges, see, e.g., Ref. [85], where it described a two-particle backscattering off the random potential.

The action (4.59) is identical to that for two coupled spinless LLs, characterized by the Luttinger constant K_-^{TLL} for the antisymmetric field φ_-^{TLL} , if one changes $K_- \rightarrow K_-^{\text{TLL}}/4$ and rescales $\varphi_- \rightarrow \varphi_-^{\text{TLL}}/4$. One importance consequence of this mapping is that the system of two strongly correlated HLLs with $K_- \simeq 1/4$ behaves similarly to weakly interacting LLs. In particular, there is a Berezinskii-Kosterlitz-Thouless (BKT) transition in the limit of $g \rightarrow 0$ at $K_- = 1/4$ [35]. Specifically, the RG equations for the coupling constants K_- and $\beta_b = g/2\pi v_-$, which characterize the action (4.59), read

$$\frac{dK_-}{d\ell} = -8\beta_b^2 K_-^2, \quad \frac{d\beta_b}{d\ell} = 2(1 - 4K_-)\beta_b, \quad (4.60)$$

where $\ell = \ln(T_d/\Lambda')$ with the running cutoff Λ' .

On the ultraviolet scale, the coupling constant β_b is quadratic in $g_{1\perp}$ and can be taken as $\beta_b \propto g_{1\perp}^2 F(K_-, K_+)$, with $F(K_-, K_+)$ from Eq. (D.62). Importantly, the function $F(K_-, K_+)$ is nonzero for all values of K_{\pm} , so that the second-order backscattering is always generated.

The integral curves

$$\beta_b(K) = \left[\beta_{b0}^2 + 2 \left(\frac{1}{4K_-} - \frac{1}{4K_0} - \ln \frac{K_0}{K_-} \right) \right]^{1/2} \quad (4.61)$$

of the RG flow for different initial conditions β_{b0} and K_0 are shown in Fig. 4.3. The separatrix

$$\beta_b^s(K) = \left[2 \left(\frac{1}{4K_-} - 1 - \ln \frac{1}{4K_-} \right) \right]^{1/2} \quad (4.62)$$

divides the phase space into the basin of attraction for the line of weak-coupling fixed points with $\beta_b = 0$ and $K_- > 1/4$ and the region in which the flow is to strong coupling (diverging β_b with $K_- < 1/4$). In the strong-coupling limit, backscattering locks the phase φ_- at the minima of the cosine potential in Eq. (4.59), which means the formation of a zigzag charge-density wave in the double-edge system. This is similar to the strong-coupling regime for two conventional spinless Luttinger liquids with repulsive interactions [92, 94]. The difference is that there is a threshold value for the strength of repulsive interactions above which the charge-density wave forms in HLLs, whereas arbitrarily small repulsion between electrons drives the system into the strong-coupling regime in conventional Luttinger liquids. We will discuss Coulomb drag between HLLs for the case of strong coupling in Sec. 4.3.4.

One can formulate a simple criterion for whether the strong- or weak-coupling regime is realized in a system of two helical edges separated by a distance d by varying the ratio of d and the radius of interaction d_0 . For $d \ll d_0$, the bare coupling constants for interactions inside and between the edges are close to each other ($g_{2\parallel} \simeq g_{2\perp}$), so that the bare Luttinger constant $K_0 \simeq 1$ [Eq. (4.53)], as illustrated by point A in Fig. 4.3. According to Eq. (4.62), the system is then in the weak-coupling regime. That is, the strong-coupling regime is only possible in our model of helical edges if $d \gtrsim d_0$. More precisely, since, as mentioned above, the bare coupling constant $\beta_{b0} \ll 1$ irrespective of $k_F d$ or d/d_0 , the transition to the strong-coupling regime is attained at K_0 close to $1/4$, which corresponds to the bare value of the difference $(g_{2\parallel} - g_{2\perp})/2\pi u_- \simeq 15/17$. It follows that the necessary condition for

the strong-coupling regime is a combination of (i) strong interactions inside the edge ($g_{2\parallel} \sim 1$) and (ii) the distance between the edges being larger than the radius of interaction ($d \gtrsim d_0$).

Note that the behavior of β_b as a function of T reduces, for $\beta_{b0} \ll 1$, to a simple power law (one can neglect the renormalization of K_-):

$$\beta_b(T) = \beta_{b0} \left(\frac{T}{T_d} \right)^{8K_0-2}. \quad (4.63)$$

For $K_0 < 1/4$ (by way of illustration, point B in Fig. 4.3), backscattering becomes stronger as T is decreased. The characteristic temperature T^* at which the zigzag charge-density wave is formed is obtained as a solution to $\beta_b(T^*) \sim 1$. For the interwire potential specified below Eq. (4.5), the result for T^* is given by (with $K_- = K_0$)

$$T^* = T_d \alpha_b^{1/(1-4K_-)} \propto \exp\left(-\frac{2k_F d}{1-4K_-}\right). \quad (4.64)$$

The behavior of the system in the strong-coupling regime will be discussed in Sec. 4.3.4.

4.3.3 Luttinger-liquid renormalization of the drag resistivity

In this section we calculate the drag resistivity in the high-frequency regime $\omega \gg \tau_D^{-1}$ incorporating renormalization effects due to Luttinger liquid physics. In second order perturbation theory in the interwire Coulomb interaction, the high-frequency drag resistivity is given by [97]

$$\rho_D = \int_0^\infty dq \int_0^\infty d\omega \frac{q^2 V_{12}^2(q)}{4\pi^3 n_1 n_2 T} \frac{\text{Im}\Pi_1(q, \omega) \text{Im}\Pi_2(q, \omega)}{\sinh^2\left(\frac{\omega}{2T}\right)}, \quad (4.65)$$

where $\text{Im}\Pi_\sigma(q, \omega)$ is the imaginary part of the retarded density-density correlation function of wire $\sigma = 1, 2$ and $n_\sigma = K_\sigma k_F / \pi$ is the electron density of wire σ . The drag resistivity obtained by this formula is equivalent to the high-frequency drag calculated previously using the kinetic equation approach [104]. However, the current formulation is more convenient for the present analysis, since it expresses the drag as an integral over the imaginary part of the polarization operator which can be calculated by standard means in the bosonized language. The calculation of the high-frequency drag resistivity is presented in App. D.5. We find

$$\rho_D \propto \alpha_b^2 \left(\frac{k_F}{k_0} \right)^4 \left(\frac{aT}{v} \right)^{4K} T. \quad (4.66)$$

We note that the parametric dependence of the drag resistivity is consistent with our weak coupling analysis in Eqs. (D.30) in the limit $K \rightarrow 1$.

It is instructive to obtain the derived temperature scaling $\rho_D \propto T^{4K+1}$ from the RG solution of the model in Eq. (4.52). For weak electron-electron interaction and $T \ll v_F/d$ the kinetic equation yields the rate in Eq. (D.30):

$$\rho_D \propto \alpha_b^2(T) T \quad (4.67)$$

where the dimensionless strength of backscattering $\alpha_b(T)$ is defined in (4.58). The effect of forward scattering can be taken into account by using a renormalized interaction coupling constant $\alpha_b(T)$ at

$K \neq 1$. The drag in the regime $\mu \gg T$ is mediated by $g_{1\perp}$ scattering, which has the scaling dimension $\Delta_{1,\perp} = 2K_- + 2$. This scaling dimension can be interpreted as the scaling of the operator $\cos(\sqrt{8\pi}\varphi)$ which we denote as $\Delta_{\text{op}} = 2K_-$ together with the scaling of the vertex momentum factors $\Delta_{\text{vert}} = 2$ that arise due to the rotation to the helical basis in Eq. (4.3). The renormalization due to the latter is already present in the weakly interacting case and yields $\alpha_b(T) = \alpha_b(Ta/v_F)^2$ for $K_- = 1$. The interaction constant is renormalized by the Luttinger parameter only due to the scaling dimension $\Delta_{1,\perp}$ since the momentum factors are not affected by Luttinger liquid effects. In combination this produces the renormalized interaction $\alpha_b(T) = \alpha_b(Ta/v_-)^{2K_-}$. Inserted into Eq. (4.67) this indeed yields the power law behavior $\rho_D(T) \propto T^{4K_-+1}$.

As we have pointed out in Sec. 4.3.2, the backscattering operator in Eq. (4.52), which itself is irrelevant, can generate relevant operators under the RG flow. These describe higher order backscattering processes that contribute to the drag resistivity in order α^4 . As we will see shortly, we cannot neglect these contributions, even though they are higher order in the interedge interaction strength, since they scale with a lower power of the temperature than the first order backscattering contributions for $K_- < 1/3$.

The effect of the higher order backscattering is not captured by the formula for the resistivity in Eq. (D.65), which neglects interedge correlations. To obtain the drag conductivity due to these processes we have to calculate the drag conductivity using Kubo's formula,

$$\sigma_D(\omega) = -\frac{i}{\omega} \lim_{q \rightarrow 0} \langle j_1(q, \Omega_n) j_2(-q, -\Omega_n) \rangle \Big|_{i\Omega_n \rightarrow \omega + i0^+}, \quad (4.68)$$

where $j_\sigma(x, \tau) = eK_\sigma v_\sigma \partial_x \theta(x, \tau) / \sqrt{\pi}$ is the current in edge $\sigma = 1, 2$. Here, the correlation function is calculated with respect to the action $S = S_0 + S_1 + S_2$ in Eq. (4.59),

$$\langle \dots \rangle = \frac{\int \mathcal{D}\varphi_- \dots e^{-S[\varphi_-]}}{\int \mathcal{D}\varphi_- e^{-S[\varphi_-]}} \quad (4.69)$$

The calculation is standard and yields in addition to the contribution due to first order backscattering discussed above the contribution $\text{Re}\sigma_D(\omega) = e^2 v_- \tau_D^{\infty, \beta_b} / \pi \omega^2$ with the high-frequency rate

$$\begin{aligned} \frac{1}{\tau_D^{\infty, \beta_b}} &= \beta_b^2 \left(\frac{\pi a T}{v_-} \right)^{16K_- - 3} \frac{v_-}{a} f(K_-), \\ f(K_-) &= \frac{4}{\pi} \sin(8\pi K_-) \cot(4\pi K_-) \Gamma^2\left(\frac{1}{2} - 4K_-\right) \Gamma^2(4K_-), \end{aligned} \quad (4.70)$$

where $\Gamma(x)$ is the Euler gamma function. As we have seen in Sec. 4.2.3 the same rate also parametrically determines the dc resistivity as $\rho_D \propto 1/\tau_D^\infty$.

The total drag resistivity is thus a sum of the contribution in Eq. (D.73), due to first order backscattering and the contribution in Eq. (4.70), resulting from second order backscattering. We note that even though the latter contribution is of higher order in the interedge interaction strength ($\beta_b \sim \alpha^4$) it scales with a lower power of the temperature if $K_- < 1/3$.

In summary, we have shown that the Luttinger liquid renormalization of the 1D theory leads to the anomalous power-law temperature dependence of the resistivity $\rho_D \propto T^\gamma$ for temperatures $T \ll T_d \sim T_1$. The exponent γ takes the value $\gamma = 4K_- + 1$ for $K_- > 1/3$ and $\gamma = 16K_- - 3$ for $1/4 < K_- < 1/3$. The different power laws originate from first order backscattering and second order backscattering processes, respectively.

The latter become relevant in the RG sense at $K_- < 1/4$ and drive the system into a strong-coupling phase. The behavior of the drag resistivity in this regime will be discussed in the next section.

4.3.4 Coulomb drag in the strong-coupling limit

In this section we will discuss the strong-coupling fixed point of the RG flow derived in Sec. 4.3.2 and analyze the behavior of the drag resistivity in the strong-coupling phase. The problem of Coulomb drag in this regime bears strong resemblance to the drag between spinless LLs discussed in the work by Klesse and Stern [94] and to the problem of pinned charge density waves (see e.g. the works by Rice *et al.*[119] and Maki [120]). To keep our analysis self contained, we will reproduce the main results of their discussion here referring to the original works for more details. In the strong-coupling limit, with $\beta_b \gg 1$ and $K_- \ll 1/4$, the action in (4.59) is minimized by the uniform mean-field configurations $\sqrt{32\pi}\varphi_-(x) \equiv \phi_m = (2m+1)\pi$, that minimize the potential energy term. Physically, φ_- describes the displacement of electrons in edge 2 with respect to electrons in wire 1. A uniform mean field therefore describes two interlocked charge density waves. At finite temperature there exist massive harmonic fluctuations around this mean field. However these excitations do not carry an antisymmetric current.

Electron transport from one end of the active wire to the other only occurs if the mean-field value changes from ϕ_m to $\phi_{m\pm 1}$. Depending on the temperature the transition between ground states occurs due to quantum tunneling or due to thermal activation. The excitations carrying the current are either (anti-)solitons that move along the wire, or soliton-antisoliton pairs that are formed inside the edge and dissociated by the applied electric field. The energy E_s and width W_s of a classical soliton are [120]

$$E_s = \sqrt{\frac{2\beta_b}{\pi^2 K_-}} \frac{v_-}{a}, \quad W_s = \frac{1}{4\sqrt{K_- \beta_b}} a. \quad (4.71)$$

We consider the regime where the soliton width is much smaller than the system length, $W_s \ll L$, and the temperature regime where solitons are excited thermally. In this limit the drag resistivity is determined by the creation of soliton-antisoliton pairs and reads as [119]

$$\rho_{\text{therm}} = \frac{h}{32\pi e^2 \ell_s} \sqrt{\frac{E_s T a^2}{2\beta_b K_- v_-}} e^{E_s/T}, \quad (4.72)$$

where the phenomenological parameter ℓ_s denotes the soliton mean free path.

Based on the above mapping, one concludes that for $K_- < 1/4$ the drag resistivity has a local minimum at a characteristic temperature T^* , Eq. (4.64), at which the coupling constant β_b for the second-order backscattering becomes of the order of unity, below this temperature, $\rho_D(T)$ starts growing exponentially due to thermally activated transitions between neighboring ground states of the potential energy. On the other hand, if $K_- > 1/4$, this local minimum does not occur and the drag resistivity vanishes as a power law as $T \rightarrow 0$.

We emphasize that the above conclusion is based on retaining only the terms S_0 and S_2 in the bosonized action (4.59). If the mapping onto the conventional theory of 1D drag worked for helical edges, for $K_- < 1/4$ one would obtain $\rho_D = -\rho_{12} \rightarrow \infty$ at $T \rightarrow 0$. However, from the general structure of the resistivity tensor, it follows that the diagonal (intraedge) resistivity should diverge simultaneously: $\rho_{11} \rightarrow \infty$. Indeed, for clean (no disorder) systems we have $\rho_{11} = -\rho_{12}$. Thus, the divergence of the drag resistivity would mean that the interedge coupling destroys the topological protection of the (otherwise) conducting helical edge states. Specifically, on both sides of the quantum spin-Hall transition driven by the closing and re-opening of the gap in the 2D bulk of the system (gap inversion), we would then have non-conducting edge states. However, at zero gap the 2D bulk state is still conducting; therefore, the delocalized bulk state should transform into the conducting edge state at one side of the QSH transition.

The situation is especially transparent in the “horizontal” drag setup, where the two parallel helical edges belong to the two 2D samples placed in the same plane (not one above the other as in the “vertical” setup of Fig. 4.1). Clearly, the interaction between the two halves of the sample cannot affect the 2D bulk properties away from the cut along which the 1D drag is observed. Each of the two samples still remains a 2D topological insulator and hence possesses conducting edges. Even if one obtains $\rho_{11} = \rho_{22} = \infty$ for the original edges, the true conducting edges are expected to re-appear deeper into the sample: this would correspond to an “edge repulsion” or, in other words, to the shift of the true conducting edges towards the bulk due to the “edge reconstruction”. The drag resistivity of the new edge states would not be then infinite at $T = 0$.

We speculate that, on a formal level of the effective edge theory, this “topological protection” might be related to the difference between the HLL and normal TLL: the former contains an additional term S_1 in the action (α -term). While in the weak-coupling regime this term is highly irrelevant, when the β -term S_2 enters the strong-coupling limit, the α -term might again become relevant, destroying the charge-density wave. In this scenario, the topological protection is maintained due to the competition of α and β terms in the action, leading to non-perturbative effects in the strong-coupling regime. A somewhat similar situation was encountered in Ref. [15] devoted to the 2D surface states of 3D topological insulators. There, the perturbative (weak-coupling) RG suggested the localization of surface states due to the Altshuler-Aronov-type corrections, but the nonperturbative effect of the topological protection resulted in the emergence of a critical state in the strong-coupling regime

To conclude this section, the behavior of the drag resistivity at sufficiently strong intraedge interaction, $K_- < 1/4$, is expected to be governed by the interplay of the tendency to formation of a charge-density wave due to the second-order backscattering (term S_2 in the action) and topological protection encoded in the α -term S_1 . This interplay might lead to a non-monotonous temperature dependence of ρ_D at low T with a local minimum around T^* and a local maximum at yet lower T . The behavior of the drag resistivity at finite T would then demonstrate an “apparent metal-insulator transition” driven by the decreasing K_- . Based on the weak-coupling RG formalism, we cannot make definite conclusions on the nature of zero- T drag for $K_- < 1/4$. We relegate the corresponding analysis to future work.

4.4 Discussion of the drag resistivity

In this section, we combine the results obtained so far and discuss the resulting qualitative behavior of the drag resistivity. The high-frequency drag rate τ_D^∞ has been obtained in Sec. 4.2.2 and we have shown in Sec. 4.2.3 that the same rate also determines the parametric dependence of the dc-drag resistivity as $\rho_D \propto 1/\tau_D^\infty$. The results obtained in the kinetic equation framework hold down to temperatures $T \sim T_d \sim T_1$, below which Luttinger liquid effects become important. In Sec. 4.3.3 we have shown that the Luttinger liquid renormalization leads, as usual, to anomalous power law temperature dependence. Let us, by way of illustration, discuss the behavior of the high-frequency rate (or equivalently the dc-drag resistivity) for a fixed chemical potential $\mu \ll T_{p0}$, as depicted in Figs. D.2 and D.3. At lowest temperatures, the rate is determined by the particle-hole contribution. The drag rate, given in Eq. (D.30), grows as a power law. Electron-electron forward scattering further renormalizes the exponent, which yields

$$\frac{1}{\tau_{D,\text{ph}}^\infty} \propto \alpha^2 \left(\frac{\mu}{v_F k_0} \right)^4 \left(\frac{T}{T_d} \right)^\gamma T_d e^{-4k_F d}. \quad (4.73)$$

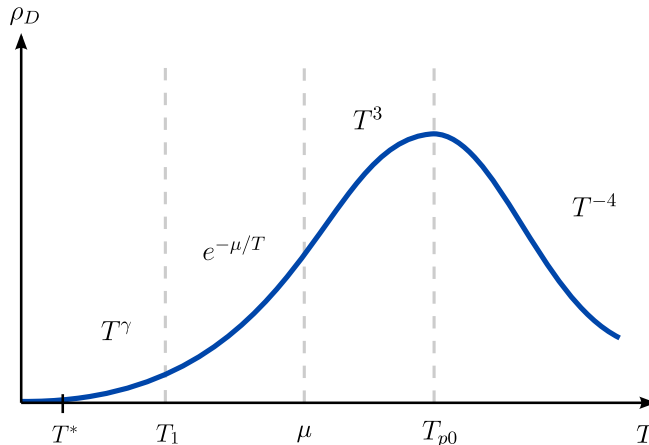


Figure 4.4: Sketch of the T dependence of the drag resistivity ρ_D for two helical liquids for $\mu \ll T_{p0}$, where T_{p0} is the temperature above which the plasmon damping leads to a strong suppression of the drag rate. For $T \gg T_1$, electron-hole excitations in two edges couple to each other through plasmon modes (“plasmon-mediated Coulomb drag”). For $T \ll T_1$, Coulomb drag is determined by direct backscattering of electrons close to the Fermi surface. The exponent of the power law in this regime is $\gamma = 4K_- + 1$, if $K_- > 1/3$ and $\gamma = 16K_- - 3$ if $K_- < 1/3$. As T decreases, the system enters the strong-coupling regime at $T \sim T^*$ (Sec. 4.3.2).

Here, the exponent γ takes the value $\gamma = 4K_- + 1$ for $K_- > 1/3$ and $\gamma = 16K_- - 3$ for $1/4 < K_- < 1/3$. The different power laws originate from first order backscattering and second order backscattering processes, respectively.

At higher temperatures a crossover to the plasmon-dominated regime occurs at the characteristic scale

$$T_1 = \frac{1}{4} \frac{\mu}{\ln(k_0/k_F) + k_F d}. \quad (4.74)$$

For temperatures above T_1 , particle-hole fluctuations in one edge transfer momentum to plasmons which, in turn, transfer momentum to the other edge. The coupling to plasmons occurs through g_5 -type scattering processes making the plasmon mediated drag a feature unique to the HLL. For $T \ll \mu$ the drag rate contains the activation factor $\exp(-\mu/T)$, because g_5 Umklapp processes are thermally activated which lead to the drag rate in (D.43),

$$\frac{1}{\tau_{D,P1}^\infty} \propto \alpha^2 \left(\frac{\mu}{v_F k_0} \right)^4 \left(\frac{\mu}{\pi T} \right)^2 T e^{-\frac{\mu}{T}}. \quad (4.75)$$

For $\mu \ll T_p$, the activation behavior of the rate crosses over at $T \sim \mu$ to the power-law growth given by Eq. (D.44):

$$\frac{1}{\tau_D^\infty} \propto \alpha^2 \left(\frac{\mu}{v_F k_0} \right)^2 \left(\frac{T}{v_F k_0} \right)^2 T. \quad (4.76)$$

At the highest temperatures, $T \gg \max\{\mu, T_p\}$, the drag rate decreases as described by Eq. (D.47):

$$\frac{1}{\tau_D^\infty} \propto \alpha^2 \left(\frac{\mu}{v_F k_0} \right)^2 \left(\frac{T_p}{v_F k_0} \right)^2 \left(\frac{T_p}{T} \right)^4 T_p. \quad (4.77)$$

The overall temperature dependence of the high-frequency drag rate for $\mu \ll T_p$ is shown schematically in Fig. 4.4. The T dependence of $1/\tau_D^\infty$ for $\mu \gg T_p$ is qualitatively similar, with the maximum shifted towards $T \sim \mu$. Most importantly, as we discuss in Sec. 4.3.4, we expect that the drag resistivity always vanishes at $T = 0$, due to the topological origin of the HLL. This is in stark contrast to the behavior of conventional LLs, where the formation of a zig-zag order at lowest temperatures inevitably leads to an exponentially diverging drag resistivity at lowest temperatures.

4.5 Summary of chapter 4

We have presented a theory of Coulomb drag between clean (no disorder) HLLs based on the kinetic equation approach supplemented with bosonization to take into account Luttinger liquid renormalization. We assume that the spin-rotational invariance of the helical liquid is broken by Rashba spin-orbit coupling in the bulk of the topological insulator, which allows for interedge backscattering events without breaking TRS. We find that the drag in a HLL differs significantly from a LL both in its magnitude and temperature dependence.

The main result of our analysis concerns the behavior of the dc-drag resistivity as a function of the temperature depicted in Fig. 4.4. For temperatures below a characteristic scale T_1 , drag occurs due to backscattering of electrons in the passive edge at the Fermi surface caused by particle-hole fluctuations in the active edge. The drag resistivity in this regime generically behaves as a power law with anomalous exponent determined by the Luttinger parameter of the relative density mode K_- . At higher temperatures, on the other hand, we find that the dominant contribution to the resistivity derives from plasmon mediated drag. The discovery of this novel mechanism of plasmon mediated drag in one dimensional systems constitutes the second main result of this chapter. The mechanism can be thought of as unique to the HLL because it necessarily requires the existence of a Dirac point in the spectrum.

Finally, we have argued that, unlike in the case of coupled LLs, the drag resistivity of coupled HLLs does not increase exponentially at lowest temperatures but rather goes to zero as a power law. This behavior was attributed to the topologically nontrivial origin of the HLL. It is in particular this feature of the drag resistivity that might be used to experimentally distinguish the drag between helical liquids.

5

Chapter 5

Emergent topological properties in one-dimensional conductors with spin-orbit coupling

Topological states of matter are typically characterized by a gapped bulk spectrum and gapless edge states with unique properties. In the previous chapters, we have studied the transport properties of the gapless one-dimensional edge modes that emerge at the boundary of 2D TIs with preserved TRS. The transport properties of these modes are particularly interesting since they are topologically protected against localization by disorder as long as the intra-edge interaction is not too strong. So far, we have only considered TIs that are bulk insulators, however, the origin of the bulk gap can be diverse.

In particular, we have shown in Ch. 1 that strong interactions in one-dimensional electron systems can lead to strong coupling phases where spectral gaps are generated dynamically without spontaneous breaking of any continuous symmetry. A particularly fascinating example of such a dynamically generated state is the Luther-Emery liquid [121], in which the charge sector remains critical (gapless), while the spin degrees of freedom acquire a gap. This can quite naturally occur for attractive interactions, in which case pairs of spins form singlets and the system exhibits many properties akin to superconductivity [35, 44, 122]. If the interactions are repulsive, however, the spin gap may only form if $SU(2)$ spin-rotational symmetry is broken in the system [35, 44]. While both cases have the same thermodynamic spectrum, the states are rather different, with the dominant correlations in the repulsive case being of the SDW type.

A natural way to break the $SU(2)$ symmetry in the spin sector while preserving TRS is by including SOC terms into the model. In this chapter we will study the model of one-dimensional electrons in the presence of Rashba SOC and show that the SDW phase indeed can be realized for a certain regime of parameters. Subsequently, we investigate, if this gapped phase exhibits properties akin to topological insulators. In particular, we are interested in the transport properties in the presence of non-magnetic disorder and the excitation spectrum at the boundary of the 1D system to the vacuum.

The chapter is organized as follows. First, we discuss a minimal model for one-dimensional electrons in the presence of SOC in Sec. 5.1. The SOC breaks the $SU(2)$ spin-rotational symmetry but preserves TRS. We then show in Sec. 5.2 that interactions can drive the system into the SDW phase for strong SOC, where the spin sector becomes gapped. Subsequently, we investigate the transport properties of the gapped phase in the presence of disorder in Sec. 5.3 and analyze the excitation spectrum at the boundary of the SDW phase to the vacuum with respect to the presence or absence of localized zero modes in Sec. 5.3.2. Lastly, we summarize our findings in Sec. 5.4.

This chapter is based in part on Ref. [123].

5.1 Model for interacting one-dimensional electrons in the presence of SOC

In this section we introduce a minimal lattice model for interacting one-dimensional electrons in the presence of Rashba-type spin-orbit coupling. We will consider the experimentally relevant situation, that the 1D channel is produced by constraining the motion of particles in a two-dimensional electron gas along one direction by external gates. To motivate the form of the lattice model it is therefore useful to first review the origin of Rashba SOC in 2D electron gases.

Typically, the electrons in the 2D electron gas originate in atomic s and p orbitals. The electrons are subject to atomic spin-orbit coupling, described by the single particle Hamiltonian $H_{SO} = \Delta_{SO} \mathbf{L} \times \mathbf{S}$, with spin \mathbf{S} and angular momentum \mathbf{L} . Furthermore the electrons experience an electric field perpendicular to the 2D surface, which generates an asymmetric potential that confines them to the plane [124]. The electric field has two main effects on the band structure. First, it breaks the inversion symmetry and generates a gap 2Δ between the s and p bands. Second, it hybridizes the bands. In the lattice model, this is described by a finite hopping with amplitude t_1 between the orbitals on adjacent sites. The Rashba effect can be understood as a process in second order perturbation theory, where an electron hops from the s orbital to the p orbital with amplitude t_1 and then uses the atomic SOC to flip its spin and hop back to the s orbital with amplitude Δ_{SO} . Note that overall the electron flipped spin and hopped one site in the same band. The amplitude of this process is $\alpha \sim a_0 t_1 \Delta_{SO} / \Delta$, with the lattice constant a_0 .

Based on these considerations, let us now formulate the model. We consider electrons with orbital quantum number $n = a, b$ and spin $\sigma = \uparrow, \downarrow$ with next nearest neighbor hopping on a 1D lattice. The hopping can be either intraorbital or interorbital. Each of the orbital states has an onsite energy, such that the bands corresponding to these orbitals have a bandgap 2Δ . Including SOC and Hubbard on-site interaction the Hamiltonian consists of four parts.

$$H = H_0 + H_1 + H_{SO} + H_{\text{int}}. \quad (5.1)$$

The kinetic part reads as

$$H_0 = -\Delta \sum_{j,\sigma} \left[a_{j,\sigma}^\dagger a_{j,\sigma} - b_{j,\sigma}^\dagger b_{j,\sigma} \right] - t \sum_{j,\sigma} \left[a_{j,\sigma}^\dagger a_{j+1,\sigma} + b_{j,\sigma}^\dagger b_{j+1,\sigma} + \text{H.c.} \right]. \quad (5.2)$$

Here, $a_{j,\sigma}$ destroys an electron in band a with spin $\sigma = \uparrow, \downarrow$ at site j and analogously for $b_{j,\sigma}$. The hopping amplitude between next nearest neighbors is denoted by t and the on-site energy by Δ . We use dimensions where the lattice spacing $a_0 = 1$ and we assume periodic boundary conditions.

The hybridization between the bands is described by the Hamiltonian

$$H_1 = -t_1 \sum_{j,\sigma} \left[a_{j,\sigma}^\dagger b_{j+1,\sigma} + b_{j,\sigma}^\dagger a_{j+1,\sigma} + \text{H.c.} \right], \quad (5.3)$$

and the spin-orbit coupling term reads as

$$H_{SO} = -i\alpha \sum_{j,\sigma,\sigma'} \left[a_{j,\sigma}^\dagger \sigma_{\sigma,\sigma'}^z a_{j+1,\sigma'} + b_{j,\sigma}^\dagger \sigma_{\sigma,\sigma'}^z b_{j+1,\sigma'} + \text{H.c.} \right]. \quad (5.4)$$

Here σ^i , with $i \in \{x, y, z\}$ denotes the set of Pauli matrices in spin space. Note, that the Rashba SOC with coupling strength α breaks the SU(2) spin-rotational symmetry of the model down to U(1) but preserves time-reversal symmetry. Here, the operation of time reversal Θ acts as $\Theta a_{j,\sigma} \Theta^{-1} = i\sigma_{\sigma,\sigma'}^y a_{j,\sigma'}$, $\Theta b_{j,\sigma} \Theta^{-1} = i\sigma_{\sigma,\sigma'}^y b_{j,\sigma'}$ and $\Theta i \Theta^{-1} = -i$.

Finally, the Hubbard interaction is given by

$$H_{\text{int}} = U \sum_j n_{j,\uparrow} n_{j,\downarrow}. \quad (5.5)$$

with the coupling constant U and the electron density operator $n_{j,\sigma} = a_{j,\sigma}^\dagger a_{j,\sigma} + b_{j,\sigma}^\dagger b_{j,\sigma}$.

Throughout this work, we assume the hopping and spin-orbit amplitudes as positive, $t, t_1, \alpha > 0$ and repulsive interactions, $U > 0$.

5.1.1 Diagonalization of the non-interacting Hamiltonian

In the presence of interorbital hopping, described by H_1 , the Hamiltonian in Eq. (5.1) is no longer diagonal. Before we diagonalize the noninteracting part of the Hamiltonian, it is instructive to first discuss the model in the single-channel approximation. In this approximation, usually employed in the study of electron transport in quantum wires, one neglects the coupling to energetically higher bands ($t_1 = 0$) and considers only the lowest band in the orbital basis. We will show that in this approximation the SOC term only leads to a trivial renormalization of the parameters of the model.

The noninteracting part of the Hamiltonian in Eq. (5.1) with $t_1 = 0$ can be written in diagonal form by transforming to momentum space. Considering only the lower band, it reads as

$$H_0 = \sum_{k,\sigma} a_{k,\sigma}^\dagger [-2t \cos(k) + 2\alpha s \sin(k)] a_{k,\sigma}, \quad (5.6)$$

where $s = \pm 1$ are the eigenvalues of σ^z . Using the harmonic addition theorem, this can be recast into the form

$$H_0 = -2t_0 \sum_{k,\sigma} \cos(k - sq_0) a_{k,\sigma}^\dagger a_{k,\sigma}. \quad (5.7)$$

Here, $t_0 = \sqrt{t^2 + \alpha^2}$ is the renormalized hopping amplitude and $q_0 = \arctan(\alpha/t)$.

Therefore, SOC renormalizes the hopping amplitude and shifts the spectrum by a constant momentum $\pm q_0$, for spin up and down respectively. However, this shift can always be removed by a spin dependent gauge transformation and therefore has no observable effect on the thermodynamic properties of the system, which only depend on the spectrum.

This statement can be made explicit by considering the Hamiltonian in Eq. (5.6) in real space:

$$H_0 = -2t_0 \sum_{j,\sigma} e^{iq_0 j \sigma} a_{j,\sigma}^\dagger a_{j+1,\sigma} = -2t_0 \sum_{j,\sigma} d_{j,\sigma}^\dagger d_{j+1,\sigma}, \quad (5.8)$$

where we defined the fermion operator $d_{j,\sigma} = e^{iq_0 j \sigma} a_{j,\sigma}$. The model in the presence of SOC is therefore unitarily equivalent to a model without SOC but with renormalized hopping parameter [125]. Note that this statement remains true in the presence of interactions since the transformation leaves the density $n_{j,\sigma} = a_{j,\sigma}^\dagger a_{j,\sigma} = d_{j,\sigma}^\dagger d_{j,\sigma}$ invariant and thus does not change the form of the interaction term

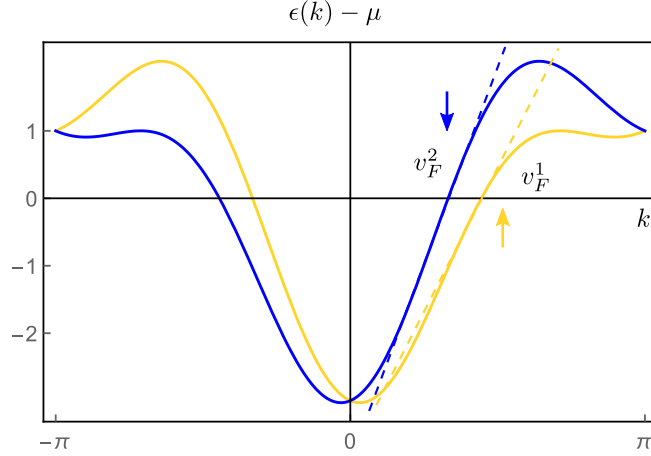


Figure 5.1: Dispersion of the lower bands $\epsilon_{\sigma,-}(k)$ of the lattice model in Eq. (5.9) for parameters $\alpha/t = 0.3$ and $t_1/t = 0.5$. Spin orbit coupling lifts the degeneracy of the bands labelled by the z -component of the spin and leads to different Fermi velocities v_F^1 and v_F^2 .

H_{int} . For repulsive electron-electron interaction the system is in the Luttinger liquid phase (see section 5.2.2), irrespective of the presence or absence of SOC.

The reason why spin-orbit may be gauged out in the single-channel approximation is quite simple. Since the electrons only move along one direction, there is no “orbital” motion possible, so the spin-orbit may only couple as a pure gauge.¹ To obtain nontrivial effects of the spin-orbit coupling beyond the single channel approximation we necessarily have to include a coupling between different orbitals.

Let us therefore consider the complete noninteracting part in Eq. (5.1). Introducing the vector of operators $\mathbf{c}_{k,\sigma} = (a_{k,\sigma}, b_{k,\sigma})^T$, it takes the form

$$H_0 = \sum_{k,\sigma} \mathbf{c}_{k,\sigma}^\dagger [\mathbf{n}\boldsymbol{\tau} - 2t_0 \cos(k - sq_0)] \mathbf{c}_{k,\sigma}, \quad (5.9)$$

where $\mathbf{n} = (-2t_1 \cos k, 0, \Delta)^T$ and $\boldsymbol{\tau}$ is the vector of Pauli matrices in orbital space. Next, we introduce fermionic operators \mathbf{f} in the band basis, which are related to the orbital basis by the unitary transformation $\mathbf{f}_{k,\sigma} = U \mathbf{c}_{k,\sigma}$, with $U = \exp(i\gamma_k \tau_y)$. Choosing $\tan 2\gamma_k = n_1(k)/|\mathbf{n}(k)|$, the Hamiltonian takes the diagonal form

$$H_0 = \sum_{k,\sigma,m} \epsilon_{\sigma,m}(k) \mathbf{f}_{k,\sigma,m}^\dagger \mathbf{f}_{k,\sigma,m}, \quad (5.10)$$

where $m = \pm$ denotes the band index and

$$\epsilon_{\sigma,m}(k) = -2t_0 \cos(k - sq_0) + m \sqrt{\Delta^2 + 4t_1^2 \cos^2 k}. \quad (5.11)$$

We note that the spin in z -direction is still a good quantum number and the time reversal symmetry of the model is still preserved and therefore the spectrum has the symmetry $\epsilon_\sigma(k) = \epsilon_{-\sigma}(-k)$.

Let us now consider the lower two bands with $m = -1$. They are characterized by the z -component of the spin and shifted by a constant momentum q_0 . The band structure is depicted in Fig. 5.1. Notice

¹One should be careful, however, that this does not mean that there are no observable effects of spin-orbit, see Ref. [125].

that the inversion symmetry is broken due to the SOC and thus $\epsilon_\sigma(k) \neq \epsilon_\sigma(-k)$. While this is also true when $t_1 = 0$, the hybridisation between the orbitals leads to different Fermi velocities at the Fermi points of each band [cf. Fig. 2], and hence the symmetry cannot be restored by a trivial gauge transformation. This difference of Fermi velocities is the main effect of SOC on the spectrum.

Let us find an analytical estimate for the velocity difference of band $\sigma = +1$ in the limit when $t_0 \gg t_1$ and the chemical potential is tuned to the bottom of the band. For simplicity, we also set $\Delta = 0$, which would only renormalize the bandwidth. In this case, we can expand the spectrum around $k = q_0$. We first find the Fermi points of the band, determined by the equation $\epsilon_\uparrow(k_{F,\uparrow}^1) = \epsilon_\uparrow(k_{F,\uparrow}^2) = \mu$, and the corresponding Fermi velocities $v_{F,\uparrow}^{1,2} = \partial E / \partial k|_{k=k_{F,\uparrow}^{1,2}}$. Due to the preserved time reversal symmetry the Fermi points and Fermi velocities are not independent but rather $k_{F,\uparrow}^{1,2} = -k_{F,\downarrow}^{1,2} \equiv k_F^{1,2}$ and $v_{F,\uparrow}^{1,2} = -v_{F,\downarrow}^{1,2} \equiv v_F^{1,2}$. We find the dimensionless velocity difference

$$\Delta v = \frac{v_F^1 - v_F^2}{v_F^1 + v_F^2} \simeq \cot \sqrt{2} \frac{t_1}{\sqrt{t^2 + \alpha^2}} \sin(q_0). \quad (5.12)$$

Notice that the velocity difference vanishes either in the absence of SOC, $\alpha = 0$, or interband hopping, $t_1 = 0$. For weak SOC, it is of the order of $\delta v \sim \alpha t_1 / t^2$.

To summarize, by using an explicit hopping model for one-dimensional fermions in the presence of SOC, we have identified two main effects of SOC on the spectrum of noninteracting electrons. First, it breaks the SU(2) spin-rotational symmetry and therefore lifts the spin degeneracy of the spectrum. Second, it breaks inversion symmetry leading to different Fermi velocities $v_F^1 \neq v_F^2$. In the next section we will investigate how this affects the phase diagram in the presence of interaction.

5.2 Interaction effects

To find the effective low-energy form of the Hamiltonian in Eqs. (5.9) and (5.5) we linearize the spectrum of the lower band near the Fermi points $k_F^{1,2}$, see Fig. 5.2, and expand the fermionic operators in continuum modes that vary slowly on the scale of the inverse Fermi momentum:

$$\begin{aligned} f_{j,\uparrow,-} &\rightarrow \psi_\uparrow(x) = R_\uparrow(x) e^{ik_F^1 x} + L_\uparrow(x) e^{-ik_F^2 x}, \\ f_{j,\downarrow,-} &\rightarrow \psi_\downarrow(x) = R_\downarrow(x) e^{ik_F^2 x} + L_\downarrow(x) e^{-ik_F^1 x}. \end{aligned} \quad (5.13)$$

This yields the density

$$n_{j,\sigma} \rightarrow R_\sigma^\dagger R_\sigma + L_\sigma^\dagger L_\sigma + R_\sigma^\dagger L_\sigma e^{-i2k_F x} + L_\sigma^\dagger R_\sigma e^{i2k_F x}. \quad (5.14)$$

where we defined $k_F = (k_F^1 + k_F^2)/2$.

The low-energy form of the Hamiltonian density is given by $\mathcal{H} = \mathcal{H}_0 + \mathcal{H}_{\text{int}}$, with

$$\mathcal{H}_0 = -iv_F^1 \left(R_\uparrow^\dagger \partial_x R_\uparrow - L_\downarrow^\dagger \partial_x L_\downarrow \right) - iv_F^2 \left(R_\downarrow^\dagger \partial_x R_\downarrow - L_\uparrow^\dagger \partial_x L_\uparrow \right), \quad (5.15)$$

$$\mathcal{H}_{\text{int}} = U \left(R_\uparrow^\dagger R_\uparrow + L_\uparrow^\dagger L_\uparrow \right) \left(R_\downarrow^\dagger R_\downarrow + L_\downarrow^\dagger L_\downarrow \right) + U \left(R_\uparrow^\dagger L_\uparrow L_\downarrow^\dagger R_\downarrow + \text{H.c.} \right). \quad (5.16)$$

Here, v_F^1 and v_F^2 are considered as phenomenological parameters of the low-energy theory which describe the different Fermi velocities at the left and right Fermi point. On the basis of our analysis of the hopping model in section 5.1 we expect the velocity difference to be small but in principle tunable

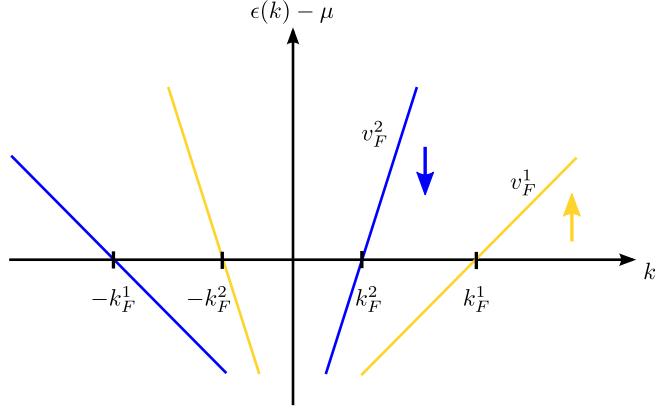


Figure 5.2: Band structure $\epsilon(k)$ of the low-energy theory. Due to time reversal invariance the dispersions of the two bands are connected as $\epsilon_{\uparrow}(k) = \epsilon_{\downarrow}(-k)$. The low-energy excitations for up spins are right moving particles with velocity v_F^1 at Fermi momentum k_F^1 and left moving particles with velocity $-v_F^2$ at Fermi momentum $-k_F^2$ [analogously for down spins].

through the Rashba parameter α . We remind the reader that the Rashba SOC arises due to the asymmetry associated with the potential that constricts electrons to the two-dimensional plane. The asymmetry, and therefore the Rashba SOC, can be further controlled by applying an external gate voltage [126–128].

5.2.1 Bosonization

To account for the effects of interaction it is useful to pass to a bosonic description of the model using the bosonization rules outlined in App. A. After bosonization, the quadratic part of the Hamiltonian density takes the form

$$\mathcal{H}_0 = \frac{v_F}{2} \sum_{\sigma} \left[(\partial_x \varphi_{\sigma})^2 + \Pi_{\sigma}^2 \right] + \frac{\delta v}{2} \left[\partial_x \varphi_{\uparrow} \Pi_{\uparrow} - \partial_x \varphi_{\downarrow} \Pi_{\downarrow} \right], \quad (5.17)$$

where we introduced the difference $\delta v = v_F^1 - v_F^2$ and average $v_F = (v_F^1 + v_F^2)/2$ of Fermi velocities .

We now introduce the usual spin and charge operators

$$\varphi_c = \frac{\varphi_{\uparrow} + \varphi_{\downarrow}}{\sqrt{2}}, \quad \varphi_s = \frac{\varphi_{\uparrow} - \varphi_{\downarrow}}{\sqrt{2}}. \quad (5.18)$$

The system is symmetric under time reversal. Using the transformation properties of the lattice fermions defined below Eq. (5.4) and the low-energy decomposition in Eq. (5.13) we find that under time reversal, $R_{\uparrow} \rightarrow L_{\downarrow}$, $L_{\uparrow} \rightarrow R_{\downarrow}$, $R_{\downarrow} \rightarrow -L_{\uparrow}$ and $L_{\downarrow} \rightarrow -R_{\uparrow}$. This implies the following transformation properties in the spin-charge basis

$$\varphi_c(x) \rightarrow \varphi_c(x), \quad \varphi_s(x) \rightarrow -\varphi_s(x), \quad \theta_c(x) \rightarrow -\theta_c(x), \quad \theta_s(x) \rightarrow \theta_s(x). \quad (5.19)$$

The importance of the TRS for the model will become clear once we discuss the transport properties in the presence of disorder.

In the new basis, the (time-reversal invariant) Hamiltonian density including electron-electron interaction reads as

$$\begin{aligned}\mathcal{H}_c &= \frac{v_c}{2} \left[K_c \Pi_c^2 + K_c^{-1} (\partial_x \varphi_c)^2 \right], \\ \mathcal{H}_s &= \frac{v_s}{2} \left[K_s \Pi_s^2 + K_s^{-1} (\partial_x \varphi_c)^2 \right] + \frac{g_\perp}{2(\pi a)^2} \cos(\sqrt{8\pi} \varphi_s), \\ \mathcal{H}_{SO} &= \frac{\delta v}{2} \left[\partial_x \varphi_c \Pi_s + \partial_x \varphi_s \Pi_c \right].\end{aligned}\tag{5.20}$$

Here, the Luttinger parameters and plasmon velocities are defined as

$$K_\mu = 1 + \frac{g_\mu}{2\pi v_F}, \quad v_\mu K_\mu = v_F.\tag{5.21}$$

where $\mu = c, s$. In terms of the lattice parameters, we have

$$g_c = -g_s = -g_\perp = -a_0 U,\tag{5.22}$$

where we reinstated the lattice constant a_0 . In particular for repulsive interaction $U > 0$, we find $K_c < 1$ and $K_s > 1$.

We notice that the charge sector in Eq. (5.20) is a LL with coupling constants v_c and K_c . The spin sector is also a LL but includes a backscattering term that can generate a spin gap if it becomes relevant in the RG sense. We point out that the coupling constant in front of the cosine term is the same that determines the Luttinger constant in the spin sector, i.e. $g_s = g_\perp$. This is no peculiarity of the Hubbard model, but holds for any spin SU(2) invariant model. In the absence of SOC the RG flow of the model is described by the well known BKT equations (5.31) and the relation between the bare parameters constrains the flow exactly along the separatrix, see Fig. 5.3. In this case the cosine term is irrelevant and the spinsector is a gapless Luttinger liquid.

The different Fermi velocities and thus the SOC manifest themselves only in the term \mathcal{H}_{SO} that breaks the spin-charge separation. Usually, the (marginal) term \mathcal{H}_{SO} would be neglected as it only produces small corrections under the RG. In the present case, however, we have to keep it, since the conventional flow is exactly along the separatrix and thus even a marginal term may drive the system into a new phase.

For the subsequent analysis it is convenient to switch to an imaginary time action formalism. The partition function of the model is then

$$Z = \int \mathcal{D}\varphi_c \mathcal{D}\varphi_s e^{-S_s[\varphi_s] - S_c[\varphi_c] - S_{SO}[\varphi_c, \varphi_s]},\tag{5.23}$$

$$S_c = \int \frac{dx d\tau}{2v_F} \left[(\partial_\tau \varphi_c)^2 + (v_c^*)^2 (\partial_x \varphi_c)^2 \right],\tag{5.24}$$

$$S_s = \int \frac{dx d\tau}{2v_F} \left[(\partial_\tau \varphi_s)^2 + \left\{ v_s^2 - \frac{(\delta v)^2}{4} \right\} (\partial_x \varphi_s)^2 \right] + \frac{g_\perp}{2(\pi a)^2} \int dx d\tau \cos(\sqrt{8\pi} \varphi_s),\tag{5.25}$$

$$S_{SO} = \frac{i\delta v}{2v_F} \int dx d\tau \left[\partial_x \varphi_c \partial_\tau \varphi_s + \partial_x \varphi_s \partial_\tau \varphi_c \right].\tag{5.26}$$

Here we introduced the renormalized coupling constants

$$K_c^* = K_c \left(1 - \frac{\delta v^2}{4v_c^2} \right)^{-\frac{1}{2}}, \quad v_c^* = v_F / K_c^*.\tag{5.27}$$

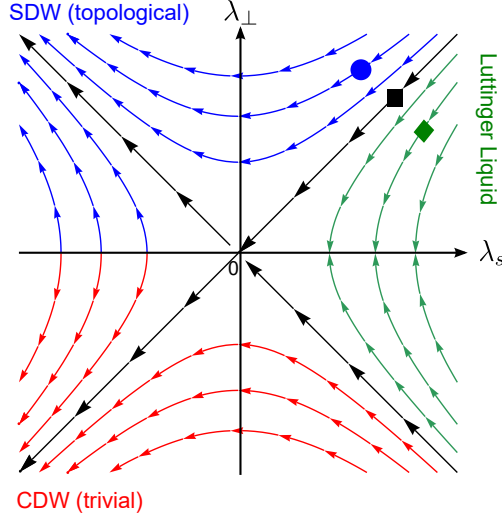


Figure 5.3: RG flow of Eq. (5.31) describing the phase diagram of interacting 1D fermions. In the presence of spin-orbit coupling the starting point of the flow is changed away from the $SU(2)$ invariant line (black rectangle) to the region of strong-coupling flow (blue circle) for strong spin-orbit coupling ($\overline{\delta v} > 2\overline{U}$) or to the region of flow towards the Luttinger liquid phase (green diamond) for weak spin orbit coupling ($\overline{\delta v} < 2\overline{U}$).

Next, we integrate out the (quadratic) charge sector which yields an effective action $S_{\text{eff},s} = S_0 + S_{\text{int}}$ in the spin sector:

$$S_0 = \frac{1}{2} \int \frac{dq}{2\pi} \frac{d\omega}{2\pi} \varphi_s(q, \omega) \varphi_s(-q, -\omega) \left[\frac{1}{v_s(q, \omega) K_s(q, \omega)} \omega^2 + \frac{v_s(q, \omega)}{K_s(q, \omega)} q^2 \right], \quad (5.28)$$

$$S_{\text{int}} = \frac{g_{\perp}}{2(\pi a)^2} \int dx d\tau \cos(\sqrt{8\pi} \varphi_s).$$

The effective spin velocity and the Luttinger parameter obey the following equations

$$v_s(q, \omega) K_s(q, \omega) = v_F, \quad (5.29)$$

$$\frac{v_s(q, \omega)}{K_s(q, \omega)} = \frac{v_s}{K_s} - v_F \left(\frac{\delta v}{2v_F} \right)^2 \left[1 - \frac{4\omega^2}{\omega^2 + (v_c^* q)^2} \right]. \quad (5.30)$$

Note that v_s and K_s are the coupling constants of the system without SOC. The effective propagator in the spin sector is affected in two ways by SOC as can be seen in Eq. (5.30): (i) The parameters in the spin sector are explicitly renormalized by a δv term and (ii) there is a contribution from the charge degrees of freedom where v_c^* is renormalized according to Eq. (5.27).

5.2.2 Renormalization-group analysis

To determine the phase diagram in the presence of interactions we derive the RG equations of the effective action in Eq. (5.28) employing a perturbative Wilson RG procedure in momentum space. To

this end we integrate out all high energy degrees of freedom between the momentum cutoff Λ and a lower cutoff Λ' to obtain the low-energy physics of the model. Details of the calculation can be found in Appendix B of [123]. The result of this procedure is encoded in differential equations for the dimensionless strength of backscattering $\lambda_{\perp} = g_{\perp}/\pi v_F$ and the dimensionless coupling constant $\lambda_s = 2(1 - K_s - \delta v^2/8v_s^2)$. The equations are of the BKT type and read as

$$\begin{aligned}\frac{d\lambda_{\perp}}{d\ell} &= -\lambda_{\perp}(\ell)\lambda_s(\ell), \\ \frac{d\lambda_s}{d\ell} &= -\lambda_{\perp}^2(\ell).\end{aligned}\tag{5.31}$$

Here, $\ell = \ln(\Lambda/\Lambda')$ and the initial values are given by $\lambda_{\perp}(0) = \bar{U}$ and $\lambda_s(0) = \bar{U} + \bar{\delta v} f(\bar{U}, \bar{\delta v})$. They are determined by the dimensionless strength of interaction $\bar{U} = a_0 U/\pi v_F$ and the dimensionless velocity difference $\bar{\delta v} = (\delta v/2v_F)^2$. The RG equations have been derived for both $\bar{U} \ll 1$ and $\bar{\delta v} \ll 1$.

The function $f(\bar{U}, \bar{\delta v})$, that appears in the bare value of λ , is nonuniversal; that is, it depends on the cutoff procedure of the RG. However, independent of the way the cutoff is introduced, one can show that it changes sign at some point,

$$\text{sign} f = \text{sign} \left(\frac{2\bar{U}}{\bar{\delta v}} - 1 \right).\tag{5.32}$$

The flow of the coupling constants in Eq. (5.31) is plotted in Fig 5.3. The flow in the absence of SOC and the characterization of the strong-coupling phases has been discussed in Sec. 1.3.1 and we briefly summarize the main results at this point: Without SOC, the bare parameters are constrained to the separatrix $\lambda_{\perp} = \lambda_s$. If interactions in the spin sector are repulsive the system flows to a Luttinger liquid phase with renormalized Luttinger parameter and plasmon velocity. If, on the other hand, the interactions in the spin sector are attractive the flow is to a strong-coupling phase (CDW), where interactions dynamically open a gap in the spin sector.

In the presence of SOC the bare coupling constants move away from the separatrix. For attractive interaction, the flow is still to the CDW phase and SOC just yields a small renormalization of parameters. If, on the other hand, interactions are repulsive, one of two possible scenarios is realized. For weak SOC, $\bar{\delta v} < 2\bar{U}$, the system flow to the Luttinger liquid fixed point and for strong SOC $\bar{\delta v} > 2\bar{U}$ the system flows to another strong-coupling fixed point (SDW), where the operator $\sim \cos(\sqrt{8\pi}\varphi_s)$ opens a gap in the spin sector. It is crucial to note that *the gapped phases for different signs of λ_{\perp} are not equivalent*. It will turn out that the SDW phase for $\lambda_{\perp} > 0$ is topologically nontrivial, while the CDW phase for $\lambda_{\perp} < 0$ is topologically trivial. We point out that while the spin-mode is gapped in this phase the charge mode still remains gapless. This leads to peculiar physical properties of the strong-coupling phase that we will discuss in the next sections.

Before we proceed to characterize the properties of the strong-coupling phases in more detail, we want to get an estimate of the magnitude of the spin-gap m that emerges in the in the strong-coupling SDW phase To this end, we integrate the RG flow (5.31) up to a scale $l^* = \ln(\Lambda/\Delta_s)$ where $\lambda_{\perp}(l^*) \sim 1$. This yields the estimate

$$\Delta_s = \Lambda e^{-\pi/\bar{\delta v}^2}.\tag{5.33}$$

The spin gap is therefore exponentially small.

5.3 Disorder

We now consider the effect of disorder on the phase diagram of the interacting electron system in the presence of spin orbit coupling. In particular we will be interested in the fate of the CDW and SDW phases, where interactions open spectral gaps in the spin sector. First, we consider a single impurity and then generalize the discussion to random disorder. We will find that the impact of disorder in general, and a single impurity in particular, varies greatly depending on the type of the order in the spin sector. We will find that the CDW phase generically becomes localized in the presence of impurities. For the SDW phase, there are two distinct scenarios, depending on the value of the Luttinger constant in the charge sector. The phase either remains a ballistic conductor at zero temperature in the presence of an impurity or the impurity becomes relevant and effectively cuts the wire into two parts, each with a spin gap. We show that in the latter scenario the conducting phase has emergent topological properties; namely it hosts zero-energy bound states with fractional spin at the site of the impurity. Possible experimental features of the topological phase are discussed at the end of this section.

5.3.1 Single impurity

Let us start our discussion by considering the action of nonmagnetic disorder given by

$$S_{\text{dis}} = \int dx d\tau \mathcal{U}_f(x) \left(R_\sigma^\dagger R_\sigma + L_\sigma^\dagger L_\sigma \right) + \int dx d\tau \left[\mathcal{U}_b(x) R_\sigma^\dagger L_\sigma + \text{H.c.} \right]. \quad (5.34)$$

Here, $\mathcal{U}_{f,b}$, denotes the potential for disorder forward scattering and backscattering respectively. While \mathcal{U}_f is real the potential \mathcal{U}_b is in general complex. Forward scattering plays no role for the transport properties and we will neglect it from now since it is well known that it can be removed via a gauge transformation of the fields [44]. Let us first consider a single impurity, with potential $\mathcal{U}_b(x) = \mathcal{U}_b \delta(x)$. We will assume that the potential is inversion symmetric and thus the parameter \mathcal{U}_b is real. Upon bosonization, this term takes the form

$$S_{\text{imp}} = -\lambda_{\text{imp}} v_s \int \frac{d\tau}{a} \cos(\sqrt{2\pi}\varphi_s(0, \tau)) \sin(\sqrt{2\pi}\varphi_c(0, \tau)), \quad (5.35)$$

with the dimensionless coupling constant $\lambda_{\text{imp}} = 2\mathcal{U}_b/(\pi v_s)$. In higher order in a perturbative expansion in λ_{imp} , scattering off the impurity generates two particle coherent scattering processes, described by the action

$$S_{\text{coh}} = v_s \int \frac{d\tau}{a} \left[\lambda_{\text{imp},s} \cos(\sqrt{8\pi}\varphi_s(0, \tau)) + \lambda_{\text{imp},c} \cos(\sqrt{8\pi}\varphi_c(0, \tau)) \right]. \quad (5.36)$$

Here, the first term corresponds physically to the backscattering of two incoming electrons with opposite spin, incident from the left and right of the impurity. The resulting scattering process effectively backscatters a particle with spin 1 but zero charge. The second term in Eq. (5.36) describes a process where two electrons with opposite spin are incident from the same side of the impurity and are coherently backscattered. This process effectively backscatters a singlet with charge $2e$. These coherent scattering processes become important when either the charge or the spin sector are gapped and electronic excitations are prohibited.

The action of interacting electrons in the presence of SOC and disorder has five parts $S = S_{\text{LL}} + S_{\delta} + S_{\text{SG}} + S_{\text{imp}} + S_{\text{coh}}$, where

$$\begin{aligned}
S_{\text{LL}} &= \frac{1}{2} \sum_{\mu} \frac{1}{K_{\mu}} \int d^2r \left(\nabla \varphi_{\mu} \right)^2, \\
S_{\delta} &= \frac{\delta}{2K_c} \int d^2r \left[(\partial_{r_1} \varphi_c)^2 - (\partial_{r_2} \varphi_c)^2 \right], \\
S_{\text{SG}} &= \lambda_{\perp} \int \frac{d^2r}{a^2} \cos(\sqrt{8\pi} \varphi_s(\mathbf{r})), \\
S_{\text{imp}} &= -\lambda_{\text{imp}} \int \frac{dr_2}{a} \cos(\sqrt{2\pi} \varphi_s(0, r_2)) \cos(\sqrt{2\pi} \varphi_c(0, r_2)), \\
S_{\text{coh}} &= \int \frac{dr_2}{a} \left[\lambda_{\text{imp},s} \cos(\sqrt{8\pi} \varphi_s(0, r_2)) + \lambda_{\text{imp},c} \cos(\sqrt{8\pi} \varphi_c(0, r_2)) \right].
\end{aligned} \tag{5.37}$$

Here, we defined the dimensionless coupling constants $\lambda_{\perp} = g_{1,\perp}/(2\pi^2 v_s)$ and $\lambda_{\text{imp}} = 2\mathcal{U}_b/(\pi v_s)$, as well as the coordinates $\mathbf{r} = (r_1, r_2) = (x, v_s \tau)^T$ and the dimensionless velocity difference $\delta = 1 - v_c/v_s$. The expansion of S_{LL} to linear order in δ leads to the appearance of the term S_{δ} in the action. However, we find that this term does not flow under the RG and also does not influence any of the other flow equations.

At this point we have to make one important remark. Note that we did not include the SO term in Eq. (5.26) into the action in Eq. (5.37). This is because this term is marginal and will not change the overall flow significantly. Its presence, however, is included implicitly by treating the two bare parameters of the flow $K_s(0)$ and $\lambda_{\perp}(0)$ as independent. The phase diagram of the model in Eq. (5.37) determined by the interplay of the impurity scattering, described by the terms S_{imp} and S_{coh} and the interaction described by the SG term. To gain a better understanding of this interplay we can study the perturbative RG equations of the action in Eq. (5.37). They are given by

$$\begin{aligned}
\frac{dK_s}{d\ell} &= -\frac{1}{2} K_s^2 \lambda_{\perp}^2, \\
\frac{d\lambda_{\perp}}{d\ell} &= (2 - 2K_s) \lambda_{\perp}, \\
\frac{d\lambda_{\text{imp}}}{d\ell} &= \left[1 - \frac{1}{2}(K_s + K_c) \right] \lambda_{\text{imp}} - \frac{1}{2} \lambda_{\text{imp}} \lambda_{\text{imp},c} - \frac{1}{2} \lambda_{\text{imp}} \lambda_{\text{imp},s} - \frac{1}{4\sqrt{2\pi}} \lambda_{\perp} \lambda_{\text{imp}}, \\
\frac{d\lambda_{\text{imp},s}}{d\ell} &= (1 - 2K_s) \lambda_{\text{imp},s} - \frac{1}{4} \lambda_{\text{imp}}^2 - \frac{1}{2} \lambda_{\perp} \lambda_{\text{imp},s}, \\
\frac{d\lambda_{\text{imp},c}}{d\ell} &= (1 - 2K_c) \lambda_{\text{imp},c} - \frac{1}{4} \lambda_{\text{imp}}^2.
\end{aligned} \tag{5.38}$$

The only weak coupling fixed point of these equations is $\lambda_i = 0$ for all i . The corresponding phase is

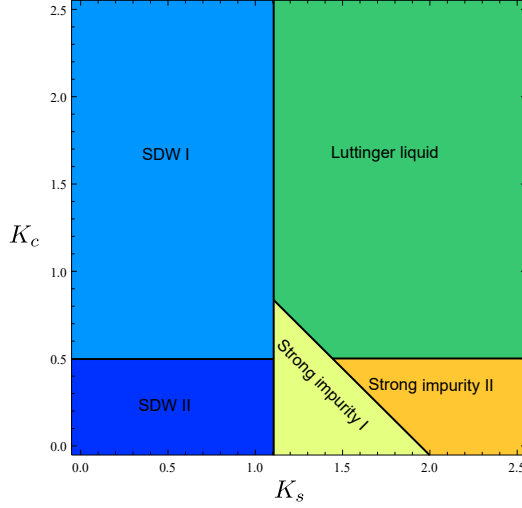


Figure 5.4: Phase diagram of the model in Eq. (5.37), describing interacting 1D electrons in the presence of both spin-orbit coupling and a single impurity. The classification of the phases is defined in Eqs. (5.39). The bare parameters of the flow are chosen as $\lambda_{\perp}^0 = 0.2$, $\lambda_{imp,s}^0 = 0.1$ and $\lambda_{imp,c}^0 = 0.1$. The phase boundary between the two SDW phases, as well as between the impurity II and Luttinger liquid phase, is $K_c = 1/2$. The boundary between the SDW phases and the neighboring phases is $\lambda_{\perp}^0 > 2(K_s^0 - 1)$ and the boundary between the impurity I and the impurity II and the Luttinger liquid phase is $K_c^0 + K_s^0 = 2$.

the spinful Luttinger liquid phase. There is also a number of strong-coupling fixed points.

$$\begin{aligned}
 \lambda_{\perp} \rightarrow 0, \lambda_{imp,s} \rightarrow 0, \lambda_{imp,c} \rightarrow 0, \lambda_{imp} \rightarrow \pm\infty &\Rightarrow \text{Strong impurity I,} \\
 \lambda_{\perp} \rightarrow 0, \lambda_{imp,s} \rightarrow 0, \lambda_{imp,c} \rightarrow \infty, \lambda_{imp} \rightarrow 0 &\Rightarrow \text{Strong impurity II,} \\
 \lambda_{\perp} \rightarrow 0, \lambda_{imp,s} \rightarrow \infty, \lambda_{imp,c} \rightarrow 0, \lambda_{imp} \rightarrow 0 &\Rightarrow \text{Strong impurity III,} \\
 \lambda_{\perp} \rightarrow \infty, \lambda_{imp,s} \rightarrow 0, \lambda_{imp,c} \rightarrow 0, \lambda_{imp} \rightarrow 0 &\Rightarrow \text{SDW I,} \\
 \lambda_{\perp} \rightarrow \infty, \lambda_{imp,s} \rightarrow 0, \lambda_{imp,c} \rightarrow \infty, \lambda_{imp} \rightarrow 0 &\Rightarrow \text{SDW II,} \\
 \lambda_{\perp} \rightarrow -\infty, \lambda_{imp,s} \rightarrow 0, \lambda_{imp,c} \rightarrow 0, \lambda_{imp} \rightarrow \infty &\Rightarrow \text{CDW.}
 \end{aligned} \tag{5.39}$$

Note that the equations for λ_{\perp} and K_s decouple from the rest. This result is very natural, since the local disorder term cannot affect the physics in the bulk. This can be used to classify the strong-coupling phases above into three strong impurity phases, where the spin gap does not develop and three phases with a gap in the spin sector.

If λ_{\perp} flows to zero, the fixed points correspond to those encountered in the study of a single impurity in the Luttinger liquid phase [63, 66]. There are then three possible strong-coupling phases. In phase

I, the impurity term becomes relevant. Physically, the impurity potential perfectly reflects incoming electrons at zero temperature in the thermodynamic limit and the system is effectively cut into two parts, each being in the LL phase. The impurity phases II and III describe impurity potentials that perfectly transmit spin but no charge, or vice versa. We will not discuss these phases in detail here but refer to the original publications [63, 66]. There is, however, one difference between these works and the current discussion. In the presence of the SG term, the bulk interaction K_s is also subject to renormalization. This renormalization slightly shifts the phase boundaries between the impurity phases in the K_s - K_c -plane compared to the model with $\lambda_\perp = 0$. Since the SG term is irrelevant in this region of the phase diagram, the shift of the phase boundaries is very minor.

Let us now discuss the opposite situation, when λ_\perp grows under the RG flow. As we have already discussed, the criterion for the opening of a spin gap is the relation $|\lambda_\perp^0| > 2(K_s^0 - 1)$ between the bare parameters of the RG. The nature of the fixed point then additionally depends on the sign of λ_\perp . For $\lambda_\perp < 0$, the strong-coupling fixed point is of the CDW type. In this case the development of CDW order in the bulk goes hand in hand with the flow of the impurity to strong coupling. In the thermodynamic limit and at zero temperature, the impurity potential becomes perfectly reflecting and cuts the wire into two parts, each exhibiting a CDW order.

In the SDW phase, on the other hand, the impurity potential always renormalizes to zero. Whether the system remains conducting or becomes insulating in the thermodynamic limit then depends on the coupling $\lambda_{\text{imp},c}$ that is generated by the impurity in second order. We find that the corresponding term becomes relevant for $K_c < 1/2$ independently of the physics in the spin sector. Then there are two disordered SDW phases. In the SDW I phase, the system remains a ballistic conductor at zero temperature, while the system in the SDW II phase is cut into two parts by the impurity analogously to the CDW phase.

The phase diagram for $\lambda_\perp^0 > 0$ is depicted in Fig. 5.4. In the remainder of this section we will substantiate this analysis by calculating the conductance in the opposite limits of a strong and weak impurity. In the first case, we study the tunneling current between the ends of two spin-gapped wires and in the second case we calculate the conductance of a single wire in the SDW phase in the presence of a weak impurity.

Weak impurity limit Let us first investigate the influence of a weak impurity in the spin gap phase, corresponding to the parameter regime $|\lambda_\perp| \gg 1 \gg \lambda_{\text{imp}}$. To this end we first perform a mean field analysis of the action in Eq. (5.37). If the strength of the SG potential defines the highest energy scale in the problem, the mean field is the one that minimizes the SG cosine term. At zero temperature the mean field takes one² of the values $\phi_s^{\text{SDW}} = \pi(n + 1/2)$ for $\lambda_\perp > 0$ or $\phi_s^{\text{CDW}} = \pi n$, for $\lambda_\perp < 0$ with n being integer. Here, we introduced the rescaled fields $\phi_\mu(x, \tau) = \sqrt{2\pi}\varphi_\mu$ for notational convenience.

To account for small fluctuations around the mean field solution, we expand the cosine term to quadratic order in fluctuations

$$\delta\phi_s(x, \tau) \equiv \phi_s(x, \tau) - \phi_s^{\text{CDW/SDW}} \quad (5.40)$$

²Note, that a constant mean field spontaneously breaks the discrete symmetry $\varphi_s \rightarrow \varphi_s + \sqrt{\pi/2}n$ of the cosine term. The solution only holds at $T = 0$, where the action in Eq. (5.37) describes a (1+1) dimensionell field theory and the spontaneous breaking of a discrete symmetry is allowed. At finite temperatures soliton solutions that interpolate between different minima restore the symmetry.

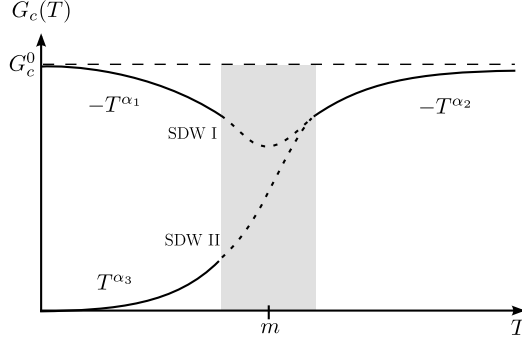


Figure 5.5: The temperature dependence of the conductance in the disordered SDW phase. At high temperatures there are power law corrections to the perfect conductance $G_c^0 = 2e^2/h$ with exponent $\alpha_1 = K_c + K_s - 2$ due to electron backscattering. At temperatures below the spin gap m there are two distinct possibilities. For $K_c > 1/2$, the system is in the SDW I phase, and for $K_c < 1/2$, it is in the SDW II phase. In the SDW II phase transport proceeds by weak tunneling and the conductance vanishes as a power law with exponent $\alpha_3 = K_c^{-1} + K_s^{-1} - 2$ as $T \rightarrow 0$. In the SDW I phase impurity scattering remains a weak perturbation and leads to corrections to the quantized conductance with power law $\alpha_2 = 4K_c - 2$.

This generates a mass term these fluctuations,

$$S_{\text{SG}} = \lambda_{\perp} \frac{v_s}{a} \int dx d\tau \cos(2\phi_s) = \frac{m^2}{4\pi v_s K_s} \int dx d\tau \delta\phi_s^2 \quad (5.41)$$

In the last equality we defined the mass $m^2 = 8\pi v_s^2 K_s |g_{\perp}|/a^2$. This term adds to the Luttinger liquid term, so that the quadratic action reads as

$$S_0 = \frac{1}{4\pi v_c K_c} \int_{\omega, q} |\phi_c(q, \omega)|^2 (\omega^2 + v_c^2 q^2) + \frac{1}{4\pi v_s K_s} \int_{\omega, q} |\delta\phi_s(q, \omega)|^2 (\omega^2 + v_s^2 q^2 + m^2) \quad (5.42)$$

Expanding the impurity contribution to the action in Eq. (5.37) around the SDW and CDW mean fields, respectively, we find

$$S_{\text{imp}} \simeq (-1)^{n+1} \lambda_{\text{imp}} \frac{v_s}{a} \int d\tau \cos \phi_c(0, \tau), \quad (\text{CDW}) \quad (5.43)$$

$$S_{\text{imp}} \simeq (-1)^n \lambda_{\text{imp}} \frac{v_s}{a} \int d\tau \cos \phi_c(0, \tau) \sin \delta\phi_s(0, \tau). \quad (\text{SDW}) \quad (5.44)$$

By power counting we see that the impurity operator in the CDW phase is a relevant perturbation — it becomes relevant already for $K_c < 2$. In the thermodynamic limit, the impurity becomes perfectly reflecting and the system is effectively cut into two parts, each in the CDW phase.

In the SDW phase the effect of disorder is more subtle. Let us integrate out the massive fluctuations in the spin sector to obtain an effective action for the charge sector,

$$e^{-S_{\text{eff}}} = \int \mathcal{D}[\delta\phi_s] e^{-S_{0,s}} e^{-S_{\text{imp}}} = \langle e^{-S_{\text{imp}}} \rangle_s \simeq e^{-\langle S_{\text{imp}} \rangle + \frac{1}{2} (\langle S_{\text{imp}}^2 \rangle - \langle S_{\text{imp}} \rangle^2)} \quad (5.45)$$

where the last step is an perturbative expansion in λ_{imp} to second order. In App. A, we derive the correlation function for massive bosonic fields

$$\langle \delta\phi_s(0, \tau_1) \delta\phi_s(0, \tau_2) \rangle = K_s K_0(m|\tau_1 - \tau_2|) \quad (5.46)$$

where $K_0(z)$ is the zeroth modified Bessel function. Using the asymptotics of this function, $K_0(x) \sim e^{-|x|}/\sqrt{x}$ for $x \rightarrow \infty$ and $K_0(x) \simeq -\ln(x/2)$ for $x \rightarrow 0$ we obtain

$$\langle \sin \delta\phi_s(0, \tau) \rangle = 0, \quad (5.47)$$

$$\langle \sin \delta\phi_s(0, \tau_1) \sin \delta\phi_s(0, \tau_2) \rangle = e^{-K_s K_0(ma/v_s)} \sinh(K_s K_0(m|\tau_1 - \tau_2|)). \quad (5.48)$$

Substituting this into the expression for the effective action in Eq. (5.45) yields

$$\begin{aligned} S_{\text{eff}} &= (-1)^n \left(\frac{\lambda_{\text{imp}} v_s}{a} \right)^2 \int d\tau_1 d\tau_2 \cos \phi_c(0, \tau_1) \cos \phi_c(0, \tau_2) \langle \sin \delta\phi_s(0, \tau_1) \sin \delta\phi_s(0, \tau_2) \rangle \\ &\simeq \lambda_{\text{imp},c} \frac{v_s}{a} \int d\tau \cos 2\phi_c(0, \tau), \end{aligned} \quad (5.49)$$

where we performed a gradient expansion in $m|\tau_1 - \tau_2| \ll 1$ and defined the dimensionless constant $\lambda_{\text{imp},c} = (-1)^n \lambda_{\text{imp}}^2 (1/2) (v_s m a / 2)^{K_s - 1} \times \int dx \sinh(K_s K_0(x))$. This means that the impurity itself is effectively absent in the SDW phase for energy scales below the gap, see also the discussion of the strong-coupling phases of the RG below Eq. (5.39). However, it generates an effective two-particle scattering potential in second order perturbation theory in Eq. (5.49). This term is the $\lambda_{\text{imp},c}$ term in Eq. (5.37). In the effective theory the massive spin sector is then integrated out and the resulting action takes the form

$$S = \frac{1}{4\pi} \int dx d\tau \left[\frac{1}{v_c K_c} (\partial_\tau \phi_c)^2 + \frac{v_c}{K_c} (\partial_x \phi_c)^2 \right] + \lambda_{\text{imp},c} \int d\tau \cos 2\phi_c(0, \tau). \quad (5.50)$$

with the effective frequency UV cutoff m . This model can be mapped exactly to the Kane-Fisher model [63] with $K_c \rightarrow 2K_c$. The scattering off the impurity thus only becomes relevant for $K_c < 1/2$. For $K_c > 1/2$, the impurity yields small corrections to the charge conductance of a finite system given by [63]

$$G_c^{\text{SDW I}} \simeq \frac{2e^2}{h} K_c \left[1 - c_{K_c, K_s}^0 \lambda_{\text{imp}} \left(\frac{T}{\Lambda} \right)^{K_c + K_s - 2} \Theta(T - m) - c_{K_c, K_s}^1 \lambda_{\text{imp}}^2 \left(\frac{T}{\Lambda} \right)^{4K_c - 2} \right], \quad (5.51)$$

where Λ denotes the UV cutoff and $c_{K_c, K_s}^{0,1}$ are dimensionless positive numbers that depend on the parameters K_c and K_s and the cutoff procedure. We see that below the spin gap single particle scattering off the impurity is absent. Physically, this is because the creation of a spin- $\frac{1}{2}$ particle or hole costs at least the energy of the gap. The next important scattering channel is for electron pairs with opposite spins, with contributes to the conductance in order λ_{imp}^2 . Above the gap, this contribution is subleading compared to the first correction in Eq. (5.51) originating from single particle backscattering off the impurity. The qualitative behavior of the conductance is plotted in Fig. 5.5.

Note that the conductance goes to the quantized value $G_c^0 = \frac{2e^2}{h} K_c$ as $T \rightarrow 0$ as long as $K_c > 1/2$. Consequently, there exists a disordered SDW phase (SDW I), realized for $K_c > 1/2$, in which the system remains a ballistic conductor at zero temperature.

If, on the other hand, $K_c < 1/2$, the effective disorder term in Eq. (5.50) becomes relevant and drives the system to another phase (SDW II). In this phase, we expect that disorder cuts the wire into two parts, each having a spin gap. To substantiate this claim we next analyze the limit of a strong impurity.

Before, however, let us briefly comment on the effect of magnetic impurities on the transport properties of the system. Consider an impurity potential whose scattering strength depends on the spin of the incoming electrons. The backscattering part is then

$$\begin{aligned}
S'_{\text{dis}} &= \int d\tau \left[\mathcal{U}_{b,\sigma} R_\sigma^\dagger(0, \tau) L_\sigma(0, \tau) + \text{H.c.} \right] \\
&= -\lambda_{\text{imp}} v_s \int \frac{d\tau}{a} \cos(\sqrt{2\pi}\varphi_s(0, \tau)) \sin(\sqrt{2\pi}\varphi_c(0, \tau)) \\
&\quad - \lambda_{\text{imp,magn}} v_s \int \frac{d\tau}{a} \cos(\sqrt{2\pi}\varphi_c(0, \tau)) \sin(\sqrt{2\pi}\varphi_s(0, \tau))
\end{aligned} \tag{5.52}$$

with $\lambda_{\text{imp}} = (\mathcal{U}_{b,\uparrow} + \mathcal{U}_{b,\downarrow})/\pi v_s$ and $\lambda_{\text{imp,magn}} = (\mathcal{U}_{b,\uparrow} - \mathcal{U}_{b,\downarrow})/\pi v_s$. The first term denotes nonmagnetic impurities, while the second models magnetic ones. After expanding around the SDW mean field and integrating out massive fluctuations, the magnetic impurity term generates an effective potential for the charge degrees of freedom $\sim \lambda_{\text{imp,magn}} \cos(\sqrt{2\pi}\varphi_c(0, \tau))$. This term becomes relevant already for $K_c < 2$ and drives the system into the SDW II phase. Note, however, that the nonmagnetic impurity potential is odd under TR and thus the SDW phase is protected against this perturbation as long as TR is not broken. This also motivated the inclusion of spin-orbit coupling as the mechanism that drives the Luttinger liquid to the SDW phase. The SDW phase can also be realized by applying a magnetic field perpendicular to the system, which however breaks time reversal, in which case the system is no longer protected against generic impurity scattering [129].

Weak tunneling limit: We now study the phase with a bulk spin gap and a strong impurity, i.e. the regime $\lambda_{\text{imp}} \gg |\lambda_\perp| \gg 1$. In this limit we expect that the impurity cuts the system into two parts. In this case we may ask the question whether the phase is stable against the application of a weak voltage that induces a tunneling current between the two parts. If the tunneling current diverges for small voltages, we have perturbed around the wrong ground state and the correct one is in fact a single (conducting) system.

Again, in the strong-coupling limit, we study the classical mean field of the action in (5.37). The bosonic field in the spin sector develops a finite expectation value $\phi_s^{\text{SDW}} = \pi(n + 1/2)$ for $g_\perp > 0$ or $\phi_s^{\text{CDW}} = \pi n$, for $g_\perp < 0$ that minimizes the potential energy of the SG term in the bulk. At the origin, however, the bosonic fields will be pinned to the minima of the impurity term, since the impurity potential is now the strongest energy scale in the problem. The local mean field at the origin is then

$$(\phi_c^{\text{imp}}, \phi_s^{\text{imp}}) = ((m + l)\pi, (m - l)\pi), \tag{5.53}$$

where we assumed that $\lambda_{\text{imp}} > 0$ and m and l are both integers.

Let us now anticipate on physical grounds the behavior of the system under the application of a small tunneling voltage across the two wires. Tunneling through the potential barrier induced by the impurity can be understood as inserting an additional electron at the end of the wire.

Consider first the case of CDW order in the bulk. Adding an electron at the end of the wire creates $\pm\pi$ soliton-like kinks in both charge and spin fields. Therefore, since the mean-field value of the spin field at the end of the wire and in the bulk differs by an integer multiple of π , see Fig 5.6, electrons may only be added in pairs. The tunneling action of such processes is given by the dual theory of the

action in Eq. (5.51) and the tunneling term becomes relevant only for $K_c > 2$ [63, 66]. Consequently, the disordered CDW phase is robust against weak tunneling.

The situation changes significantly if we consider bulk SDW order. In this case, the mean-field value of the spin field at $x = 0$ and in the bulk differs by a minimal amount of $\pm\pi/2$. Therefore, the potential barrier already distorts the bulk SDW order and adding an electron at the edge merely changes the ‘‘polarity’’ of the distortion. For now, we postpone a physical discussion of this situation to Sec. 5.3.2. Here, let us derive a perturbative expression for the tunneling current if both wires are in the SDW phase.

Our starting point is the action $S = S_0 + S_{\text{imp}}$ with

$$\begin{aligned} S_0 &= \frac{1}{2v_c K_c} \int_{\omega, q} |\varphi_c(q, \omega)|^2 (\omega^2 + v_c^2 q^2) + \frac{1}{2v_s K_s} \int_{\omega, q} |\phi_s(q, \omega)|^2 (\omega^2 + v_s^2 q^2 + m^2), \\ S_{\text{imp}} &= -\lambda_{\text{imp}} \frac{v_s}{a} \int d\tau \cos \phi_s(0, \tau) \cos \phi_c(0, \tau). \end{aligned} \quad (5.54)$$

Since the action is quadratic in fields except for the point $x = 0$, we can integrate out all degrees of freedom except those at the origin, which yields the effective action

$$e^{-S_{\text{eff}}} = \int \mathcal{D}\phi_s \int \mathcal{D}\varphi_c \delta[\varphi_s(\tau) - \phi_s^{\text{SDW}} - \phi_s(0, \tau)] \delta[\varphi_c(\tau) - \phi_c(0, \tau)] e^{-S}. \quad (5.55)$$

Performing the integration we get

$$S_{\text{eff}} = \frac{1}{2\pi K_c} \int_{\omega} |\omega| |\varphi_c(\omega)|^2 + \frac{1}{2\pi K_s} \int_{\omega} \sqrt{\omega^2 + m^2} |\varphi_s(\omega)|^2 - \lambda_{\text{imp}} \frac{v_s}{a} \int d\tau \cos \varphi_s(\tau) \cos \varphi_c(\tau). \quad (5.56)$$

Note that the action is similar to that of a Brownian particle with coordinate (φ_c, φ_s) moving in a periodic potential and coupled to a dissipative environment. In our model, the low-lying spin and charge excitations in the bulk cause the dissipation. Hence our 1D problem is now reduced to the problem of a quantum-mechanical problem, i.e. a 0D field theory. We point out that, since the spin sector of the model is gapped, there exist no low lying excitations and hence no dissipation in the spin sector for energies below the gap.

Our goal now is to calculate the tunneling current. Since the bosonic fields at the origin are pinned to the minima of the impurity potentials, this current is carried by instantons that connect neighboring minima. To find a perturbative expression for this tunneling current, we adapt a formalism developed in Ref. [66]. The dissipation suffered by the particle at the coordinate (φ_c, φ_s) can be expressed with a linear coupling to harmonic oscillators, i.e we should study the action

$$\begin{aligned} S &= \int_0^\beta d\tau \mathcal{L}(\{x_{1j}\}, \{x_{2k}\}, \varphi_s, \varphi_c), \\ \mathcal{L} &= \sum_j \left[\frac{m_{1j}}{2} (\partial_\tau x_{1j})^2 + \frac{m_{1j}}{2} \omega_{1j}^2 x_{1j}^2 + g_{1j} x_{1j} \varphi_c + \frac{g_{1j}^2}{2m_{1j}\omega_{1j}^2} \varphi_c^2 \right] \\ &+ \sum_k \left[\frac{m_{2k}}{2} (\partial_\tau x_{2k})^2 + \frac{m_{2k}}{2} \omega_{2k}^2 x_{2k}^2 + g_{2k} x_{2k} \varphi_s + \frac{g_{2k}^2}{2m_{2k}\omega_{2k}^2} \varphi_s^2 \right] \\ &- \lambda_{\text{imp}} \frac{v_s}{a} \int d\tau [\cos \varphi_s(\tau) \cos \varphi_c(\tau) - 1] \end{aligned} \quad (5.57)$$

with the spectral functions for the oscillators $\{x_{1j}\}$ and $\{x_{2k}\}$

$$\begin{aligned}
J_1(\omega) &= \sum_j \frac{\pi g_{1j}^2}{2m_{1j}\omega_{1j}} \delta(\omega - \omega_{1j}) = \frac{\omega}{\pi K_c} \Theta(\omega), \\
J_2(\omega) &= \sum_k \frac{\pi g_{1k}^2}{2m_{2k}\omega_{2k}} \delta(\omega - \omega_{2k}) = \frac{\sqrt{\omega^2 - m^2}}{\pi K_s} \Theta(\omega - m).
\end{aligned} \tag{5.58}$$

Here, the expressions on the right hand side are obtained from the analytical continuation of the propagator [56] in the action in Eq. (5.54)

$$J_{1,2}(\omega) = -\lim_{\delta \rightarrow 0} \text{Im} G_{c,s}^{-1}(-i\omega + \delta). \tag{5.59}$$

The tunneling probability to lowest order in the electron tunneling matrix element t_e is obtained using Fermis golden rule for tunneling between the neighboring minima $(\varphi_c, \varphi_s) = (0, 0)$ and (π, π) :

$$\begin{aligned}
\mathcal{P}_{(0,0) \rightarrow (\pi,\pi)} &= 2\pi t_e^2 \sum_{i,f} |\langle f|i \rangle|^2 e^{-\beta E_i} \delta(E_f - E_i - eV) \bigg/ \sum_i e^{-\beta E_i} \\
&= t_e^2 \int_{-\infty}^{\infty} dt_0 \langle e^{-iH_f t_0} e^{iH_i t_0} \rangle_i e^{ieV t_0},
\end{aligned} \tag{5.60}$$

where V is the applied voltage and $|i\rangle$ ($|f\rangle$) represent eigenstates of H_i (H_f) with eigenvalues E_i (E_f). The thermal average is defined as $\langle X \rangle_i = \text{Tr}(X e^{-\beta H_i}) / \text{Tr}(e^{-\beta H_i})$. The initial and final state Hamiltonians are obtained from \mathcal{L} in Eq. (5.57) by setting $(\phi_c, \phi_s) = (0, 0)$ and (π, π) , respectively. The average is calculated by quantizing the oscillator modes which yields the tunneling probability

$$\begin{aligned}
&\mathcal{P}_{(0,0) \rightarrow (\pi,\pi)} \\
&= t_e^2 \int_{-\infty}^{\infty} dt_0 \exp \left[ieV t_0 - \pi \int_{-\infty}^{\infty} \frac{d\omega}{\omega^2} (J_1(\omega) + J_2(\omega)) [(1 - \cos \omega t) \coth(\beta\omega/2) + i \sin \omega t] \right].
\end{aligned} \tag{5.61}$$

The probability of the reverse process, $(\varphi_c, \varphi_s) = (\pi, \pi) \rightarrow (0, 0)$ is obtained the same way as Eq. (5.60) but with i and f interchanged

$$\mathcal{P}_{(\pi,\pi) \rightarrow (0,0)} = t_e^2 \int_{-\infty}^{\infty} dt_0 \langle e^{-iH_i t_0} e^{iH_f t_0} \rangle_f e^{-ieV t_0} = e^{-\beta eV} \mathcal{P}_{(0,0) \rightarrow (\pi,\pi)}. \tag{5.62}$$

Here, the last equality represents the detailed balance. The net charge current is given by the difference of the tunneling probabilities

$$\begin{aligned}
j_c &= 2e(\mathcal{P}_{(0,0) \rightarrow (\pi,\pi)} - \mathcal{P}_{(\pi,\pi) \rightarrow (0,0)}) = 2et_e^2(1 - e^{-\beta eV}) \\
&\times \int_{-\infty}^{\infty} dt_0 \exp \left[ieV t_0 - \int \frac{d\omega}{\omega^2} [J_1(\omega) + J_2(\omega)] \left((1 - \cos \omega t_0) \coth \frac{\beta\omega}{2} + i \sin \omega t_0 \right) \right],
\end{aligned} \tag{5.63}$$

where the factor 2 comes from the spin degeneracy. From this result, we obtain the charge current at zero temperature as a function of the voltage

$$j_c = 2et_e^2 \int_{-\infty}^{\infty} dt_0 \exp \left[ieV t_0 - \int \frac{d\omega}{\omega^2} [J_1(\omega) + J_2(\omega)] e^{-\omega/\Lambda} (1 - e^{-i\omega t_0}) \right]. \tag{5.64}$$

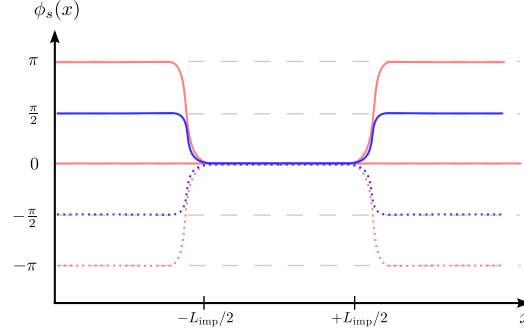


Figure 5.6: Spatial profile of the $\phi_s(x)$ field in the topological SDW phase (blue) or the topologically trivial CDW phase (red) in the presence of an impurity with finite range L_{imp} located at the origin. The kink (solid line) and anti-kink (dotted line) configurations correspond to the two degenerate groundstates at the boundary, where the field has to minimize the backscattering potential. Addition of a single electron changes the field by $\pm\pi$ and therefore costs no energy in the SDW phase since it switches the polarity of the kink, which corresponds to the transition between degenerate states at the boundary. In the CDW phase single-electron excitations are gapped but the addition of two electrons with parallel spin, which corresponds to the transition of red kink and antikink, or the addition of a singlet pair of electrons (straight solid line) is allowed.

Evaluating the integral, we find the expression for the charge current

$$j_c = d_{K_c,0} \left(\frac{eV}{\Lambda} \right)^{\frac{1}{K_c}-1} \Theta(m - eV) + d_{K_c,K_s} \left(\frac{eV}{\Lambda} \right)^{\frac{1}{K_c} + \frac{1}{K_s}-1} \Theta(eV - m), \quad (5.65)$$

with $d_{K_c,K_s} = 4\pi e t_e^2 / (\Lambda \Gamma(\frac{1}{K_c} + \frac{1}{K_s}))$. For voltages above the gap, the tunneling current coincides with that of a spinful Luttinger liquid [56]. At voltages below the gap, the tunneling conductance behaves as $G_c = dj_c/dV \sim V^{\frac{1}{K_c}-2}$ which vanishes for $V \rightarrow 0$ if $K_c < 1/2$.

To summarize, we have shown that there exist two distinct SDW phases. In the SDW II phase, realized for $K_c < 1/2$, a weak impurity grows under the RG flow. In the strong-coupling regime the impurity potential becomes perfectly reflecting effectively cutting the wire into two parts, each exhibiting SDW order. This phase is stable against a weak tunneling current.

In the SDW I phase, realized for $K_c > 1/2$, a weak impurity flows towards weak coupling. We have shown that in this phase a strong impurity also becomes weaker at lower energy scales (an infinitesimal weak tunneling voltage already creates a finite tunneling current driving the system into the conducting regime).

5.3.2 Boundary zero modes

The robustness of the SDW I phase against impurity scattering observed above can physically be explained by the presence of zero-energy modes localized at the impurity site. In order to show the existence of zero modes, we introduce a strong impurity at site $x = 0$ with finite range L_{imp} , that effectively cuts the system into two parts. If we assume that the backscattering potential generated the strongest energy scale in the problem, the action is minimized by pinning the spin and charge field at the position of the impurities to one of the values $(\phi_c^{\text{imp}}, \phi_s^{\text{imp}}) = ((m+n)\pi, (m-n)\pi)$. In the bulk, on

the other hand, the spin field is locked to $\phi_s^{\text{SDW}} = \pi(n + 1/2)$. This implies that the field has to change by a minimal amount $\pm \frac{\pi}{2}$ close to the boundary, see Fig. 5.6. These kink and antikink configurations can be interpreted as the two degenerate ground states of a mode located at the boundary. This mode carries half of the electron spin, which is determined by size of the (anti-)kink at the boundary

$$S_z = \lim_{\delta \rightarrow 0} \int_{-L_{\text{imp}} - \delta}^{-L_{\text{imp}} + \delta} dx \rho_s(x) = \frac{1}{2\pi} \int_{-L_{\text{imp}} - \delta}^{-L_{\text{imp}} + \delta} dx \partial_x \phi_s(x) = \pm \frac{1}{4}. \quad (5.66)$$

This agrees with recent findings in an analogous model in Ref. [130].

Tunneling of a spin- $\frac{1}{2}$ particle into the edge requires flipping the (anti-)kink by a magnitude $\pm\pi$. Since the two states are degenerate, this does not cost any energy – in the thermodynamic limit we can neglect the charging energy, which scales as $1/L$, that is required to add an additional particle. In terms of the edge state, we can interpret this as follows. The electron is added at the edge but does not have to pay the cost for the creation of a spin- $\frac{1}{2}$ in the gapped spin sector, since the spin change triggers a transition between the degenerate spin- $\frac{1}{4}$ ground states of the edge mode.

To summarize, we expect the topological phase to host zero-energy edge modes with fractional spin in the spin sector that are located at the boundary. The existence of such edge modes is topologically protected since the values of the field ϕ_s deep in the bulk for $x \rightarrow \infty$ and at the impurity site are fixed. Alternatively, the presence of edge states can be shown by refermionizing the Luttinger model with SG term at the special value $K_s = 1/2$ and solving the eigenvalue equation for zero energy eigenstates of the Hamiltonian. This program is performed in App. D of [131] and yields eigenstates exponentially localized at the boundary of the 1D system. While it is not mentioned in the original publication, the edge state wave function is only normalizable for $g_{1\perp} > 0$.

Physical argument for the current We can use the physical picture of edge states to motivate the behavior of the tunneling conductance obtained in Sec. 5.3.1, following an argument by Ref. [56]. Due to the zero-energy state, the local density of states in the spin sector takes the form $\nu_s(x = 0, \epsilon) = \nu_s^0 \delta(\epsilon) + \nu_s^{\text{reg}}(\epsilon)$, where $\nu_s^{\text{reg}}(\epsilon)$ is the contribution of massive modes above the SDW gap. On the other hand, the charge sector is still massless and the end-chain density of states is given by $\nu_c(x = 0, \epsilon) = \epsilon^{\frac{1}{2K_c} - 1}$ [56].

Since charge and spin sector factorize, the total density of states at the edge is a convolution of the two individual densities of states,

$$\nu_{\text{edge}}(x = 0, \omega) \sim \int_0^\omega d\epsilon \nu_c(x = 0, \epsilon) \nu_s(x = 0, \omega - \epsilon) \sim \nu_c(x = 0, \omega) \sim \omega^{\frac{1}{2K_c} - 1}. \quad (5.67)$$

The tunneling current between the two parts of the system is obtained as

$$j_c(V) \sim \int_0^V d\omega \nu_{\text{edge}}(x = 0-, \omega) \nu_{\text{edge}}(x = 0+, \omega) \sim V^{\frac{1}{K_c} - 1}, \quad (5.68)$$

which agrees with the result of the perturbative calculation performed in Sec. 5.3.1.

5.3.3 Disorder

Let us now discuss the influence of disorder on the transport properties in the presence of SOC. The action describing nonmagnetic disorder is

$$\begin{aligned}
S_{\text{dis}} &= \sum_{\sigma} \int dx d\tau \mathcal{U}_f(x) \left(R_{\sigma}^{\dagger} R_{\sigma} + L_{\sigma}^{\dagger} L_{\sigma} \right) + \int dx \left[\mathcal{U}_b(x) R_{\sigma}^{\dagger} L_{\sigma} + \text{H.c.} \right]. \\
&= \frac{2}{\sqrt{\pi}} \int dx d\tau \mathcal{U}_f(x) \partial_x \varphi_c - \frac{i}{4\pi} \int dx \mathcal{U}_b(x) e^{-\sqrt{2\pi}\varphi_c} \cos(\sqrt{2\pi}\varphi_s) + \text{H.c.} .
\end{aligned} \tag{5.69}$$

The disorder fields have the usual correlation functions $\langle \mathcal{U}_f(x) \mathcal{U}_f(x') \rangle_{\text{dis}} = \langle \mathcal{U}_b(x) \mathcal{U}_b^*(x') \rangle_{\text{dis}} = D\delta(x - x')$, and zero otherwise. As we already discussed, forward scattering can be removed from the partition function through a gauge transformation. After introducing replicas and performing the disorder average, the action has four parts $S = S_c + S_s + S_{\text{SO}} + S_b$, with

$$\begin{aligned}
S_c &= \frac{1}{2K_c^* v_c^*} \sum_n \int dx d\tau \left[(\partial_{\tau} \varphi_{cn})^2 + (v_c^*)^2 (\partial_x \varphi_{cn})^2 \right], \\
S_s &= \frac{1}{2K_s^* v_s^*} \sum_n \int dx d\tau \left[(\partial_{\tau} \varphi_{sn})^2 + (v_s^*)^2 (\partial_x \varphi_{sn})^2 \right] + \frac{g_{\perp}}{2(\pi a)^2} \sum_n \int dx d\tau \cos(\sqrt{8\pi}\varphi_{sn}), \\
S_{\text{SO}} &= i \frac{\delta v}{v_F} \sum_n \int dx d\tau \partial_{\tau} \varphi_{cn} \partial_x \varphi_{sn}, \\
S_b &= \frac{D}{(\pi a)^2} \sum_{n,m} \int dx d\tau_1 d\tau_2 \cos(\sqrt{2\pi}[\varphi_{cn}(1) - \varphi_{cm}(2)]) \cos(\sqrt{2\pi}\varphi_{sn}(1)) \cos(\sqrt{2\pi}\varphi_{sm}(2)).
\end{aligned} \tag{5.70}$$

Here, n, m denote replica indices and the asterisk symbolizes that the parameters already contain renormalization effects due to the velocity difference δv .

We consider the scenario that $\lambda_{\perp} \gg 1$ and the spin gap has already established. In this case we may neglect the marginal term S_{SO} and expand φ_s around the mean field as in Eq. (5.40). Integrating out the massive fluctuations $\delta\varphi_s$, the model maps to the Giamarchi-Schulz model [67] with $K \rightarrow 2K_c^*$. Disorder thus becomes relevant for $K_c^* < 3/4$.

This result can also be deduced from the result for a single impurity by the following heuristic reasoning [56]. For a single nonmagnetic impurity the conductance has been calculated in Eq. (5.51) and reads as

$$G = \frac{2e^2}{h} - c_{K_c, K_s}^1 \lambda_{\text{imp}}^2 \left(\frac{\epsilon}{m} \right)^{4K_c - 2}, \tag{5.71}$$

where c_{K_c, K_s}^1 is a nonuniversal constant and $\epsilon = \max(T, eV)$. To establish the boundary between localized and delocalized regime for the case of weak disorder, it is sufficient to replace $\epsilon \rightarrow 1/L$ and multiply δG by the number of impurities $N_{\text{imp}} \sim 1/L$. Now if G grows with increasing L , the system is in the localized regime, else it is in the delocalized regime. This yields the threshold $K_c < 3/4$ for localization in the presence of nonmagnetic impurities and $K < 3$ for magnetic impurities. This situation is very similar to the effect of disorder in quantum-spin-Hall edge states [85]. The edge states are also protected against nonmagnetic impurities for weak interactions $K_c > 3/8$ but are expected to localize if the interactions in the system become too strong.

5.3.4 Experimental signatures

There are several signatures of the SDW I phase studied above that can be tested in experiment. First, our theory predicts that the conductance as a function of temperature behaves as Eq. (5.51). Unlike in the Luttinger liquid phase in the presence of an impurity or in the disordered CDW phase, the conductance does not go to zero in the limit of low temperatures, but reaches its quantized value. This can be used as a clear experimental signature of the SDW I phase.

Another experiment is the measurement of the tunneling density of states (TDOS) using scanning tunneling microscopy. In the topologically nontrivial SDW I phase, we expect to see signatures of edge modes at the end of a finite wire. At low bias, the TDOS at the impurity site is expected to show a power-law zero bias anomaly, see Eq. (5.68). In the bulk of the wire, on the other hand, there is a hard gap of the size of the spin gap m for single-electron tunneling. We expect an overall behavior,

$$\nu(\epsilon)/\nu_0 \sim \begin{cases} (\epsilon/m)^{1/2K_c-1}, & \text{close to the edges} \\ \Theta(\epsilon - m), & \text{in the bulk} \end{cases} \quad (5.72)$$

where ν_0 is the bare value of the tunneling density of states and ϵ is the excitation energy measured from the Fermi surface.

5.4 Summary of chapter 5

In this chapter, we investigated the influence of Rashba SOC on the phase diagram and transport properties of one-dimensional electrons. The main role of the spin-orbital interactions is to break the spin-rotational symmetry in the spin sector, which enables the realization of previously symmetry-protected phases. The most interesting situation occurs when the dimensionless strength of SOC is stronger than the strength of interactions. In this case, electron-electron interactions drive the spin sector of the system to a strong-coupling phase with quasi-long-range spin-density-wave order where a spectral gap is dynamically generated. This prediction was established by treating interactions using bosonization and a weak-coupling renormalization-group analysis which is controlled by the small parameters of dimensionless interaction \bar{U} and spin-orbit-coupling strength $\bar{\delta}v$.

We show that this gapped SDW phase exhibits properties akin to those of TIs. It differs, however, from conventional band insulators due to the fact that only the spin sector is gapped, while the charge sector of the liquid is still massless. Since physical electrons carry both spin and charge, the whole electron liquid forms an unusual topological state. The topological nature manifests itself mainly in two properties: First, the bulk of the system is protected against nonmagnetic impurity scattering for interaction strengths $K_c > 3/4$, for high impurity concentration and for $K_c > 1/2$ in the case of a single impurity. Second, we find zero-energy edge modes at the boundary of a finite system that carry fractional electron spin. These topological properties are protected by the bulk spin-gap.

There are several signatures of this novel topological state that may be used to verify it experimentally. The conductance of the system in the topological phase is expected to show a non-monotonous behavior as a function of temperature according to Eq. (5.51) which is depicted in Fig. 5.5. Furthermore, the tunneling density of states, as described by Eq. (5.72) shows distinct behavior in the bulk and at the edge of the wire. Due to the spin gap, there is a hard gap for single-particle tunneling in the bulk, while the tunneling density of states at the boundary shows power law behavior as a function of the bias.

Conclusion

In this thesis we have analyzed the effect of topology, interactions and disorder, as well as their mutual interplay on the transport properties of one-dimensional quantum systems. This chapter presents a brief summary of the main results and outlines related further research projects.

Ch. 3 is concerned with the impact of electron-electron interactions and disorder on the transport properties of the HLL, that emerges at the boundary of 2D QSH insulators in the topological regime. The discerning property of this quantum liquid is its topological protection against disorder scattering. In the presence of nonmagnetic disorder, *elastic* backscattering between Kramers partners is exactly forbidden by time-reversal symmetry. As a result, the $T = 0$ conductance is given by $G_0 = 2e^2/h$ independently of the strength of disorder (as long as the two-dimensional bulk is insulating). However, at nonzero T , we find that *inelastic* backscattering is generically triggered beyond S_z -conserving models and gives rise to dissipation, even in the absence of disorder, modifying significantly the transport properties of both a clean and disordered helical liquid. We have identified two main sources of inelastic scattering in the microscopic low-energy theory. First, the existence of a Dirac point in the spectrum of helical electrons allows for the presence of a unique Umklapp process, termed g_5 process. This perturbation breaks specific conservation laws, present in the usual LL, and hence generates dissipation, even in the absence of disorder. If the edge is disordered, the physics becomes even richer. In this case composite scattering processes, containing both forward scattering from impurities and interaction induced backscattering, are present in the theory and determine the behavior of transport observables at low temperatures. In this context, it is of conceptual importance that forward scattering off disorder, in contrast to disorder induced backscattering, plays the primary role in these combined effects.

Our main result concerns the temperature dependence of the *dc* resistivity, depicted in Fig. 3.5, and the dependence of the conductivity on the frequency of the driving field at fixed temperature, depicted in Fig. 3.6. Both generically show an anomalous power-law temperature or frequency dependence similar to the conventional LL. By complementing the perturbative analysis with a weak-coupling RG procedure, we have shown that the HLL is stable against perturbations that may open a gap for intraedge interactions smaller than the critical value $K = 1/2$. In fact, the protection against the opening of a gap at the edge for $K > 1/2$ is facilitated by the disorder backscattering term. The disorder scattering does not affect transport, but destroys the phase coherence of electrons leading to less repulsive interaction under the RG flow. For more repulsive interactions we have identified the existence of various strong-coupling fixed points of the RG, but their characterization remains an open problem for future work. However, we have presented qualitative arguments that even if the edge modes were to develop a gap an edge reconstruction deeper inside the bulk would take place. The “new” edge states are expected to exhibit the weak-coupling transport properties of the original edge modes.

The central topic of Ch. 4 has been the investigation of Coulomb drag between helical liquids. The Coulomb drag provides a sensitive measure of the electron-electron correlations in a material and is therefore of particular interest in the HLL, since the intraedge dissipation is generated solely by inelastic scattering events. The main result of our analysis concerns the behavior of the *dc*-drag resistivity as a function of the temperature depicted in Fig. 4.4. For temperatures below a characteristic scale T_1 , drag occurs due to backscattering of electrons in the passive edge at the Fermi surface caused by particle-hole

fluctuations in the active edge. The drag resistivity in this regime generically behaves as a power law with anomalous exponent determined by the Luttinger parameter of the relative density mode K_- . At higher temperatures, on the other hand, we find that the dominant contribution to the resistivity derives from plasmon mediated drag. The discovery of this novel mechanism of plasmon mediated drag in 1D systems constitutes the second main result of this chapter. Finally, we have presented qualitative arguments similar to Ch. 3 that, unlike in the case of coupled LLs, the drag resistivity of coupled HLLs does not increase exponentially at lowest temperatures but rather goes to zero as a power law. This behavior was attributed to the topologically nontrivial origin of the HLL. It is in particular this feature of the drag resistivity that might be used to experimentally observe the drag between helical liquids.

The results in both Ch. 3 and 4 have been obtained using a combination of weak-coupling perturbation theory and RG methods. First, by treating the electron-electron interaction perturbatively, we solve the kinetic equation for the model and obtain the resistivity in the high-frequency and low-frequency regimes. These regimes are distinguished by the relation between the frequency of the driving field and the relevant inelastic relaxation rate. Next, we bosonized the model and studied the high frequency resistivity in linear response. The combination of both method allows us to make predictions about the resistivity in a large parameter regime. Finally, the behavior at lowest temperatures is investigated by employing a weak-coupling RG analysis.

Finally, in Ch. 5 we investigated the influence of Rashba SOC on the phase diagram and transport properties of interacting 1D electrons. The main role of the spin-orbital interactions is to break the spin-rotational symmetry in the spin sector, which enables the realization of previously symmetry-protected phases. The most interesting situation occurs when the dimensionless strength of SOC is stronger than the dimensionless strength of interactions. In this case, electron-electron interactions drive the spin sector of the system to a strong-coupling phase with quasi-long-range spin-density-wave order where a spectral gap is dynamically generated. On the other hand, the charge sector remains gapless. This prediction was established by treating interactions using bosonization and a weak-coupling renormalization-group analysis which is controlled by the small parameters of dimensionless interaction and spin-orbit-coupling strength.

We show that this gapped SDW phase exhibits properties akin to those of TIs. It differs, however, from conventional band insulators due to the fact that only the spin sector is gapped, while the charge sector of the liquid is still massless. Since physical electrons carry both spin and charge, the whole electron liquid forms an unusual topological state. The topological nature manifests itself mainly in two properties: First, the bulk of the system is protected against nonmagnetic impurity scattering for interaction strengths $K_c > 3/4$, for high impurity concentration and for $K_c > 1/2$ in the case of a single impurity. Second, we find zero-energy edge modes at the boundary of a finite system that carry fractional electron spin. These topological properties are protected by the bulk spin-gap.

There are several signatures of this novel topological state that may be used to verify it experimentally. The conductance of the system in the topological phase is expected to show a non-monotonic behavior as a function of temperature according to Eq. (5.51) which is depicted in Fig. 5.5. Furthermore, the tunneling density of states, as described by Eq. (5.72) shows distinct behavior in the bulk and at the edge of the wire. Due to the spin gap, there is a hard gap for single-particle tunneling in the bulk, while the tunneling density of states at the boundary shows power-law behavior as a function of the bias.

Naturally, many aspects presented in this thesis deserve further study. Firstly, we have discovered in Ch. 3, that scattering off impurities does not generate any dissipation to lowest order in perturbation theory, even if the impurities are dressed by arbitrarily strong Friedel oscillations. It was recently confirmed in [89] that this is an exact property of the model, to any order in perturbation theory. It

would therefore be interesting to analyze if the protection is caused by some hidden conservation law.

Another aspect that deserves further study concerns the nature of the strong coupling regimes in both the single edge and double edge setups studied in this thesis. One of the main arguments presented in the main text is that the edge cannot be studied disentangled from the bulk and therefore we expect that the edge conduction persists as long as the bulk remains in the topological regime even in the presence of strong interactions at the edge. Nonetheless, it is interesting to study how this protection arises microscopically. Thereby, one first has to answer the question if the protection can be seen in the edge theory itself or if one has to study the bulk simultaneously with the edge. Oftentimes we noticed that transport properties are determined by higher order scattering events describing pairs of fermions. Therefore a promising approach to further investigate the strong-coupling fixed points of the HLL might be to express the low energy field theory in terms of composite fermions and study their properties in turn.

Finally, open questions remain concerning the topological SDW phase discussed in Ch. 5. Our analysis of the weak-tunneling regime was based on the mapping of the 1D quasiclassical theory to a 0D quantum theory. In the problem of the single impurity in a LL, there exists a further method to gain complementary insight into the problem which consist of deriving the dual theory using an instanton expansion [66]. It would be interesting to develop such a dual theory also in our case. In particular we expect that the presence of zero-energy edge modes generates additional terms in the field theory which might lead to distinct signatures in the spin conductance.

In conclusion, we have seen in this thesis that the three central aspects of quantum transport in one dimension outlined in the introduction – topology, interaction and disorder – are inherently related.

Topological materials generically host gapless edge modes with unique properties symmetry-protected against impurity scattering. Ch. 3 showed that this protection is typically broken in the presence of interactions at the edge. While the edge states are still protected against Anderson localization by TRS, corrections to the exact quantization of the edge conductance do arise, due to elastic scattering off disorder dressed by Friedel oscillations. Even in the absence of disorder, we have seen that the interplay of topology and interaction leads to novel transport phenomena in 1D quantum systems. In particular, in the context of Coulomb drag, we have seen that the drag at sufficiently high temperatures is mediated by plasmons, since usual interaction channels are suppressed due to the topological origin of the edge liquid. Finally, Ch. 5 provided the proof of principle that strong interactions in 1D systems can generate gapped phases where topological properties emerge dynamically.

On a more general level, the work presented in this thesis accomplishes the following main achievements. Conceptually, this thesis has shown that the edge states of TIs remain conducting even in the presence of disorder and weak interactions. By the bulk-boundary correspondence this suggests that the classification of TIs in the periodic table remains stable in the presence of weak interactions. Further, we have been able to formulate exact criteria for the critical strength of the interaction for which the topological protection breaks down, by treating the edge modes in the framework of the exactly solvable Luttinger model. Furthermore, we have shown that interactions in 1D systems can lead to strong-coupling phases, where topological properties emerge dynamically. These phases have no noninteracting analogue, but still poses properties akin to topological insulators. In particular they exhibit a bulk-boundary correspondence. Taken together, this thesis shows that one-dimensional quantum systems not only provide a useful theoretical framework to study the impact of strong interactions on topological phases of matter but also provide promising candidate materials for the ongoing experimental search for exotic new topological phases of matter.

List of publications

In the following a list of the publications of the author of this thesis is presented:

1. N. Kainaris, *Interaction and disorder in edge states of two-dimensional topological insulators*, diploma thesis (2013). Ref. [86] in the bibliography.
2. N. Kainaris, I. V. Gornyi, S. T. Carr and A. D. Mirlin, *Conductivity of a generic helical liquid*, Phys. Rev. **B** 90, 075118 (2014). Ref. [85] in the bibliography.
3. N. Kainaris and S. T. Carr, *Emergent topological properties in interacting one-dimensional systems with spin-orbit coupling*, Phys. Rev. **B** 92, 035139 (2015). Ref. [123] in the bibliography.
4. N. Kainaris, R. A. Santos, D. B. Gutman, S. T. Carr, *Interaction induced topological protection in one-dimensional conductors*, arXiv:1605.06058 (to be published in Fortschritte der Physik). Ref. [132] in the bibliography.
5. N. Kainaris, I. V. Gornyi, A. Levchenko and D. G. Polyakov, *Coulomb drag between helical liquids*, arXiv:1610.01100 (submitted to PRB). Ref. [114] in the bibliography.

Bibliography

- [1] L. D. Landau. On the theory of phase transitions. *Zh. Eksp. Teor. Fiz.*, 7(19-32), 1937.
(Cited on page vii.)
- [2] K. v. Klitzing, G. Dorda, and M. Pepper. New method for high-accuracy determination of the fine-structure constant based on quantized hall resistance. *Phys. Rev. Lett.*, 45:494–497, Aug 1980.
(Cited on page vii.)
- [3] R. B. Laughlin. Quantized hall conductivity in two dimensions. *Phys. Rev. B*, 23:5632–5633, May 1981.
(Cited on page vii.)
- [4] D. J. Thouless, M. Kohmoto, M. P. Nightingale, and M. den Nijs. Quantized hall conductance in a two-dimensional periodic potential. *Phys. Rev. Lett.*, 49:405–408, Aug 1982.
(Cited on page vii.)
- [5] F. D. M. Haldane. Model for a quantum hall effect without landau levels: Condensed-matter realization of the "parity anomaly". *Phys. Rev. Lett.*, 61:2015–2018, Oct 1988.
(Cited on page vii.)
- [6] C. L. Kane and E. J. Mele. Z_2 topological order and the quantum spin hall effect. *Phys. Rev. Lett.*, 95:146802, Sep 2005.
(Cited on pages vii, 28, and 33.)
- [7] C. L. Kane and E. J. Mele. Quantum spin hall effect in graphene. *Phys. Rev. Lett.*, 95:226801, Nov 2005.
(Cited on page vii.)
- [8] B. Andrei Bernevig and Shou-Cheng Zhang. Quantum spin hall effect. *Phys. Rev. Lett.*, 96:106802, Mar 2006.
(Cited on pages viii and 25.)
- [9] Markus König, Steffen Wiedmann, Christoph Brüne, Andreas Roth, Hartmut Buhmann, Laurens W. Molenkamp, Xiao-Liang Qi, and Shou-Cheng Zhang. Quantum spin hall insulator state in hgte quantum wells. *Science*, 318(5851):766–770, 2007.
(Cited on pages viii, ix, 25, 29, and 33.)
- [10] Andreas P. Schnyder, Shinsei Ryu, Akira Furusaki, and Andreas W. W. Ludwig. Classification of topological insulators and superconductors in three spatial dimensions. *Phys. Rev. B*, 78:195125, Nov 2008.
(Cited on pages viii and 21.)

- [11] D. Hsieh, D. Qian, L. Wray, Y. Xia, Y. S. Hor, R. J. Cava, and M. Z. Hasan. A topological dirac insulator in a quantum spin hall phase. *Nature*, 452(7190):970–974, Apr 2008.
(Cited on page viii.)
- [12] Ivan Knez, Rui-Rui Du, and Gerard Sullivan. Evidence for helical edge modes in inverted InAs/GaSb quantum wells. *Phys. Rev. Lett.*, 107:136603, Sep 2011.
(Cited on pages viii, 30, and 33.)
- [13] X.L. Qi and S.-C. Zhang. *Rev. Mod. Phys.*, 83:1057, 2011.
(Cited on pages viii, 19, 25, and 33.)
- [14] Alexei Kitaev. Periodic table for topological insulators and superconductors. *AIP Conference Proceedings*, 1134(1):22–30, 2009.
(Cited on pages viii and 21.)
- [15] P. M. Ostrovsky, I. V. Gornyi, and A. D. Mirlin. Interaction-induced criticality in \mathbb{Z}_2 topological insulators. *Phys. Rev. Lett.*, 105:036803, Jul 2010.
(Cited on pages viii, 21, 60, and 81.)
- [16] Shinsei Ryu, Joel E. Moore, and Andreas W. W. Ludwig. Electromagnetic and gravitational responses and anomalies in topological insulators and superconductors. *Phys. Rev. B*, 85:045104, Jan 2012.
(Cited on page viii.)
- [17] Yuval Oreg, Gil Refael, and Felix von Oppen. Helical liquids and majorana bound states in quantum wires. *Phys. Rev. Lett.*, 105:177002, Oct 2010.
(Cited on page viii.)
- [18] Jason Alicea, Yuval Oreg, Gil Refael, Felix von Oppen, and Matthew P. A. Fisher. Non-abelian statistics and topological quantum information processing in 1d wire networks. *Nat Phys*, 7(5):412–417, May 2011.
(Cited on page viii.)
- [19] Piet W. Brouwer, Mathias Duckheim, Alessandro Romito, and Felix von Oppen. Topological superconducting phases in disordered quantum wires with strong spin-orbit coupling. *Phys. Rev. B*, 84:144526, Oct 2011.
(Cited on page viii.)
- [20] Bertrand I. Halperin, Yuval Oreg, Ady Stern, Gil Refael, Jason Alicea, and Felix von Oppen. Adiabatic manipulations of majorana fermions in a three-dimensional network of quantum wires. *Phys. Rev. B*, 85:144501, Apr 2012.
(Cited on page viii.)
- [21] A.Yu. Kitaev. Fault-tolerant quantum computation by anyons. *Annals of Physics*, 303(1):2 – 30, 2003.
(Cited on page viii.)
- [22] Chetan Nayak, Steven H. Simon, Ady Stern, Michael Freedman, and Sankar Das Sarma. Non-abelian anyons and topological quantum computation. *Rev. Mod. Phys.*, 80:1083–1159, Sep 2008.
(Cited on page viii.)

-
- [23] V. Mourik, K. Zuo, S. M. Frolov, S. R. Plissard, E. P. A. M. Bakkers, and L. P. Kouwenhoven. Signatures of majorana fermions in hybrid superconductor-semiconductor nanowire devices. *Science*, 336(6084):1003–1007, 2012.
(Cited on page viii.)
- [24] Anindya Das, Yuval Ronen, Yonatan Most, Yuval Oreg, Moty Heiblum, and Hadas Shtrikman. Zero-bias peaks and splitting in an al-inas nanowire topological superconductor as a signature of majorana fermions. *Nat Phys*, 8(12):887–895, Dec 2012.
(Cited on page viii.)
- [25] Leonid P. Rokhinson, Xinyu Liu, and Jacek K. Furdyna. The fractional a.c. josephson effect in a semiconductor-superconductor nanowire as a signature of majorana particles. *Nat Phys*, 8(11):795–799, Nov 2012.
(Cited on page viii.)
- [26] H. O. H. Churchill, V. Fatemi, K. Grove-Rasmussen, M. T. Deng, P. Caroff, H. Q. Xu, and C. M. Marcus. Superconductor-nanowire devices from tunneling to the multichannel regime: Zero-bias oscillations and magnetoconductance crossover. *Phys. Rev. B*, 87:241401, Jun 2013.
(Cited on page viii.)
- [27] Lukasz Fidkowski and Alexei Kitaev. Effects of interactions on the topological classification of free fermion systems. *Phys. Rev. B*, 81:134509, Apr 2010.
(Cited on page viii.)
- [28] Lukasz Fidkowski and Alexei Kitaev. Topological phases of fermions in one dimension. *Phys. Rev. B*, 83:075103, Feb 2011.
(Cited on page viii.)
- [29] Ari M. Turner, Frank Pollmann, and Erez Berg. Topological phases of one-dimensional fermions: An entanglement point of view. *Phys. Rev. B*, 83:075102, Feb 2011.
(Cited on page viii.)
- [30] Cenke Xu and J. E. Moore. Stability of the quantum spin hall effect: Effects of interactions, disorder, and F_2 topology. *Phys. Rev. B*, 73:045322, Jan 2006.
(Cited on page viii.)
- [31] Congjun Wu, B. Andrei Bernevig, and Shou-Cheng Zhang. Helical liquid and the edge of quantum spin hall systems. *Phys. Rev. Lett.*, 96:106401, Mar 2006.
(Cited on page viii.)
- [32] Sin-itiro Tomonaga. Remarks on bloch’s method of sound waves applied to many-fermion problems. *Progress of Theoretical Physics*, 5(4):544–569, 1950.
(Cited on page ix.)
- [33] J. M. Luttinger. An exactly soluble model of a many-fermion system. *Journal of Mathematical Physics*, 4(9):1154–1162, 1963.
(Cited on page ix.)
- [34] F D M Haldane. ‘luttinger liquid theory’ of one-dimensional quantum fluids. i. properties of the luttinger model and their extension to the general 1d interacting spinless fermi gas. *Journal of*

- Physics C: Solid State Physics*, 14(19):2585, 1981.
(Cited on page ix.)
- [35] T. Giamarchi. *Quantum Physics in One Dimension*. Oxford University Press, Oxford, 2004.
(Cited on pages ix, 1, 4, 12, 51, 59, 77, 85, 133, and 161.)
- [36] T. Lorenz, M. Hofmann, M. Gruninger, A. Freimuth, G. S. Uhrig, M. Dumm, and M. Dressel. Evidence for spin-charge separation in quasi-one-dimensional organic conductors. *Nature*, 418(6898):614–617, Aug 2002.
(Cited on page ix.)
- [37] O. M. Auslaender, H. Steinberg, A. Yacoby, Y. Tserkovnyak, B. I. Halperin, K. W. Baldwin, L. N. Pfeiffer, and K. W. West. Spin-charge separation and localization in one dimension. *Science*, 308(5718):88–92, 2005.
(Cited on page ix.)
- [38] Vikram V. Deshpande and Marc Bockrath. The one-dimensional wigner crystal in carbon nanotubes. *Nat Phys*, 4(4):314–318, Apr 2008.
(Cited on page ix.)
- [39] Marc Bockrath, David H. Cobden, Jia Lu, Andrew G. Rinzler, Richard E. Smalley, Leon Balents, and Paul L. McEuen. Luttinger-liquid behaviour in carbon nanotubes. *Nature*, 397(6720):598–601, Feb 1999.
(Cited on page ix.)
- [40] I. Safi and H. J. Schulz. Transport in an inhomogeneous interacting one-dimensional system. *Phys. Rev. B*, 52:R17040–R17043, Dec 1995.
(Cited on page ix.)
- [41] Dmitrii L. Maslov and Michael Stone. Landauer conductance of luttinger liquids with leads. *Phys. Rev. B*, 52:R5539–R5542, Aug 1995.
(Cited on page ix.)
- [42] Hadar Steinberg, Gilad Barak, Amir Yacoby, Loren N. Pfeiffer, Ken W. West, Bertrand I. Halperin, and Karyn Le Hur. Charge fractionalization in quantum wires. *Nat Phys*, 4(2):116–119, Feb 2008.
(Cited on page ix.)
- [43] H. Kamata, N. Kumada, and K. and Fujisawa T. Hashisaka, M. and Muraki. Fractionalized wave packets from an artificial tomonaga-luttinger liquid. *Nat Nano*, 9(3):177–181, Mar 2014. Letter.
(Cited on page ix.)
- [44] Alexander O. Gogolin, Alexander A. Nersesyan, and Alexei M. Tsvelik. *Bosonization and strongly correlated systems*. Cambridge University Press, 1. publ. edition, 1998.
(Cited on pages ix, 1, 4, 11, 51, 58, 85, 94, and 135.)
- [45] Lingjie Du, Ivan Knez, Gerard Sullivan, and Rui-Rui Du. Robust helical edge transport in gated InAs/GaSb bilayers. *Phys. Rev. Lett.*, 114:096802, Mar 2015.
(Cited on pages ix, 30, and 33.)

-
- [46] Tingxin Li, Pengjie Wang, Hailong Fu, Lingjie Du, Kate A. Schreiber, Xiaoyang Mu, Xiaoxue Liu, Gerard Sullivan, Gábor A. Csáthy, Xi Lin, and Rui-Rui Du. Observation of a helical luttinger liquid in InAs/GaSb quantum spin hall edges. *Phys. Rev. Lett.*, 115:136804, Sep 2015.
(Cited on pages ix, 30, and 57.)
- [47] Joseph Maciejko, Chaoxing Liu, Yuval Oreg, Xiao-Liang Qi, Congjun Wu, and Shou-Cheng Zhang. Kondo effect in the helical edge liquid of the quantum spin hall state. *Phys. Rev. Lett.*, 102:256803, Jun 2009.
(Cited on pages ix and 57.)
- [48] Thomas L. Schmidt, Stephan Rachel, Felix von Oppen, and Leonid I. Glazman. Inelastic electron backscattering in a generic helical edge channel. *Phys. Rev. Lett.*, 108:156402, Apr 2012.
(Cited on pages ix, 36, 57, and 65.)
- [49] Natalie Lezmy, Yuval Oreg, and Micha Berkooz. Single and multiparticle scattering in helical liquid with an impurity. *Phys. Rev. B*, 85:235304, Jun 2012.
(Cited on pages ix and 57.)
- [50] Jan Carl Budich, Fabrizio Dolcini, Patrik Recher, and Björn Trauzettel. Phonon-induced backscattering in helical edge states. *Phys. Rev. Lett.*, 108:086602, Feb 2012.
(Cited on page ix.)
- [51] N.F. Mott and W.D. Twose. The theory of impurity conduction. *Advances in Physics*, 10(38):107–163, 1961.
(Cited on pages 1 and 12.)
- [52] Alexander Altland and Ben D. Simons. *Condensed matter field theory*. Cambridge Univ. Press, 2. ed. edition, 2010.
(Cited on pages 1 and 50.)
- [53] John L. Cardy. *Scaling and renormalization in statistical physics*. Cambridge University Press, 2002.
(Cited on pages 1, 141, and 158.)
- [54] D. Sénéchal. An introduction to bosonization. *arXiv:cond-mat/9908262*, August 1999.
(Cited on pages 1, 4, and 7.)
- [55] Jan von Delft and Herbert Schoeller. Bosonization for beginners — refermionization for experts. *Annalen der Physik*, 7(4):225–305, 1998.
(Cited on pages 4 and 7.)
- [56] O. A. Starykh, D. L. Maslov, W. Haeusler, and L. I. Glazman. Gapped Phases of Quantum Wires. In T. Brandes, editor, *Low-Dimensional Systems. Interactions and Transport Properties*, volume 544 of *Lecture Notes in Physics*, Berlin Springer Verlag, page 37, 2000.
(Cited on pages 9, 11, 102, 103, 104, and 105.)
- [57] D. L. Maslov. Fundamental aspects of electron correlations and quantum transport in one-dimensional systems. *arXiv:cond-mat/0506035*, June 2005.
(Cited on pages 9, 39, and 56.)
-

- [58] J M Kosterlitz and D J Thouless. Ordering, metastability and phase transitions in two-dimensional systems. *Journal of Physics C: Solid State Physics*, 6(7):1181, 1973.
(Cited on page 11.)
- [59] Sam T. Carr, Boris N. Narozhny, and Alexander A. Nersesyan. Spinful fermionic ladders at incommensurate filling: Phase diagram, local perturbations, and ionic potentials. *Annals of Physics*, 339(0):22 – 80, 2013.
(Cited on page 11.)
- [60] I. V. Gornyi, A. D. Mirlin, and D. G. Polyakov. Electron transport in a disordered luttinger liquid. *Phys. Rev. B*, 75:085421, Feb 2007.
(Cited on pages 12 and 16.)
- [61] V. L. Berezinskii. Kinetics of a quantum particle in a one-dimensional random potential. *Sov. Phys. JETP*, 38(3):620, March 1974.
(Cited on page 12.)
- [62] A. A. Gogolin, V. I. Mel’nikov, and E. I. Rashba. Conductivity in a disordered one-dimensional system induced by electron-phonon interaction. *Sov. Phys. JETP*, 42(1):168, September 1975.
(Cited on page 12.)
- [63] C. L. Kane and Matthew P. A. Fisher. Transmission through barriers and resonant tunneling in an interacting one-dimensional electron gas. *Phys. Rev. B*, 46:15233–15262, Dec 1992.
(Cited on pages 14, 96, 97, 99, and 101.)
- [64] K. A. Matveev, Dongxiao Yue, and L. I. Glazman. Tunneling in one-dimensional non-luttinger electron liquid. *Phys. Rev. Lett.*, 71:3351–3354, Nov 1993.
(Cited on page 14.)
- [65] Dongxiao Yue, L. I. Glazman, and K. A. Matveev. Conduction of a weakly interacting one-dimensional electron gas through a single barrier. *Phys. Rev. B*, 49:1966–1975, Jan 1994.
(Cited on page 14.)
- [66] Akira Furusaki and Naoto Nagaosa. Single-barrier problem and anderson localization in a one-dimensional interacting electron system. *Phys. Rev. B*, 47:4631–4643, Feb 1993.
(Cited on pages 14, 96, 97, 101, and 109.)
- [67] T. Giamarchi and H. J. Schulz. Anderson localization and interactions in one-dimensional metals. *Phys. Rev. B*, 37:325–340, Jan 1988.
(Cited on pages 15, 105, and 143.)
- [68] M. Z. Hasan and C. L. Kane. Topological insulators. *Rev. Mod. Phys.*, 82:3045, 2010.
(Cited on pages 19 and 33.)
- [69] A. D. Mirlin, F. Evers, I. V. Gornyi, and P. M. Ostrovsky. Anderson transitions: Criticality, symmetries and topologies. *International Journal of Modern Physics B*, 24(12n13):1577–1620, 2010.
(Cited on pages 19 and 21.)

-
- [70] T. L. Schmidt G. Dolcetto, M. Sasseti. Edge physics in two-dimensional topological insulators. *Rivista del Nuovo Cimento*, 39:113–154, March 2016.
(Cited on pages 19 and 30.)
- [71] Eugene Paul Wigner. *Group theory and its application to the quantum mechanics of atomic spectra*. Acad. Press, exp. and impr. ed., 4. pr. edition, 1964.
(Cited on page 20.)
- [72] Martin R. Zirnbauer. Riemannian symmetric superspaces and their origin in random matrix theory. *Journal of Mathematical Physics*, 37(10):4986–5018, 1996.
(Cited on page 21.)
- [73] Alexander Altland and Martin R. Zirnbauer. Nonstandard symmetry classes in mesoscopic normal-superconducting hybrid structures. *Phys. Rev. B*, 55:1142–1161, Jan 1997.
(Cited on page 21.)
- [74] Andreas P. Schnyder, Shinsei Ryu, Akira Furusaki, and Andreas W. W. Ludwig. Classification of topological insulators and superconductors. *AIP Conference Proceedings*, 1134(1):10–21, 2009.
(Cited on page 21.)
- [75] W. P. Su, J. R. Schrieffer, and A. J. Heeger. Solitons in polyacetylene. *Phys. Rev. Lett.*, 42:1698–1701, Jun 1979.
(Cited on page 22.)
- [76] B. Andrei Bernevig, Taylor L. Hughes, and Shou-Cheng Zhang. Quantum spin hall effect and topological phase transition in hgte quantum wells. *Science*, 314(5806):1757–1761, 2006.
(Cited on pages 25 and 33.)
- [77] Chaoxing Liu, Taylor L. Hughes, Xiao-Liang Qi, Kang Wang, and Shou-Cheng Zhang. Quantum spin hall effect in inverted type-ii semiconductors. *Phys. Rev. Lett.*, 100:236601, Jun 2008.
(Cited on page 27.)
- [78] Haijun Zhang, Chao-Xing Liu, Xiao-Liang Qi, Xi Dai, Zhong Fang, and Shou-Cheng Zhang. Topological insulators in bi_2se_3 , bi_2te_3 and sb_2te_3 with a single dirac cone on the surface. *Nat Phys*, 5(6):438–442, Jun 2009.
(Cited on page 28.)
- [79] D. G. Rothe, R. W. Reithaler, C.-X. Liu, L. W. Molenkamp, S.-C. Zhang, and E. M. Hankiewicz. Fingerprint of different spin-orbit terms for spin transport in hgte quantum wells. *New Journal of Physics*, 12(6):065012, 2010.
(Cited on page 28.)
- [80] Ivan Knez, Charles T. Rettner, See-Hun Yang, Stuart S. P. Parkin, Lingjie Du, Rui-Rui Du, and Gerard Sullivan. Observation of edge transport in the disordered regime of topologically insulating InAs/GaSb quantum wells. *Phys. Rev. Lett.*, 112:026602, Jan 2014.
(Cited on pages 30 and 33.)
- [81] Christoph Brune, Andreas Roth, Hartmut Buhmann, Ewelina M. Hankiewicz, Laurens W. Molenkamp, Joseph Maciejko, Xiao-Liang Qi, and Shou-Cheng Zhang. Spin polarization of the quantum spin hall edge states. *Nat Phys*, 8(6):485–490, Jun 2012.
(Cited on page 30.)
-

- [82] Katja C. Nowack, Eric M. Spanton, Matthias Baenninger, Markus König, John R. Kirtley, Beena Kalisky, C. Ames, Philipp Leubner, Christoph Brüne, Hartmut Buhmann, Laurens W. Molenkamp, David Goldhaber-Gordon, and Kathryn A. Moler. Imaging currents in hgte quantum wells in the quantum spin hall regime. *Nat Mater*, 12(9):787–791, Sep 2013. Letter.
(Cited on page 30.)
- [83] Eric M. Spanton, Katja C. Nowack, Lingjie Du, Gerard Sullivan, Rui-Rui Du, and Kathryn A. Moler. Images of edge current in InAs/GaSb quantum wells. *Phys. Rev. Lett.*, 113:026804, Jul 2014.
(Cited on page 30.)
- [84] Andreas Roth, Christoph Brüne, Hartmut Buhmann, Laurens W. Molenkamp, Joseph Maciejko, Xiao-Liang Qi, and Shou-Cheng Zhang. Nonlocal transport in the quantum spin hall state. *Science*, 325(5938):294–297, 2009.
(Cited on page 33.)
- [85] Nikolaos Kainaris, Igor V. Gornyi, Sam T. Carr, and Alexander D. Mirlin. Conductivity of a generic helical liquid. *Phys. Rev. B*, 90:075118, Aug 2014.
(Cited on pages 34, 45, 71, 77, 105, and 111.)
- [86] Nikolaos Kainaris. Interaction and disorder in edge states of two dimensional topological insulators. Master’s thesis, Karlsruhe Institute of Technology, Department of Physics, Institut für Theorie der Kondensierten Materie, 2013.
(Cited on pages 34, 41, and 111.)
- [87] Anders Ström, Henrik Johannesson, and G. I. Japaridze. Edge dynamics in a quantum spin hall state: Effects from rashba spin-orbit interaction. *Phys. Rev. Lett.*, 104:256804, Jun 2010.
(Cited on pages 36 and 59.)
- [88] A. Rosch and N. Andrei. Conductivity of a clean one-dimensional wire. *Phys. Rev. Lett.*, 85:1092–1095, Jul 2000.
(Cited on page 42.)
- [89] Hong-Yi Xie, Heqiu Li, Yang-Zhi Chou, and Matthew S. Foster. Topological protection from random rashba spin-orbit backscattering: Ballistic transport in a helical luttinger liquid. *Phys. Rev. Lett.*, 116:086603, Feb 2016.
(Cited on pages 54 and 108.)
- [90] Florian Geissler, Francois Crépin, and Björn Trauzettel. Random rashba spin-orbit coupling at the quantum spin hall edge. *Phys. Rev. B*, 89:235136, Jun 2014.
(Cited on page 57.)
- [91] Karsten Flensberg. Coulomb drag of luttinger liquids and quantum hall edges. *Phys. Rev. Lett.*, 81:184–187, Jul 1998.
(Cited on page 63.)
- [92] Yuli V. Nazarov and D. V. Averin. Current drag in capacitively coupled luttinger constrictions. *Phys. Rev. Lett.*, 81:653–656, Jul 1998.
(Cited on pages 63 and 77.)

-
- [93] V. V. Ponomarenko and D. V. Averin. Coulomb drag between one-dimensional conductors. *Phys. Rev. Lett.*, 85:4928–4931, Dec 2000.
(Cited on page 63.)
- [94] Rochus Klesse and Ady Stern. Coulomb drag between quantum wires. *Phys. Rev. B*, 62:16912–16925, Dec 2000.
(Cited on pages 63, 77, and 80.)
- [95] A. Komnik and R. Egger. Transport and coulomb drag for two interacting carbon nanotubes. *Eur. Phys. J. B*, 19(2):271–280.
(Cited on page 63.)
- [96] B. Trauzettel, R. Egger, and H. Grabert. Coulomb drag shot noise in coupled luttinger liquids. *Phys. Rev. Lett.*, 88:116401, Feb 2002.
(Cited on page 63.)
- [97] M. Pustilnik, E. G. Mishchenko, L. I. Glazman, and A. V. Andreev. Coulomb drag by small momentum transfer between quantum wires. *Phys. Rev. Lett.*, 91:126805, Sep 2003.
(Cited on pages 63, 78, and 160.)
- [98] P. Schlottmann. Coulomb drag effect between luttinger liquids. *Phys. Rev. B*, 69:035110, Jan 2004.
(Cited on page 63.)
- [99] Thomas Fuchs, Rochus Klesse, and Ady Stern. Coulomb drag between quantum wires with different electron densities. *Phys. Rev. B*, 71:045321, Jan 2005.
(Cited on page 63.)
- [100] Gregory A. Fiete, Karyn Le Hur, and Leon Balents. Coulomb drag between two spin-incoherent luttinger liquids. *Phys. Rev. B*, 73:165104, Apr 2006.
(Cited on page 63.)
- [101] J. Peguiron, C. Bruder, and B. Trauzettel. Temperature dependence of coulomb drag between finite-length quantum wires. *Phys. Rev. Lett.*, 99:086404, Aug 2007.
(Cited on page 63.)
- [102] D. N. Aristov. Luttinger liquids with curvature: Density correlations and coulomb drag effect. *Phys. Rev. B*, 76:085327, Aug 2007.
(Cited on pages 63 and 160.)
- [103] A. V. Rozhkov. *Phys. Rev. B*, 77:125109, 2008.
(Cited on page 63.)
- [104] A. P. Dmitriev, I. V. Gornyi, and D. G. Polyakov. Coulomb drag between ballistic quantum wires. *Phys. Rev. B*, 86:245402, Dec 2012.
(Cited on pages 63, 65, 71, 72, 78, and 160.)
- [105] A. P. Dmitriev, I. V. Gornyi, and D. G. Polyakov.
(Cited on page 63.)
-

- [106] P Debray, P Vasilopoulos, O Raichev, R Perrin, M Rahman, and W.C Mitchel. Experimental observation of coulomb drag in parallel ballistic quantum wires. *Physica E*, 6(1–4):694 – 697, 2000.
(Cited on page 63.)
- [107] P Debray, V Zverev, O Raichev, R Klesse, P Vasilopoulos, and R S Newrock. Experimental studies of coulomb drag between ballistic quantum wires. *J. Phys.: Condens. Matter*, 13(14):3389, 2001.
(Cited on page 63.)
- [108] P Debray, V N Zverev, V Gurevich, R Klesse, and R S Newrock. Coulomb drag between ballistic one-dimensional electron systems. *Semicond. Sci. Technol.*, 17(11):R21, 2002.
(Cited on page 63.)
- [109] M. Yamamoto, M. Stopa, Y. Tokura, Y. Hirayama, and S. Tarucha. Coulomb drag between quantum wires: magnetic field effects and negative anomaly. *Physica E*, 12(1–4):726 – 729, 2002.
(Cited on page 63.)
- [110] M. Yamamoto, M. Stopa, Y. Tokura, Y. Hirayama, and S. Tarucha. Negative coulomb drag in a one-dimensional wire. *Science*, 313(5784):204–207, 2006.
(Cited on page 63.)
- [111] D. Laroche, G. Gervais, M. P. Lilly, and J. L. Reno. Positive and negative Coulomb drag in vertically integrated one-dimensional quantum wires. *Nat. Nanotechnol.*, 6(12):793–797, dec 2011.
(Cited on page 63.)
- [112] D. Laroche, G. Gervais, M. P. Lilly, and J. L. Reno. 1d-1d coulomb drag signature of a luttinger liquid. *Science*, 343(6171):631–634, 2014.
(Cited on page 63.)
- [113] Vladimir A. Zyuzin and Gregory A. Fiete. Coulomb drag between helical edge states. *Phys. Rev. B*, 82:113305, Sep 2010.
(Cited on pages 63 and 64.)
- [114] N. Kainaris, I. V. Gornyi, A. Levchenko, and D. G. Polyakov. Coulomb drag between helical luttinger liquids. *arXiv:cond-mat/1610.01100*, 2016.
(Cited on pages 64 and 111.)
- [115] B. N. Narozhny and A. Levchenko. Coulomb drag. *Rev. Mod. Phys.*, 88:025003, 2016.
(Cited on page 71.)
- [116] M. Schütt, P. M. Ostrovsky, I. V. Gornyi, and A. D. Mirlin. Coulomb interaction in graphene: Relaxation rates and transport. *Phys. Rev. B*, 83:155441, Apr 2011.
(Cited on pages 71 and 72.)
- [117] B. N. Narozhny, M. Titov, I. V. Gornyi, and P. M. Ostrovsky. Coulomb drag in graphene: Perturbation theory. *Phys. Rev. B*, 85:195421, May 2012.
(Cited on page 71.)

-
- [118] A. G. Yashenkin, I. V. Gornyi, A. D. Mirlin, and D. G. Polyakov. Quantum interference and spin-charge separation in a disordered luttinger liquid. *Phys. Rev. B*, 78:205407, Nov 2008.
(Cited on page 71.)
- [119] M. J. Rice, A. R. Bishop, J. A. Krumhansl, and S. E. Trullinger. Weakly pinned fröhlich charge-density-wave condensates: A new, nonlinear, current-carrying elementary excitation. *Phys. Rev. Lett.*, 36:432–435, Feb 1976.
(Cited on page 80.)
- [120] Kazumi Maki. Creation of soliton pairs by electric fields in charge-density—wave condensates. *Phys. Rev. Lett.*, 39:46–48, Jul 1977.
(Cited on page 80.)
- [121] A. Luther and V. J. Emery. Backward scattering in the one-dimensional electron gas. *Phys. Rev. Lett.*, 33:589–592, Sep 1974.
(Cited on page 85.)
- [122] Alexander Seidel and Dung-Hai Lee. The luther-emery liquid: Spin gap and anomalous flux period. *Phys. Rev. B*, 71:045113, Jan 2005.
(Cited on page 85.)
- [123] Nikolaos Kainaris and Sam T. Carr. Emergent topological properties in interacting one-dimensional systems with spin-orbit coupling. *Phys. Rev. B*, 92:035139, Jul 2015.
(Cited on pages 86, 93, and 111.)
- [124] E. I. Rashba. Properties of semiconductors with an extremum loop. 1. cyclotron and combinational resonance in a magnetic field perpendicular to the plane of the loop. *Sov. Phys. Solid State*, 2:1109–1122, 1960.
(Cited on page 86.)
- [125] Florian Goth and Fakher F. Assaad. Equivalence of rashba-hubbard and hubbard chains. *Phys. Rev. B*, 90:195103, Nov 2014.
(Cited on pages 87 and 88.)
- [126] Junsaku Nitta, Tatsushi Akazaki, Hideaki Takayanagi, and Takatomo Enoki. Gate control of spin-orbit interaction in an inverted $\text{In}_{0.53}\text{Ga}_{0.47}\text{As}/\text{In}_{0.52}\text{Al}_{0.48}\text{As}$ heterostructure. *Phys. Rev. Lett.*, 78:1335–1338, Feb 1997.
(Cited on page 90.)
- [127] G. Engels, J. Lange, Th. Schäpers, and H. Lüth. Experimental and theoretical approach to spin splitting in modulation-doped $\text{In}_x\text{Ga}_{1-x}\text{As}/\text{InP}$ quantum wells for $b \rightarrow 0$. *Phys. Rev. B*, 55:R1958–R1961, Jan 1997.
(Cited on page 90.)
- [128] Dirk Grundler. Large rashba splitting in InAs quantum wells due to electron wave function penetration into the barrier layers. *Phys. Rev. Lett.*, 84:6074–6077, Jun 2000.
(Cited on page 90.)
- [129] Suhas Gangadharaiah, Jianmin Sun, and Oleg A. Starykh. Spin-orbital effects in magnetized quantum wires and spin chains. *Phys. Rev. B*, 78:054436, Aug 2008.
(Cited on page 100.)
-

- [130] Anna Keselman and Erez Berg. Gapless symmetry-protected topological phase of fermions in one dimension. *Phys. Rev. B*, 91:235309, Jun 2015.
(Cited on page 104.)
- [131] M. Fabrizio and Alexander O. Gogolin. Interacting one-dimensional electron gas with open boundaries. *Phys. Rev. B*, 51:17827–17841, Jun 1995.
(Cited on page 104.)
- [132] N. Kainaris, R. A. Santos, D. B. Gutman, and S. T. Carr. Interaction induced topological protection in one-dimensional conductors. *arXiv:cond-mat/1605.06058*, May 2016.
(Cited on page 111.)
- [133] Zoran Ristivojevic, Aleksandra Petković, Pierre Le Doussal, and Thierry Giamarchi. Phase transition of interacting disordered bosons in one dimension. *Phys. Rev. Lett.*, 109:026402, Jul 2012.
(Cited on page 144.)

List of Figures

1.1	Interaction processes in a Tomonaga Luttinger liquid	8
1.2	RG flow diagram of one-dimensional fermions with repulsive interaction	10
1.3	Strong-coupling phases of the 1D interacting electron gas and their excitations	12
1.4	RG flow diagram of the disordered Luttinger liquid	16
2.1	Su-Schrieffer-Heeger chain	24
2.2	Band structure of HgTe and CdTe near the Γ point	25
2.3	AlSb/InAs/GaSb/AlSb heterostructure	27
2.4	Nonlocal conductance measurement in HgTe/CdTe heterostructures	29
2.5	Experimental evidence for the HLL	30
3.1	Illustration of the spin orientation and dispersion of a helical liquid	36
3.2	Two-particle electron-electron scattering processes in a helical Luttinger liquid	37
3.3	Diagrammatic representation of the second order perturbation theory of the helical Luttinger model	43
3.4	Most important scattering mechanisms in a HLL	47
3.5	Behavior of the dc resistivity of a helical Luttinger liquid	55
3.6	Behavior of the conductivity of a helical Luttinger liquid	56
3.7	Possible strong-coupling regimes of a HLL	59
4.1	Schematics of a Coulomb drag measurement between helical edges of two quantum spin Hall systems	64
4.2	Momentum configurations for the two-particle scattering processes between two helical liquids	68
4.3	RG flow diagram for the inter-edge interaction strength of two coupled helical Luttinger models	76
4.4	Sketch of the temperature dependence of the high-frequency drag scattering rate between two weakly interacting helical liquids	82
5.1	Energy dispersion of one-dimensional electrons subject to spin-orbit coupling	88
5.2	Band structure of one-dimensional electrons subject to spin-orbit coupling in the low-energy limit	90
5.3	RG flow diagram of interacting one-dimensional electrons subject to spin-orbit interaction	92
5.4	Phase diagram of one-dimensional electrons subject to spin-orbit coupling in the presence of a single impurity	96
5.5	Temperature dependence of the conductance in the disordered spin-density wave phase	98
5.6	Spatial profile of the spin displacement field in the SDW phase in the presence of a single impurity	103
D.1	Diagramms determining the Coulomb drag between helical liquids	151

D.2	Sketch of the parametric behavior of the particle-hole contribution to the high-frequency Coulomb drag rate between helical liquids	153
D.3	Sketch of the parametric behavior of the plasmon contribution to the high-frequency Coulomb drag rate between helical liquids	155

Acronyms

- 1BZ** first Brillouin zone. 21, 23
- 1D** one dimensional. vii–x, 1, 4, 5, 7, 10, 12, 13, 17, 19, 22, 23, 33, 85, 104, 108, 109
- 2D** two dimensional. vii–x, 25, 27, 28, 30, 33, 60, 85
- BHZ** Bernevig-Hughes-Zhang. 24, 26, 28
- BIA** bulk-inversion asymmetry. 28
- BKT** Berezinskii-Kosterlitz-Thouless. 11, 91, 93
- CDW** charge-density wave. 10, 11, 93, 94, 97, 98, 100, 101, 103, 106
- HLL** helical Luttinger liquid. ix, x, 33, 34, 36, 38, 47, 51, 54–56, 58–60, 63, 64, 70, 77, 82, 83, 107–109, 135, 143, 151
- IR** infrared. 2, 132
- LL** Luttinger liquid. ix, x, 1, 4, 8, 9, 14, 59, 60, 64, 66, 70, 71, 77, 80, 83, 91, 97, 107–109
- PHS** particle-hole symmetry. 20, 23, 24
- QHE** quantum Hall effect. vii, viii
- QSH** quantum spin Hall. viii, x, 27, 28, 30, 33, 57, 64
- RG** renormalization group. 1–3, 9, 10, 15–17, 56, 59, 61, 91–93, 95, 97, 99, 141–143, 145
- RPA** Random phase approximation. 66, 69–71, 73
- SDW** spin-density wave. 11, 12, 85, 93, 94, 96–101, 103, 104, 106, 108, 109
- SG** sine-Gordon. 10, 95, 97, 100, 104
- SIA** structural-inversion asymmetry. 28
- SOC** spin-orbit coupling. vii, viii, x, 25, 26, 28, 33–36, 85–93, 95, 105, 106
- SSH** Su-Schrieffer-Heeger. 22–24
- TI** Topological insulators. viii–x, 19–23, 25, 27–30, 60, 85, 106, 108, 109
- TRS** time-reversal symmetry. vii, ix, 20, 21, 23, 25, 26, 28–30, 34, 39, 59, 63–65, 83, 85, 90, 109
- UV** ultraviolet. 2, 34, 49, 56, 99

Notations and conventions

Here we present a list of notations and conventions used throughout this thesis

1. We use units where $\hbar = k_B = c = 1$, where \hbar is the reduced Planck's quantum, k_B is Boltzmann's constant and c is the velocity of light.

2. The symbol \int_k denotes the normalized integration over momenta:

$$\int_k \dots = \int \frac{dk}{2\pi} \dots$$

3. In order to distinguish between operators in Fock space and quantum fields the former are depicted with hats whereas the latter are not (see e.g. $\hat{\varphi}$ Eq. (1.13) and $\varphi(z, \bar{z})$ in Eq. (1.15)).

4. The Pauli matrices are defined as

$$\begin{aligned} \sigma_0 = \tau_0 &= \begin{pmatrix} 1 & 0 \\ 0 & 1 \end{pmatrix}, & \sigma_x = \tau_x &= \begin{pmatrix} 0 & 1 \\ 1 & 0 \end{pmatrix}, \\ \sigma_y = \tau_y &= \begin{pmatrix} 0 & -i \\ i & 0 \end{pmatrix}, & \sigma_z = \tau_z &= \begin{pmatrix} 1 & 0 \\ 0 & -1 \end{pmatrix}, \end{aligned}$$

where we use the symbol σ refers to the microscopic spin of the electron and τ refers to pseudospin.

5. The commutator $[\cdot, \cdot]$ and anticommutator $\{\cdot, \cdot\}$ are defined as

$$[\hat{A}, \hat{B}] := \hat{A}\hat{B} - \hat{B}\hat{A}, \quad \{\hat{A}, \hat{B}\} = \hat{A}\hat{B} + \hat{B}\hat{A}$$

for two operators \hat{A} and \hat{B} .

6. For binary quantum numbers a bar over the quantum number index denotes negation, i.e. if the spin $\sigma = \uparrow$ then $\bar{\sigma} = \downarrow$.

7. The Fermi-Dirac distribution function is denoted by

$$n_F(\epsilon) = \frac{1}{1 + \exp \frac{\epsilon - \mu}{k_B T}}$$

Next we present the basic notation used in this thesis:

e	elementary charge
v_F	Fermi velocity
k_F	Fermi momentum
E_F	Fermi energy
μ	chemical potential
$\nu(\epsilon)$	single particle density of states at energy ϵ
$\psi_{\eta,\sigma}$	fermionic Grassmann field for chirality η and (pseudo-) spin σ
φ	bosonic displacement field
θ	bosonic phase field
$\phi_{R,L}$	chiral bosonic fields
$\Theta(x)$	Heaviside step function
$\text{sign}(x)$	signum function
K_μ	Luttinger parameter in the charge ($\mu = c$) or spin ($\mu = s$) sector
v_μ	plasmon velocity in the charge ($\mu = c$) or spin ($\mu = s$) sector
a	short distance cutoff of the bosonic theory
a_0	lattice constant
λ	dimensionless coupling constant
\simeq	approximately
\propto	proportional
\sim	asymptotic
Re and Im	real and imaginary part
\mathcal{P}	principal value
$\delta(x)$	delta function
δ_{ij}	Kronecker delta
$\Gamma(x)$	Euler Gamma function
$B(x, y)$	Euler beta function
$K_m(x)$	modified Bessel function of the second kind
H.c.	Hermitian conjugate
c.c.	complex conjugate

A

Appendix A

Bosonization dictionary

In this Appendix we state the bosonization conventions used in this thesis and present some useful relations.

Bosonization conventions. We use the bosonization conventions

$$\psi_{+,\sigma}(x) = \frac{\kappa_{+,\sigma}}{\sqrt{2\pi a}} e^{i\sqrt{4\pi}\phi_{+,\sigma}(x)}, \quad \psi_{-,\sigma}(x) = \frac{\kappa_{-,\sigma}}{\sqrt{2\pi a}} e^{-i\sqrt{4\pi}\phi_{-,\sigma}(x)}. \quad (\text{A.1})$$

where a is the bosonic UV cutoff. The Klein factors are introduced to ensure that the fermionic operators obey the correct anticommutation relations. They obey the Clifford algebra

$$\{\kappa_{\eta,\sigma}, \kappa_{\eta',\sigma'}\} = 2\delta_{\eta,\eta'}\delta_{\sigma,\sigma'} \quad (\text{A.2})$$

Since they are not dynamic variables we are free to choose a specific representation. In particular in Ch. 5 we choose

$$\kappa_{\eta,\sigma}^2 = 1, \quad \kappa_{\eta,\uparrow}\kappa_{\eta,\downarrow} = -\kappa_{\eta,\downarrow}\kappa_{\eta,\uparrow} = i. \quad (\text{A.3})$$

We also introduce the dual fields

$$\varphi_\sigma = \phi_{+,\sigma} + \phi_{-,\sigma}, \quad \theta_\sigma = \phi_{+,\sigma} - \phi_{-,\sigma}. \quad (\text{A.4})$$

such that $\Pi = -\partial_x\theta$ is the conjugate momentum to φ . Vertex operators are multiplied according to the rule

$$e^{i\alpha\varphi} e^{i\beta\varphi'} = e^{i(\alpha\varphi+\beta\varphi')} e^{-\alpha\beta(\varphi\varphi')}, \quad (\text{A.5})$$

The spin and charge degrees of freedom are given by

$$\varphi_c = \frac{\varphi_\uparrow + \varphi_\downarrow}{\sqrt{2}}, \quad \varphi_s = \frac{\varphi_\uparrow - \varphi_\downarrow}{\sqrt{2}}. \quad (\text{A.6})$$

In terms of these fields the nonoscillatory part of the charge density and the z-component of the spin-density read as

$$\begin{aligned} \rho_c(x) &= \sum_\sigma \psi_\sigma^\dagger(x) \psi_\sigma(x) = \sqrt{\frac{2}{\pi}} \partial_x \varphi_c(x), \\ \rho_s^z(x) &= \sum_\sigma \psi_\sigma^\dagger(x) S_{\sigma\sigma'}^z \psi_{\sigma'}(x) = \frac{1}{2} \sum_\sigma \psi_\sigma^\dagger(x) \sigma_{\sigma\sigma'}^z \psi_\sigma(x) = \frac{1}{\sqrt{2\pi}} \partial_x \varphi_s(x). \end{aligned} \quad (\text{A.7})$$

Bosonic correlation functions The action of a real bosonic field is given by

$$\begin{aligned}
S &= \int dx d\tau \left[i\partial_x \theta \partial_\tau \varphi + \frac{uK}{2} (\partial_x \theta)^2 + \frac{u}{2K} (\partial_x \varphi)^2 \right] \\
&= \int_{q, \omega_n} \left\{ iq\omega_n \theta(q, \omega_n) \varphi_{-q, -\omega_n} + \frac{uK}{2} q^2 \theta(q, \omega_n) \theta(-q, -\omega_n) + \frac{u}{2K} q^2 \varphi_{q, \omega_n} \varphi_{-q, -\omega_n} \right\} \\
&= \frac{1}{2} \int_{q, \omega_n} \begin{pmatrix} \theta(q, \omega_n) & \varphi(q, \omega_n) \end{pmatrix} \underbrace{\begin{pmatrix} Kuq^2 & iq\omega_n \\ iq\omega_n & \frac{u}{K} q^2 \end{pmatrix}}_{\equiv \hat{G}^{-1}} \begin{pmatrix} \theta(-q, -\omega_n) \\ \varphi(-q, -\omega_n) \end{pmatrix}.
\end{aligned} \tag{A.8}$$

Inverting the propagator matrix yields

$$\hat{G}(q, \omega_n) = \frac{1}{v^2 q^2 + \omega_n^2} \begin{pmatrix} vK & -\frac{i\omega_n}{q} \\ -\frac{i\omega_n}{q} & vK \end{pmatrix}. \tag{A.9}$$

First we note that e.g.

$$i\omega_n \langle \varphi(\mathbf{q}) \varphi(-\mathbf{q}) \rangle = vqK \langle \theta(\mathbf{q}) \varphi(-\mathbf{q}) \rangle \tag{A.10}$$

That means inside correlation functions we may use the relation $i\omega_n \varphi(\mathbf{q}) = vqK\theta(\mathbf{q})$. Analogously one finds $i\omega_n K\theta(\mathbf{q}) = vq\varphi(\mathbf{q})$. This yields the duality relations

$$i\partial_\tau \varphi(x, \tau) = vK \partial_x \theta(x, \tau), \quad i\partial_\tau \theta(x, \tau) = \frac{v}{K} \partial_x \varphi(x, \tau) \tag{A.11}$$

Next, we calculate the φ correlation function at $T = 0$. In this case we can replace the sum over Matsubara frequencies by an integral

$$T \sum_{\omega_n} \rightarrow \int_{\omega} \tag{A.12}$$

The propagator then reads as

$$G_\varphi(x, \tau) = \langle \varphi(x, \tau) \varphi(0, 0) \rangle = \int \frac{d^2 q}{(2\pi)^2} \frac{K}{\mathbf{q}^2 + m^2} e^{i\mathbf{q}\mathbf{x}}, \tag{A.13}$$

Here, we defined the vectors $\mathbf{q} = (vq, \omega)^T$ and $\mathbf{x} = (x/v, \tau)^T$ and introduced a small mass term m to regularize the integral in the IR. The integral is most conveniently performed in polar coordinates, which yields

$$\begin{aligned}
G_\varphi(x, \tau) &= \frac{K}{4\pi^2} \int_0^\infty dr \int_0^{2\pi} d\phi \frac{r}{r^2 + m^2} e^{i|\mathbf{x}|r \cos \phi} = \frac{K}{2\pi} \int_0^\infty dr \frac{r}{r^2 + m^2} J_0(|\mathbf{x}|r) \\
&= \frac{K}{2\pi} K_0(m|\mathbf{x}|).
\end{aligned} \tag{A.14}$$

Here, $J_0(x)$ denotes the zeroth Bessel function and $K_0(x)$ the zeroth modified Bessel function of the second kind; we used the identities

$$\int_0^{2\pi} d\phi e^{ix \cos(\phi)} = 2\pi J_0(|x|), \quad (\text{A.15})$$

$$\int_0^\infty dx \frac{x J_0(ax)}{x^2 + k^2} = K_0(ak). \quad (\text{A.16})$$

The modified Bessel function behaves asymptotically as $K_0(x) \sim \sqrt{\pi/2x} \exp(-|x|)$ for $x \rightarrow \infty$ and as $K_0(x) \sim -\ln(x/2)$ for $x \rightarrow 0$. This yields the correlation function

$$\langle \varphi(x, \tau) \varphi(0, 0) \rangle = -\frac{K}{4\pi} \ln \left\{ m^2 (x^2 + v^2 \tau^2) \right\}, \quad \text{for } m|\mathbf{x}| \rightarrow 0, \quad (\text{A.17})$$

$$\langle \varphi(x, \tau) \varphi(0, 0) \rangle = \frac{K}{2\pi} \sqrt{\frac{\pi}{2m|\mathbf{x}|}} e^{-m|\mathbf{x}|}, \quad \text{for } m|\mathbf{x}| \gg 1. \quad (\text{A.18})$$

At finite temperature, we obtain the correlation function in the limit of vanishing mass by the substitution $m x_\pm \rightarrow \frac{v}{\pi a T} \sinh(x_\pm)$ with $x_\pm = x \pm i v \tau$ [35].

Correlation functions containing exponentials of bosonic fields. In this thesis we often encounter correlation functions such as

$$\langle \theta'(1) \theta'(2) e^{i\alpha[\varphi(3) - \varphi(4)]} \rangle, \quad (\text{A.19})$$

where we denoted $\partial_x \theta(x, \tau) = \theta'(x, \tau)$ and $(i) = (x_i, \tau_i)$. We can calculate them using the following trick:

$$\begin{aligned} & \langle \theta'(1) \theta'(2) e^{i\alpha[\varphi(3) - \varphi(4)]} \rangle \\ &= \frac{1}{\alpha^2} \partial_{I_1} \partial_{I_2} \langle e^{\alpha[\varphi(3) - \varphi(4) + I_1 \theta'(1) - I_2 \theta'(2)]} \rangle \Big|_{I_1=I_2=0} \\ &= \left\{ \langle \theta'(1) \theta'(2) \rangle - \alpha^2 \langle \theta'(1) [\varphi(3) - \varphi(4)] \rangle \langle \theta'(2) [\varphi(3) - \varphi(4)] \rangle \right\} e^{-\frac{\alpha^2}{2} \langle [\varphi(3) - \varphi(4)]^2 \rangle}. \end{aligned} \quad (\text{A.20})$$

B

Appendix B

Electron transport in a helical Luttinger liquid

In this Appendix we present some details of the calculation of the high-frequency conductivity of the disordered HLL performed in Sec. 3.3.1 in the main part of the thesis. Throughout this appendix we will use the notation $(i) \equiv (x_i, \tau_i)$ for space-time coordinates.

B.1 Expressions for the current and diamagnetic susceptibility

To couple the theory of the disordered HLL to an external electric field we perform the minimal substitution $\partial_{x_1}\theta(1) \rightarrow \partial_{x_1}\theta(1) + eA(1)/\sqrt{\pi}$ [44] in the model in (3.57). In doing so, we neglect the terms S_3 and S_f in the action, since we know from the results of the kinetic equation section that they do not contribute to transport properties. Therefore, we are left with the action $S = S_{LL} + S_{\text{dis}} + S_5$ with $S_{\text{dis}} = S_{1P} + S_{2P} + S_b$. The current j and diamagnetic susceptibility χ^{dia} are then obtained by varying with respect to the vector potential. The current density is given by

$$j_n(1) = \left. \frac{\delta S}{\delta A_n(1)} \right|_{A=0} = j_n^{(0)}(1) + j_n^{(\text{dis})}(1) + j_n^{(5)}(1). \quad (\text{B.1})$$

Here, we defined the current of the Luttinger model $j_n^{(0)}(1) = \frac{eKv}{\sqrt{\pi}}\partial_{x_1}\theta_n(1)$ and the *anomalous* contributions to the current $j_n^{(5)}$ and $j_n^{(\text{dis})} = j_n^{(1P)} + j_n^{(b)}$ with

$$\begin{aligned} j_n^{(5)}(1) &= -\lambda_{5,1} \frac{ev}{\sqrt{\pi}} \partial_{x_1} \cos(\sqrt{4\pi}\varphi_n(1) - 2k_F x_1) - \lambda_{5,2} \frac{ev}{\sqrt{\pi}a} \sin(\sqrt{4\pi}\varphi_n(1) - 2k_F x_1), \\ j_n^{(1P)}(1) &= 2\lambda_{1P,1} \frac{ev^2 a}{\sqrt{\pi}} \sum_m \int d\tau_2 \partial_{x_1} \left(\partial_{x_1}^2 \theta_m(x_1, \tau_2) \cos \left\{ \sqrt{4\pi} [\varphi_n(x_1, \tau_1) - \varphi_m(x_1, \tau)] \right\} \right) \\ &\quad + 2\lambda_{1P,2} \frac{ev^2}{\sqrt{\pi}} \sum_m \int d\tau_2 \partial_{x_1}^2 \theta_b(x_1, \tau_2) \sin \left\{ \sqrt{4\pi} [\varphi_m(x_1, \tau_2) - \varphi_n(x_1, \tau_1)] \right\} \\ &\quad + 2\lambda_{1P,2} \frac{ev^2}{\sqrt{\pi}} \sum_m \int d\tau_2 \partial_{x_1} \theta_m(x_1, \tau_2) \partial_{x_1} \sin \left\{ \sqrt{4\pi} [\varphi_n(x_1, \tau_1) - \varphi_m(x_1, \tau_2)] \right\}, \\ j_n^{(b)}(1) &= -2\mathcal{D}_b \frac{ev^2}{\sqrt{\pi}a} \sum_m \int d\tau_2 \partial_{x_1} \theta_b(x_1, \tau_2) \cos \left\{ \sqrt{4\pi} [\varphi_n(x_1, \tau_1) - \varphi_m(x_1, \tau_2)] \right\}. \end{aligned} \quad (\text{B.2})$$

The diamagnetic susceptibility is given by

$$\chi_{nm}^{\text{dia}}(x_1 - x_2, \tau_1 - \tau_2) = - \left. \frac{\delta S}{\delta A_n(1) \delta A_m(2)} \right|_{A=0} = \chi_{nm}^{(0)}(1-2) + \chi_{nm}^{(\text{dis})}(1-2), \quad (\text{B.3})$$

where we defined

$$\chi_{nm}^{(0)}(1-2) = \frac{e^2 v K}{\pi} \delta(x_1 - x_2) \delta(\tau_1 - \tau_2) \delta_{nm}, \quad (\text{B.4})$$

and $\chi_{nm}^{(\text{dis})} = \chi_{nm}^{(1\text{P})} + \chi_{nm}^{(b)}$ with

$$\chi_{nm}^{(1\text{P})}(1-2) = 2\lambda_{1\text{P},2} \frac{e^2 v^2}{\pi} \delta(x_1 - x_2) \delta_{nm} \partial_{x_1} \sin \left\{ \sqrt{4\pi} [\varphi_n(x_1, \tau_1) - \varphi_n(x_1, \tau_2)] \right\}, \quad (\text{B.5})$$

$$\chi_{nm}^{(b)}(1-2) = 2\mathcal{D}_b \frac{e^2 v^2}{\pi a} \cos \left\{ \sqrt{4\pi} [\varphi_a(x_1, \tau_1) - \varphi_b(x_1, \tau_2)] \right\} \delta(x_1 - x_2) \delta_{nm}. \quad (\text{B.6})$$

These expressions are needed to obtain the *ac* conductivity in Appendix B.2.

Correlation functions. Let us define the correlation functions

$$G_{\theta\varphi}^{(i)}(1-2) = \langle \partial_{x_1}^i \theta(1) \varphi(2) \rangle, \quad (\text{B.7})$$

$$G_{\theta\theta}^{(i)}(1-2) = \langle \partial_{x_1}^i \theta(1) \partial_{x_2}^i \theta(2) \rangle. \quad (\text{B.8})$$

In particular we will need the correlation function with respect to the Luttinger liquid fixed point action

$$\begin{aligned} \langle [\varphi(x, \tau) - \varphi(0, 0)]^2 \rangle_0 &= \frac{K}{2\pi} \ln \left\{ \left(\frac{v}{\pi a T} \right)^2 \sinh x_- \sinh x_+ \right\} \equiv \frac{K}{2\pi} F(x, \tau), \\ \langle \partial_x \varphi(x, \tau) \partial_x \varphi(0, 0) \rangle_0 &= - \frac{K}{4\pi} \left(\frac{\pi T}{v} \right)^2 \left(\frac{1}{\sinh^2 x_+} + \frac{1}{\sinh^2 x_-} \right), \\ \langle \partial_x^2 \varphi(x, \tau) \partial_x^2 \varphi(0, 0) \rangle_0 &= \frac{K}{2\pi} \left(\frac{\pi T}{v} \right)^4 \left(\frac{1 + 2 \cosh^2 x_+}{\sinh^4 x_+} + \frac{1 + 2 \cosh^2 x_-}{\sinh^4 x_-} \right), \\ \langle \varphi(x, \tau) \partial_x \theta(0, 0) \rangle_0 &= - \frac{1}{4\pi} \left(\frac{\pi T}{v} \right) (\coth x_+ - \coth x_-), \\ \langle \varphi(x, \tau) \partial_x \varphi(0, 0) \rangle_0 &= - \frac{K}{4\pi} \left(\frac{\pi T}{v} \right) (\coth x_+ + \coth x_-), \\ \langle \varphi(x, \tau) \partial_x^2 \theta(0, 0) \rangle_0 &= - \frac{K}{4\pi} \left(\frac{\pi T}{v} \right)^2 \left(\frac{1}{\sinh^2 x_+} - \frac{1}{\sinh^2 x_-} \right). \end{aligned} \quad (\text{B.9})$$

Here, we defined $x_{\pm} = \frac{\pi T}{v}(x \pm iv\tau)$. At short space-time distances the arguments are cut off as $x \rightarrow x + a \text{sign}(x)$ if $\tau = 0$ and $\tau \rightarrow \tau + \frac{a}{v} \text{sign}(\tau)$ if $x = 0$. The correlation functions above can be obtained from the $\varphi\varphi$ correlator by differentiation and use of the duality relations.

B.2 Calculation of the conductivity

We now outline how to obtain the high-frequency conductivity in (3.58). To this end we expand the current-current correlation function to leading order in coupling constants, which yields

$$\begin{aligned} \langle j_n(1)j_m(2) \rangle &\simeq \langle j_n^{(0)}(1)j_m^{(0)}(2) \rangle_0 - \langle j_n^{(0)}(1)j_m^{(0)}(2)S_{\text{dis}} \rangle_0 + 2 \langle j_n^{(0)}(1)j_n^{(\text{dis})}(2) \rangle_0 \\ &+ \frac{1}{2} \langle j_n^{(0)}(1)j_m^{(0)}(2)S_5^2 \rangle_0 - 2 \langle j_n^{(0)}(1)j_m^{(5)}(2)S_5 \rangle_0 + \langle j_n^{(5)}(1)j_m^{(5)}(2) \rangle_0 . \end{aligned} \quad (\text{B.10})$$

Contributions due to inelastic impurity scattering. Let us start with the contribution due to S_{dis} . Due to the neutrality condition, only the replica diagonal term of S_{dis} yields a nonvanishing correlation function at this order in perturbation theory. We write the replica sum explicitly as $S_{\text{dis}} = \sum_l S_{\text{dis},l}$. The average over replicas thus takes the form

$$\begin{aligned} &\frac{1}{N} \sum_{m,n,l} \langle j_n^{(0)}(1)j_m^{(0)}(2)S_{\text{dis},l} \rangle_0 \\ &= \frac{1}{N} \sum_{m,n} \left(\sum_{l=m} \langle j_n^{(0)}(1)j_m^{(0)}(2)S_{\text{dis},m} \rangle_0 + \sum_{l \neq m} \langle j_n^{(0)}(1)j_m^{(0)}(2)S_{\text{dis},l} \rangle_0 \right) \\ &= \frac{1}{N} \sum_{n=1}^N \left(\langle j_n^{(0)}(1)j_m^{(0)}(2)S_{\text{dis},m} \rangle_0 + (N-1) \langle j_n^{(0)}(1)j_m^{(0)}(2) \rangle_0 \langle S_{\text{dis},l \neq m} \rangle_0 \right) \\ &\xrightarrow{N \rightarrow 0} \langle j^{(0)}(1)j^{(0)}(2)S_{\text{dis}} \rangle_0 - \langle j^{(0)}(1)j^{(0)}(2) \rangle_0 \langle S_{\text{dis}} \rangle_0 \equiv \langle j^{(0)}(1)j^{(0)}(2)S_{\text{dis}} \rangle_c , \end{aligned} \quad (\text{B.11})$$

where we defined the connected average in the last equality and used that only the $m = n$ term in the replica summation remains after taking the limit $N \rightarrow 0$. Hence, we can drop the replica indices in the final expression.

Next, we define the contributions to the current-current correlator, linear in disorder strength, as

$$\Sigma^{(\text{dis})}(1-2) = - \langle j^{(0)}(1)j^{(0)}(2)S_{\text{dis}} \rangle_c + 2 \langle j^{(0)}(1)j^{(\text{dis})}(2) \rangle_c . \quad (\text{B.12})$$

The contribution to the conductivity due to disorder scattering is then obtained as

$$\sigma^{(\text{dis})}(\omega) = - \frac{i}{\omega} \lim_{q \rightarrow 0} \left[\Sigma^{(\text{dis})}(q, \omega_n) + \chi^{(\text{dis})}(q, \omega_n) \right] \Big|_{i\omega_n \rightarrow \omega + i\delta} . \quad (\text{B.13})$$

We obtain $\Sigma^{(\text{dis})} = \Sigma^{2\text{P}} + \Sigma^{1\text{P}} + \Sigma^b$ with

$$\Sigma^{2\text{P}}(q=0, \omega_n) = 32 \frac{e^2 v^2 K^2}{\omega_n^2} \lambda_{2\text{P}} \int_0^{1/T} d\tau e^{-4KF(\tau)} \left[1 - e^{i\omega_n \tau} \right] , \quad (\text{B.14})$$

$$\Sigma^{1\text{P}}(q=0, \omega_n) = 8 \frac{e^2 v^2 K^2}{\omega_n^2} \lambda_{1\text{P},1} \int_0^{1/T} d\tau G_{\theta\theta}^{(2)}(0, \tau) e^{-KF(\tau)} \left[1 - e^{i\omega_n \tau} \right] , \quad (\text{B.15})$$

$$\begin{aligned} \Sigma^b(q=0, \omega_n) &= 8 \frac{e^2 v^2 K^2}{\omega_n^2} \mathcal{D}_b \int_0^{1/T} d\tau e^{-KF(\tau)} \left[1 - e^{-i\omega_n \tau} \right] \left\{ G_{\theta\theta}^{(1)}(0, \tau) - 4\pi [G_{\theta\varphi}^{(1)}(0, \tau)]^2 \right\} \\ &+ 16 \frac{e^2 K v}{\omega_n} \mathcal{D}_b \int_0^{1/T} d\tau G_{\theta\varphi}^{(1)}(0, \tau) e^{-KF(\tau)} \left[1 - e^{-i\omega_n \tau} \right] , \end{aligned} \quad (\text{B.16})$$

and

$$\chi^{(\text{dis})}(q=0, \omega_n) = -2\mathcal{D}_b \frac{e^2}{\pi} \int d\tau e^{-KF(\tau)} e^{i\omega_n \tau}. \quad (\text{B.17})$$

The conductivity due to 1P and 2P processes is then

$$\sigma_{2\text{P}}(\omega) = 32i \frac{e^2 v^2 K^2}{\omega^3} \lambda_{2\text{P}} \left(\frac{\pi a T}{v} \right)^{8K} \mathcal{J}_{8K}(\omega, T), \quad (\text{B.18})$$

$$\sigma_{1\text{P}}(\omega) = 8i \frac{e^2 v^2 K}{\pi a^4 \omega^3} \lambda_{1\text{P},1} \left(\frac{\pi T}{v} \right)^{2K+4} (3\mathcal{J}_{2K+4}(\omega, T) - 2\mathcal{J}_{2K+2}(\omega, T)), \quad (\text{B.19})$$

where we defined

$$\begin{aligned} \mathcal{J}_{2K}(\omega, T) &= \int_0^{1/T} d\tau \frac{1 - e^{i\omega_n \tau}}{\sin^{2K}(\pi \tau T)} \Big|_{i\omega_n \rightarrow \omega + i\delta} \\ &= \frac{2^{2K}}{T} \Gamma(1 - 2K) \left[\frac{1}{\Gamma^2(1 - K)} - \frac{\sin(\pi K)}{\pi} \frac{\Gamma(K - i\frac{\omega}{2\pi T})}{\Gamma(1 - K - i\frac{\omega}{2\pi T})} \right]. \end{aligned} \quad (\text{B.20})$$

Here, $\Gamma(x)$ is the gamma function. These results appear in Eq. (3.71) and Eq. (3.72) of the main text.

In the case of backscattering off the impurity we obtain

$$\begin{aligned} \Sigma^b(q=0, \omega) &= -4e^2 K \mathcal{D}_b \frac{v^2}{a} \left(\frac{\pi a T}{v} \right)^{2K} \\ &\quad \times \left\{ \left(\frac{\pi T}{\omega} \right)^2 \left[(2K + 1) \mathcal{J}_{2K+2}(\omega, T) - 2K \mathcal{J}_{2K}(\omega, T) \right] + \frac{2T}{\omega} \mathcal{L}_K(\omega, T) \right\}, \end{aligned} \quad (\text{B.21})$$

$$\chi^{(\text{dis})}(q=0, \omega) = 2\mathcal{D}_b \frac{e^2 v^2}{\pi a} \left(\frac{\pi a T}{v} \right)^{2K} \frac{1}{\pi T} \sin(K\pi) B(K - i\frac{\omega}{2\pi T}, 1 - 2K). \quad (\text{B.22})$$

Here, $B(x, y)$ denotes the Euler beta function and we defined

$$\begin{aligned} \mathcal{L}_K(\omega, T) &= \int d\tau \frac{1 - e^{-i\omega_n \tau}}{\sin^{2K+1}(\pi T \tau)} \cos(\pi T \tau) = (-i) \sin(\pi K) \frac{2^{2K}}{\pi T} \\ &\quad \times \left\{ B(K, -2K) - B(K - i\frac{\omega}{2\pi T}, -2K) + B(K + 1, -2K) - B(K + 1 - i\frac{\omega}{2\pi T}, -2K) \right\}. \end{aligned} \quad (\text{B.23})$$

We find that the current-current correlation function is exactly canceled by the diamagnetic susceptibility, i.e. $\Sigma^b(0, \omega) + \chi^{(\text{dis})}(q=0, \omega) = 0$, after some simplification using Mathematica. This result is discussed in Sec. 3.3.1.

Contributions due to electron-electron scattering. Now let us discuss the contribution due to g_5 Umklapp scattering. As in the disordered case we define $\Sigma^{(5)}(1-2) \equiv \frac{1}{2} \langle j^{(0)}(1) j^{(0)}(2) S_5^2 \rangle_c - 2 \langle j^{(0)}(1) j^{(5)}(2) S_5 \rangle_c + \langle j^{(5)}(1) j^{(5)}(2) \rangle_c$. Adding all the terms we are left with only one term contributing to the real part of the conductivity

$$\Sigma^{(5)}(1-2) = \frac{e^2 K^2 v^4}{\pi} \lambda_{5,1}^2 \int d^3 d^4 \langle \partial_{x_1} \theta(1) \partial_{x_2} \theta(2) \partial_{x_3}^2 \theta(3) \partial_{x_4}^2 \theta(4) e^{i\sqrt{4\pi}(\varphi(3) - \varphi(4)) - 2ik_F(x_3 - x_4)} \rangle_0 \quad (\text{B.24})$$

Evaluating the correlation function we obtain

$$\sigma_{g_5}(\omega) = \frac{i}{\omega^3} \frac{e^2 v^4 K^2}{h} \frac{2^6}{\pi^2} \left(\frac{g_5}{v}\right)^2 \left(\frac{k_F}{k_0}\right)^2 \frac{1}{(ak_0)^2} \mathcal{I}_K(\omega, T). \quad (\text{B.25})$$

Here, we defined

$$\begin{aligned} \mathcal{I}_K(\omega, T) &= \int dx d\tau \left\{ G_{\theta\theta}^{(2)}(x, \tau) + 4\pi [G_{\theta\varphi}^{(2)}(x, \tau)]^2 \right\} e^{-KF(x, \tau)} e^{2ik_F x} \left[1 - e^{i\omega_n \tau} \right] \Big|_{i\omega_n \rightarrow \omega + i\delta} \\ &= \frac{1}{(2a)^4 \pi v} \left(\frac{2\pi T a}{v} \right)^{2K+4} \left(\frac{v}{\pi T} \right)^2 \sin(K\pi) \left[\frac{1}{K} \{ \mathcal{M}(\omega, -K, -K-2) + \mathcal{M}(\omega, -K-2, -K) \} \right. \\ &\quad \left. + \left(\frac{6}{K} + 1 \right) \{ \mathcal{M}(\omega, -K, -K-4) + \mathcal{M}(\omega, -K-4, -K) \} - 2\mathcal{M}(\omega, -K-2, -K-2) \right], \end{aligned} \quad (\text{B.26})$$

with

$$\begin{aligned} \mathcal{M}(\omega, \nu, \mu) &= B(-iS_-^0 - \frac{\nu}{2}, \nu+1) B(-iS_+^0 - \frac{\mu}{2}, \mu+1) \\ &\quad - B(-iS_- - \frac{\nu}{2}, \nu+1) B(-iS_+ - \frac{\mu}{2}, \mu+1), \end{aligned} \quad (\text{B.27})$$

and $S_{\pm} = \frac{\omega}{4\pi T} \pm \frac{vk_F}{2\pi T}$, $S_{\pm}^0 = S_{\pm}(\omega = 0)$. The behavior of the clean conductivity is discussed in Sec. 3.3.1 in the main part of the thesis.

C

Appendix C

Renormalization group analysis of the disordered HLL

In this Appendix we derive the renormalization group equations for the model of the disordered HLL using the formalism of the operator product expansion [53]. We perform the calculation for finite system size L and at zero temperature.

It is convenient to introduce complex coordinates (\bar{z}) and (z) as

$$z = v\tau - ix, \quad \bar{z} = v\tau + ix, \quad (\text{C.1})$$

where $\tau = -it$ is the imaginary time variable. The corresponding derivatives transform as

$$\partial_x = -i(\partial_z - \partial_{\bar{z}}), \quad \partial_\tau = iv(\partial_z + \partial_{\bar{z}}). \quad (\text{C.2})$$

Furthermore, we introduce the short hand notations $1 \equiv (z_1, \bar{z}_1)$ and $z_{12} \equiv z_1 - z_2$. By expanding the partition function of the model defined in Eq. (3.57) in powers of the coupling constants and reexponentiating, we find the effective action [53] up to second order in the coupling constants,

$$S_{\text{eff}} = \langle S_1 \rangle + \frac{1}{2} \left[\langle S_1 \rangle^2 - \langle S_1^2 \rangle \right], \quad (\text{C.3})$$

where $\langle \rangle$ denotes the averaging with respect to the fixed point action S_{LL} and $S_1 \equiv S_3 + S_5 + S_{2\text{P}} + S_{1\text{P}} + S_f + S_b$. In the real space RG procedure performed here we increase the short distance cutoff a in each step by an infinitesimal amount $\ell \ll 1$ as $a \rightarrow a' = ab \simeq a(1 + \ell)$ and demand that the action remains invariant under this rescaling of the cutoff. The cutoff appears in two ways in the action. First, each term in the action contains powers of a needed to make the coupling constant of the term dimensionless. Second, in all spatial integrations a defines the minimal relative distance between two points. We stress, that a only limits spatial integrations and not those over the imaginary time.

To calculate the correlation functions that appear in the RG procedure we need the $\varphi_n \varphi_m$ correlation function of replicated displacement fields,

$$\langle \varphi_n(z, \bar{z}) \varphi_m(0, 0) \rangle = -\frac{K}{4\pi} \delta_{n,m} \ln \left[\left(\frac{2\pi}{L} \right)^2 (z\bar{z} + a^2) \right]. \quad (\text{C.4})$$

The correlation function for θ_n fields can be obtained by using the duality relations $K\partial_z\theta_n = \partial_z\varphi_n$ and $K\partial_{\bar{z}}\theta_n = -\partial_{\bar{z}}\varphi_n$, which hold inside correlation functions. With the help of these duality relations and

the correlation function in Eq. (C.4) we can generate further expectation values

$$\langle \partial_{x_1} \theta_\alpha(x_1, \tau_1) \partial_{x_2} \theta_m(x_2, \tau_2) \rangle = -\frac{\delta_{n,m}}{4\pi K} \left[\frac{z_{12}^2}{[a^2 + |z_{12}|^2]^2} + \frac{\bar{z}_{12}^2}{[a^2 + |z_{12}|^2]^2} \right], \quad (\text{C.5})$$

$$\langle \partial_{x_1} \theta_n(x_1, \tau_1) \varphi_m(x_2, \tau_2) \rangle = \frac{i}{4\pi} \delta_{n,m} \left[\frac{z_{12}}{a^2 + |z_{12}|^2} + \frac{\bar{z}_{12}}{a^2 + |z_{12}|^2} \right], \quad (\text{C.6})$$

$$\langle \partial_{x_1} \varphi_n(x_1, \tau_1) \varphi_m(x_2, \tau_2) \rangle = \frac{i}{4\pi} \delta_{n,m} \left[\frac{z_{12}}{a^2 + |z_{12}|^2} - \frac{\bar{z}_{12}}{a^2 + |z_{12}|^2} \right]. \quad (\text{C.7})$$

Derivation of composite operators: We first derive the form of the composite 1P and 2P operators, which are generated in second order perturbation theory under the RG flow. The derivation is most conveniently performed before taking the disorder average. In this case the action is

$$\begin{aligned} S_3 &= \bar{g}_3 \left(\frac{2\pi a}{L} \right)^{4K} \frac{v}{a^2} \sum_n \int dx d\tau \cos(4\sqrt{\pi}\varphi_n - 4k_F x), \\ S_5 &= \bar{g}_{5,1} \left(\frac{2\pi a}{L} \right)^K v \sum_n \int dx d\tau \partial_x^2 \theta_n \cos(2\sqrt{\pi}\varphi_n - 2k_F x) \\ &\quad - \bar{g}_{5,2} \left(\frac{2\pi a}{L} \right)^K \frac{v}{a} \sum_n \int dx d\tau \partial_x \theta_n \sin(2\sqrt{\pi}\varphi_n - 2k_F x), \\ S_f &= -\frac{D_f}{2\pi} \sum_{n,m} \int dx d\tau d\tau' \partial_x \varphi_n(x, \tau) \partial_x \varphi_m(x, \tau'), \end{aligned} \quad (\text{C.8})$$

with the dimensionless coupling constants $\bar{g}_3 = g_3(2v_F k_F^2)/(\pi^2 k_0^4 a^2 v)$, $\bar{g}_{5,1} = g_5(2v_F k_F)/(\sqrt{\pi^3} k_0^2 a v)$ and $\bar{g}_{5,2} = g_5(8v_F k_F^2)/(\sqrt{\pi^3} k_0^2 v)$.

Let us illustrate how to obtain the effective operators. In second order, the effective action in Eq. (C.3) contains mixed terms, such as

$$\begin{aligned} & - \langle S_{5,1} S_f \rangle + \langle S_{5,1} \rangle \langle S_f \rangle \\ &= \frac{\bar{g}_{5,1}}{\sqrt{\pi}} \left(\frac{2\pi a}{L} \right)^K v \sum_{n,m} \int_{|x_{12}| > ab} dx_1 dx_2 d\tau_1 d\tau_2 \frac{1}{2} \sum_{\sigma=\pm} U_f(x_1) \\ &\quad \times \langle \partial_{x_1} \varphi_n(1) \partial_{x_2}^2 \theta_m(2) e^{i\sigma\sqrt{4\pi}\varphi_m(2)} \rangle e^{-i\sigma 2k_F x_2} \\ &\sim -\bar{g}_{5,1} \left(\frac{2\pi a}{L} \right)^K v \sum_{n,m} \int_{ab > |x_{12}| > a} dx_1 dx_2 d\tau_1 d\tau_2 \frac{1}{2} \sum_{\sigma=\pm} U_f(x_1) i\sigma \langle \partial_{x_1} \varphi_n(1) \varphi_m(2) \rangle \\ &\quad \times \langle \partial_{x_2}^2 \theta_m(2) e^{i\sigma\sqrt{4\pi}\varphi_m(2)} \rangle e^{-i\sigma 2k_F x_2} \\ &= -\frac{2K}{\pi} \bar{g}_{5,1} \ell \left(\frac{2\pi a}{L} \right)^K a \sum_{n,m} \int dx d\tau U_f(x) \langle \partial_x^2 \theta_n \sin(\sqrt{4\pi}\varphi_n - 2k_F x) \rangle \end{aligned} \quad (\text{C.9})$$

In the second equation we split the spatial integration $\int_{|x_{12}|>ab} = \int_{|x_{12}|>a} - \int_{ab>|x_{12}|>a}$ and kept only the second integration – the first integral leads to a less relevant term. Additionally we used that the correlator $\langle \partial_x \varphi_n(1) \partial_x \theta_m(2) \rangle$ is odd in τ_{12} and therefore vanishes upon integration over the relative coordinate. In the last equation, we performed the integration over the relative coordinate, keeping only the contribution of close times since the integral over times $|\tau_{12}| > a/v$ generates a less relevant term. Specifically,

$$\begin{aligned} & \int_{ab>|x_{12}|>a} \int_{|\tau_{12}|<a/v} dx_{12} d\tau_{12} \langle \partial_{x_1} \varphi_n(1) \varphi_m(2) \rangle \\ &= -\frac{K}{2\pi} \int_{ab>|x_{12}|>a} \int_{|\tau_{12}|<a/v} dx_{12} d\tau_{12} \frac{x_{12}}{x_{12}^2 + v^2 \tau_{12}^2 + a^2} = -\frac{K}{\pi v} a \ell. \end{aligned} \quad (\text{C.10})$$

In the last equality we evaluated the integral by setting $x_{12} = a$ in an interval of length $2a\ell$ and $\tau_{12} = 0$ in an interval of length $2a$. To keep the action invariant under the rescaling of the short distance cutoff, we have to add a counterterm of the form

$$S_{1P,1} = g_{1P,1}(\ell) \left(\frac{2\pi a}{L} \right)^K a \sum_n \int dx d\tau \mathcal{U}_f(x) \partial_x^2 \theta_n \sin(\sqrt{4\pi} \varphi_n - 2k_F x), \quad (\text{C.11})$$

to the action. If we choose $g_{1P,1}(\ell) = g_{1P,1}(0)(1 - (K-1)\ell) + 2K\bar{g}_{5,1}\ell/\pi$, the average of this action exactly cancels the contribution (C.9) that appears in second order perturbation theory. Analogously we can derive the terms

$$S_{1P,2} = g_{1P,2} \left(\frac{2\pi a}{L} \right)^K \sum_n \int dx d\tau \mathcal{U}_f(x) \partial_x \theta_n \cos(\sqrt{4\pi} \varphi_n - 2k_F x), \quad (\text{C.12})$$

$$S_{2P} = g_{2P} \left(\frac{2\pi a}{L} \right)^{4K} \frac{v}{a^2} \sum_n \int dx d\tau \mathcal{U}_f(x) \sin(\sqrt{16\pi} \varphi_n - 4k_F x), \quad (\text{C.13})$$

with coupling constants $g_{1P,2}(\ell) = g_{1P,2}(0)(1 - K\ell) + 2K\bar{g}_{5,2}\ell/\pi$ and $g_{2P}(\ell) = g_{2P}(0)(1 - 4K\ell) + 4K\bar{g}_3\ell/\pi$. By refermionizing these terms, we obtain the effective operators in Eqs. (3.40) and (3.41) in the main text. After performing the disorder average we obtain the composite terms in the bosonic action in Eq. (3.57).

Renormalization of bare interaction by disorder: We now outline how to derive the RG equations of the disordered HLL defined by the action in Eq. (3.57). In order to derive the RG equations we follow the procedure introduced by Giamarchi and Schulz [67], and single out the ultraviolet contribution of close times $v|\tau_{12}| < a$, by splitting the disorder terms into two parts. For disorder forward scattering this yields

$$\begin{aligned} S_f &= -\mathcal{D}_f \frac{v^2}{a} \int_{v|\tau_{12}|>a} dx d\tau_1 d\tau_2 \sum_{n,m} \partial_x \varphi_n(x, \tau_1) \partial_x \varphi_m(x, \tau_2) \\ &\quad - 2\mathcal{D}_f v \int dx d\tau \sum_{n,m} \partial_x \varphi_n(x, \tau) \partial_x \varphi_m(x, \tau) \end{aligned} \quad (\text{C.14})$$

The second term in Eq. (C.14) is local in imaginary time and can therefore be absorbed into the fixed point action. The replica diagonal part renormalizes the bare value of v/K in the diagonal part of the

action as

$$\frac{\tilde{v}}{\tilde{K}} = \frac{v}{K} - 4\mathcal{D}_f v K^2 \quad (\text{C.15})$$

On the other hand the replica off diagonal term introduces a new contribution to the bosonic correlation function $G_{nm}(q, \omega) = \langle \varphi_n(q, \omega) \varphi_m(-q, -\omega) \rangle$ which now reads as

$$G_{n,m}^{-1}(q, \omega) = \frac{1}{vK} [(vq)^2 + \omega^2 + m^2] \delta_{n,m} - 4\mathcal{D}_f v q^2 \quad (\text{C.16})$$

where we introduced an infinitesimal mass m to regularize the propagator in the IR. For the matrix of the form $M_{nm} = M_1 \delta_{nm} + M_2$ we use $M_{nm}^{-1} = \delta_{nm}/M_1 - M_2/M_1^2$ valid in the replica limit $N \rightarrow 0$ [133]. This yields

$$G_{nm} = \frac{vK}{(vq)^2 + \omega^2 + m^2} \delta_{nm} + \mathcal{D}_f \frac{4K^2}{v} \frac{q^2}{[(vq)^2 + \omega^2 + m^2]^2}. \quad (\text{C.17})$$

Performing the Fourier transform to real space, we obtain the propagator $G_{nm}(x, \tau) = G_0(x, \tau) \delta_{nm} + G_f(x, \tau)$, with

$$G_0(x, \tau) = \frac{K}{2\pi} K_0(m\sqrt{x^2 + v^2\tau^2 + a^2}), \quad (\text{C.18})$$

$$G_f(x, \tau) = \frac{\mathcal{D}_f K^2}{\pi} [K_0(m|x|) - m|x|K_1(m|x|)]. \quad (\text{C.19})$$

Here, K_m denotes the m -th modified Bessel function of the second kind. Their asymptotic behavior for small arguments is given by $K_0(x) \simeq -\ln(e^{\gamma_E} x/2)$, with the Euler constant γ_E and $K_1(x) \simeq 1/x$. As we have mentioned the diagonal part of G_f can be absorbed into a redefinition of the parameters v and K . The offdiagonal part, on the other hand can be neglected to leading order in \mathcal{D}_f , which will be considered here.

For backscattering we split the action according to

$$S_b = -\mathcal{D}_b \left(\frac{2\pi a}{L} \right)^{2K} \frac{v^2}{a} \int_{v|\tau_{12}| > a} dx d\tau_1 d\tau_2 \sum_{n,m} \partial_x \theta_n(x, \tau_1) \partial_x \theta_m(x, \tau_2) e^{i\sqrt{4\pi}[\varphi_n(x, \tau_1) - \varphi_m(x, \tau_2)]} \quad (\text{C.20})$$

$$-\mathcal{D}_b \left(\frac{2\pi a}{L} \right)^{2K} \frac{v^2}{a} \int_{v|\tau_{12}| < a} dx d\tau_1 d\tau_2 \sum_{n,m} \partial_x \theta_n(x, \tau_1) \partial_x \theta_m(x, \tau_2) e^{i\sqrt{4\pi}[\varphi_n(x, \tau_1) - \varphi_m(x, \tau_2)]}. \quad (\text{C.21})$$

For close times we can perform the OPE, for $x_1 = x_2$ and $v|\tau_{12}| < a$,

$$\begin{aligned} & (L/2\pi a)^{2K} \langle \partial_{x_1} \theta_n(1) e^{i\sqrt{4\pi}\varphi_n(1)} \partial_{x_2} \theta_m(2) e^{i\sqrt{4\pi}\varphi_m(2)} \rangle \\ &= \langle \partial_{x_1} \theta_n \partial_{x_2} \theta_m e^{i\sqrt{4\pi}[\varphi_n - \varphi_m]} \rangle + i\sqrt{4\pi} \langle \partial_{x_2} \theta_m \varphi_n \rangle \langle \partial_{x_1} \theta_n e^{i\sqrt{4\pi}[\varphi_n - \varphi_m]} \rangle \\ & \quad - i\sqrt{4\pi} \langle \partial_{x_1} \theta_n \varphi_m \rangle \langle \partial_{x_2} \theta_m e^{i\sqrt{4\pi}[\varphi_n - \varphi_m]} \rangle \\ & \quad + \{4\pi \langle \partial_{x_1} \theta_n \varphi_m \rangle \langle \partial_{x_2} \theta_m \varphi_n \rangle + \langle \partial_{x_1} \theta_n \partial_{x_2} \theta_m \rangle\} \langle e^{i\sqrt{4\pi}[\varphi_n - \varphi_m]} \rangle \\ & \simeq \langle (\partial_x \theta_n)^2 \rangle \left\{ 1 - 2vK\tau_{12} \left[\frac{z_{12}}{a^2 + |z_{12}|^2} + \frac{\bar{z}_{12}}{a^2 + |z_{12}|^2} \right] \right. \\ & \quad \left. + \frac{(vK)^2}{2} \tau_{12}^2 \left[\frac{1}{K} \left(\frac{z_{12}^2}{[a^2 + |z_{12}|^2]^2} + \frac{\bar{z}_{12}^2}{[a^2 + |z_{12}|^2]^2} \right) + \left(\frac{z_{12}}{a^2 + |z_{12}|^2} + \frac{\bar{z}_{12}}{a^2 + |z_{12}|^2} \right)^2 \right] \right\}, \end{aligned} \quad (\text{C.22})$$

where we omitted the space-time arguments for simplicity. The space time argument (x_1, τ_1) always appears together with the replica index n and the same for (x_2, τ_2) and m . In the second equality we inserted the explicit expressions for the correlation functions, expanded the normal ordered terms in small time differences and used the duality relation $i\partial_\tau\varphi_n = vK\partial_x\theta_n$. To obtain the action at close times in Eq. (C.21), we have to perform the integration over the relative time. Since τ at small times is always cut by the small distance cutoff as $v\tau \rightarrow 0 + a\text{sign}\tau$, we perform the integration, by setting $\int_{v|\tau_{12}|<a} d\tau_{12} f(\tau_{12}) = 2a/v \times f(0)$, which is correct up to a nonuniversal multiplicative constant. To keep the action invariant, we have to add a term of the form

$$-2\mathcal{D}_b v(1-K)(1-2K) \int dx d\tau \sum_n (\partial_x \theta_n)^2. \quad (\text{C.23})$$

This term renormalizes the bare value of the parameter vK in the quadratic part of the action as

$$\tilde{v}\tilde{K} = vK - 4v\mathcal{D}_b(1-K)(1-2K). \quad (\text{C.24})$$

First order RG: In the first order of the weak coupling expansion, the effective action is given by $S_{\text{eff}} = \langle S_1 \rangle$. Let us first consider the S_3 term,

$$\langle S_3 \rangle = \lambda_3 \left(\frac{2\pi a}{L} \right)^{4K} \frac{\tilde{v}}{a^2} \int dx d\tau \sum_n \langle \cos(\sqrt{16\pi}\varphi_n - \delta) \rangle, \quad (\text{C.25})$$

with $\delta = 4k_F x$. To derive the beta-function we increase the low distance cutoff by an infinitesimal amount $a \rightarrow a' = ab$, but keep the large distance cutoff L invariant. The action is then only invariant if we define the new coupling constant $\lambda_3(b) \equiv b^{2-4K}\lambda_3$. To derive the beta function, we make the RG step infinitesimal $b = 1 + \ell$, and take the derivative, which yields

$$\frac{d\lambda_3}{d\ell} = (2 - 4K)\lambda_3. \quad (\text{C.26})$$

Next, we turn to the forward scattering term. After increasing the cutoff $a \rightarrow ab$ we split the integration over relative times into two parts,

$$\int_{\tilde{v}|\tau_{12}|>ab} d\tau_1 d\tau_2 = \int_{\tilde{v}|\tau_{12}|>a} d\tau_1 d\tau_2 - \int_{ab>\tilde{v}|\tau_{12}|>a} d\tau_1 d\tau_2 \quad (\text{C.27})$$

In the first integral the factors ab only appear in front of the integrand to make the expression dimensionless. They can be treated similar to the case of the umklapp term and renormalize $\mathcal{D}_f \rightarrow \mathcal{D}_f(b) = \mathcal{D}_f b$. On the other hand the second term yields a contribution to the effective action of the form

$$\mathcal{D}_f \frac{\tilde{v}^2}{ab} \int_{ab>\tilde{v}|\tau_{12}|>a} d\tau_1 d\tau_2 \sum_n \langle \partial_x \varphi_n(x, \tau_1) \partial_x \varphi_n(x, \tau_2) \rangle = 2\mathcal{D}_f \tilde{v} \ell \int dx d\tau \sum_n \langle [\partial_x \varphi_n(x, \tau)]^2 \rangle \quad (\text{C.28})$$

In the last step we dropped the factor b in front of the integral to leading order in ℓ , since the integral itself already is linear in ℓ . This term renormalizes the coupling constants in the quadratic part of the action as $\tilde{v}(\ell)/\tilde{K}(\ell) = \tilde{v}/\tilde{K} - 4\tilde{v}\mathcal{D}_f\ell$.

We treat the disorder backscattering term and the 2P term in the same way which yields the renormalized coupling constant $\mathcal{D}_b(b) = \mathcal{D}_b b^{1-2K}$, $\lambda_{2P}(b) = \lambda_{2P} b^{3-8K}$ and the renormalization to the quadratic part of the action $\tilde{v}(\ell)\tilde{K}(\ell) = \tilde{v}\tilde{K} - 4\tilde{v}\mathcal{D}_b(1-\tilde{K})(1-2\tilde{K})\ell - 16\pi\lambda_{2P}\tilde{v}\tilde{K}^2\ell$.

Second order RG: Let us first consider the contribution of the S_3 term to the effective action in Eq. (C.3) in second order:

$$\frac{1}{2} [\langle S_3 \rangle^2 - \langle S_3^2 \rangle] = -\frac{1}{8} \lambda_3^2(b) \frac{\tilde{v}^2}{a^4} \left(\frac{2\pi a}{L} \right)^{8K} \int_{|x_{12}| > ab} dx_1 dx_2 d\tau_1 d\tau_2 \sum_{n,m} \sum_{\sigma, \sigma'} \quad (C.29)$$

$$\{ \langle e^{i\sigma\sqrt{16\pi}\varphi_n(1)} e^{i\sigma'\sqrt{16\pi}\varphi_m(2)} \rangle - \langle e^{i\sigma\sqrt{16\pi}\varphi_n(1)} \rangle \langle e^{i\sigma'\sqrt{16\pi}\varphi_m(2)} \rangle \} e^{-i\sigma\delta x_1} e^{-i\sigma'\delta x_2}$$

To proceed, we split the space time integration over relative coordinates as

$$\int_{|x_{12}| > ab} dx_{12} d\tau_{12} \quad (C.30)$$

$$= \int_{|x_{12}| > a} dx_{12} d\tau_{12} - \int_{ab > |x_{12}| > a} dx_{12} \int_{|\tau_{12}| > a} d\tau_{12} - \int_{ab > |x_{12}| > a} dx_{12} \int_{|\tau_{12}| < a} d\tau_{12}$$

The first two terms generate new, less relevant operators, and will be neglected. Since the integration in the last term is proportional $\sim \ell$ we can again neglect the renormalization of the coupling constant in front. Furthermore, we take into account only terms with $\sigma = -\sigma'$ in the summation in Eq. (C.29), since the other terms yield cosine operators with higher harmonics, that are less relevant. This yields

$$S_{\text{eff}} = \frac{1}{8} \lambda_3^2 \frac{\tilde{v}^2}{a^4} \int_{ab > |x_{12}| > a} dx_{12} \int_{|\tau_{12}| < a} d\tau_{12} \int dR_{12} dT_{12} \quad (C.31)$$

$$\times \sum_{n, \sigma} \langle e^{i\sigma\sqrt{16\pi}(\varphi_n(1) - \varphi_n(2))} \rangle e^{-i\sigma\delta x_{12}}$$

where we defined the absolute coordinates $R_{12} = x_1 + x_2/2$ and $T_{12} = \tau_1 + \tau_2/2$. Performing a gradient expansion in the term in brackets and using the duality relations, we find

$$S_{\text{eff}} = -8\pi g_{\text{um}}^2(b) v \ell \int dx d\tau \sum_n \left[c_1(\delta a) (\partial_x \varphi_n)^2 - c_2(\delta a) K^2 (\partial_x \theta_n)^2 \right] \quad (C.32)$$

where we defined the dimensionless functions

$$c_1(\delta a) = \frac{1}{4\ell} \int_{b > |x| > 1} dx \int_{|y| < 1} dy x^2 \cos(\delta a x), \quad (C.33)$$

$$c_2(\delta a) = \frac{1}{4\ell} \int_{b > |x| > 1} dx \int_{|y| < 1} dy y^2 \cos(\delta a x). \quad (C.34)$$

The explicit form of these functions depends on the choice of cutoff procedure. For our purposes it is sufficient to know the limiting behavior. For $\delta a \rightarrow 0$ we have $c_1(0) = c_2(0) = 1$. On the other hand for large values of δa the integrand in Eq. (C.34) is strongly oscillating and the integration vanishes, yielding $c_1(\delta a \gg 1) = c_2(\delta a \gg 1) = 0$.

The effective action in Eq. (C.32) has the same form as the quadratic part of the action. In order to the partition function invariant under the cutoff rescaling one has to introduce counterterms that cancel the terms above. This leads to the additional terms in the couplings of the quadratic part of the action

$$\tilde{v} \tilde{K} \rightarrow \tilde{v} \tilde{K} - 16c_2(\delta a) \pi v K^2 \lambda_3^2 \ell, \quad (C.35)$$

$$\frac{\tilde{v}}{\tilde{K}} \rightarrow \frac{\tilde{v}}{\tilde{K}} + 16c_1(\delta a) \pi v K^2 \lambda_3^2 \ell. \quad (C.36)$$

The second term in the effective action we have to consider is the mixed term of forward and backscattering off disorder

$$\begin{aligned}
- \langle S_b S_f \rangle + \langle S_b \rangle \langle S_f \rangle &= -\mathcal{D}_b \mathcal{D}_f \frac{\tilde{v}^4}{a^2 b^2} \left(\frac{2\pi ab}{L} \right)^{2K} \int_{|x_{12}|>a} dx_1 dx_2 \int_{v|\tau_{12}|>ab} \int_{v|\tau_{34}|>ab} d\tau_1 \cdots d\tau_4 \\
&\times \sum_{n,m,\gamma,\delta} \left[\langle \partial_{x_1} \varphi_n \partial_{x_1} \varphi_m \partial_{x_2} \theta_\gamma \partial_{x_2} \theta_\delta e^{i\sqrt{4\pi}(\varphi_\gamma - \varphi_\delta)} \rangle - \langle \partial_{x_1} \varphi_n \partial_{x_1} \varphi_m \rangle \langle \partial_{x_2} \theta_\gamma \partial_{x_2} \theta_\delta e^{i\sqrt{4\pi}(\varphi_\gamma - \varphi_\delta)} \rangle \right]
\end{aligned} \tag{C.37}$$

We split the spatial integral and keep only the part of close distances $\int_{|x_{12}|>ab} dx \rightarrow -\int_{ab>|x_{12}|>a} dx$ and consider only the time integration, where $\tau_1 \sim \tau_3$ and $\tau_2 \sim \tau_4$. There is another contribution due to times $\tau_1 \sim \tau_4$ and $\tau_2 \sim \tau_3$ that gives the same result and yields a factor of two. Thus we find

$$\begin{aligned}
& -\mathcal{D}_b \mathcal{D}_f \frac{\tilde{v}^4}{a^2} \left(\frac{2\pi a}{L} \right)^{2K} \int_{ab>|x_{12}|>a} dx_1 dx_2 \int_{v|\tau_{12}|>a} \int_{v|\tau_{13}|<a} \int_{v|\tau_{24}|<a} d\tau_1 \cdots d\tau_4 \\
& \times 4\pi \sum_{n,m,\gamma,\delta} \langle \partial_{x_1} \varphi_n \varphi_\gamma \rangle \langle \partial_{x_1} \varphi_m \varphi_\delta \rangle \langle \partial_{x_2} \theta_\gamma \partial_{x_2} \theta_\delta e^{i\sqrt{4\pi}(\varphi_\gamma - \varphi_\delta)} \rangle \\
& = -4\mathcal{D}_b \mathcal{D}_f \ell \tilde{K}^2 \frac{\tilde{v}^2}{a} \left(\frac{2\pi a}{L} \right)^{2K} \int dx \int_{v|\tau_{12}|>a} d\tau_1 d\tau_2 \\
& \times \sum_{n,m} \langle \partial_x \theta_n(x, \tau_1) \partial_x \theta_m(x, \tau_2) e^{i\sqrt{4\pi}(\varphi_n(x, \tau_1) - \varphi_m(x, \tau_2))} \rangle
\end{aligned} \tag{C.38}$$

In the last equality we performed the integration over relative space times

$$\begin{aligned}
& 4\pi \int_{ab>|x_{12}|>a} \int_{|\tau_{13}|<a} \int_{|\tau_{24}|<a} dx_{12} d\tau_{13} d\tau_{24} \langle \partial_{x_1} \varphi_n \varphi_\gamma \rangle \langle \partial_{x_1} \varphi_m \varphi_\delta \rangle \\
& = \frac{\tilde{K}^2}{\pi} \int_{ab>|x_{12}|>a} \int_{|\tau_{13}|<a} \int_{|\tau_{24}|<a} dx_{12} d\tau_{13} d\tau_{24} \frac{x_{12}^2}{(x_{12}^2 + \tau_{13}^2 + a^2)(x_{12}^2 + \tau_{24}^2 + a^2)} = \frac{a}{v^2} \tilde{K}^2 \ell.
\end{aligned} \tag{C.39}$$

In the last step we set $x_{12} \simeq a$ on an infinitesimal interval of length $2a\ell$ and evaluated the remaining integral using polar coordinates for radius $r \ll a$. To keep the partition function invariant under the cutoff rescaling we have to add a counterterm that cancels the contribution above and which adds to the scaling of \mathcal{D}_b as $\mathcal{D}_b \rightarrow \mathcal{D}_b + 4\mathcal{D}_b \mathcal{D}_f \tilde{K}^2 \ell$.

Beta functions: We now collect all renormalizations derived in the previous parts and reformulate

the flow equations of $\tilde{v}\tilde{K}$ and \tilde{v}/\tilde{K} in terms of the flow equations for \tilde{v} and \tilde{K} . This yields

$$\begin{aligned}
\frac{d\tilde{K}}{d\ell} &= -2\mathcal{D}_b(1-\tilde{K})(1-2\tilde{K}) + 2\mathcal{D}_f\tilde{K}^2 - 8\pi\tilde{K}^2\lambda_3^2[c_1(\delta a) + c_2(\delta a)] - 8\pi\tilde{K}^2\lambda_{2P}^2, \\
\frac{d\tilde{v}}{d\ell} &= -2\mathcal{D}_b\tilde{v}\frac{(1-\tilde{K})(1-2\tilde{K})}{\tilde{K}} - 2\mathcal{D}_f\tilde{v}\tilde{K} + 8\pi\lambda_3^2\tilde{v}\tilde{K}[c_1(\delta a) - c_2(\delta a)] - 8\pi\tilde{v}\tilde{K}\lambda_{2P}^2, \\
\frac{d\lambda_3}{d\ell} &= (2-4\tilde{K})\lambda_3, \\
\frac{d\lambda_{2P}}{d\ell} &= (3-8\tilde{K})\lambda_{2P}, \\
\frac{d\mathcal{D}_f}{d\ell} &= \mathcal{D}_f, \\
\frac{d\mathcal{D}_b}{d\ell} &= (1-2\tilde{K})\mathcal{D}_b + 4\mathcal{D}_b\mathcal{D}_f\tilde{K}^2.
\end{aligned} \tag{C.40}$$

These equations are perturbative in the couplings λ_{2P} , \mathcal{D}_f and \mathcal{D}_b up to first order and perturbative in λ_3 up to second order but exact in \tilde{K} and \tilde{v} .

As we have mentioned the coupling constants \tilde{K} and \tilde{v} already contain renormalizations due to disorder. They are related to the bare parameters as

$$\frac{\tilde{v}}{\tilde{K}} = \frac{v}{K} - 4v\mathcal{D}_f, \tag{C.41}$$

$$\tilde{v}\tilde{K} = vK - 4v\mathcal{D}_b(1-K)(1-2K). \tag{C.42}$$

If we reformulate the flow equations in terms of the clean parameters and redefine $\lambda_3 \rightarrow \lambda_3/\sqrt{16\pi}$ and $\lambda_{2P} \rightarrow \lambda_{2P}/8\pi$ we find

$$\begin{aligned}
\frac{dK}{d\ell} &= -4\mathcal{D}_b(1-K)(1-2K)K - \lambda_3^2K^2\frac{c_1(\delta a) + c_2(\delta a)}{2} + K^2(8K-2)\lambda_{2P}, \\
\frac{dv}{d\ell} &= -4\mathcal{D}_bv(1-K)(1-2K) + \lambda_3^2vK\frac{c_1(\delta a) - c_2(\delta a)}{2} + vK(8K-2)\lambda_{2P}, \\
\frac{d\lambda_3}{d\ell} &= (2-4K)\lambda_3 - 8\mathcal{D}_f\lambda_3K^2 + 8\mathcal{D}_b\lambda_3(1-K)(1-2K), \\
\frac{d\lambda_{2P}}{d\ell} &= (2-4K)\lambda_{2P}, \\
\frac{d\mathcal{D}_f}{d\ell} &= \mathcal{D}_f, \\
\frac{d\mathcal{D}_b}{d\ell} &= (1-2K)\mathcal{D}_b.
\end{aligned} \tag{C.43}$$

These equations will be discussed in Sec. 3.5 in the main text.

D

Appendix D

Coulomb drag between helical Luttinger liquids

D.1 Polarization operator for edge states of quantum spin Hall insulators

In this Appendix, we derive the polarization operator and the dynamically screened RPA interaction for a clean 1D system of helical fermions. The bare polarization operator of fermions in edge $\sigma = 1, 2$ is given by the density-density correlation function

$$\Pi_\sigma(q, i\Omega_m) = -\langle \rho_\sigma(q, i\Omega_m) \rho_\sigma(-q, -i\Omega_m) \rangle_0 \quad (\text{D.1})$$

where $\Omega_m = 2\pi mT$ are bosonic Matsubara frequencies and the brackets denote the functional average

$$\langle O(x, \tau) \rangle = \frac{\int \mathcal{D}[\psi, \bar{\psi}] O(x, \tau) e^{-S_0}}{\int \mathcal{D}\psi \mathcal{D}[\bar{\psi}] e^{-S_0}} \quad (\text{D.2})$$

with respect to the Gaussian action

$$S_0 = \int_k (-i\omega_n + \eta v_F k - \mu) \bar{\psi}_{k, \eta, \sigma} \psi_{k, \eta, \sigma}. \quad (\text{D.3})$$

The density of helical fermions is given by

$$\rho_\sigma(q) = \sum_{\eta_1, \eta_2} \int_k \bar{\psi}_{k+q, \eta_1, \sigma} \psi_{k, \eta_2, \sigma} b_{\eta_1, \eta_2}(k+q, k), \quad (\text{D.4})$$

with the matrix elements b defined in Eq. (4.5). The polarization operator can be expressed as a sum of the chiral components with small q ,

$$\Pi_\eta(q, i\Omega_m) = -\int_k T \sum_n G_{0, \eta}(k+q, i\omega_n + i\Omega_m) G_{0, \eta}(k, i\omega_n) \quad (\text{D.5})$$

and the components with q near $2k_F$,

$$\Pi_{\eta\bar{\eta}}(q, i\Omega_m) = -\int_k T \sum_n G_{0, \bar{\eta}}(k+q, i\omega_n + i\Omega_m) G_{0, \eta}(k, i\omega_n) b_{\eta\bar{\eta}}(k, k+q) b_{\bar{\eta}\eta}(k+q, k), \quad (\text{D.6})$$

with the bare fermion propagator

$$G_{0,\eta}(k) = (-i\omega_n + v_F\eta k - \mu)^{-1}. \quad (\text{D.7})$$

Performing the integrations we readily find the expression for the chiral bubble

$$\Pi_\eta(q, i\Omega_m) = \frac{1}{2\pi v_F} \frac{\eta v_F q}{\eta v_F q - i\Omega_m}. \quad (\text{D.8})$$

In the expression for the $2k_F$ bubble we first perform summation over Matsubara frequencies. This yields

$$\Pi_{\eta\bar{\eta}}(q, i\Omega_m) = -\frac{1}{k_0^4} \int_k \frac{[k^2 - (k+q)^2]^2}{i\Omega_m + 2v_F\eta k + v_F\eta q} [n_F(v_F\eta k) - n_F(-v_F\eta k - v_F\eta q)]. \quad (\text{D.9})$$

where $n_F(\epsilon) = (1 + \exp[(\epsilon - \mu)/T])^{-1}$ is the thermal distribution function. To obtain the retarded polarization operator we perform the analytical continuation to real frequencies $i\Omega_m \rightarrow \Omega + i0$ and use Dirac's identity $\frac{1}{x+i0} = \mathcal{P}\frac{1}{x} - i\pi\delta(x)$ to obtain the real and imaginary part:

$$\text{Re } \Pi_{\eta,\bar{\eta}}^R(q, \Omega) = -\frac{1}{2\pi v_F} \frac{q^2}{v_F^2 k_0^4} \mathcal{P} \int_{-v_F k_0}^{v_F k_0} d\epsilon \frac{(2\epsilon + \epsilon_q)^2}{2\epsilon + \epsilon_q + \Omega} n_F(\epsilon + \mu) + (\Omega \rightarrow -\Omega), \quad (\text{D.10})$$

$$\text{Im } \Pi_{\eta,\bar{\eta}}^R(q, \Omega) = \frac{1}{4v_F} \frac{(v_F q)^2 \Omega^2}{(v_F k_0)^4} \frac{\sinh\left(\frac{\Omega}{2T}\right)}{\cosh\left(\frac{\Omega}{2T}\right) + \cosh\left(\frac{v_F q \eta}{2T} + \frac{\mu}{T}\right)}. \quad (\text{D.11})$$

Here, we defined $\epsilon = v_F\eta k$ and $\epsilon_q = v_F\eta q + 2\mu$.

We will neglect the real part of the umklapp polarization operator with respect to the real part of the chiral operator since it can be shown to only diverge logarithmically and it is additionally small in q/k_0 . The real and imaginary part of the total retarded polarization operator $\Pi^R = \sum_{\eta_1, \eta_2} \Pi_{\eta_1, \eta_2}^R$ are then given by

$$\begin{aligned} \text{Re } \Pi^R(q, \Omega) &= \frac{1}{\pi v_F} \frac{(v_F q)^2}{(v_F q)^2 - \Omega^2}, \\ \text{Im } \Pi^R(q, \Omega) &= \frac{\Omega}{2v_F} [\delta(v_F q - \Omega) + \delta(v_F q + \Omega)] \\ &\quad + \frac{1}{4v_F} \frac{(v_F q)^2 \Omega^2}{(v_F k_0)^4} \frac{\sinh\left(\frac{\Omega}{2T}\right)}{\cosh\left(\frac{\Omega}{2T}\right) + \cosh\left(\frac{v_F q}{2T} + \frac{\mu}{T}\right)} \\ &\quad + \frac{1}{4v_F} \frac{(v_F q)^2 \Omega^2}{(v_F k_0)^4} \frac{\sinh\left(\frac{\Omega}{2T}\right)}{\cosh\left(\frac{\Omega}{2T}\right) + \cosh\left(\frac{v_F q}{2T} - \frac{\mu}{T}\right)}. \end{aligned} \quad (\text{D.12})$$

It is easy to check that the polarization operator fulfills the usual limits, $\lim_{q \rightarrow 0} \Pi(q, \Omega) = 0$ and $\lim_{q \rightarrow 0} \lim_{\Omega \rightarrow 0} \Pi(q, \Omega) = \nu_0 = \frac{1}{\pi v_F}$, where ν_0 denotes the density of states.

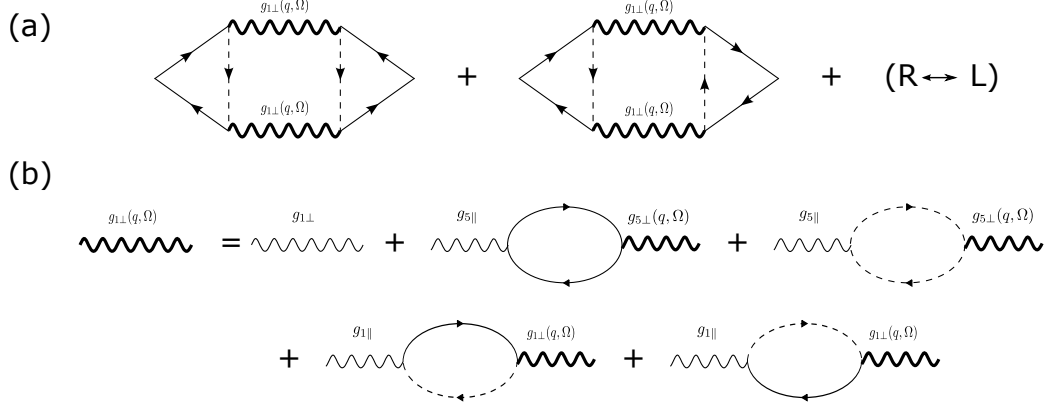


Figure D.1: (a) Aslamazov-Larkin diagrams describing the lowest order contribution to drag. The solid (dotted) lines refer to quasiparticle Greens functions of right (left) movers and the wiggly line denotes the dynamically screened RPA interaction. (b) Diagrammatic representation of the Dyson equation for $g_{1\perp}$ type interaction. We note that the coupling to plasmons (chiral polarization bubbles) is due to g_5 type interaction lines unique to the HLL. In both (a) and (b) we have set $g_{1\parallel} = g_{3\parallel}$ and $g_{1\perp} = g_{3\perp}$.

D.2 RPA-screened interaction

For a double layer system the intraedge interaction $V_{\sigma,\sigma}(q, \Omega)$ and the interedge interaction $V_{\sigma,-\sigma}(q, \Omega)$ fulfill the Dyson equation

$$\begin{pmatrix} V_{11} & V_{12} \\ V_{12} & V_{22} \end{pmatrix} = \begin{pmatrix} V_{0\parallel} & U_0 \\ U_0 & V_{0\parallel} \end{pmatrix} - \begin{pmatrix} V_{0\parallel} & U_0 \\ U_0 & V_{0\parallel} \end{pmatrix} \begin{pmatrix} \Pi_1 & 0 \\ 0 & \Pi_2 \end{pmatrix} \begin{pmatrix} V_{11} & V_{12} \\ V_{12} & V_{22} \end{pmatrix}, \quad (\text{D.13})$$

where Π_σ denotes the total polarization operator in edge σ and $U_0 \equiv V_{0\perp} \exp(-|q|d)$ is the bare strength of the interwire interaction. Since tunneling is neglected the off-diagonal components of the polarization matrix are zero. Inverting the matrix equation yields

$$V_{11} = \frac{V_0 + \Pi_2[(V_{0\parallel})^2 - (U_0)^2]}{1 + (\Pi_1 + \Pi_2)V_{0\parallel} + \Pi_1\Pi_2[(V_{0\parallel})^2 - (U_0)^2]}, \quad (\text{D.14})$$

$$V_{22} = \frac{V_0 + \Pi_1[(V_{0\parallel})^2 - (U_0)^2]}{1 + (\Pi_1 + \Pi_2)V_{0\parallel} + \Pi_1\Pi_2[(V_{0\parallel})^2 - (U_0)^2]}, \quad (\text{D.15})$$

$$V_{12} = \frac{U_0}{1 + (\Pi_1 + \Pi_2)V_{0\parallel} + \Pi_1\Pi_2[(V_{0\parallel})^2 - (U_0)^2]}. \quad (\text{D.16})$$

To simplify the following calculations we are going to set $V_{0\parallel} = V_{0\perp} \equiv V_0$. It is straightforward to check that this does not change the results qualitatively. Substituting $U_0 = V_0 \exp(-|q|d)$ the interedge RPA screened interaction can be brought into the form

$$U(q, \Omega) = \frac{1}{e^{|q|d}[V_0^{-1} + \Pi_1 + \Pi_2] + 2 \sinh(|q|d)\Pi_1\Pi_2V_0}. \quad (\text{D.17})$$

For identical edges with polarization operator $\Pi = \Pi' + i\Pi''$ this expression simplifies to

$$U(q, \Omega) = \frac{1}{e^{|q|d}[V_0^{-1} + 2\Pi'] + 2 \sinh(|q|d) [(\Pi')^2 - (\Pi'')^2] V_0 + 2i\Pi'' (e^{|q|d} + 2 \sinh(|q|d)\Pi'V_0)}. \quad (\text{D.18})$$

We substitute the polarization operator in Eq. (D.12) into Eq. (D.18) and use $\Pi' \gg \Pi''$ which yields

$$U(q, \Omega) = \frac{V_0 e^{-|q|d} [(v_F q)^2 - \Omega^2]^2}{(\Omega^2 - \Omega_+^2)(\Omega^2 - \Omega_-^2) + 2i\Pi'' V_0 [(v_F q)^2 - \Omega^2]^2 (1 + 2e^{-|q|d} \sinh(|q|d)\Pi'V_0)}. \quad (\text{D.19})$$

The poles Ω_{\pm} are obtained as the solution of the equation

$$[(v_F q)^2 - \Omega^2]^2 + 2\alpha(v_F q)^2 [(v_F q)^2 - \Omega^2] + 2\alpha^2 e^{-|q|d} \sinh(|q|d) (v_F q)^4 = 0, \quad (\text{D.20})$$

where $\alpha = V_0/(\pi v_F)$. The solution to the quadratic equation are the plasmon poles

$$\Omega_{\pm}^2 = [1 + \alpha_{\pm}(|q|d)] (v_F q)^2 \equiv v_{\pm}^2 q^2, \quad (\text{D.21})$$

where we defined the dimensionless interaction parameters

$$\alpha_{\pm}(|q|d) = \alpha (1 \pm e^{-|q|d}). \quad (\text{D.22})$$

and the plasmon velocities $v_{\pm}^2 = [1 + \alpha_{\pm}]v_F^2$ as given in the main text in Eq. (1.37).

We write the denominator of Eq. (D.19) as

$$[(\Omega + i\Gamma_+)^2 - \Omega_+^2] [(\Omega + i\Gamma_-)^2 - \Omega_-^2]. \quad (\text{D.23})$$

The plasmon decay rates Γ_{\pm} are determined by demanding that expression (D.23) is identical to the denominator in Eq. (D.19) at the poles Ω_{\pm} .

For $\Omega = \Omega_+$ we demand that

$$\begin{aligned} & [(\Omega_+ + i\Gamma_+)^2 - \Omega_+^2] [(\Omega_+ + i\Gamma_-)^2 - \Omega_-^2] = 2i\Gamma_+ \Omega_+ (\Omega_+^2 - \Omega_-^2) + \mathcal{O}(\Gamma^2) \\ & = 2i\Pi''(q, \Omega_+) V_0 [(v_F q)^2 - \Omega_+^2]^2 (1 + 2e^{-|q|d} \sinh(|q|d)\Pi'(q, \Omega_+) V_0). \end{aligned} \quad (\text{D.24})$$

Using the polarization operator in Eq. (D.12) and the relations in Eqs. (D.21) and (D.22) we find the rate

$$\begin{aligned} \Gamma_+(q) & \simeq \alpha_+^2 \frac{\alpha - \alpha_-}{\alpha_+ - \alpha_-} v_F q \frac{v_F}{u_+} [\Pi''(q, \Omega_+) v_F] \\ & \simeq \alpha_+^2 \frac{v_F q}{8} \left(\frac{q}{k_0}\right)^4 \left[\frac{\sinh(\frac{v_F q}{2T})}{\cosh(\frac{v_F q}{2T}) + \cosh(\frac{v_F q}{2T} + \frac{\mu}{T})} + \frac{\sinh(\frac{v_F q}{2T})}{\cosh(\frac{v_F q}{2T}) + \cosh(\frac{v_F q}{2T} - \frac{\mu}{T})} \right]. \end{aligned} \quad (\text{D.25})$$

In the last line we expanded to leading order in weak interaction $\alpha \ll 1$. Equivalently, we find for $\Omega = \Omega_-$:

$$\Gamma_-(q) \simeq \alpha_-^2 \frac{v_F q}{8} \left(\frac{q}{k_0}\right)^4 \left[\frac{\sinh(\frac{v_F q}{2T})}{\cosh(\frac{v_F q}{2T}) + \cosh(\frac{v_F q}{2T} + \frac{\mu}{T})} + \frac{\sinh(\frac{v_F q}{2T})}{\cosh(\frac{v_F q}{2T}) + \cosh(\frac{v_F q}{2T} - \frac{\mu}{T})} \right]. \quad (\text{D.26})$$

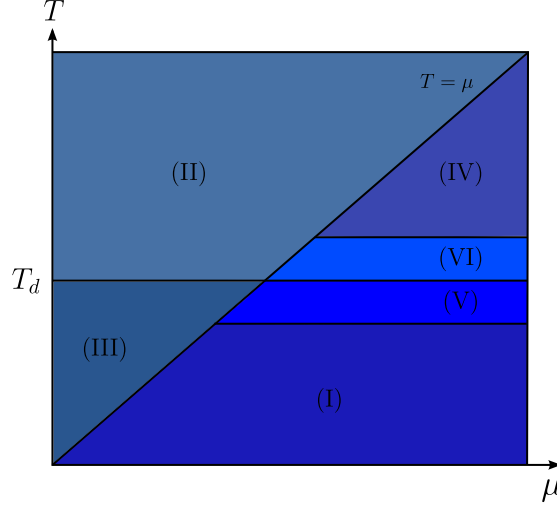


Figure D.2: Sketch of the parametric behavior of the particle-hole contribution to the high-frequency drag rate of coupled helical liquids in the $T - \mu$ -plane. The line 3 denotes the crossover temperature T_3 between different regimes discussed in the main text.

In summary, using the plasmon poles in Eq. (D.21) and the decay rates in Eqs. (D.25) and (D.26) the RPA screened inter-edge interaction for high temperatures, $\mu \ll T$, can be expressed as

$$V_{12}^R(q, \Omega) = \frac{V_0 e^{-|q|d} \left[(v_F q)^2 - \Omega^2 \right]^2}{\left[(\Omega + i\Gamma_+)^2 - \Omega_+^2 \right] \left[(\Omega + i\Gamma_-)^2 - \Omega_-^2 \right]}. \quad (\text{D.27})$$

In our derivation of the RPA screened interaction all g-ology interaction parameters have been set equal to V_0 . However we point out, that the coupling to the plasmon modes, determined by the chiral polarization bubbles, occurs solely due to umklapp processes. This can be seen by considering the diagrammatic expansion depicted in Fig. (D.1). Since these interaction processes only take place in the presence of a Dirac point in the excitation spectrum, the presence of plasmon poles in the screened interaction in Eq. (D.27) can be seen as a unique feature of the helical liquid.

D.3 Calculation of high-frequency drag rate

In this Appendix we present details of the calculation of the high-frequency drag rate discussed in Sec. 4.2.2 in the main text.

D.3.1 High-frequency Coulomb drag: Particle-hole contribution

We first consider the particle-hole contribution to the drag rate, obtained by setting $V_{12}(q, Q) = V_0 \exp(-|q|d)$ in Eq. (4.19). In this case, the integration over Q can be performed exactly. This yields

$$\frac{1}{\tau_{D,\text{eh}}^\infty} = \frac{2}{\pi} V_0^2 \left(\frac{T}{v_F k_0} \right)^4 \int dq e^{-2|q|d} \frac{q^4}{k_0^4} F_{\text{ph}} \left(\frac{v_F q}{2T}, \frac{\mu}{T} \right) \quad (\text{D.28})$$

where we defined the function

$$\begin{aligned}
F_{\text{eh}}(x, y) = & \frac{1}{60} \left\{ -4 \left[15(x+y)^4 + 30\pi^2(x+y)^2 + 7\pi^4 \right] \text{csch}^2(x+y) \right. \\
& + \text{csch}(x)\text{csch}(y) \left\{ -2 \left[(x-y)^2 + \pi^2 \right] \left[3(x-y)^2 + 7\pi^2 \right] [x-y] \text{csch}(x-y) \right. \\
& - [x+y] \left[(x+y)^2 + \pi^2 \right] \left[3(x+y)^2 + 7\pi^2 \right] \\
& \left. \left. \times \left[-2 \cosh(2(x+y)) + \cosh(2x) + \cosh(2y) \right] \text{csch}^3(x+y) \right\} \right\}. \tag{D.29}
\end{aligned}$$

The function $F_{\text{eh}}(\frac{v_F q}{2T}, \frac{\mu}{T})$ is strongly peaked around momenta $q \sim -2k_F$ with width of the order of the temperature. The main contribution to the integral in Eq. (D.28) comes either from momenta of the order of the negative Fermi momentum in a range of the temperature or from momenta of the order of the inverse interedge distance. Which of the momentum ranges yields the dominant contribution depends on the relation between the momentum scales in the integrand.

The integrand of Eq. (D.28) contains three energy scales. The first scale $T_d = v_F/d$ characterizes the momentum dependence of the interaction potential. The energy of thermally excited particle-hole pairs, T , is the second scale and the chemical potential μ the third one.

Let us first consider the regime $T \ll \min\{v_F/d, \mu\}$. In this case the integrand in Eq. (D.28) is strongly peaked around $q \sim -2k_F$ in a range of the order of the temperature. Therefore, we replace $e^{-2|q|d}(q/k_0)^4$ in the integrand by $e^{-4k_F d}(2k_F/k_0)^4$ and perform the remaining integral which yields

$$\text{(I) : } \quad \frac{1}{\tau_{D,\text{eh}}^\infty} \simeq \frac{64}{5} \pi \alpha^2 \left(\frac{\mu}{v_F k_0} \right)^4 \left(\frac{T}{v_F k_0} \right)^4 T e^{-4k_F d}, \tag{D.30}$$

with $\alpha = V_0/\pi v_F$.

In the opposite limit of high T , for $\max\{v_F/d, \mu\} \ll T$ we get the temperature independent rate,

$$\text{(II) : } \quad \frac{1}{\tau_{D,\text{eh}}^\infty} \simeq \frac{\pi}{5} (3\pi^4 - 35\pi^2 + 60) \alpha^2 \left(\frac{\mu}{v_F k_0} \right)^2 \frac{1}{(k_0 d)^7} v_F k_0. \tag{D.31}$$

At temperatures T between the scales v_F/d and μ , the contribution stemming from momenta $|q| \sim 1/d$ begins to compete with the contribution from the vicinity of the Fermi edge $|q \pm 2k_F| \sim T$. The result then depends on which of the scales is larger:

$$\text{(III) : } \quad \frac{1}{\tau_{D,\text{eh}}^\infty} \simeq \frac{512}{315} \left(\frac{22}{15} \pi^2 + 13 \right) \pi \alpha^2 \left(\frac{\pi T}{v_F k_0} \right)^6 \left(\frac{\mu}{v_F k_0} \right)^2 T \tag{D.32}$$

for $\mu \ll T \ll v_F/d$ and

$$\text{(IV) : } \quad \frac{1}{\tau_{D,\text{eh}}^\infty} \simeq 18 \pi \alpha^2 \left(\frac{\mu}{v_F k_0} \right)^8 \left(\frac{v_F}{T d} \right)^4 \frac{1}{(k_F d)^3} T e^{-\frac{2\mu}{T}}, \tag{D.33}$$

for $v_F/d \ll T \ll \mu$. In both cases there is a strong compensation between the contributions from $g_{1\perp}$ and $g_{3\perp}$ processes. In both cases, the main contribution to $\frac{1}{\tau_{D,\text{eh}}^\infty}$ comes from $|q| \sim 1/d$; the difference is that the characteristic Q is given by T in Eq. (D.32) and by k_F in Eq. (D.33). The crossover between

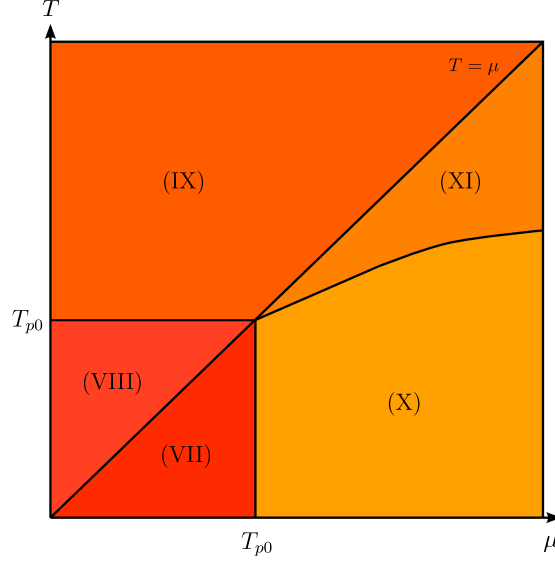


Figure D.3: Sketch of the parametric behavior of the plasmon contribution to the high-frequency drag rate of coupled helical liquids in the $T-\mu$ -plane. The line 2 denotes the crossover temperature T_2 between different regimes discussed in the main text.

the limits $T \ll v_F/d \ll \mu$ and $v_F/d \ll T \ll \mu$ [Eqs. (D.33) and Eq. (D.30), respectively] has the form of a singularity at $T = T_d$, where $T_d = v_F/2d$. Specifically,

$$(V) : \quad \frac{1}{\tau_{D,\text{eh}}^\infty} \simeq 192\pi\alpha^2 \left(\frac{\mu}{v_F k_0}\right)^8 \left(\frac{T_d}{\mu}\right)^4 T_d e^{-\frac{2\mu}{T_d}} \left(\frac{T_d}{T_d - T}\right)^6, \quad (\text{D.34})$$

for $v_F/k_F d^2 \ll T_d - T \ll T_d$ and

$$(VI) : \quad \frac{1}{\tau_{D,\text{eh}}^\infty} \simeq \frac{384}{5}\pi\alpha^2 \left(\frac{\mu}{v_F k_0}\right)^8 \left(\frac{T_d}{\mu}\right)^3 T_d e^{-\frac{2\mu}{T_d}} \left(\frac{T_d}{T - T_d}\right)^5, \quad (\text{D.35})$$

for $v_F/k_F d^2 \ll T - T_d \ll T_d$. The behavior of the particle-hole contribution to the high-frequency drag rate in different regimes in the $T-\mu$ -plane is plotted in Fig. D.2.

D.3.2 High-frequency Coulomb drag: Plasmon contribution

The plasmon drag rate is obtained by performing the integration over Q in Eq. (4.19) by closing the contour in the upper complex plane and taking into account only contributions of the plasmon poles, at $Q = v_\pm q/2v_F + i\Gamma_\pm/2v_F$ and $Q = -v_\pm q/2v_F + i\Gamma_\pm/2v_F$. This yields the intermediary result

$$\frac{1}{\tau_{D,\text{pl}}^\infty} = \frac{1}{32\pi} \frac{V_0^2}{T k_0^8} \int dq q^4 e^{-2|q|d} F_{\text{pl}}(q, k_F), \quad (\text{D.36})$$

where

$$F_{\text{pl}}(q, k_F) \equiv A_+(q, k_F)B_+(q, k_F) + A_-(q, k_F)B_-(q, k_F) \quad (\text{D.37})$$

and we defined

$$A_{\pm}(q) \equiv \frac{2\pi i}{v_F^5} \left(\frac{v_{\pm}}{v_F}\right)^4 \left[1 - \left(\frac{v_{\pm}}{v_F}\right)^2\right]^4 \frac{(v_F q)^{12}}{\cosh\left(\frac{v_F q}{2T} + \frac{\mu}{T}\right) + \cosh\left(\frac{v_{\pm} q}{2T}\right)} \quad (\text{D.38})$$

$$\times \left[\frac{1}{\cosh\left(\frac{v_{+} q}{2T}\right) + \cosh\left(\frac{v_F q}{2T} + \frac{\mu}{T}\right)} - \frac{1}{\cosh\left(\frac{v_{+} q}{2T}\right) + \cosh\left(\frac{v_F q}{2T} - \frac{\mu}{T}\right)} \right],$$

and

$$B_{\pm}(q) \equiv \frac{1}{2i\Gamma_{\pm}} \frac{1}{v_{\pm} q} \operatorname{Re} \left\{ \frac{1}{v_{\pm} q + i\Gamma_{\pm}} \frac{1}{(v_{+} + v_{-})q + i(\Gamma_{+} + \Gamma_{-})} \frac{1}{(v_{+} - v_{-})q + i(\Gamma_{+} + \Gamma_{-})} \right. \quad (\text{D.39})$$

$$\left. \times \frac{1}{(v_{+} - v_{-})q + i(\Gamma_{+} - \Gamma_{-})} \frac{1}{(v_{+} + v_{-})q + i(\Gamma_{+} - \Gamma_{-})} \right\}.$$

Using the explicit expressions in Eq. (4.22) and (4.24) we now simplify these functions to leading order in the dimensionless interaction α . To simplify the functions B_{\pm} we compare the differences and sums of the plasmon kinetic energy $(v_{+} \pm v_{-})|q|$ and plasmon decay rates $\Gamma_{+} \pm \Gamma_{-}$ that appear in the denominators. We notice that we can always neglect the decay rates with respect to the sum of plasmon excitation energies, since the rates are suppressed by an additional small factor $\alpha(q/k_0)^4$. On the other hand, the difference of plasmon velocities becomes exponentially small for $|q|d \gg 1$. In this case there exists a critical momentum scale q_p for which we can no longer neglect $\Gamma_{+} + \Gamma_{-}$ w.r.t. $(v_{+} - v_{-})|q|$. This scale is determined by the equation

$$\Gamma_{+}(q_p) + \Gamma_{-}(q_p) = |v_{+} - v_{-}|q_p = v_F q \alpha e^{-|q_p|d}. \quad (\text{D.40})$$

We note that the structure of this equation fixes the relation between the momentum scale q_p and the inverse interedge distance d^{-1} . Since the left hand side of the equation is parametrically smaller than the right hand side, the equality can only hold if the exponential factor is small i.e. for $q_p d \gg 1$. In particular, for $v q_p \gg \max T, \mu$, the equation can be solved to logarithmic accuracy and we obtain $q_p \simeq d^{-1} \ln(k_0^4 d^4 / \alpha)$

For momenta in the range $q < q_p$ we neglect all plasmon rates in the denominator of Eq. (D.39) and expand to leading order in α which yields

$$B_{\pm}(q) \simeq \frac{1}{2i\Gamma_{\pm}} \frac{1}{(v_F q)^6} \frac{1}{(\alpha_{+} - \alpha_{-})^2}. \quad (\text{D.41})$$

Substituting this back into Eq. (D.37) and expanding to leading order in the dimensionless interaction strength α yields the expression for the plasmon drag rate

$$\frac{1}{\tau_{D,PI}^{\infty}} = \frac{\pi^3}{32} \alpha^2 \frac{v_F^2}{T k_0^4} \frac{\sinh \frac{\mu}{T}}{\cosh^3 \frac{\mu}{2T}} \int_q q^5 \left(1 + e^{-2|q|d}\right) \left[\frac{1}{\cosh \frac{v_F q}{2T} \cosh \frac{v_F q - \mu}{2T}} - (q \rightarrow -q) \right]. \quad (\text{D.42})$$

We note that the expression in Eq. (D.42) contains two energy scales, the chemical potential μ , and the temperature $T_p = v_F q_p / 2$. While the interedge distance d also explicitly appears in the integrand it only changes the numerical prefactor of the drag rate and does not affect the temperature dependence.

In the limit of low T , for $T \ll \mu \ll v_F / d$, we obtain

$$\text{(VII):} \quad \frac{1}{\tau_{D,PI}^{\infty}} \simeq \frac{\pi^3}{6} \pi \alpha^2 \left(\frac{\mu}{v_F k_0}\right)^4 \left(\frac{\mu}{\pi T}\right)^2 T e^{-\frac{\mu}{T}}. \quad (\text{D.43})$$

In stark contrast to the particle-hole contribution to the drag rate, which vanishes as $T \rightarrow 0$ as a power law of T , the plasmon contribution is thermally activated. The main contribution to Eq. (D.43) comes from momenta from all $q \in (0, k_F)$.

Next, for $\mu \ll T \ll v_F/d$ we have

$$(VIII) : \quad \frac{1}{\tau_{D,P1}^\infty} \simeq \frac{7\pi^3}{24} \pi \alpha^2 \left(\frac{\pi T}{v_F k_0} \right)^2 \left(\frac{\mu}{v_F k_0} \right)^2 T. \quad (D.44)$$

with characteristic $|q| \sim T/v_F$. For $v/d \ll \max\{T, \mu\}$, the exponential term $e^{-2|q|d}$ in (D.42) can be neglected, so that $1/\tau_{D,P1}^\infty$ is obtained by multiplying the results in (D.43) (for $T \ll v_F/d \ll \mu$) and (D.44) (for $\mu \ll v_F/d \ll T$) by a factor $1/2$.

Now, let us turn to the case $\max\{T, \mu\} \gg T_p$, where the plasmon damping starts to modify the plasmon-mediated drag. In this limit the drag rate can be represented as

$$\frac{1}{\tau_{D,P1}^\infty} = \frac{\pi^3}{32} \alpha^2 \frac{v_F^2}{T k_0^4} \frac{\sinh \frac{\mu}{T}}{\cosh^3 \frac{\mu}{2T}} \int_q q^5 \frac{1}{s(q)} \left[\frac{1}{\cosh \frac{v_F q}{2T} \cosh \frac{v_F q - \mu}{2T}} - (q \rightarrow -q) \right], \quad (D.45)$$

with

$$s(q) = 1 + 16\alpha^2 \left(\frac{2q}{k_0} \right)^8 e^{2|q|d} \sinh^2 \frac{v_F q}{2T} \left[\frac{1}{\cosh \frac{v_F q}{2T} + \cosh \frac{v_F q - \mu}{2T}} + (q \rightarrow -q) \right]^2 \quad (D.46)$$

Here, the integral is determined by all q in the interval $0 < |q| < q_p$, with $q_p \ll \max\{T/v_F, k_F\}$.

We obtain, for $\max\{\mu, T_p\} \ll T$:

$$(IX) : \quad \frac{1}{\tau_{D,P1}^\infty} \simeq \frac{2}{7} \pi^2 \alpha^2 \left(\frac{\mu}{v_F k_0} \right)^2 \left(\frac{T}{v_F k_0} \right)^2 \left(\frac{T_p}{T} \right)^7 T, \quad (D.47)$$

where

$$T_p = \frac{v_F}{2d} \ln \left[\frac{(k_0 d)^4 T d}{\alpha v_F} \right]. \quad (D.48)$$

Next, in the regime $T \ll T_p \ll \mu$ we get

$$(X) : \quad \frac{1}{\tau_{D,P1}^\infty} \simeq \frac{16}{3\pi^2} \alpha^2 \left(\frac{\pi T}{v_F k_0} \right)^4 \left(\frac{T_p}{T} \right)^6 T e^{-\frac{\mu}{T}}, \quad (D.49)$$

where

$$T_p = \frac{v_F}{2d} \left\{ \frac{\mu}{T} + \ln \left[\frac{(k_0 d)^4}{\alpha} \right] \right\}. \quad (D.50)$$

Finally, for $T_p \ll T \ll \mu$:

$$(XI) : \quad \frac{1}{\tau_{D,P1}^\infty} \simeq \frac{32}{7\pi^2} \alpha^2 \left(\frac{\pi T}{v_F k_0} \right)^4 \left(\frac{T_p}{T} \right)^7 T e^{-\frac{\mu}{T}}, \quad (D.51)$$

where

$$T_p = \frac{v_F}{2d} \left\{ \frac{\mu}{T} + \ln \left[\frac{(k_0 d)^4 T d}{\alpha v_F} \right] \right\}. \quad (\text{D.52})$$

The term μ/T in Eqs. (D.50) and (D.52) appears because the plasmon damping rate obeys the Arrhenius law with activation gap μ for temperatures $T \ll \mu$. Here, $T_{p0} = \frac{v_F}{2d} \ln \left[\frac{(k_0 d)^4}{\alpha} \right]$ and the border between the regimes (X) and (XI) is given by the solution of $T_p = T$ with T_p from Eq. (D.50) which behaves as $T_{p0} + T_d \mu / 4T_{p0}$ for $\mu \ll T_{p0} \ln \frac{(k_0 d)^4}{\alpha}$ and $\sqrt{T_d \mu} / 2$ for $\mu \gg T_{p0} \ln \frac{(k_0 d)^4}{\alpha}$. The behavior of the plasmon contribution to the high-frequency drag rate in different regimes in the $T-\mu$ -plane is plotted in Fig. D.3. A discussion of the qualitative behavior of the sum of plasmon and particle-hole drag rates is presented in Sec. 4.4.

D.4 Second-order backscattering

In this Appendix, we perform a real-space RG procedure using the operator product expansion [53] to derive the most relevant operator generated by the backscattering term in Eq. (4.52):

$$S_1 = \frac{g_{1\perp}}{\pi} \int dx d\tau \cos(\sqrt{8\pi}\varphi_-) \left[(\partial_x \theta_+)^2 - (\partial_x \theta_-)^2 \right]. \quad (\text{D.53})$$

The general form for an OPE for two operators \mathcal{O}_i and \mathcal{O}_j is

$$:\mathcal{O}_i(\mathbf{r}_{\lambda,1}) :: \mathcal{O}_j(\mathbf{r}_{\lambda,2}) := \sum_k \frac{c_{ijk}}{|\mathbf{r}_{\lambda,1} - \mathbf{r}_{\lambda,2}|^{\Delta_i + \Delta_j - \Delta_k}} : \mathcal{O}_k \left(\frac{\mathbf{r}_{\lambda,1} + \mathbf{r}_{\lambda,2}}{2} \right) : \quad (\text{D.54})$$

where $:\mathcal{O}:$ denotes normal ordering, Δ_i is the scaling dimension of \mathcal{O}_i , and $\mathbf{r}_\lambda = (x, v_\lambda \tau)^T$ denotes coordinates in space-time. The above equality does not hold on the level of operators, but it is valid when used within the correlation functions, i.e., when the averaging is performed with another set of operators, at a distance much larger than $|\mathbf{r}_1 - \mathbf{r}_2|$ from \mathbf{r}_1 or \mathbf{r}_2 .

It is convenient to introduce the complex coordinates (\bar{z}_λ) and (z_λ) as

$$z_\lambda = v_\lambda \tau + ix, \quad \bar{z}_\lambda = v_\lambda \tau - ix, \quad (\text{D.55})$$

where $\tau = -it$ is the imaginary time variable. We further introduce the short-hand notations $1_\lambda \equiv (z_{\lambda,1}, \bar{z}_{\lambda,1})$ and $z_{\lambda,12} \equiv z_{\lambda,1} - z_{\lambda,2}$. By expanding the partition function of the model defined in Eq. (4.52) in powers of $g_{1\perp}$, followed by the reexponentiation, we find the effective action [53] to the second order in the coupling constant,

$$S_2 = \frac{1}{2} \left[\langle S_{1\perp} \rangle^2 - \langle S_{1\perp}^2 \rangle \right], \quad (\text{D.56})$$

where $\langle \dots \rangle$ denotes the averaging with respect to the fixed-point action. Within the RG procedure, we increase the short-distance cutoff a at each step by an infinitesimal amount, $a \rightarrow a' = (1 + \ell)a$, which reproduces the action, but with renormalized coupling constants, and may lead to the emergence of

new operators. To study the terms in the effective action, we need the time-ordered $\varphi_\lambda \varphi_\lambda$ correlation function of the $\lambda = \pm$ fields,

$$\langle \varphi_\lambda(z_\lambda, \bar{z}_\lambda) \varphi_\lambda(0, 0) \rangle = -\frac{K_\lambda}{4\pi} \ln \left[\frac{|z_\lambda|^2 + a^2}{a^2} \right]. \quad (\text{D.57})$$

The correlation function for the θ_λ fields can be obtained by using the duality relations

$$K_\lambda \partial_{z_\lambda} \theta_\lambda = \partial_{z_\lambda} \varphi_\lambda, \quad K_\lambda \partial_{\bar{z}_\lambda} \theta_\lambda = -\partial_{\bar{z}_\lambda} \varphi_\lambda, \quad (\text{D.58})$$

which, similarly to the OPE, hold when used for the averages that produce the correlation functions.

The most relevant perturbation in the effective action (D.56) is obtained by contracting all $\partial_x \theta$ terms for small space time distances $a < |z_{-,12}| < a'$. Using the correlation function of the bosonic fields and the duality relations (D.58), we find the OPEs

$$\begin{aligned} & \left[(\partial_x \theta_+)^2 e^{i\sqrt{8\pi}\varphi_-} \right]_1 \left[(\partial_x \theta_+)^2 e^{i\sqrt{8\pi}\varphi_-} \right]_2 \\ \rightarrow & \frac{1}{4(\pi K_+)^2} \frac{(z_{+,12}^2 + \bar{z}_{+,12}^2)^2}{(a^2 + |z_{+,12}|^2)^4} \left(\frac{|z_{-,12}|^2 + a^2}{a^2} \right)^{2K_-} \\ & \times e^{i\sqrt{8\pi}[\varphi_-(1_-) + \varphi_-(2_-)]}, \end{aligned} \quad (\text{D.59})$$

and

$$\begin{aligned} & \left[(\partial_x \theta_-)^2 e^{i\sqrt{8\pi}\varphi_-} \right]_1 \left[(\partial_x \theta_-)^2 e^{i\sqrt{8\pi}\varphi_-} \right]_2 \\ \rightarrow & \frac{1}{(4\pi)^2} \left[\frac{2}{K_-^2} \frac{(z_{-,12}^2 + \bar{z}_{-,12}^2)^2}{(a^2 + |z_{-,12}|^2)^4} + 4 \frac{(z_{-,12} + \bar{z}_{-,12})^4}{(a^2 + |z_{-,12}|^2)^4} \right. \\ & \left. - \frac{8}{K_-} \frac{(z_{-,12} + \bar{z}_{-,12})^2}{(a^2 + |z_{-,12}|^2)^2} \frac{z_{-,12}^2 + \bar{z}_{-,12}^2}{(a^2 + |z_{-,12}|^2)^2} \right] \\ & \times \left(\frac{|z_{-,12}|^2 + a^2}{a^2} \right)^{2K_-} e^{i\sqrt{8\pi}[\varphi_-(1_-) + \varphi_-(2_-)]}. \end{aligned} \quad (\text{D.60})$$

Here, we neglected less relevant terms in the OPE. We perform the integration over the relative coordinates by introducing the polar coordinates $z_{-,12} = re^{-i\phi}$ and $z_{+,12} = re^{-i\phi} + r\tilde{v} \cos \phi$ with the parameter $\tilde{v} = v_+/v_- - 1 = K_-/K_+ - 1$. The radial and angular integrations decouple and we perform the radial integration over an infinitesimal shell $r \in (a, a')$ by setting $r = a$. After integrating out the relative coordinates, we obtain the following contribution to the effective action:

$$\delta S_2 = \frac{g_{1,\perp}^2 F(K_-, K_+) \ell}{(2\pi)^2 v_-} \int \frac{dx d\tau}{\pi a^2} \cos[\sqrt{32\pi}\varphi_-(x, \tau)], \quad (\text{D.61})$$

with the dimensionless function

$$F(K_-, K_+) = 2^{2K_-} [f_1(K_-, K_+) + f_2(K_-)], \quad (\text{D.62})$$

where

$$f_1(x, y) = 4y^2 \int_0^{2\pi} \frac{d\phi}{2\pi} \frac{\left[(x^2 + y^2) \cos^2 \phi - y^2 \right]^2}{\left[2y^2 + (x^2 - y^2) \cos^2 \phi \right]^4} = \frac{5x^6 + 45x^4y^2 + 7x^2y^4 + 7y^6}{32\sqrt{2}(x^2 + y^2)^{7/2}} \quad (\text{D.63})$$

and

$$\begin{aligned} f_2(x) &= \frac{1}{(4x)^2} \int_0^{2\pi} \frac{d\phi}{2\pi} \left[1 - 4x + 6x^2 - 8x(1-x) \cos 2\phi + (1 - 4x + 2x^2) \cos 4\phi \right] \\ &= \frac{1 - 4x + 6x^2}{16x^2}. \end{aligned} \quad (\text{D.64})$$

Importantly, the function $F(K_-, K_+)$ is nonzero for $K_{\pm} > 0$. We thus see that, upon renormalization, the new coupling constant is always generated in the effective action, even if it is absent at the ultraviolet scale. The effect of the term (D.61) on the phase diagram of capacitively coupled helical edge modes is discussed in Sec. 4.3.2.

D.5 Renormalization of the drag resistivity

In this Appendix, we derive the asymptotics of the drag resistivity at $T \rightarrow 0$ for $K_- > 1/3$. We assume for simplicity that the interedge interaction is weak. To the lowest order in the interwire interaction, the dc drag resistivity can be expressed as [97, 102]:

$$\rho_D = \int_0^{\infty} dq \int_0^{\infty} d\omega \frac{q^2 V_{12}^2(q)}{4\pi^3 n_1 n_2 T} \frac{\text{Im}\Pi_1(q, \omega) \text{Im}\Pi_2(q, \omega)}{\sinh^2\left(\frac{\omega}{2T}\right)}, \quad (\text{D.65})$$

where $\text{Im}\Pi_{\sigma}(q, \omega)$ is the imaginary part of the retarded density-density correlation function of wire $\sigma = 1, 2$ and $n_{\sigma} = K_{\sigma} k_F / \pi$ is the electron density of wire σ . The drag resistivity obtained by this conventional formula is equivalent to that obtained from the high-frequency drag conductivity using the kinetic equation approach [104].

We write the density operator of helical fermions by employing the expansion in Eq. (4.3). This yields

$$\begin{aligned} \rho_{\sigma}(x) &= \psi_{\sigma, \uparrow}^{\dagger} \psi_{\sigma, \uparrow} + \psi_{\sigma, \downarrow}^{\dagger} \psi_{\sigma, \downarrow} \simeq R_{\sigma}^{\dagger} R_{\sigma} + L_{\sigma}^{\dagger} L_{\sigma} \\ &+ \frac{2k_F}{k_0^2} \left\{ i \left[(\partial_x R_{\sigma}^{\dagger}) L_{\sigma} - R_{\sigma}^{\dagger} \partial_x L_{\sigma} \right] e^{-i2k_F x} + \text{H.c.} \right\}. \end{aligned} \quad (\text{D.66})$$

The polarization operators entering Eq. (D.65) are calculated in the presence of the intrawire interaction which would lead to the Luttinger-liquid renormalization of the drag resistivity, but neglecting correlations between the edges. This amounts to setting $g_{2\perp} = 0$ and $g_{4\perp} = 0$. Then the quadratic part of the total Hamiltonian separates into two independent sectors in the edge basis. As in the main text, we will restrict the discussion to equal edges with Luttinger parameter $K_1 = K_2 \equiv K$ (or, equivalently, $K_- = K_+ = K$) and plasmon velocity $v_1 = v_2 \equiv v$. In the bosonic language, the $2k_F$ -part of the density-density correlation function, which determines the behavior of the drag resistivity at low temperatures, can be cast in the form

$$\Pi^{2k_F}(x, \tau) = \frac{4k_F^2}{\pi a^2 k_0^4} e^{-i2k_F x} \langle \partial_x \theta(x, \tau) \partial_x \theta(0, 0) e^{i\sqrt{4\pi}[\varphi(x, \tau) - \varphi(0, 0)]} \rangle + \text{H.c.} \quad (\text{D.67})$$

The analytic continuation to real time and the Fourier transform to the frequency-momentum space is standard [35] and yields

$$\Pi^{2k_F}(q, \omega) = \tilde{\Pi}^{2k_F}(q + 2k_F, \omega) + \tilde{\Pi}^{2k_F}(q - 2k_F, \omega) \quad (\text{D.68})$$

with $\tilde{\Pi}^{2k_F}(q, \omega)$ given by

$$\tilde{\Pi}^{2k_F}(q, \omega) = - \left(\frac{k_F}{k_0} \right)^2 \frac{1}{(k_0 a)^2} \left(\frac{\pi a T}{v} \right)^{2K} \frac{1}{\pi^4 T^2} \mathcal{K}_K \left(\frac{qv}{4\pi T}, \frac{\omega}{4\pi T} \right). \quad (\text{D.69})$$

Here

$$\mathcal{K}_K(x, y) = \left(\frac{1}{K} + 1 \right) \mathcal{I}_{K+2,2}(x, y) - 2\mathcal{I}_{K,0}(x, y) + \mathcal{J}_{K+1}(x, y) \quad (\text{D.70})$$

and we have defined the functions

$$\mathcal{I}_{\gamma,\delta}(x, y) = \sin(\pi\gamma) 2^{2\gamma-\delta-2} B \left(-i(x+y) + \frac{\gamma-\delta}{2}, -\gamma + \delta + 1 \right) B \left(-i(y-x) + \frac{\gamma}{2}, -\gamma + 1 \right) + (x \rightarrow -x), \quad (\text{D.71})$$

and

$$\begin{aligned} \mathcal{J}_\gamma(x, y) &= \frac{v}{(\pi T)^2} 2^{2\gamma-4} \sin(\pi\gamma) \\ &\times \left\{ \left[B \left(-i(x+y) + \frac{\gamma}{2} - \frac{1}{2}, -\gamma + 1 \right) + B \left(-i(x+y) + \frac{\gamma}{2} + \frac{1}{2}, -\gamma + 1 \right) \right] \right. \\ &\times \left. \left[B \left(-i(y-x) + \frac{\gamma}{2} - \frac{1}{2}, -\gamma + 1 \right) + B \left(-i(y-x) + \frac{\gamma}{2} + \frac{1}{2}, -\gamma + 1 \right) \right] \right\}, \end{aligned} \quad (\text{D.72})$$

where $B(x, y)$ is the Euler beta-function. When deriving this result, we used

$$\int_0^\infty dX e^{-\mu X} \sinh^\nu(\gamma X) = \frac{1}{2^{\nu+1}\gamma} B(\mu/2\gamma - \nu/2, \nu + 1),$$

where the identity holds as long as $\text{Re}\gamma > 0$, $\text{Re}\nu > -1$ and $\text{Re}\mu > \text{Re}(\gamma\nu)$. In our problem, there exist integrals for which the condition $\text{Re}\nu > -1$, which ensures the infrared convergence, is not fulfilled. In that case, the integrals over time t are cut off at small t by a/v and, consequently, the integrals over X are cut off by $\pi T a/v$.

For $T \rightarrow 0$, the function $\text{Im} \mathcal{K}([q - 2k_F]/4\pi T, \omega/4\pi T)$ is strongly peaked around $q = 2k_F$ with a width of the peak of the order of T/v . Therefore, we can neglect the term $\text{Im} \mathcal{K}_K([q + 2k_F]/4\pi T, \omega/4\pi T)$ in the integral over positive momenta in Eq. (D.65). Then, we find

$$\rho_D \sim I_K \frac{[V_{12}(2k_F)]^2}{u^2} \left(\frac{k_F}{k_0} \right)^4 \frac{T}{(k_0 a)^4} \left(\frac{\pi a T}{u} \right)^{4K}, \quad (\text{D.73})$$

where

$$I_K = \int_0^\infty d\Omega \frac{[\text{Im} \mathcal{K}_K(0, \Omega/4\pi)]^2}{\sinh^2(\Omega/2)}$$

with $\Omega = \omega/T$. As discussed in the main text, the natural ultraviolet cutoff here is provided by the distance between the edges, $a \sim d$. The parametric dependence of the drag resistivity obtained by means of bosonization reproduces in the limit $K \rightarrow 1$ the result (4.41) of the kinetic-equation analysis.